NATIONAL RESEARCH CENTER
"KURCHATOV INSTITUTE"
PETERSBURG NUCLEAR PHYSICS INSTITUTE

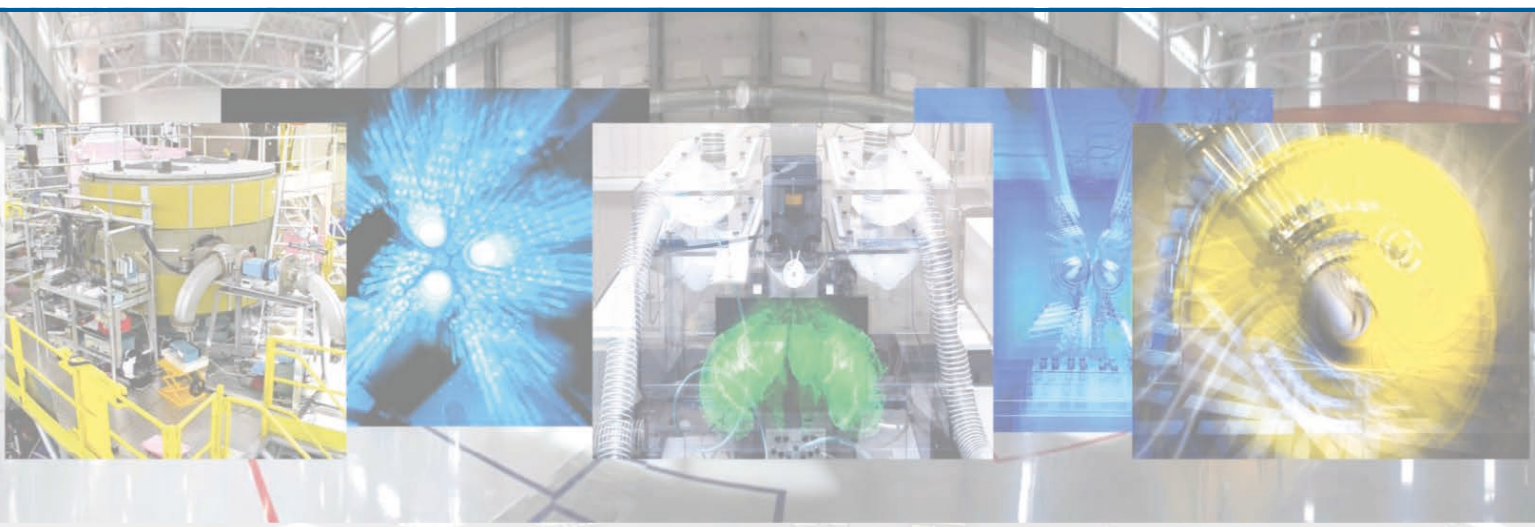

PNPI Scientific Highlights

2015

Gatchina • 2016

Chief-editors:
Victor L. Aksenov
Svetlana V. Sarantseva

Editors:
Georgy D. Alkhazov
Alexey A. Vorobyov
Vladimir V. Voronin
Andrey L. Konevega
Geliy F. Mikheev
Victor Yu. Petrov
Sergey R. Friedmann
Yury P. Chernenkov

Proofreaders:
Alena M. Arkhipova
Elena Yu. Orobets
Nadezhda V. Silinskaya
Anastasia I. Zaitseva (translation)

Technical editing and design:
Tatiana A. Parfeeva

Layout composition:
Elena V. Veselovskaya
Anastasiya B. Kudryavtseva

Publisher:
Petersburg Nuclear Physics Institute
NRC "Kurchatov Institute"
Publishing Office

Orlova Roscha,
Gatchina, Leningrad District,
Russian Federation

PNPI Scientific Highlights 2015 (136 pages) contains a number of short overview reports of the main research results of PNPI NRC "Kurchatov Institute" achieved in 2015. The links for the leading Russian and foreign scientific journals containing the full versions of each paper are listed below each article.

Printed on Konica Minolta bizhub PRO C1060L

ISBN 978-5-86763-383-7

Table of contents

Preface

B.P. Konstantinov Petersburg Nuclear Physics Institute of the National Research Center "Kurchatov Institute" (PNPI NRC KI) is a multidisciplinary research center. It conducts fundamental and applied research in various directions of particle and high-energy physics, nuclear physics, condensed matter physics, molecular and radiation biophysics.

The scientific achievements of PNPI NRC KI researchers have been awarded the Lenin and State prizes, the prizes of the Government of the Russian Federation and the Academic prizes. Three PNPI NRC KI employees were elected full members and seven employees – the corresponding members of the Russian Academy of Sciences. PNPI NRC KI currently employs 1 989 people including 585 researchers, 72 Doctors of Sciences and 267 Candidates of Sciences. At the moment, one of PNPI NRC KI employees is a full member and two are the corresponding members of the Russian Academy of Sciences.

PNPI NRC KI consists of five research divisions sharing a common infrastructure:

- Theoretical Physics Division;
- Neutron Research Division;
- High Energy Physics Division;
- Molecular and Radiation Biophysics Division;
- Knowledge Transfer Division.

The long-term and short-term research program of the Institute can be found in two documents, which are the program concerning the activity of the NRC "Kurchatov Institute" and the Research and Development program of the Institute in accordance with the State assignment.

Just like other institutes within the NRC "Kurchatov Institute", PNPI NRC KI takes an active part in various international projects and collaborates with the largest international research centers within its main research areas.

PNPI NRC KI possesses a number of operating installations as well as designs new set-ups for the physical research.

The WWR-M research reactor (built in 1959) was temporarily shut down in December 2015 owing to the end of its operating license and the lack of funds necessary to carry out the repair works mandatory for the license renewal.

The proton synchrocyclotron built in 1970 performed 1 874 hours in 2015 for the different applied scientific research.

In December 2014, the physical launching of the C-80 cyclotron took place. The start-up operations were carried out together with the D.V. Efremov Institute of the Electrophysical Apparatus (NIIEFA).

The beam ejection and the beginning of the physical investigations are scheduled for 2016.

The year 2015 was an important phase in the creation of the PIK-based International Center for Neutron Research (ICNR). The positive conclusion of the Main State Expert Review Board of the Russian Federation and the Federal Service for Ecological, Technological and Nuclear Supervision (Rostekhnadzor) enables the completion of the PIK reactor construction. The implementation of the investment projects on the modernization and the reconstruction of the PIK infrastructure shall be continued in 2016.

At the moment, seven stations transferred from the Helmholtz Center Geesthacht (Germany) undergo the starting-up and adjustment procedures. The project was funded by a grant from the Federal Ministry of Education and Research of Germany and is related to the first step of Instrumentation Program for the PIK reactor. To implement the second step, the first meeting of the International Advisory Committee on Neutron Sciences of the NRC "Kurchatov Institute" was held in Gatchina in March 2015. The concept of the facility with 20 experimental stations was considered and six international expert groups were formed, each in different directions of the experimental research. During last year, these groups carried out an analysis of the Institute proposals and came up with the suggestions on their implementation. The activity will be continued next year.

The year 2015 was an eventful year in terms of both scientific and social life. On 5–8 February 2015, the holiday "Russian Science Day" was celebrated for the first time at the Institute. The program organized by the Committee of young researchers and specialists included the lessons for schoolchildren, the lecture "Brain and Freedom of Will" given by T. Chernigovskaya, the member of the President's Council for Science and Education, the professor of Saint Petersburg University. The celebration ended with a winter ball.

February and March saw the memorial seminars devoted to the 85th anniversary of the first director of the Institute, the corresponding member of the USSR Academy of Sciences O.I. Sumbaev and the founders of the Theoretical Physics Department – the corresponding member of the USSR Academy of Sciences V.N. Gribov and professor V.M. Shekhter.

In 2015 the Institute convened 15 scientific conferences, including the traditional Winter schools and the Third annual international conference "Large Hadron Collider Physics" attended by 350 participants from 35 countries. The conference was a great success.

The works of our Institute won various scientific prizes. One of the prizes of the European Physical Society (EPS) in 2015 was awarded to the academician L.N. Lipatov and professor Yu.L. Dokshitzer for an outstanding contribution to High Energy Physics. The famous Dokshitzer–Gribov–Lipatov–Altarelli–Parisi equation is the basis for the description of the scattering processes at high energies.

At the end of the year 2015 the organizational structure of the NRC "Kurchatov Institute" underwent certain changes. On 7 December 2015, the president of the Russian Federation V.V. Putin signed a decree on the appointment of M.V. Kovalchuk as a president of the NRC "Kurchatov Institute" for the period of 5 years starting from 31 December 2015. In all institutes within NRC "Kurchatov institute" a new job title "Science Director" was introduced. At PNPI NRC KI the corresponding member of the Russian Academy of Sciences V.L. Aksenov was appointed its Science Director and professor D.Yu. Minkin was appointed the Director of the Institute.

The most significant PNPI NRC KI results of 2015 were summarized and presented in this volume. The scientific achievements of the Institute employees have been published in 565 articles in the leading Russian and foreign reviewed editions and presented at 139 national and international conferences. The general information about the Institute is given in the conclusive part of this document.

Director of PNPI
NRC "Kurchatov Institute"
Professor D.Yu. Minkin

Science Director of PNPI NRC "Kurchatov Institute"
Corresponding member of the Russian Academy
of Sciences V.L. Aksenov

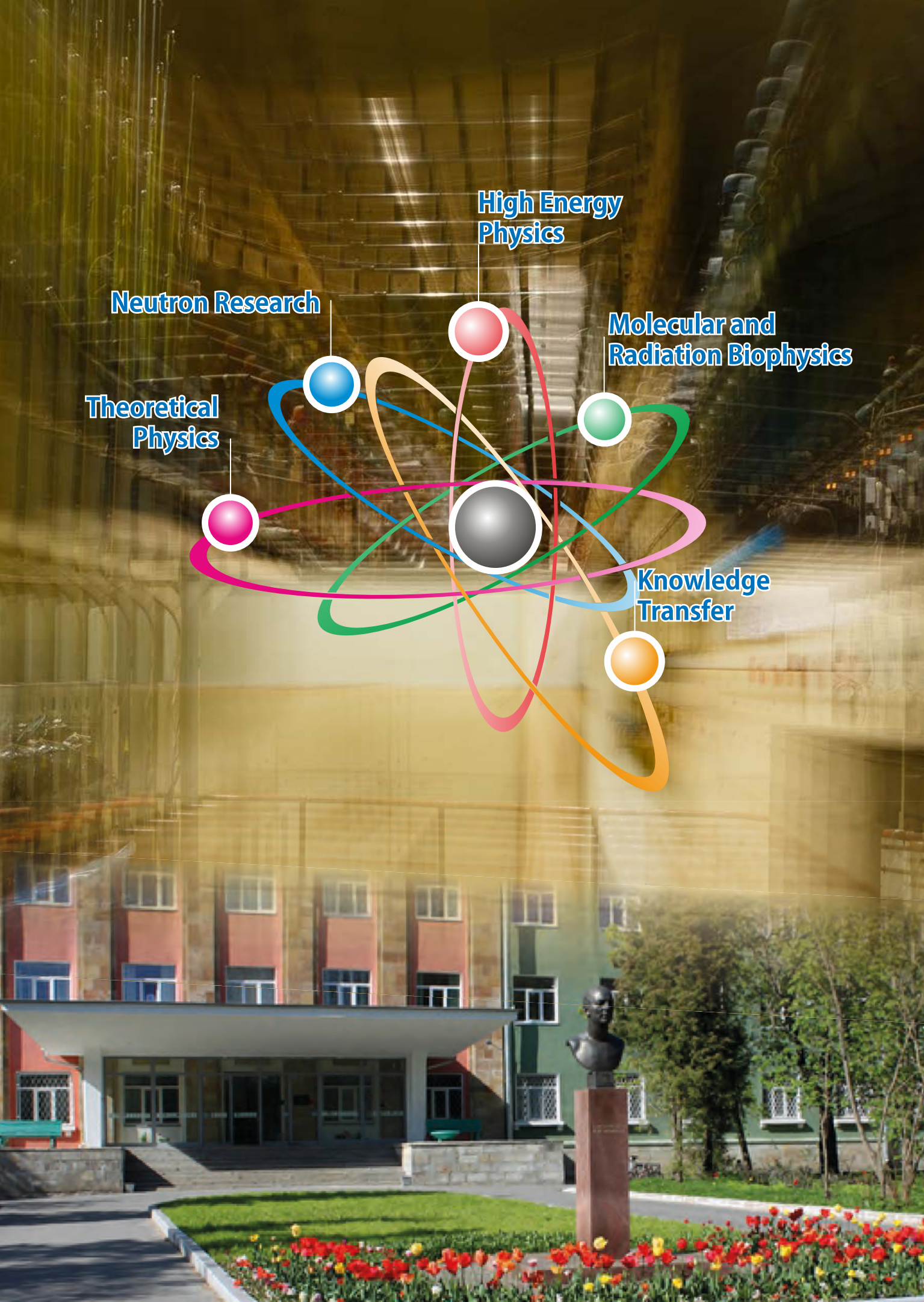
High Energy Physics
Neutron Research
Molecular and Radiation Biophysics
Theoretical Physics
Knowledge Transfer

Research Divisions

Theoretical Physics Division

Theoretical Physics Division (TPD) headed by Lev N. Lipatov (member of the Russian Academy of Sciences) consists of seven departments:

– Theory of Electroweak Interactions (headed by Dr. Gennady S. Danilov)**;**
– Theory of Strong Interactions (headed by Dr. Victor Yu. Petrov)**;**
– Quantum Field Theory (headed by Dr. Vyacheslav A. Kudryavtsev)**;**
– High Energy Theory (acting head Dr. Victor Yu. Petrov)**;**
– Condensed Matter Theory (headed by Dr. Saul L. Ginzburg)**;**
– Nuclear Theory (headed by Dr. Mikhail G. Ryskin)**;**
– Atomic Theory (headed by Dr. Alexander I. Mikhailov)
and a Group of Physics of Nuclear Reactors (headed by Dr. Mikhail S. Onegin)**.**

TPD employs 69 research staff members (28 Doctors of Sciences and 32 Candidates of Sciences).

Lev N. Lipatov
Member of the Russian Academy of Sciences,
Head of TPD

TPD research covers most of the branches of modern theoretical physics: from elementary particle physics and quantum field theory to physics of nuclear reactors.

Scattering at high energies is a traditional area of TPD research. It can be noted that for a long time the activity of TPD researchers has determined the frontier in this field. In 2015 L.N. Lipatov *et al.* continued the investigation of BFKL (Balitsky, Fadin, Kuraev, Lipatov) equation determining the asymptotics of the scattering amplitude at high energies. In particular, the behavior of the BFKL pomeron Green function with running coupling constant was determined. The quasiclassical solution of the BFKL equation was found for the theory with massive gluons in the Higgs phase. Effective Lagrangian for Gribov reggeon field theory was obtained both for Yang–Mills theory and gravity. Also Euler–Lagrange equations in the effective theory were derived.

TPD is also one of the world leaders in the field of so-called AdS/CFT duality (anti-de Sitter/conformal field theory), which is currently one of the hot topics in theoretical physics. The duality means that some non-trivial field theory ($N = 4$ supersymmetric Yang–Mills theory) in $d = 4$ space-time is equivalent to string theory and both are exactly solvable. L.N. Lipatov suggested investigating the high energy behavior of $N = 4$ conformal field theory. Due to high symmetry and exact solvability of the theory one can go much further in this theory than in Quantum Chromodynamics (QCD). For example, in 2015 pomeron trajectory was calculated both for small couplings and (using AdS/CFT correspondence) also for large couplings. Also in a paper of N.A. Gromov the eigenvalues of BFKL equations were calculated in three loops using the method of algebraic curve. Analogous result is known in QCD only in two loops and was obtained by L.N. Lipatov *et al.* after 10 years of work. In principle, next loops can be easily obtained in $N = 4$ theory using the same method and one can hope that these results can help to make a progress in QCD. Another way to compute the 3rd loop correction was proposed by V.N. Velizhanin on basis of his record six-loop calculations of anomalous dimensions in $N = 4$ theory.

Recently, exact expressions for scattering amplitudes in the multiregge kinematics for $N = 4$ theory were proposed. As it was shown in 2014–2015 papers of L.N. Lipatov these expressions are wrong and should be corrected by some wrapping factor accounting for Regge cuts which should be present

together with Regge poles. In 2015 the structure of Regge singularities in $N = 4$ theory was derived for the amplitudes with seven legs.

Quark confinement is the most interesting and still unclear phenomenon in QCD. It is still impossible to study it directly, and for that reason, simpler (more symmetrical) supersymmetrical (SUSY) theories are used to clarify its mechanism. A.V. Yung has studied these theories for many years. Now this mechanism is almost completely clarified. Perhaps, it is not exactly what we need to explain confinement in QCD, however, a number of very interesting non-perturbative phenomena were revealed. One of them, which was completely unknown before, was named "instead–of–confinement mechanism". Also, for the first time the definite conclusions concerning the behavior of $N = 1$ SUSY Yang–Mills theory were made. This theory is the last hope to manifest the confinement of the type that is observed in nature.

In 2015 the effective string theories arising in the confining phase of SUSY theories were investigated. It appears that under definite conditions strings can be critical in four-dimensional space-time and possibly free of ultraviolet divergences. The theory was also developed for strings of finite length. This allows the determination of a spectrum of low-lying states in the SUSY theories.

Works of V.N. Velizhanin proved to reach the maximum accuracy in calculation of perturbative theory diagrams. In 2015 his calculations of renormalization of the Higgs coupling constant in the Standard Model (SM) in three loops and anomalous dimensions of twist two operators in $N = 4$ SUSY theory were published.

In 2015 LHCb collaboration declared observation of two pentaquark resonances. In a paper of M.I. Eides, V.Yu. Petrov and M.V. Polyakov these resonances are interpreted as a bound state of an excited state of charmonium and proton. Surprisingly, the interaction potential between these two hadrons can be estimated on the general grounds of QCD. Obtained positions of resonance and its width appeared to be close to the data. Another interpretation was proposed in the series of papers of V.V. Anisovich, A.V. Sarantsev *et al.* who adopted the diquark picture of the pentaquark. Then its mass can be easily related to the masses of recently discovered tetraquark mesons.

The theory of baryon resonances at a large number of colors was developed in the papers of V.Yu. Petrov *et al.* In this theory resonances can be viewed as a number of constituent quarks in the mean field of mesons described by effective low energy lagrangian. It is shown that all baryons below 2 GeV can be interpreted in this way and there are no missed states in this model. The masses and widths of resonances can be calculated and reasonably coincide with the data.

M.G. Ryskin with his co-authors studied diffractive and exclusive processes at Large Hadron Collider (LHC) energies. In 2015 exclusive photoproduction of charmoniums and bottoniums and low x gluons was considered at LHC energies. A large paper dedicated to elastic scattering and diffractive dissociation in the light of LHC data was also published.

The works of M.I. Eides and his co-authors prove to reach a high precision (three loops and more) Quantum Electrodynamics (QED) perturbative calculations. The precision of QED experiment has reached a fantastic level here, so these calculations are needed to explain the data. In 2015 a calculation of hard corrections hyperfine splittings in positronium and muonium in three loops were published.

The ideas concerning the origin of the hierarchy of quark masses and the Kobayashi–Maskawa matrix continue to attract attention of theoreticians. In 2015 I.T. Dyatlov published two papers, which approach these problem in the mirror symmetry theory. It was shown that such a theory can explain some of the well-known miracles of the SM. A possible mechanism of the spontaneous breakdown of mirror symmetry was presented.

A.V. Sarantsev with his group continues the work on PWA (Partial Wave Analysis) of a series of reactions with mesons and bosons. This group (so-called, Bonn–Gatchina analysis) has already become the most recognized and reputable in the world – a significant part of PDG (Particle Data Group) data is based on their results. It is important to underline that the analysis is for the first time based on a single approach to all the reactions – data from different experiments complement each other. Some new data and new hadron reactions were considered also in 2015.

A number of contributions in 2015 was also made to condensed matter physics. Magnetics are the

traditional topic of research for TPD. In particular, in the papers of A.V. Syromyatnikov with collaborators, the influence of impurities on magnetics in ordered phase and in spin liquid phase was investigated. Spiral magnetics with defects in the phase of "Bose-glass" were considered. The spectrum of singlet excitations for Heisenberg antiferromagnet on square lattice was calculated. Anomalously strong damping for the part of long-wave excitation at small temperatures was predicted.

Magnetics with non-trivial ordering (with so-called skyrmion lattice) were considered in papers of D.N. Aristov *et al.* Spectrum and wave functions of magnons in the field of skyrmion were calculated analytically and numerically for a magnetic with hexagonal skyrmion lattice. Corrections to the spectrum which are due to the interaction of magnons were also taken into account.

Nanowires have been under investigation in TPD already for a long time. In 2015 in works of D.N. Aristov *et al.* the function of four quantum wires was investigated by renormalization group method. They also discussed the renormalization of conductance for the edge states of topological insulators. Renormalization group method was also used in the paper of V.Yu. Petrov *et al*. for the problem of one impurity in the quantum wire. Conductance was calculated on the level of four loops.

The paper of A.G. Yashenkin *et al.* deals with effect of the spin Coulomb drag in two dimensional electron gas at small temperatures. The coefficient of spin transconductance appears to be much larger than expected by standard theory.

S.L. Ginzburg and N.E. Savitskaya studied disorder systems in their works. In 2015 it was shown in their paper that avalanche dynamics is always more stable for the nets with structure changing with time than for stationary nets.

A significant part of TPD publications in 2015 was devoted to the theory of atoms and molecules, as well as traditional nuclear physics. The electronic analogue of the famous Mikelson experiment was considered, the proposed experiment improved the restriction on breakdown of Lorentz symmetry by two orders of magnitude. In the papers of A.I. Mikhailov *et al.* the cross section of double ionization of helium-like atoms by high energy photons was calculated analytically. The influence of inner electrons on the photoionization of electrons from outer shells was also estimated in the paper of E.G. Drukarev *et al.* High accuracy calculations of the properties of molecules and atoms were performed. These results are needed for the future experiments measuring electrical dipole moment of an electron.

In 2015 Group of Reactor Physics continues investigations and numerical simulations of the PIK reactor. In particular, complete calculations of the PIK fuel cycle were performed for the new type of the fuel element. It appears that all requirements of nuclear safety can be fulfilled and the fuel cycle up to 30 days can be provided.

The following statistics demonstrates the results obtained by TPD employees during 2015:

– 96 research papers published in reviewed journals (including 88 papers published in foreign editions);

– One monograph published;

– 35 research reports presented at international and Russian events;

– Two theses (Candidate of Sciences) defended.

Neutron Research Division

Neutron Research Division (NRD) headed by Dr. Alexander I. Kurbakov consists of two research and four scientific and technological departments:

– Condensed State Research Department (headed by Dr. Sergey V. Grigoriev) **consists of four laboratories:**

– Disordered State Physics Laboratory (headed by Dr. Vladimir V. Runov);
– Neutron Physical and Chemical Research Laboratory (headed by Dr. Vasily T. Lebedev);
– Crystal Physics Laboratory (headed by Dr. Yury P. Chernenkov);
– Material Research Laboratory (headed by Dr. Alexander I. Kurbakov)
and two groups:
– Condensed Matter Electrodynamics Group (headed by Dr. Oleg V. Gerashchenko);
– Solid State Radiation Physics Laboratory (headed by Dr. Sergey P. Belyaev).

Neutron Physics Department (headed by Prof. Anatoly P. Serebrov) **consists of four laboratories:**

– Neutron Physics Laboratory (headed by Prof. Anatoly P. Serebrov);
– Nuclear Spectroscopy Laboratory (headed by Dr. Ivan A. Mitropolsky);
– Molecular and Atomic Beams Laboratory (headed by Dr. Victor F. Ezhov);
– *X*- and γ-Ray Spectroscopy Laboratory (headed by Prof. Valery V. Fedorov)
and two groups:
– Weak Interaction Research Group (headed by Dr. Alexander N. Pirozhkov);
– Nuclear Fission Physics Group (headed by Dr. Alexander S. Vorobyov).

Four scientific and technological departments:
– Engineering and Technological Support of Experiments on Reactors Department
(headed by Dr. Alexey P. Bulkin);
– Automation of Experiments on Reactors Department (headed by Dr. Valery A. Solovey);
– Semiconductor Nuclear Detectors Department (headed by Dr. Alexander V. Derbin);
– Department of Operation of Neutron Stations at the PIK Reactor (headed by Dr. Evgeniy V. Moskvin).

NRD employs 179 research staff members (16 Doctors of Sciences and 76 Candidates of Sciences).

Dr. Alexander I. Kurbakov
Head of NRD

The main directions of NRD research are nuclear physics, particle physics and condensed matter physics.

At the present time, the full-scale model of a source of ultracold neutrons for the WWR-M reactor is being created. In November 2015, the superfluid helium with the temperature 1.3 K at the thermal load of 15 W was obtained on a full-scale mode. It is the important result, which shows the possibility of realization of a UCN project at the WWR-M reactor and the possibility of use of superfluid helium in nuclear technologies.

In 2015 the model of an antineutrino detector of a cellular type with 16 sections was installed in the PNPI-RSIAR neutrino laboratory at the SM-3 reactor. The measurements of the antineutrino flux depending on the distance (R) from the active zone of the reactor were made. The deviation from the $1/R^2$ law was observed, which is far too early to be interpreted as the effect of neutrino oscillation, since it is necessary to check the possible systematic effect connected with the insufficiency of reactor protection.

In 2015 the Borexino collaboration, in which employees from NRD take part, published 2 056-days

data on the measurement of the geo-neutrinos flux in the Gran Sasso National Laboratory. Using the calculation of the expected geo-neutrino flux from the Earth's crust, for the first time the existence of a flow of geo-neutrinos from the mantle was firmly established, which is an important fact to determine the structure of the Earth.

The Laboratory of Low-Background Measurements of PNPI NRC KI and the Institute for Nuclear Research of the Russian Academy of Sciences (INR RAS) at the Baksan Neutrino Observatory performed a search for axions with the energy of 9.4 keV, emitted in M1-transition ^{83}Kr nuclei in the Sun. As a result, new limits on the axion-nucleon coupling constants and on the mass of hadron axion have been obtained: $m_A \leq 100$ eV at 95% C.L .

In the Laboratory of Nuclear Spectroscopy the methods for the element analysis of geological samples and refined petroleum products are developed. The study of tagamites and suevites of the Kara impact structure was performed in 2015. The content of Pt, Au, Ir, Re and 29 other elements was determined by means of chromatography and neutron activation analysis at the level of up to 10^{-8}%.

The measurements of fission fragment angular distributions of ^{235}U, ^{238}U and ^{232}Th were made in the energy range of incoming neutrons 1–200 MeV at the neutron time-of-flight spectrometer GNEIS operated on the base of the PNPI synchrocyclotron SC-1000. At the moment, the data obtained for the neutron energies above 20 MeV are the most accurate and complete.

The magneto-electronic phase separation in the doped single-crystal $La_{0.85}Sr_{0.15}CoO_3$ has been studied by linear and nonlinear magnetic ac response and neutron depolarization. A detailed characteristic of the emerging superparamagnetic cluster system as well as its temperature evolution were obtained from the data treatment using the Gilbert–Landau–Lifshitz formalism.

A comprehensive diffraction study (neutron and synchrotron powder diffraction) of the quasi-two-dimensional (2D) monoclinic compound $Na_3Co_2SbO_6$ is carried out. It is shown that magnetic Co cations in the oxygen-octahedral layers form honeycomb grids, which in condition of an antiferromagnetic type interaction between nearest neighbors, lead to a frustration in the magnetic subsystem, a complicated character of magnetic exchanges both within the magnetic layers and between the layers and the emergence of unusual types of magnetic moments ordering: the superposition of a collinear AFM ($\mathbf{k}_1$) in a general direction with a long period transversal sinusoidal ($\mathbf{k}_2$) component along the short axis.

For the first time the study of radiation resistance of fullerenols $Gd@C_{82}(OH)_X$ in a flux of fast neutrons (10^{16}–10^{19} fluences n/cm^2) has been performed, which showed that fullerenols are more stable by an order of magnitude than C_{60} and $Gd@C_{82}$complexes, which is important for biomedical applications of fullerenols as isotopic pharmaceuticals.

The magnetic properties of the core/shell nanosystem, where the core is Fe_xO and the shell is Fe_3O_4 were studied by different tenchiques: *X*-ray and neutron diffraction, Mossbauer spectroscopy, electron microscopy, EELS, magnetometers and other for two samples: small (10/2 nm, for core and shell, respectively) and large (21/9 nm). In the case of small particles, the magnetic order in the core was not detected, whereas in the larger particles the antiferromagnetic structure in the core was observed, which differs from that of the bulk.

Neutron diffraction studies of the solid solutions $(BiFeO_3)_{1-x}(PbTiO_3)_x$ showed a mixture of two nanoscale phases with different crystal structures: the rhombohedral and tetragonal. The observed enhancement of the Neel temperature by several hundred degrees in the tetragonal phase was interpreted as “the exchange bias” between particles: a phase with larger temperature “magnetizing” a phase with lower temperature. A new scenario, where “proximity effects” in an unstable nanostructured system play a crucial role in the emergence of the unusual magnetic properties was demonstrated.

For the first time the three-level structure of diamond hydrogels was discovered: the particles associated through hydration shells; linear and branched moieties (first coordination sphere) and chains forming the cells of a gel.

Small angle neutron scattering has been applied to study the supramolecular structure of new hydrogen fuel cell membranes based on fluorine-containing polymers with short side chains, synthesized by the efficient water-emulsion based method in the Boreskov Institute of Catalysis of the Siberian Branch of the RAS.

Fourier-analysis of *X*-ray scattering data has enabled the decoding of the structure of amorphous metal-carbon phase of the pyrolysates of diphthalocyanines for a number of elements (Y, La, Ce, Nd, Tb) and the determination of the laws of its formation depending on the annealing temperature, the atomic number and the mass of base element.

The critical state theory in the low field region of the Josephson medium electrodanymics has been proved experimentally for a new type of the granular superconductors. The universality of the conception has been evidenced.

The neutron resistance tests of electronic components in the wide neutron energy range of 1–1 000 MeV were continued at the neutron testing facility ISNP/GNEIS, jointly with the Branch of JSC "United Rocket and Space Corporation" – "Institute of Space Device Engineering". As a result of two irradiation shifts, the cross sections of single event upsets have been obtained for the SRAM memory chips of six technological norms.

New optimization criteria for a class of instruments – neutron reflectometers – are substantiated. It is shown that the correct choice of the working wavelength and other beam parameters may increase the luminosity of the reflectometers in several times. Such innovations as neutron-optical velocity selector, fan beam time-of-flight technique and small angle Soller collimator of special design are proposed to further increase the luminosity of the reflectometers.

In the Data Center two books with the compilation of nuclear data "Nuclear Resonance Parameters" and "Excited Nuclear States" were prepared and published in the Springer Verlag in 2015. Problem-oriented databases of nuclear structure and decays and interface programs to work with them were created and registered.

The following statistics demonstrates the results obtained by NRD employees during 2015:

– 77 research papers published in reviewed journals (including 34 papers published in foreign editions);

– Two monographs published;

– 156 research reports presented at international and Russian events;

– Three patents and five certificates of state registration of specialized programs and databases obtained;

– Two theses (Candidate of Sciences) defended.

High Energy Physics Division

High Energy Physics Division (HEPD) headed by Prof. Alexey A. Vorobyov (corresponding member of the Russian Academy of Sciences) consists of 10 laboratories:

– Elementary Particle Physics Laboratory (headed by Prof. Georgy D. Alkhazov);
– Meson Physics of Condensed Matter Laboratory (headed by Dr. Sergey I. Vorobyev);
– Relativistic Nuclear Physics Laboratory (headed by Prof. Vladimir M. Samsonov);
– Short-Lived Nuclei Laboratory (headed by Dr. Vladimir N. Panteleev);
– Meson Physics Laboratory (headed by Prof. Victorin V. Sumachev);
– Few Body System Laboratory (headed by Prof. Stanislav L. Belostotski);
– Hadron Physics Laboratory (headed by Dr. Oleg L. Fedin);
– Physics of Exotic Nuclei Laboratory (headed by Prof. Yuri N. Novikov);
– Crystal Optics of Charged Particles Laboratory (headed by Dr. Yuri M. Ivanov);
– Cryogenic and Superconductive Techniques Laboratory (headed by Dr. Alexander A. Vasilyev)
and four technical departments:
– Radio Electronics Department (headed by Dr. Viktor L. Golovtsov);
– Track Detectors Department (headed by Prof. Anatoly G. Krivshich);
– Computing Systems Department (headed by Andrei E. Shevel);
– Muon Chambers Department (headed by Vladimir S. Kozlov).

HEPD employs 147 research staff members (14 Doctors of Sciences and 66 Candidates of Sciences).

Prof. Alexey A. Vorobyov
Corresponding member
of the Russian Academy
of Sciences,
Head of HEPD

HEPD activity is mainly aimed at the experimental research in the field of elementary particle physics and nuclear physics. In addition, a solid state physics research with the use of the μSR-method is being performed. As in previous years, research works were conducted at PNPI NRC KI facilities and at accelerators of the world's leading nuclear centers.

In 2015, the following experiments were carried out

Experiments at the PNPI NRC KI synchrocyclotron:

– Production and studies of short-lived nuclei with the laser-mass spectrometer complex IRIS;
– Studies of polarization effects in proton quasi-elastic scattering off nuclei;
– Studies of η-meson production in the pion beam;
– Studies of magnetic properties of materials with the μSR-method.

Furthermore, the 1 GeV proton beam was in use for testing various experimental equipment at a special test stand.

Experiments in the European Center for Nuclear Research (CERN):

– Participation in experiments CMS, ATLAS, LHCb, and ALICE at the Large Hadron Collider (LHC);
– Production and studies of short-lived nuclei with the laser-mass spectrometer complex ISOLDE;
– Studies of possibilities to use crystal collimation of the LHC beams (experiment UA9).

Experiment at Brookhaven National Laboratory (USA):

– Experiment PHENIX. Studies of the relativistic heavy ion collision physics.

Experiment at the Paul Scherrer Institute Meson factory (Switzerland):

– Experiment MuSun. High precision studies of muon capture on deuteron.

Experiments at the electron accelerators at Bonn and Mainz universities (Germany):

– Study of nucleon structure by γ-p- and e-p-scattering.

The following experiments were completed, the data analysis being continued:

– Experiments HERMES and OLYMPUS at DESY, Germany (study of spin structure and form factors of nucleons);

– Experiment D0 at the Fermi National Accelerator Laboratory, USA (physics of proton-antiproton collisions at the Tevatron);

– Experiment EPECURE at the Institute for Theoretical and Experimental Physics (ITEP), Moscow (search for narrow resonances in π-p-scattering).

New projects:

– Preparations for experiments R3B, MATS, PANDA, and CBM at the accelerator complex FAIR (GSI, Germany);

– Experiment Compton for studies of nucleon polarizability at the accelerator MESA (Mainz, Germany);

– Project IRINA for production and studies of short-lived nuclei at the high flux neutron reactor PIK;

– Project RIC-80 for production of radioisotopes for medical applications.

One of the main activities of the HEPD was the participation in the LHC experiments CMS, ATLAS, LHCb, and ALICE. PNPI NRC KI participated in these experiments from the initial phase of design and construction of the collider detectors with essential contributions to the construction of various subsystems of these detectors. After the LHC start-up, HEPD physicists and engineers shared responsibilities in maintenance and operation of these detectors and took part in the analysis of the experimental data.

The analysis of the experimental data collected in Run 1 (2010–2012) yielded a great amount of new results crowned by the discovery of the Higgs boson. More than 150 papers were published in 2015. The list of authors in these publications includes 35 scientists from the HEPD. The main annual LHC physics conference (LHCP conference) was held in Saint Petersburg on August 31 – September 5, 2015. This conference with about 400 participants summarized physics results obtained at LHC during Run 1. The HEPD shared major responsibility in organizing this conference.

In 2015, the activities of the HEPD groups participating in the LHC experiments were focused on preparations and start-up of Run 2. As an example, in the framework of the CMS upgrade program, 76 new large muon chambers and a 2 500-channels high voltage system for the CMS muon detector have been constructed, installed, and put into operation with the active participation of HEPD specialists. Also, the projects of further upgrades of the CMS, ATLAS, LHCb, and ALICE detectors were formulated to be realized until 2019. The HEPD takes an active part in realization of these projects.

This volume presents some of the results published in 2015 obtained in the LHC experiments, as well as in experiments performed at PNPI NRC KI and in other nuclear centers with the participation of HEPD physicists.

The following statistics demonstrates scientific activity of the HEPD in 2015:

– 194 research papers published in reviewed journals (including 187 papers published in foreign editions);

– 45 research reports presented at international and Russian events;

– One thesis (Candidate of Sciences) defended.

Molecular and Radiation Biophysics Division

Molecular and Radiation Biophysics Division (MRBD) (deputy Head Dr. Andrey L. Konevega) consists of 14 laboratories:

– Biophysics of Macromolecules (headed by Dr. Vladimir V. Isaev-Ivanov);
– Genetics of Eukaryotes (headed by Dr. Vladimir G. Korolev);
– Protein Biosynthesis (headed by Dr. Andrey L. Konevega);
– Molecular Genetics (headed by Dr. Valeriy N. Verbenko);
– Biopolymers (headed by Dr. Andrey L. Timkovsky);
– Cell Biology (headed by Dr. Mikhail V. Filatov);
– Human Molecular Genetics (headed by Dr. Alexander L. Schwartzman);
– Enzymology (headed by Dr. Anna A. Kulminskaya);
– Experimental and Applied Genetics (headed by Dr. Svetlana V. Sarantseva);
– Medical Biophysics (headed by Dr. Leonid A. Noskin);
– Medical and Bioorganic Chemistry (headed by Dr. Farid M. Ibatullin);
– Proteomics (headed by Dr. Stanislav N. Naryzhny);
– Cryoastrobiology (headed by Dr. Sergey A. Bulat);
– Molecular and Cellular Biophysics (headed by Dr. Georgiy N. Rychkov)
and Scientific and Technical Department of Bioelectronics (headed by Alexander P. Roganov).

MRBD employs 122 research staff members (13 Doctors of Sciences and 62 Candidates of Sciences).

Dr. Andrey L. Konevega
Deputy Head of MRBD

The research at MRBD is focused on the most significant fundamental questions in the molecular biology, biophysics, molecular and medical genetics. The studies of macromolecular complexes by small-angle neutron scattering and molecular modeling are actively pursued at the Laboratory of Biophysics of Macromolecules.

The problem of accounting of water molecules in the docking was addressed in the work of M.G. Petukhov and A.S. Afanasyeva. AquaBridge – the method to search for all possible structural conformations of water inside of active centers of proteins (AC) – has been developed to investigate the influence of structural water on efficiency of modern docking algorithms and design of ligands. The analysis of docking of small organic molecules in the active site of proteins under study showed a significant improvement of selectivity and docking prediction of the conformation of the ligand in the case when structural water in the active site was taken into account. The method is implemented in the form of AquaBridge utility for use in software packages ICM-Pro.

The study of the molecular mechanisms of protein biosynthesis is a traditional research focus at MRBD. In 2015, a group of researchers from Germany with the active participation of Russian scientists (A.L. Konevega, Laboratory of Protein Biosynthesis), for the first time surpassed the results obtained by *X*-ray crystallography. Using the method of cryoelectron microscopy, three-dimensional structures of the ribosomal complexes with a resolution better than 3 Å were obtained.

The optimized methods for obtaining of functional ribosomal complexes and microimages sorting procedures enabled obtaining the most accurate and complete model of the bacterial ribosome in the complex with elongation factor EF-Tu, stalled by antibiotic kirromycin during decoding (reading) of mRNA. The ribosome structure, including all the 35 modified bases of ribosomal RNA, was obtained for the first time in the world.

Structural studies of dihydrouridine synthases (Dus) complexes with tRNA (P.S. Kasatsky, A.L. Konevega) have demonstrated a new way for modifying of the substrate specificity of the enzyme from the family of dihydrouridine synthases. A characteristic feature of tRNA molecules is the presence of a large number of modified nucleotides that occur in the process of primary tRNA transcript maturation. One of the most common modified nucleosides – dihydrouridine – is formed by reduction of the C5-C6 double bond of uridine. Normally, formation of dihydrouridine in tRNA is catalyzed by dihydrouridine synthases. Three species of dihydrouridine synthases (DusA, DusB and DusC) were found in *Echerichia coli*. *X*-ray analysis of dihydrouridine synthases from mesophilic and thermophilic organisms complexed with $tRNA^{Phe}$ and $tRNA^{Trp}$ showed that the Dus subfamily, which selectively modified uridine in different positions of the tRNA, bound tRNA in orientations, which differ by 160°. So, in such an elegant way, substrate specificity of this class of enzymes is controlled by a relatively simple mechanism: re-orientation of an entire tRNA molecule. Such reprogramming of enzyme specificity could be named a unique evolutionary solution for a recognition of different tRNA by the same enzyme.

One of the most significant scientific MRBD achievements includes work on the possible association of Parkinson's disease (PD) and lysosomal storage diseases (Laboratory of Human Genetics). In 2015, a study was carried out on the correlation between a level of oligomeric forms of the protein alpha-synuclein and activity of the lysosomal enzyme glucocerebrosidase (GBA) in patients with Gaucher disease. The presence of two mutant alleles of gene *GBA* is the cause of a rare hereditary disease related to a class of lysosomal storage diseases. These data provide better understanding of the PD etiology in carriers of *GBA* gene mutations as well as allow us to offer the treatment of GBA-associated PD using pharmacological chaperones GBA (eg, ambroxol, izofagomin). An extensive group of human conformational diseases called amyloidosis, is accompanied by the formation and accumulation of aggregates (oligomeric and fibrillar) amyloid proteins having toxic properties. These aggregates of amyloid proteins have a number of physiological functions and are not always associated with pathological processes. Brain protein BASP1 that is important for organism's vitality is capable of forming oligomers *in vitro*.

In the O.S. Vityuk, N.J. Guiliano and V.V. Zakharov (Laboratory of Biopolymers) study of the properties of amyloid aggregates protein BASP1, it was found that the N-terminal miristorylated peptide myr-BASP1(1-13) *in vitro* formed amyloid fibril structure similar to native BASP1 protein. Complexes of native BASP1 localized to the presynaptic membrane in rat brain neurons are present in oligomer form. These BASP1 oligomers are not toxic to the PC12 cells. These data suggest that the BASP1 oligomers are non-pathological functional form of the protein in the brain. The proposed function of BASP1 is sequestering of membrane phosphatidylinositol 4,5-diphosphate.

Study of homologous genome repair is traditional at MRBD. Microorganism *Deinococcus radiodurans* withstands extreme doses of ionizing radiation due to the efficient ability to repair DNA even with hundreds of double-strand breaks. Protein RecA – the central link homologous recombination in bacteria – is one of the key components of recombination repair, which is thoroughly studied in the Laboratory of Molecular Genetics of Eukaryotes. For the repair of DNA double-strand breaks, RecA interacts with DNA and forms nucleoprotein complex, which is a coiled filament. In the single molecule DrRecA experiment, D.M. Baytin employed optical tweezer to measure the mechanical properties of the filament, formed by the association of DrRecA or EcRecA with long double-stranded phage λ DNA. DrRecA forms complexes with double-stranded DNA much faster; the resulting coiled filament is shorter and more flexible than that with EcRecA. In addition, multiple nucleation events occur during the filament assembly. These observations suggest a difference in the number of breaks in the filaments of both proteins or a different number of clusters. These different mechanical properties are the result of a change in the balance between DNA filament nucleation events and the subsequent growth phase.

Research on the structural and functional characterization of enzymes (Laboratory of Enzymology) is conducted in MRBD for many years. Recently, A.S. Borisova in collaboration with Swedish scientists had solved a structure of cellobiohydrolase from

Geotrichum candidum (GcaCel7A). It was shown that the cellobiohydrolase had a two-domain structure consisting of cellulose binding module connected by a peptide linker with the catalytic domain similarly to the industrial enzyme from *Hypocrea jecorina* (HjeCel7A). It was found that the GcaCel7A had increased resistance to inhibition product (cellobiose) during cellulose hydrolysis. Analysis of five crystal structures obtained (two for enzyme and three for complexes with different thiooligosaccharides) revealed some conformational differences in loops located in the entrance area in the coupling cavity in the active site of the enzyme.

Nicotinamide adenine dinucleotide (NAD) is essential for cellular metabolism and plays a key role in various signaling pathways in human cells. Nicotinamide and nicotinic acid as well as nicotinamide riboside (NR) and nicotinic acid riboside (NAR) are the major precursors for NAD biosynthesis in humans. In the study of A.P. Yakimov and K.A. Shabalin, it was shown that the ribosides NR and NAR can be generated in human cells. They have demonstrated that purified recombinant human cytosolic 5'-nucleotidases (5'-NTs) CN-II and CN-III, but not CN-IA, can dephosphorylate the mononucleotides nicotinamide mononucleotide and nicotinic acid mononucleotide (NAMN) and thus catalyze NR and NAR formation *in vitro*. Moreover, they found that untransfected HeLa cells produce and release sufficient amounts of NAR and NR under normal culture conditions. Collectively, the results indicate that cytosolic 5'-NTs participate in the conversion of NAD precursors and establish NR and NAR as integral constituents of human NAD metabolism.

Laboratory of Cell Biology studies molecular and cellular mechanisms of cancerogenesis on primary tissue cultures derived from tumors, particularly, on glioblastomas. Works of A.V. Volnitsky *et al.* have demonstrated aberrant expression of stemness genes (Oct4, Sal2, Tet1,2,3) at primary human glioblastomas. In collaboration with the Proteomics Laboratory, proteome profiling of glioblastoma was carried out resulting in development of barcode and proteome profiling of glioblastoma. Lately, exosomal transport of regulatory molecules, such as siRNA and proteins has been extensively studied. Dr. Shtam *et al.* has demonstrated that exosomes are natural carriers of exogenous siRNA to human cells *in vitro*.

Closely related work of Dr. V.A. Ryzhov aims to employ superparamagnetic nanoparticles (NPs) on the basis of iron oxides (SPIONs) with sewn to them Hsp70-specific antibodies (cmHsp70.1) to target tumor cells. The stress-inducible 72 kDa heat shock protein Hsp70 is known to be expressed on the membrane of highly aggressive tumor cells including high-grade gliomas, but not on the corresponding normal cells. Membrane Hsp70 (mHsp70) is rapidly internalized into tumor cells and thus targeting of mHsp70 might provide a promising strategy for thermostatics. Superparamagnetic iron oxide nanoparticles (SPIONs) are contrast negative agents that are used for the detection of tumors with MRI. Herein, Ryzhov *et al.* conjugated the Hsp70-specific antibody (cmHsp70.1), which is known to recognize mHsp70 to SPIONs to assess tumor-specific targeting before and after ionizing irradiation. *In vitro* experiments demonstrated the selectivity of SPION–cmHsp70.1 conjugates to free and mHsp70 in different tumor cell types (C6 glioblastoma, K562 leukemia, HeLa cervix carcinoma) in a dose-dependent manner. The approach has the potential to be clinically applied for Hsp70-targeted anti-tumor diagnostic and/or therapeutic approaches.

Overall, MRBD scientists have published more than 60 papers in peer-reviewed journals during 2015, including top-rated: Nature (IF = 41.5), PNAS (IF = 9.7), J. Biol. Chem. (IF = 4.6), Retrovirology (IF = 4.2), J. Comput. Chem. (IF = 3.6) and more than 40 publications at international conferences. Three theses (Candidate of Sciences) defended.

Knowledge Transfer Division

Knowledge Transfer Division (KTD) headed by Dr. Victor F. Ezhov, consists of three laboratories:

– Holographic Information and Measuring Systems Laboratory (HIMSLab) (headed by Dr. Boris G. Turukhano)**;**
– Radiative Physics Laboratory (headed by Dr. Nikolay A. Ivanov)**;**
– Quantum Chemistry Laboratory (headed by Dr. Anatoly V. Titov)
and two departments:
– Accelerator Department (headed by Dr. Evgeny M. Ivanov)**, which includes Accelerator Physics and Technology Laboratory** (headed by Dr. Stanislav A. Artamonov)**;**
– Information Technologies and Automation Department (headed by Dr. Sergey B. Oleshko)**,**
which includes Laboratory of Informational and Computing Systems (headed by Dr. Yuri F. Ryabov)**.**

KTD employs 35 research staff members (4 Doctors of Sciences and 18 Candidates of Sciences).

Dr. Victor F. Ezhov
Head of KTD

The main accelerative facilities of the Institute are concentrated in this Division. First of all, it is the 1 GeV synchrocyclotron. It provides a widespread research program in nuclear and applied physics as well as in a medical proton therapy and production of radio pharmacology for medical purposes.

After the long-term improvement program the accelerator and experimental area are represented by a unique installation. Briefly, the main features of 1 GeV synchrocyclotron facility can be formulated as follows:

– 30% efficiency non-linear regenerative extraction system has been developed with the record efficiency for synchrocyclotrons with an open ion source central geometry.

– The original system for a long burst operation of synchrocyclotron beam has been developed. It allows the increase of the coefficient of beam temporary filling from 2 to 85%.

Proton beams of variable energy are necessary for some physical and applied experiments. For these purposes, the possibility to change the beam energy from 60 to 1 000 MeV was created. The beam diameter is about 30–80 mm, $\Delta p/p$ is about 1.3–14% and the intensity is in the range $10^7 \div 10^{12}$ s^{-1}.

There is the second proton beam with small intensity (about 1%) that acts in parallel with the main beam. It can be used both for physical and applied purposes. For instance, using this beam for proton therapy will essentially decrease the cost of medical radiation exposure.

There are some secondary beams of $\pi^{\pm}$ and $\mu^{\pm}$ mesons for scientific research. Meson beams are formed at an outer target. An additional point to emphasize is that higher energy of a proton beam in comparison with meson factories provides an opportunity for the research production of *K*-mesons and *h*-mesons, as well as investigations on higher energy of pion beams, not accessible on meson factories.

There is the neutron spallation source (GNEIS) inside the accelerator vacuum chamber. The target is made of lead and the neutron energy varies from 10^{-2} eV to 200 MeV.

The progress of space and aviation technique is connected with the use of micro- and nano-electronics. One of the main conditions of their reliable work is their ability to operate effectively in the radiation field of space and higher layer of atmosphere. At present, the standards of Russia as well as the international ones include the obligatory tests of radiation

resistance for electronic equipment used in space and aviation. In 2015 at the PNPI NRC KI synchrocyclotron the special center for tests of proton radiation resistance started its work. The energy of used protons is variable in the range 60–1 000 MeV. The center includes two stands with the beam diagnosis, dosimetry, system of automatic data treatment and infrastructure for users.

Now according to the standards and regulations of the leading countries, the electronic equipment used in space and aviation is required to be tested in neutron fields too. An international document titled "JEDEC STANDARD" orders to test this equipment using neutrons, whose energetic spectrum is equal to the atmospheric one. In 2015, the stand for such tests was created at the neutron source GNEIS by a collaboration of the group of nuclear fission from Neutron Research Division and Accelerator Department from Knowledge Transfer Division. As a result, the universal center for radiation resistance tests is in operation in PNPI NRC KI since 2015. It allows the performance of tests both by using protons and by using neutrons, whose energetic spectrum is equal to the atmospheric one.

Now the Accelerator Department in collaboration with D.E. Efremov Institute of Electro Physical Apparatus are preparing the commissioning of isochronous cyclotron Ts-80. Its proton beam will have the energy in the range 40–80 MeV and the current up to 150 μA. High energy and high intensity of proton beam allows the production of such isotopes and radiopharmaceuticals that cannot be produced at commercial cyclotrons (for example generators isotopes). The use of generators isotopes enables us to conduct positron emission tomography at the medical centers located in remote areas. Besides, a new method of producing super clean isotopes with the help of magnetic separator is in progress at the new cyclotron.

The energetic range of proton beam (60–70 MeV) at the cyclotron Ts-80 allows the creation of an ophthalmology center for radiation therapy of eye cancer disease. At present, there are no such centers in Russia. This project is developed in Accelerator Department and recently in Laboratory of Radiation Physics. In 2015, the radiation background in irradiation zone for different variants of proton beam formation was simulated. It was shown that the radiation background is to three times less if one uses collimators instead of the traditional method. Moreover, the use of collimator allows the simplification of a system of beam formation and the decrease in the quantity of magnetic elements. The equipment for ophthalmology room and the software for radiation exposure planning will be created in collaboration with Institute for Theoretical and Experimental Physics (ITEP NRC KI). It has extensive experience in eye proton therapy since about 1 400 patients were treated with the help of this technique.

The Laboratory of Holographic Information and Measuring Systems (HIMSLab) is one of the world leaders in the field of precision measuring in the range of nanometers. In HIMSLab there is a unique holographic underground vibration-freee laboratory for such type of research. On the base of this laboratory and unique stands for linear and radial holographic diffraction grating HIMSLab produces 14 different nanotechnological devices. They include photoelectric converters of linear and angle moving, long-length, coordinate-measuring machines, etc. Their resolution is equal to 10 nm and hundredths of seconds. In 2015 for the first time in the world the holographic diffraction grating with the length 1 300 mm and the resolution of 1 nm was created. These devices were awarded at the exhibition "Army 2015".

Information Technologies and Automation Department (ITAD) provides support and development of the local computer network of the Institute, including the computing cluster and PNPI NRC KI site of Worldwide LHC computing Grid (WLCG) network. One of the main activity in 2015 was the participation in the creation of the data center for PIK reactor that will be commissioned in 2017. The Laboratory of Informational and Computing Systems (as a part of ITAD) is actively working in the CERN projects such as ATLAS (DAQ and DCS) and WLCG. Its main activities in WLCG are connected with the software development for WLCG storage data systems (GridFTP, DPM, SRM) that allows the increase of the data transfer efficiency on GRID sites. The experience in advanced technologies of distributed computing and data processing will be useful in the exploitation of the data center of PIK reactor.

The discovery of subglacial lake Vostok in Antarctica became the last geographic discovery of XX century. Its exploration will allow the provision of the unique data about the origin and evolution of different

forms of life in ecosystems that are characterized by high power of oligotrophic (i. e. the lowest concentration of nutrients) and extreme conditions. These are very high oxygen concentration in water (it exceeds usual concentration to 50–100 times), high pressure (about 350 bars) and inability to use the sun energy by the ecosystem due to extremely high thickness of ice layer. PNPI NRC KI is the head organization in the research investigation of Vostok lake water. The scientists of Knowledge Transfer Division, Molecular and Radiation Biophysics Division and Neutron Research Division take part in this research. It is a complicated technical task. It is necessary to develop ecologically clean technology of penetration into water environment that will exclude the possibility of polluting the lake with the bore liquid. This task requires the development of unique devices for the registration of hydro physical, hydro chemical and microbiological parameters working online. In addition, the technology of sterile sampling of water and sediments for their further laboratory analysis is required.

Now part of this equipment was made in PNPI NRC KI. In 2015 it was tested in deep-water places of Ladoga lake. The tests were successful.

The main direction of Quantum Chemistry Laboratory activity is the development of electronic structure calculation methods for molecules containing heavy elements. This activity was initiated in 1980's by the experimental study of the *P*- and *CP*-odd effects in heavy diatomic molecules. The base of calculations became a two-step method that enabled the division of computation of such molecules to two consequent computations in valence and core regions. The presently achieved accuracy of these computations is the best in the world. In addition to the computation of the *P*- and *CP*-odd effects, the investigation of the structure of more complicated molecules is in progress. In 2015 the systematic investigation of properties of super heavy elements in solid systems was developed. It allowed the computation of the chemical properties of elements from "the island of stability" that were synthesized in Dubna and Darmstadt.

In 2015 KTD staff published 24 papers (more than 100 in collaboration with ATLAS scientists) in reviewed journals, presented 27 papers at the Russian and international scientific conferences and workshops, received four patents and defended one thesis (Candidate of Sciences).

Theoretical and Mathematical Physics

LHCb: pentaquarks as charmonium-proton bound states

M.I. Eides, V.Yu. Petrov, M.V. Polyakov
Theoretical Physics Division, PNPI NRC "Kurchatov Institute"

We interpret the newly discovered by LHCb pentaquark $P_c(4450)$ as a bound state of charmonium $\psi(2S)$ and the nucleon (Fig. 1). Heavy quarkonium is a small neutral object, which can easily penetrate the nucleon and form a true pentaquark. In the dipole approximation interaction of the charmonium and the nucleon is dominated by emission of two chromoelectric gluons in a color singlet state. The effective interaction potential is proportional to the product of chromoelectric polarizibility and the local gluon energy momentum density inside the nucleon. Chromoelectric polarizibility can be reliably calculated in the heavy quark limit when the quarkonium can be considered as a Coulomb system. It grows as the cube of the quarkonium size and therefore it is much larger for excited state. For charmonium $\psi(2S)$ attraction with proton is of order of few hundreds MeV (Fig. 2). The dependence on x is determined by distribution of gluon energy inside the proton. It can be calculated in the limit of large number of colors, in the mean field approximation.

Potential has a level with quantum numbers $3/2^-$ which can be identified with pentaquark $P_c(4450)$. The width of the state is around 12 MeV which is due to the decay to $J/\psi + p$. The second pentaquark can be interpreted as a bound state of $\chi_{c2}(3556)$ which is $1P$ state of charmonium and proton. The observed width of this pentaquark can be explained by few unresolved resonances located close to each other.

Observed pentaquarks should have partners with different spins and masses different only by superfine splittings. The value of splitting is estimated to be 10–15 MeV. Also they are members of SU(3)-multiplets (octets). The masses of other pentaquarks in the multiplet can be easily predicted.

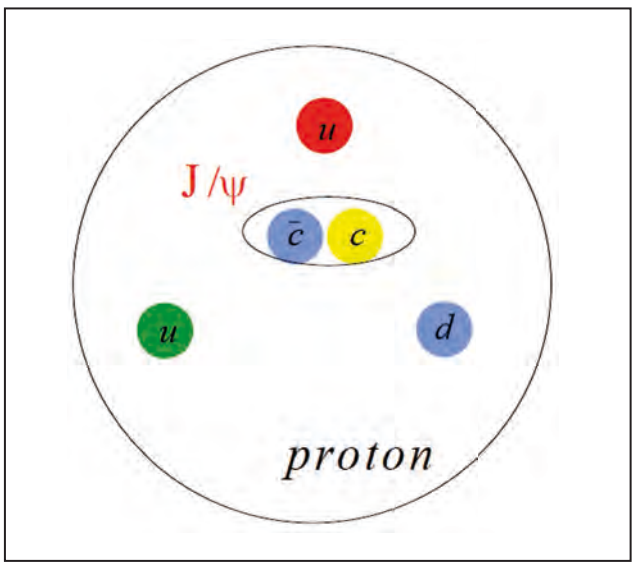

Fig. 1. Suggested structure of pentaquark

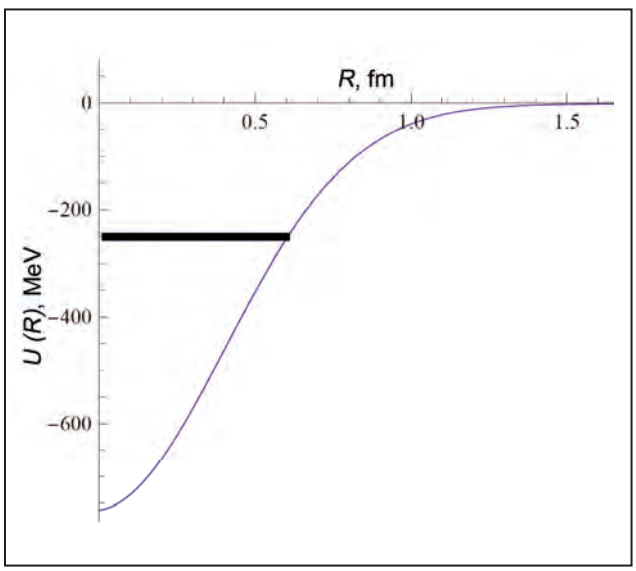

Fig. 2. Interaction potential $U(R)$ (MeV) between proton and charmonium as a function of distance (fm)

Eides M., Petrov V., Polyakov M. hep-ph: 1512.00426. Submitted to Phys. Rev. Lett.

Resonance model for non-perturbative inputs to gluon distributions in the hadrons

S.I. Troyan – Theoretical Physics Division, PNPI NRC "Kurchatov Institute"
B.I. Ermolaev – Ioffe Institute
F. Olness – Southern Methodist University

The description of hadronic reactions at high energies requires the use of Quantum Chromodynamics (QCD) in both the perturbative and non-perturbative domains. Such calculations are challenging because the non-perturbative characteristics of QCD are difficult if possible to quantify. The standard approach is to use the QCD factorization to divide the problem into perturbative and non-perturbative components, and then to use the properties of the perturbative expressions to infer basic features of the non-perturbative part.

Previously the non-perturbative inputs shown as block *T* in Fig. 1, for elastic quark-hadron scattering amplitudes in the forward kinematic region (i. e. with the zero scattering angle) for both polarized and non-polarized hadrons have been studied. The optical theorem allowed one to relate the invariant amplitudes to the quark distributions in hadrons.

In current work such an approach was extended to the case of study of the gluon components (Fig. 2). The conventional approach is purely phenomenological and constructs such inputs by matching with the experimental data. Knowledge of structure of the IR and UV divergences of the perturbative part of the amplitudes was used to obtain restrictions for the non-perturbative inputs, from the requirement of convergence of the integral for factorization convolution. In this work the resonance model for the energy dependence of the amplitudes was suggested, and validity of using the resonance factors for the both within and outside the resonance region was assessed. Succesively, starting with the basic factorization of the amplitudes, the restrictions for non-perturbative inputs were derived, that are necessary for the K_T and Collinear Factorizations.

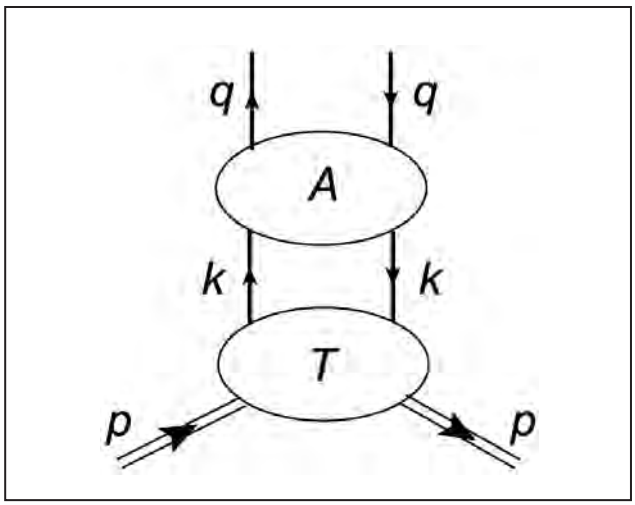

Fig. 1. Factorization of quark *q* on hadron *p* elastic scattering amplitude to perturbative *A* and non-perturbative *T* components through intermediate quark state *k*

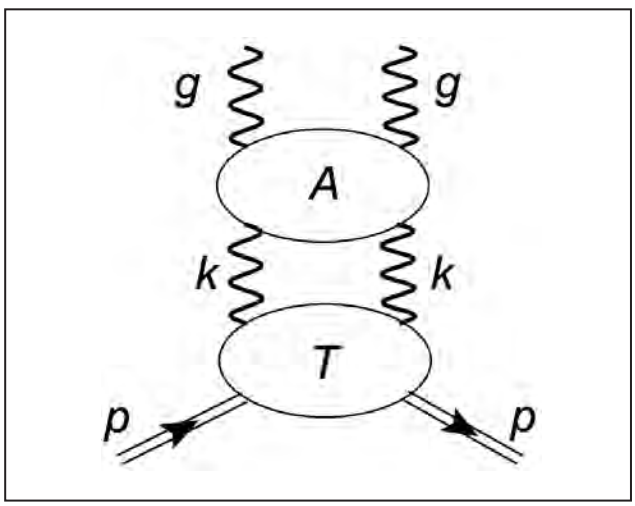

Fig. 2. Factorization of gluon *g* on hadron *p* elastic scattering amplitude to perturbative *A* and non-perturbative *T* components through intermediate gluon state *k*

1. *Ermolaev B.I., Greco M., Troyan S.I.* Eur. Phys. J. C. 2015. V. 75. P. 306.
2. *Ermolaev B.I., Olness F., Troyan S.I.* arXiv:1512.07861 [hep-ph], 2015.

Euler–Lagrange equations for effective actions in the high energy QCD and gravity

L.N. Lipatov
Theoretical Physics Division, PNPI NRC "Kurchatov Institute"

Remarkable properties of the equations of Balitsky, Fadin, Kuraev and Lipatov (BFKL) for wave functions of pomeron, odderon and other composite states of reggeized gluons in the color singlet and adjoint representations are related to their gauge-invariant formulation in terms of effective vertices and the gluon Regge trajectory. These quantities can be calculated from the Feynman diagrams for the effective action, containing apart from the usual gluon and quark fields also degrees of freedom describing the production and annihilation of the reggeized gluons. The gauge invariant Euler – Lagrange equation for effective QCD gives a possibility to calculate vertices for reggeized gluon interactions. Due to the AdS/CFT-correspondence especially simple results are obtained in the $N = 4$ supersymmetric gauge theory, where the BFKL pomeron is dual to the reggeized graviton. Thus, we consider the effective action for the high energy processes in gravity. Apart from the metric tensor it contains the fields describing the production and annihilation of reggeized gravitons. The Euler–Lagrange equation for this action is generally covariant and allows one to find the reggeized graviton interactions.

High energy effective action in quantum chromodynamics

The effective action S_{eff} for high energy processes in QCD is valid for a cluster of quarks and gluons interacting with reggeized gluons and having their rapidities y in a small interval. Apart from the gluon field v_μ being an antihermitian matrix for the group SU(N_c) we introduce also the fields $A^\pm$ describing the production and annihilation of reggeized gluons. These fields are invariant under gauge transformations with parameters $\chi(x)$ vanishing at $x \to \infty$ and satisfy the kinematical constraints $\partial_\pm A^\pm = 0$. The induced term in S_{eff} has the form

$$S_{ind} = Tr \int d^4x (V_+ \partial_\mu^2 A^+ + V_- \partial_\mu^2 A^-).$$

The currents $V_\pm = V_0 + V_3$ can be expanded in the perturbation theory series

$$V_\pm = -\frac{\partial_\pm}{g} U(x^\pm),\ U(x^\pm) = \frac{1}{D_\pm}\partial_\pm =$$
$$= 1 - \frac{g}{\partial_\pm} v_\pm + \frac{g}{\partial_\pm} v_\pm \frac{g}{\partial_\pm} v_\pm + \ldots.$$

The matrices $U(x^\pm)$ are solutions of the equation $D_\pm U(x^\pm) = 0$. In a framework of the principal value prescription for corresponding singular integrals they can be presented in terms of ratios of the Wilson P-exponents:

$$U(x^\pm) = P \frac{e^{-\frac{g}{4}\int_{-\infty}^{x^\pm} dx'^\pm v_\pm}}{e^{-\frac{g}{4}\int_{x^\pm}^{\infty} dx'^\pm v_\pm}} \equiv$$
$$\equiv \frac{e^{-\frac{g}{4} v_\pm (x^\pm) dx^\pm}}{e^{-\frac{g}{4} v_\pm (x^\pm) dx^\pm}} \frac{e^{-\frac{g}{4} v_\pm (x^\pm - dx^\pm) dx^\pm}}{e^{-\frac{g}{4} v_\pm (x^\pm + dx^\pm) dx^\pm}} \frac{e^{-\frac{g}{4} v_\pm (x^\pm - 2dx^\pm) dx^\pm}}{e^{-\frac{g}{4} v_\pm (x^\pm + 2dx^\pm) dx^\pm}} \ldots.$$

In the pure glue-dynamics the corresponding Euler–Lagrange equations takes the form

$$[D_\mu, G^{\mu\nu}]^\perp = 0,\ [D_\mu, G^{\mu\nu\pm}] = j^\pm_{ind},$$
$$j^\pm_{ind} = U(x^\pm)(\partial_\sigma^2 A^\pm) U^\pm(x^\pm).$$

In particular at the quasielastic kinematics, where $A^\pm = 0$, their solutions $V_\pm$ coincide with $A^\mp$.

High energy effective action in gravity

According to the Maldacena hypothesis the $N = 4$ supersymmetric gauge theory is equivalent to the ten-dimensional super-string model living in the anti-de-Sitter space. Here the BFKL pomeron is dual to the reggeized graviton, and the effective Gribov model for Pomerons is equivalent to the theory of self-interacting reggeized gravitons. The generally covariant effective action in the high energy gravity is formulated for a cluster of gravitons and reggeized gravitons having their rapidities in a small interval. Apart from the well known Einstein–Hilbert term this action contains the induced contribution

$$S_{ind} = -\frac{1}{2\kappa^2}\int d^4x\left(\frac{j_{++}}{2}\partial_\sigma^2 A^{++} + \frac{j_{--}}{2}\partial_\sigma^2 A^{--}\right),$$

where $A^{\pm\pm}$ (with $\partial_\pm A^{\pm\pm} = 0$) describe the production and annihilation of reggeized gravitons. The general covariance fixes the dependence of $j_{\pm\pm}$ from the metric tensor $g_{\mu\nu}$. Thi current is expressed in terms of the function $\omega^\mp$ satisfying the Hamilton–Jacobi equation:

$$j_{\pm\pm} = \partial_\pm \omega^\mp,\ g^{\rho\sigma}(\partial_\rho\omega^\mp)(\partial_\sigma\omega^\mp) = 0.$$

Its solution $\omega^\mp/2 = x^\mp - x^\mp(x^\pm, x^\perp)$ describes a light-front configuration being a plane wave at large negative or positive t. It can be considered as a coordinate transformation $x'(x)$ to the system with the global light-cone time corresponding to the metric constraint $g'^{\mp\mp} = 0$.

The Euler–Lagrange equation for the effective action in gravity has the form

$$R_{\mu\nu} - \frac{1}{2}g_{\mu\nu}R = -\theta_{\mu\nu},$$

$$\theta_{\mu\nu} = \partial_\mu x'^- \partial_\nu x'^- \partial_\sigma^2 A^{++}(x') + \partial_\mu x''^+ \partial_\nu x''^+ \partial_\sigma^2 A^{--}(x''),$$

where $x'(x)$ and $x''(x)$ are coordinate transformations to the systems with the corresponding metric constraints $g^{\mp\mp} = 0$. Solutions of this equation for $g^{\mu\nu}$ in the quasielastic kinematics, where $A^{++} = 0$, are expressed in terms of general coordinate transformations of the field A^{--}.

Using the Euler–Lagrange equations one can construct the effective vertices for interactions of an arbitrary number of reggeized gravitons in the tree approximation.

In the case of non-trivial initial and final boundary conditions there are classical solutions of these equations allowing to find effective vertices for the graviton emission in the multi-Regge kinematics of produced particles in the high energy collisions.

Lipatov L.N. // Int. J. Mod. Phys. Conf. Ser. 2015. V. 39 P. 1560082.

Heavy meson production at the Large Hadron Collider

V.A. Khoze, M.G. Ryskin, A.G. Shuvaev
Theoretical Physics Division, PNPI NRC "Kurchatov Institute"

The cross section of two J/ψ-mesons exclusive production in the process $pp \to p + J/\psi + J/\psi + p$ was calculated. It was shown that the contribution of single gluon-gluon fusion into the two J/ψ exceeds the contribution of the production via the double parton scattering channel.

In comparison with the naive estimate the cross section is suppressed by the $J_z = 0$ selection rule, which is typical for the exclusive reactions. The value of cross section and the distribution over the mass of J/ψ pair (Fig. 1) agree with the LHCb data.

Due to the Landau–Yang theorem it is impossible to create the $\chi(1^+)$-meson in the collision of two identical on-mass-shell gluons. Thus at the leading order perturbative theory the expected cross section is zero. On the other hand the experimentally observed ratio $\sigma[\chi(1^+)]/\sigma[\chi(2^+)]$ turns out to be close to 1, in spite of the fact that the $\chi(2^+)$-meson can be produced in gluon-gluon fusion already at the Leading Order (LO).

We considered the formation of $\chi(1^+)$-meson in the fusion of three gluons, $g + (gg) \to \chi(1^+)$ (Fig. 2). It was shown that thanks to the large gluon density, which we deal with at the Large Hadron Collider energies, the cross section of this process becomes comparable with that of the $\chi(2^+)$ production via the LO two gluons fusion.

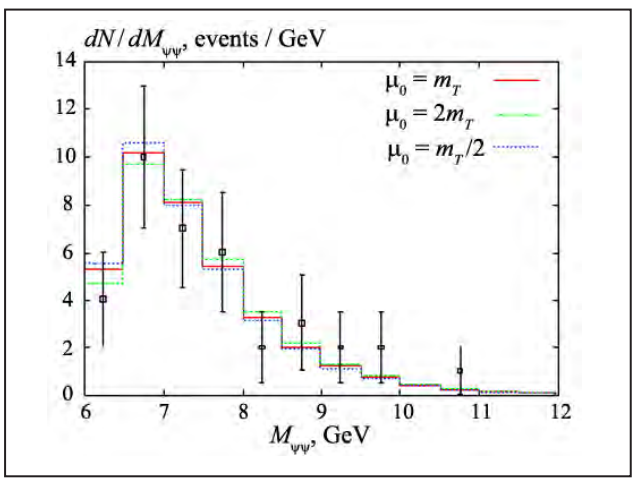

Fig. 1. Distribution over the mass of J/ψ pair produced in $pp \to p + J/\psi + J/\psi + p$ exclusive process

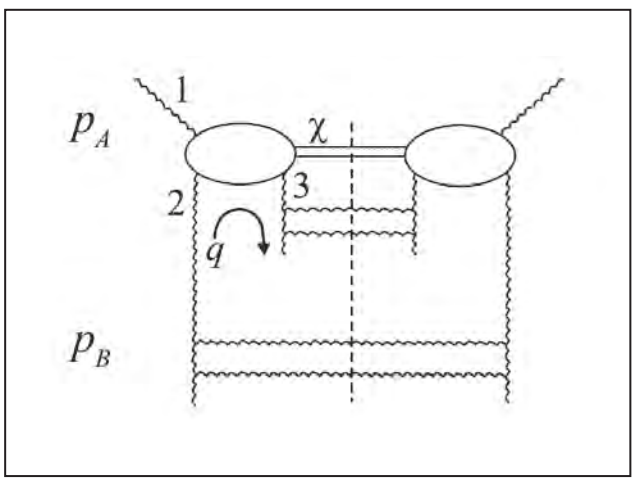

Fig. 2. Diagram for inclusive $\chi(1^+)$-meson via three gluons fusion

1. *Harland-Lang L.A., Khoze V.A., Ryskin M.G.* // J. Phys. G: Nucl. Part. Phys. 2015. V. 42. P. 055001.
2. *Ryskin M.G., Khoze V.A., Shuvaev A.G. et al.* // Eur. Phys. J. C. 2015. V. 75. P. 616.

Standard model phenomenology in the spontaneously-broken mirror symmetry

I.T. Dyatlov
Theoretical Physics Division, PNPI NRC "Kurchatov Institute"

Since the discovery by Lee and Yang (1956), attempts to understand parity non-conservation, its paradoxes, have been based on the hypothesis of mirror symmetry (MS). In MS, observed states are supplemented by particles identical to normal in all respects except their weak interactions, where the left currents change to the right ones. Mirror states are nowhere to be seen, which would make one expect them to be very heavy.

Our investigations reveal that MS can also be the hypothetical reason for some observed but unexplained qualitative phenomena of the Standard Model (SM):

– the hierarchy of elements of the quark mixing matrix (the CKM-matrix);

– the tiny value of neutrino masses (in MS one has some evolution of the well-known see-saw mechanism);

– the alternative (to CKM) structure of the weak mixing matrix for leptons;

– in the MS-scheme the observed lepton properties are indicative of the Dirac nature and inverted mass spectrum of neutrinos.

All these features appear only in systems with really very heavy mirror fermions. Their masses have to be much larger than SM ones.

The spontaneous MS breaking by means of additional scalars can be modeled to be completely similar to the SM weak symmetry violation. The necessity of two isospinor scalars is the main MS difference from SM. The first one may be attributed as the usual Higgs boson, the second would represent four states with different charges and unknown masses (similar to *K*-bosons). Such a system, qualitatively reproducing the observed SM phenomenology, also reveals the following essential general property. Non-conservations of the space-parity *P* and the charge-conjugation *C* appear here with the MS-breaking alone. However, *CP*-violation requires non-conservation of MS-symmetrical models to the time-inversion *T* and, simultaneously (according to the *CPT*-theorem), to the *C*-operation again. The *T*-"forward-back" non-invariance must take place in the initial MS-symmetrical Lagrangian before the MS-breaking.

The observed lepton phenomenology also requires that MS-models have weak processes with non-conservation of the total lepton number. Such reactions proceed only with participation of very heavy mirror neutrinos (in spite of their Dirac nature here). These properties create in MS-models suitable conditions for leptogenesis – the mechanism for generating the barion-lepton asymmetry of the Universe.

Quantitative descriptions of many new phenomena are plagued by the inevitable non-perturbative coupling of the usual Higgs-boson *H* with mirror fermions. At the same time the *H*-coupling with SM-particles remains normal, perturbative one.

1. *Dyatlov I.T.* // Yad. Fiz. 2015. V. 78. P. 1015; arXiv: 1509,07280 [hep-ph].
2. *Dyatlov I.T.* // Yad. Fiz. 2015. Sent to publish.

Strings in non-abelian gauge theories in $d = 4$

A.V. Yung
Theoretical Physics Division, PNPI NRC "Kurchatov Institute"

In a class of non-Abelian solitonic vortex strings supported in certain $N = 2$ supersymmetric gauge theories in four-dimensions we find the vortex, which behaves as a critical fundamental superstring. This vortex is supported in four-dimensional $N = 2$ Quantum Chromodynamics with the U(2) gauge group, the Fayet–Iliopoulos term, and four quark flavors. Non-Abelian string in this theory in addition to four translational moduli has another six orientational-size moduli. The world sheet theory for orientational modes is weighted $CP(2,2)$ model. The target space of this theory is a non-compact Calabi-Yau manifold. This world-sheet theory is conformally invariant. Moreover, altogether translational and orientational-size moduli form a ten-dimensional space needed for a superstring to be critical.

Non-Abelian strings are supported in a large class of four-dimensional gauge theories with gauge group U(N) and N_f quark flavors. We consider effective two dimensional world-sheet theories for non-Abelian strings assuming compactification on a cylinder with a finite circumference L and periodic boundary conditions. The dynamics of the orientational modes is described by two-dimensional $CP(N-1)$ model. We solve in the large N approximation both non-supersymmetric (bosonic) model and $N = (2,2)$ supersymmetric $CP(N-1)$ emerging in the case of 1/2-BPS saturated strings in $N = 2$ supersymmetric QCD with $N_f = N$.

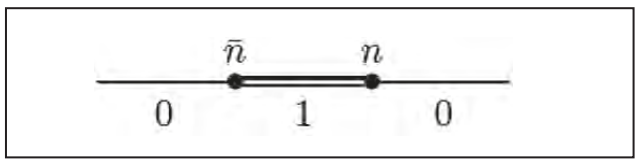

Confinement of kinks on a string

In the large-N limit we detect a phase transition. At large L the $CP(N-1)$ model develops a mass gap and is in the Coulomb/confinement phase, with exponentially suppressed finite-L effects. Confinement is interpreted as splitting between N quasivacua of $CP(N-1)$ model.

Two-dimensional kinks (they are seen as monopoles of the four-dimensional theory) which interpolate between the true vacuum and the first quasivacuum are connected by the string with a larger tension (Fig.).

At small L (high temperature) the theory is in the deconfinement phase, and the orientational modes contribute to the Lusher term. The latter becomes dependent on the rank of the bulk gauge group.

In the supersymmetric $CP(N-1)$ models at finite L the large-N solution gives a single phase independently of the value of L. The model has N degenerate vacua breaking discrete Z_N symmetry. For any value of this parameter a mass gap develops, which turns out to be independent of the string length due to holomorphy.

1. *Shifman M., Yung A.* // Phys. Lett. B. 2015. V. 750. P. 416–419: arXiv:1502.00683 [hep-th].
2. *Monin S., Shifman M., Yung A.* // Phys. Rev. D: Part. Fields. 2015. V. 92. No. 2. P. 025011: arXiv:1505.07797 [hep-th].

Double ionization of heliumlike ions by scattering of high-energy photons

A.I. Mikhailov, A.V. Nefiodov
Theoretical Physics Division, PNPI NRC "Kurchatov Institute"

The double ionization of inner-shell electrons by a single photon has been intensively investigated during recent decades. Since the incident photon interacts with each electron separately, the simultaneous ejection of two bound electrons is caused exclusively by the inter-electron interaction. The helium atom and heliumlike ions are the simplest atomic systems, where the double ionization can occur. Consideration of such targets allows one to test the quality of description of the electron-electron correlations within the framework of different theoretical approaches.

In the work we employed non-relativistic perturbation theory with respect to the electron-electron interaction. In the problem, there are two parameters, which are assumed to be small, namely, $1/Z << 1$ and $\alpha Z << 1$, where Z is the nuclear charge number and α is the fine-structure constant. As the zeroth approximation, the complete set of the Coulomb wave functions is used. The Coulomb Green's function is represented in the closed form without the partial-wave expansion. The characteristic momentum of K-shell electron and its binding energy in the Coulomb field of nucleus are given by $\eta = m\alpha Z$ and $I = \eta^2/(2m)$, respectively, where m is the electron mass ($\hbar = 1$, $c = 1$).

The atomic ionization can proceed due to both the absorption and the scattering of photons. As long as the photon energy ω is not too high ($\omega \le \eta$), the photoabsorption dominates over the Compton scattering. However, if $\omega \ge \eta$, the Compton effect becomes the dominant process. In the asymptotic energy domain characterized by the condition $I << \omega << m$, the main contribution into the cross section of the process appears from the diagram depicted in Figure, which takes into account the inter-electron interaction in the initial state. The calculation was performed analytically to the first order of perturbation theory with respect to the inter-electron interaction. For two-electron targets being in the ground state, the ratio of cross sections for double-to-single ionization by Compton scattering has the universal scaling form:

$$R_c = \sigma^{++}/\sigma^{+} = 0{,}050Z^{-2}.$$

This formula is in good agreement with the previous calculations, in particular, for helium atom ($Z = 2$). Since $1/Z$ is the formal parameter of expansion, the higher Z is, the more accurate the formula is.

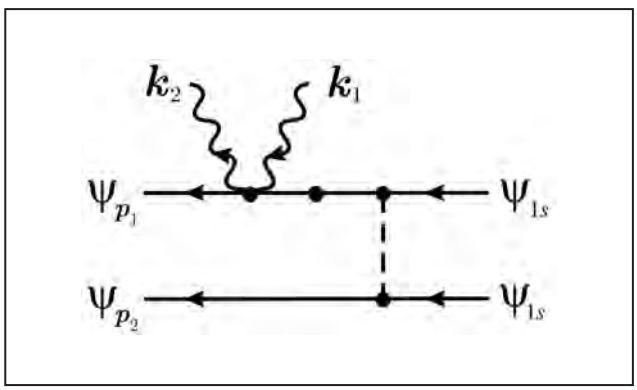

Feynman diagram, which describes the Compton ionization of K-shell

Mikhailov A.I., Nefiodov A.V. // Phys. Rev. A. 2015. V. 91. P. 013410.

Spiral magnets with Dzyaloshinskii–Moriya interaction containing defect bonds

A.V. Sizanov, A.V. Syromyatnikov, O.I. Utesov
Theoretical Physics Division, PNPI NRC "Kurchatov Institute"

In crystals without inversion center, Dzyaloshinskii–Moriya interaction (DMI) is caused by an antisymmetric spin-orbit interaction. The competition of the symmetric ferromagnetic (FM) or antiferromagnetic (AF) exchange interaction and DMI can result in a long period spiral magnetic structure.

Recently mixed B20 spiral compounds have been considered extensively. It was shown that the modulus of the spiral vector $\mathbf{q}$ in $Mn_{1-x}Fe_xGe$ depends on dopant concentration x and the magnetic chirality changes its sign (and $\mathbf{q}$ goes through zero) at $x \approx 0.75$. This observation is quite expected because MnGe and FeGe are B20 cubic helimagnets with opposite signs of the spin chirality. Evidently, such a behavior is a consequence of the fact that the exchange interaction and DMI change around dopant ions which can be considered as defects at $x << 1$ or $x \approx 1$. These experimental results are interpreted phenomenologically by renormalization of constants in the Hamiltonian describing the pure translational invariant B20 magnets. Then, a more detailed theoretical description of mixed spiral materials is required.

Motivated by this experimental activity, we address the problem of spiral magnets with DMI subject to bond disorder at small concentration c of defects. We assume that both exchange interaction and DMI are changed on imperfect bonds. Two models are considered in detail: cubic spiral magnets with B20 structure and layered spiral magnets.

We obtain qualitatively the same physical picture in both models. The one-impurity problem is addressed first. We show that the perturbation of the spiral ordering around the defect bond (i. e., values of additional turns of spins due to the defect) is described by the Poisson's equation for electric dipole. Then, the magnetic ordering disturbance made by one impurity is long range: values of additional turns of spins decay with the distance r to the defect as $1/r^2$.

At finite defects concentration $c << 1$, spiral magnets under discussion are equivalent to a dielectric with randomly distributed electric dipoles, which lead to a finite average polarization of a unit volume proportional to c. This electrical polarization corresponds to $\delta\mathbf{q} \propto c$ to the modulus of the spiral vector $\mathbf{q}$.

The analysis of the elastic neutron scattering cross section predicts magnetic Bragg peaks (satellites) on momenta transfer $Q = \pm(\mathbf{q} + \delta\mathbf{q}) + \tau$, where τ is a reciprocal lattice vector. Besides, we obtain a diffuse scattering with power-law singularities at positions of magnetic Bragg peaks, as it is shown in the Figure. We calculate also magnon spectrum renormalization due to the scattering on defects in the first order in c.

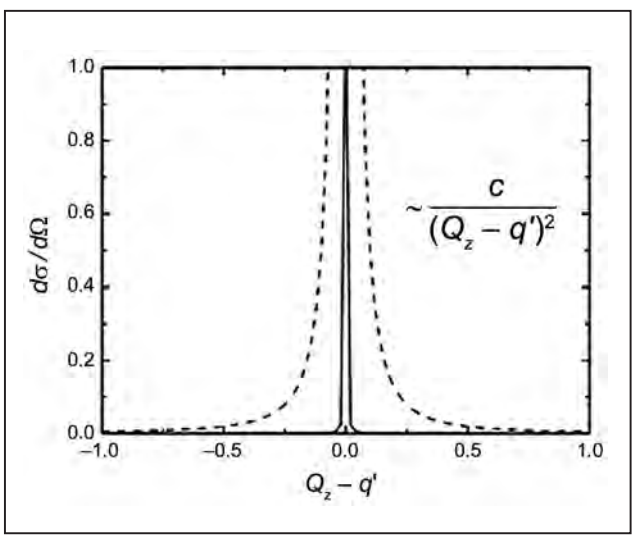

Diffuse scattering with power-law singularities at positions of magnetic Bragg peaks

Utesov O.I., Sizanov A.V., Syromyatnikov A.V. // Phys. Rev. B.: Condens. Matter. 2015. V. 92. P. 125110.

Magnons in ferromagnets with a skyrmion

D.N. Aristov, A.O. Sorokin
Theoretical Physics Division, PNPI NRC "Kurchatov Institute"

We considered the spin-wave excitations (magnons) in Heisenberg planar ferromagnet, whose ground state is characterized by one static soliton (skyrmion). It is known that the classical energy of such state is higher than of usual uniformly magnetized state, and is metastable in the absence of stabilizing interactions. We performed a semiclassical approach to the problem by considering lattice spin model, using Maleyev–Dyson representation for spin operators and finding equilibrium solution of skyrmionic character. This equilibrium solution is found in continuum limit as extremal configuration of the classical magnetization field, parametrized via Euler's angles. Thus we find a local basis of spins for each lattice site with spin quantization axis along the local magnetization, as shown in the Figure.

Expanding the Hamiltonian by inverse spin value, $1/S$, delivers the classical energy in order S^2 and linear in bosons terms, ~ $S^{3/2}$, are absent. The terms ~ S give the quantum spectrum of the problem. The usual uniform situation corresponds to the magnons in the form of plane waves and the dispersion is $E = Dk^2$. We find that in the presence of a skyrmion the magnons are the solution of Schrodinger equation with central potential at the center of the skyrmion. The spectrum shows no bound states and two non-trivial solution of zero energy. This zero of Goldstone modes arise due to broken symmetries with respect to translation and dilatation of the skyrmion. The third zero mode corresponds to broken conformal symmetry of the action, some analysis shows that in case of uniform solution it also corresponds to usual spontaneously broken symmetry with respect to the direction of total magnetization.

We also find the corrections to the Hamiltonian as the next terms in $1/S$ expansion, which define the interaction of magnons. The preliminary analysis shows that the interaction corrections to the spectrum and renormalization of the vertices are negligible. It shows that the skyrmion remains a stable configuration in the low-temperature limit.

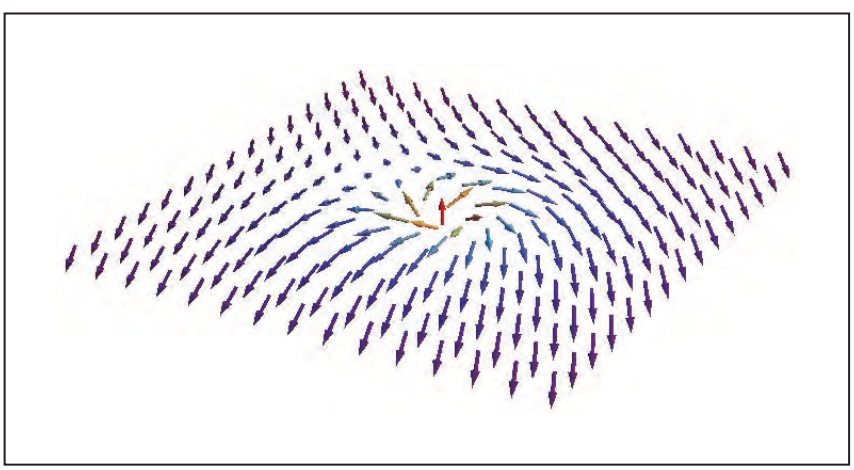

Skyrmion configuration of spins

Aristov D.N., Kravchenko S.S., Sorokin A.O. // JETP Lett. 2015. V. 102. P. 455.

Quantum spin liquid

V.R. Shaginyan
Theoretical Physics Division, PNPI NRC "Kurchatov Institute"

It is shown for the first time, that the herbertsmithite $ZnCu_3(OH)_6Cl_2$ represents a new type of strongly correlated electric insulator possessing properties of metals with heavy fermions with one exception: it does not support charge current. Properties of this insulator are defined by a quantum spin liquid formed as a result of spin-charge separation of an electron. The charge of an electron is localized on atoms of the copper, and its spin gains mobility and forms the quantum spin liquid filling the Fermi-sphere and playing the role of heavy fermion liquid. This liquid which emerges owing to the separation of spin and charge defines properties of the insulators of new type. Calculations of the thermodynamic and the thermal transport properties are in the good agreement with experimental data. For example, the thermal capacity of $ZnCu_3(OH)_6Cl_2$ at low temperatures is proportional to temperature T and corresponds to that of metals with heavy fermions, as it is seen in the Figure. Meanwhile, the thermal capacity of the common insulators is defined by phonons and proportional to T^3.

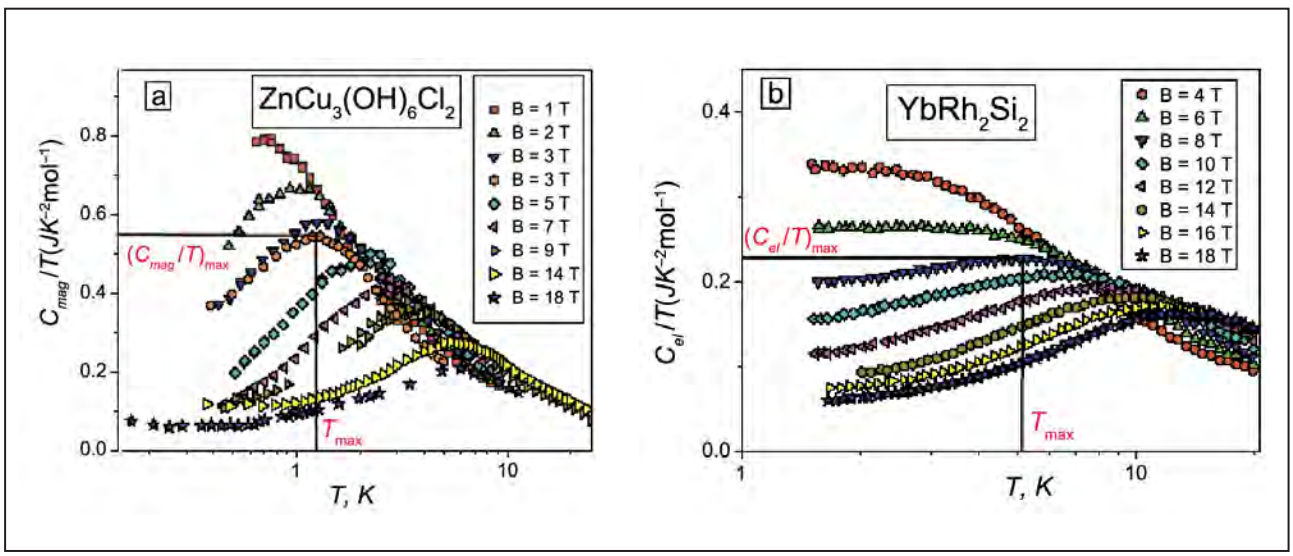

The thermal capacity C/T of the alloys with heavy fermions: the thermal capacity of the insulator (a). The thermal capacity of the conductor with heavy fermions (b). C/T measured as a function of temperature T versus magnetic field B, shown in the legends

Shaginyan V.R. et al. // Phys. Lett. A. 2015. V. 379. P. 2092.

Investigation of the possibility of ^{254}Es isotope production in the PIK reactor

M.S. Onegin
Theoretical Physics Division, PNPI NRC "Kurchatov Institute"

The isotope ^{254}Es in ground state has a half life 256 days and α decay with branching ratio about 100%. Because of its long lifetime this isotope can be used as a target for the production of the new elements with atomic number 119 in the reaction

$$^{254}\text{Es} + ^{48}\text{Ca} \rightarrow ^{302-x}119 + xn.$$

The elements with atomic numbers 114–118 were synthesized for the first time in Dubna in the fusion reaction of ^{48}Ca nucleus with Pu, Am, Cm, Bk and Cf atomic nuclei. According to estimates, the target for production of 119 element using this reaction should contain about 1 mg of Es. We have evaluated the possibility to produce this amount of isotope in the PIK reactor. For production of Es it is convenient to use 100 mg of ^{252}Cf as a target. This target can be irradiated in the Central Experimental Channel (CEC) of the PIK reactor where we have the record neutron flux: total flux – $8.6 \cdot 10^{15}$ cm$^{-2} \cdot$ s^{-1}, thermal flux – $5 \cdot 10^{15}$ cm$^{-2} \cdot$ s^{-1}. The calculations have shown at the same time that it is more profitable to produce this isotope in the core of the PIK reactor. For this purpose the new places for the sample irradiation should be provided in the core as it is done in a similar high flux reactor SM-3 in Dimitrovgrad. The total neutron flux in the core is about $3 \cdot 10^{15}$ cm$^{-2} \cdot$ s^{-1} while the thermal flux is – $2 \cdot 10^{15}$ cm$^{-2} \cdot$ s^{-1}, but the neutron spectrum is harder here and as a result the reaction rates differ considerably. The transmutation chain is shown in the Figure.

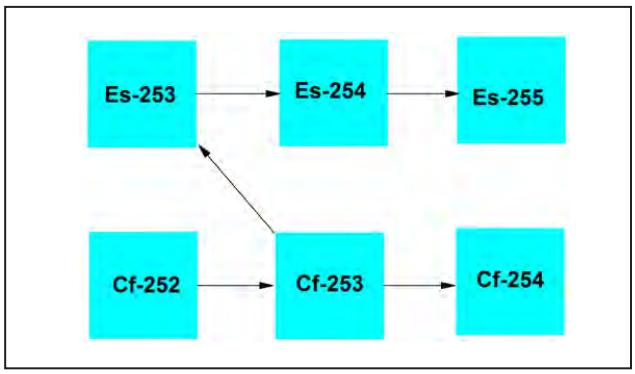

Transmutaition chains of ^{254}Es isotope production

The precious evaluation of the production rate of ^{254}Es isotope is complicated by the fact that the cross sections of some important reactions at this chart are poorly known with errors approaching 60%. There are no experimental data about ^{253}Es(*n*, *f*) reaction at all and we use here the theoretical expectation, which is now known as having a low predictability.

We have made the probability calculations for the produced mass of ^{254}Es isotope in the core and in the CEC. The mean amount of mass produced in the CEC is equal to 2.4 μg and with the probability 95% this mass is smaller than 7.7 μg. At the same time the mean amount of isotope produced in the core is equal to 37 μg and with probability 95% is smaller than 107 μg. It is evident that it is more efficient to produce isotope ^{254}Es in the core than in the CEC of the PIK reactor. The gain however slightly depends on the construction of the target for sample irradiation in the core.

Onegin M.S. // Report on Super Heavy Elements Symposium. Texas, USA, 2015.

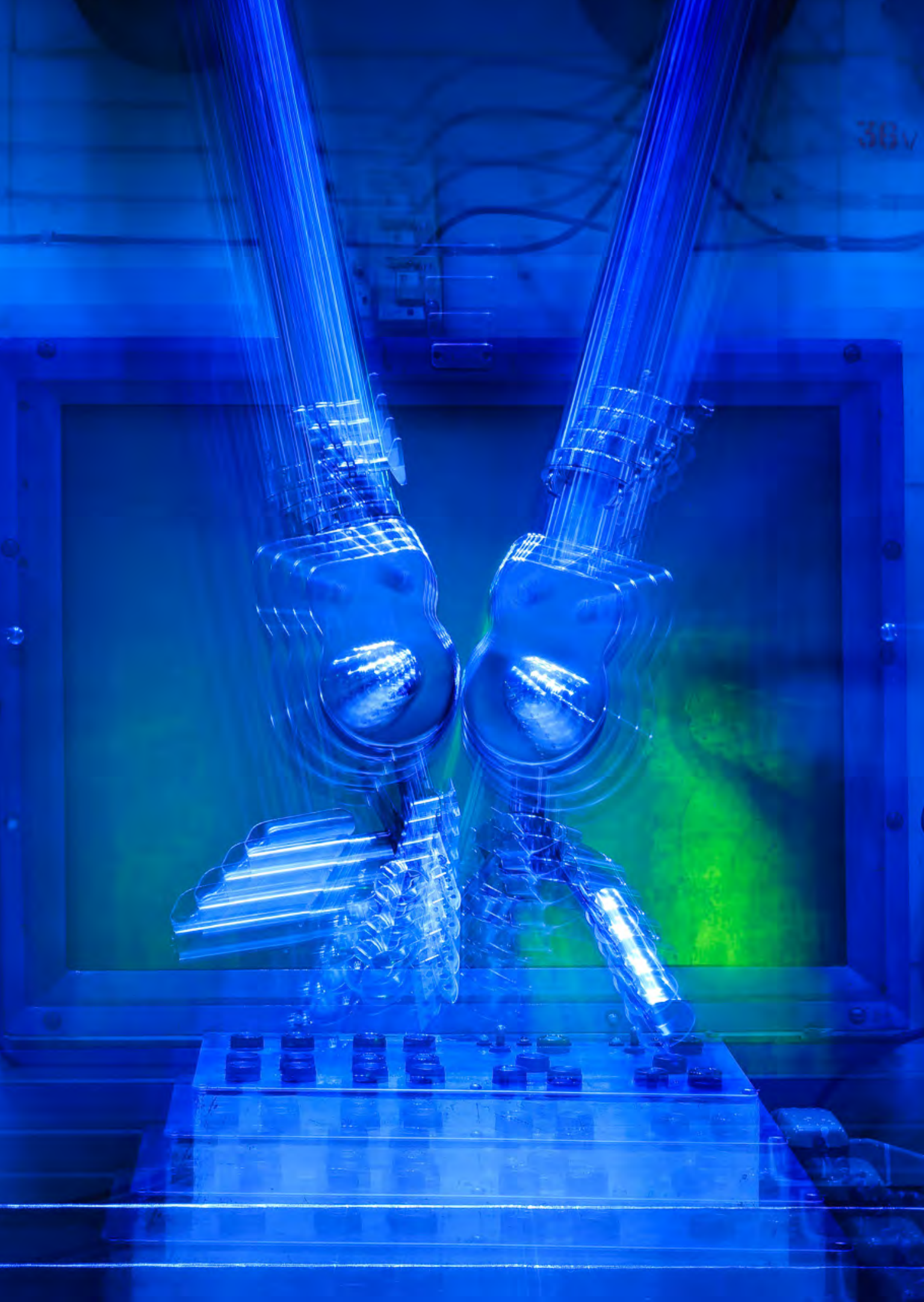

Research Based on the Use of Neutrons, Synchrotron Radiation and Muons

Controlling the Dzyaloshinskii–Moriya interaction to alter the chiral link between structure and magnetism for $Fe_{1-x}Co_xSi$

E.V. Altynbaev, N.M. Chubova, V. Dyadkin, S.V. Grigoriev, E.V. Moskvin – Neutron Research Division, PNPI NRC "Kurchatov Institute"
A. Heinemann, A. Schreyer, S.-A. Siegfried – Helmholtz Zentrum Geesthacht
D. Chernyshov – Swiss-Norwegian Beamlines at the European Synchrotron Radiation Facility
D. Menzel – Institut für Physik der Kondensierten Materie

We exploited the idea to get full control of the Dzyaloshinskii–Moriya Interaction (DMI) sign in a series of single crystalline $Fe_{1-x}Co_xSi$. The $Fe_{1-x}Co_xSi$ single crystals were grown using the Czochralski technique with the following concentrations: x = 0.5, 0.6, 0.65, 0.7 and 0.8. The same structural chirality of all grown crystals was provided by consequent use of every grown crystal as the seed for the next one.

The determination of the absolute structure is done via the refinement of the Flack-parameter. This analysis is based on the difference between the Friedel pairs: $[I(h, k, l) - I(-h, -k, -l)]$ due to a resonant contribution in the X-ray scattering amplitude. The single-crystal diffraction data were collected using the PILATUS@SNBL diffractometer at the BM01A end station of the Swiss-Norwegian Beamlines at the ESRF (Grenoble, France). All samples show the same right-handed structural chirality (Γ_C = +1) as confirmed by the absolute structure.

The large size of the single crystals makes it possible to determine the chirality of the magnetic structure by polarized neutron diffraction. The helix chirality γ_m is quantified with the help of the polarization of the scattered neutron P_s at a fixed point in the momentum space $\mathbf{Q} = \mathbf{k}$:

$$P_s(\mathbf{k}) = \frac{I^+(\mathbf{k}) - I^-(\mathbf{k})}{I^+(\mathbf{k}) + I^-(\mathbf{k})} = \gamma_m P_0,$$

where I^+ and I^- are the intensities of the scattered beam with initial polarization $\mathbf{P}_0$ parallel or antiparallel to the scattering vector $\mathbf{Q}$, respectively.

The polarized small-angle neutron scattering measurements were carried out at the SANS-1 instrument at the Heinz Meyer-Leibniz Zentrum. Figure 1 shows the polarized SANS maps for the compounds MnSi and $Fe_{1-x}Co_xSi$ with x = 0.5, 0.6 and 0.7 at $T \approx 3.5$ K.

The MnSi reference sample shows a maximum of the scattering intensity at the right part of the detector (Fig.1a). The samples with x = 0.5 (Fig. 1b) and x = 0.6 (Fig. 1c) show the similar behavior. According to the previous given definition the magnetic chirality is given a γ_m = –1. Clearly, the $Fe_{0.3}Co_{0.7}Si$ sample shows the opposite behavior (Fig. 1d) with γ_m = +1.

Furthermore, the helix wavevector k has been extracted from the low temperature scattering maps and plotted in Fig. 2a. In Figure 2b the product from the structural and magnetic chirality is shown. $k \to 0$ at the critical concentration x_C = 0.65. The helix wave vector k and the DM constant D are linked via the equation $k = SD/A$, where S is the average spin per unit cell and A is the spin wave stiffness. Expecting the spin wave stiffness and the spin value as monotonic functions of the Co content, $k \to 0$ implies $D \to 0$ at x_C. The critical concentration x_C separates two region with opposite values of the product $\gamma_m \cdot \Gamma_C$, which means that D not only goes to zero at x_C but also changes its sign.

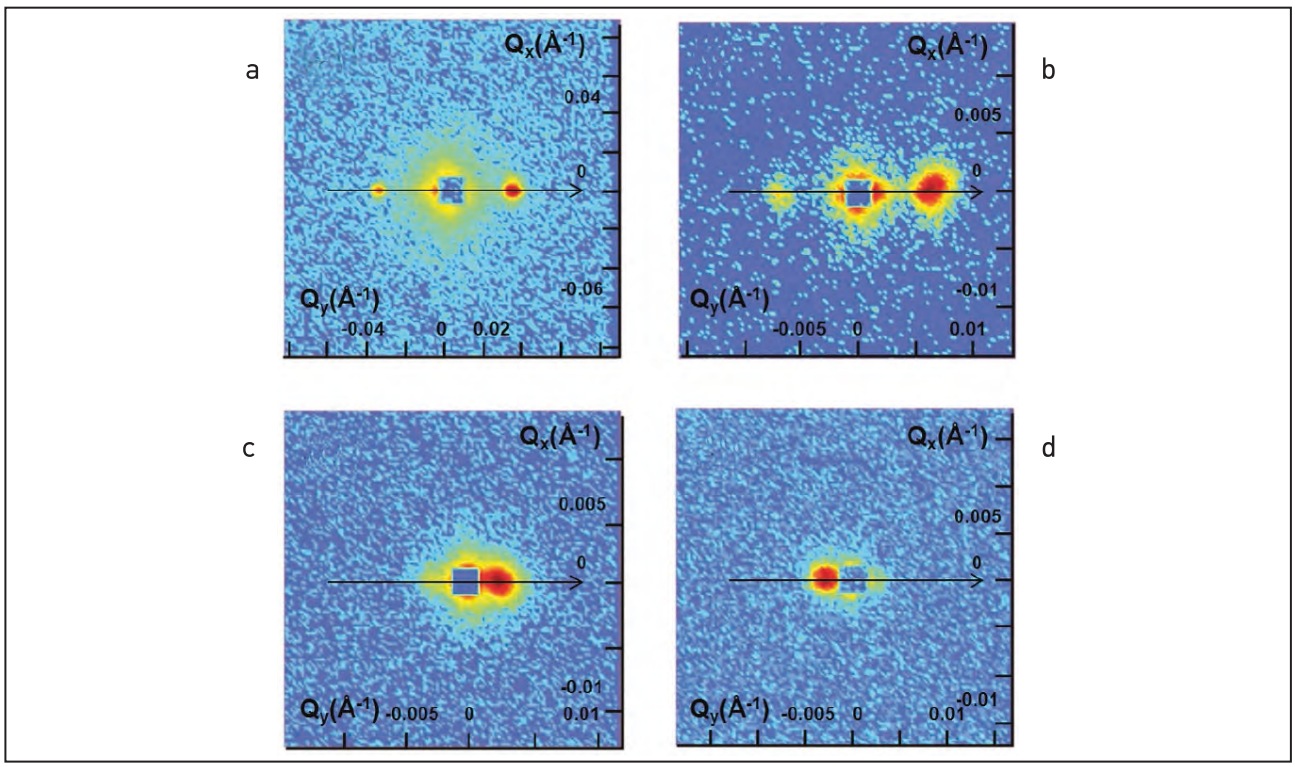

Fig. 1. Maps of polarized SANS intensities of MnSi (a) and $Fe_{1-x}Co_xSi$ with x = 0.5 (b), 0.6 (c) and 0.7 (d) for polarization $+\mathbf{P}_0$ along the field at $T \approx 3.5$ K

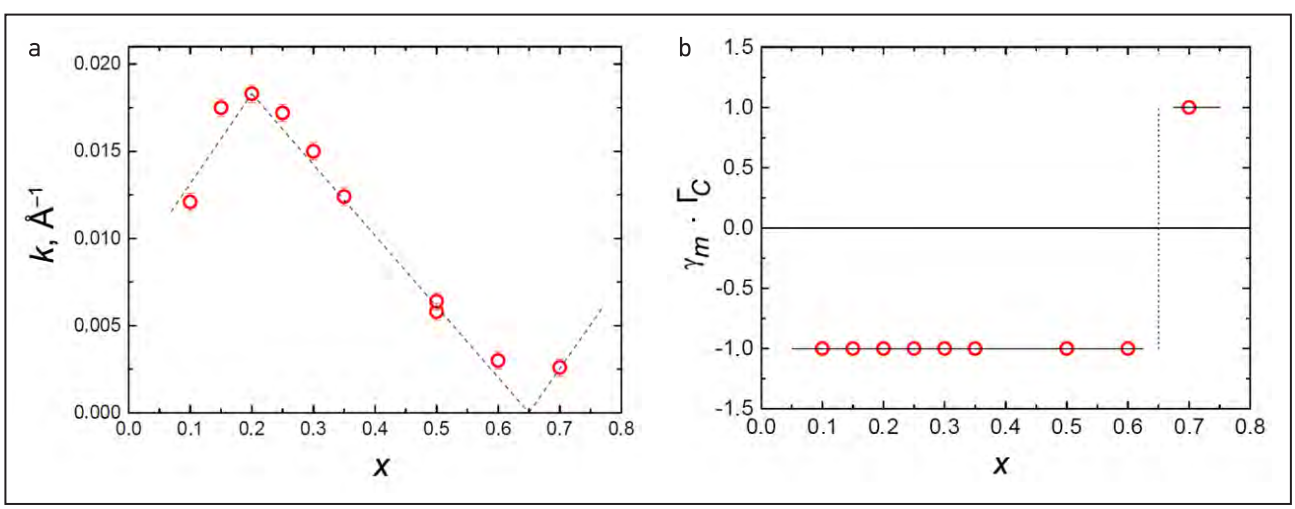

Fig. 2. Dependence of the helix wave vector k (a); the product of structural and magnetic chirality $\gamma_m \cdot \Gamma_c$ on the concentration x (b). x_c shows where k goes to zero

Siegfried S.-A., Altynbaev E.V., Chubova N.M., Dyadkin V. ..., Moskvin E.V. ..., Grigoriev S.V. // Phys. Rev. B. 2015. V. 91. P. 184406.

Spin waves if full-polarized state of Dzyaloshinskii–Moriya helimagnets

E.V. Altynbaev, S.V. Grigoriev, A.S. Sukhanov – Neutron Research Division
S.V. Maleev – Theoretical Physics Division,
PNPI NRC "Kurchatov Institute"
S.-A. Siegfried – Helmholtz Zentrum Geesthacht

The competition between the ferromagnetic exchange interaction J and the antisymmetric Dzyaloshinskii–Moriya (DM) interaction D leads to appearance of the helical magnetic structure in the cubic B20-type compounds. The external magnetic field H_{C2} is needed to transform the helix with wave vector $k_s = D/J$ into the ferromagnetic collinear Full-Polarized (FP) state. Despite the parallel ordering of the spins in FP-state, the presence of the DM interaction leads to the chirality of the dispertion relation of the spin waves. The FP-state of the DM-helimagnets is predicted to be the only known system with the excitations described by the asymmetrical dispersion relation. The dispersion relation in this case can be written as follows: $\varepsilon_{\mathbf{q}} = A(\mathbf{q} - \mathbf{k}_s)^2 + H - H_{C2}$, where A is the spin-wave stiffness.

To verify the main peculiarities of the helimagnon spectrum in FP-state, we have applied small angle scattering of polarized neutrons (SANS). MnSi crystal was chosen for this study as one of the best-known representatives of the DM-helimagnets. We have shown that the cross section contains a polarization-dependent part due to the asymmetry of the aforementioned dispertion relation. The last means that the scattering on spin-waves in FP-state of helimangets can be distinguished by the substraction of the measured intensities with the different polarization of the incident netrons from each other: $I_{SW}(\theta) = I(\theta; +\mathbf{P}_0) - I(\theta; -\mathbf{P}_0)$. Figure 1a shows the example of the polarized part of the SANS map at the field $H > H_{C2}$. As can be seen, the inelastic scattering of neutrons on magnons appears mostly around the former Bragg peak in the small angles estimated to be less than $\theta_0 = \hbar/(2m_nA)$, where m_n is the mass of the neutron. The inelastic scattering arising from the spin-wave scattering is integrated over the energy transfer in SANS experiments where it is detected as a diffuse scattering. By analyzing this diffuse scattering one can extract the value of the spin-wave stiffness of the system A. The profile of intensity contains step-like part with a characteristic cut-off angle (Fig.1b). The cut-off angle depends on the strength of the applied magnetic field: $\theta_C^2 = \theta_0^2 - \theta_0 H/E_i + \theta_B$, where E_i is the energy of the incident neutron, θ_B is the Bragg angle corresponding to the period of the HM-structure in the HM-phase. The spin-wave stiffness can be extracted from the obtained cut-off angle with high accuracy. The temperature dependence $A(T)$ has been investigated in the whole range below T_C = 30 K. Obtained data fits by power law: $A(T) = A_0[1 - c(T/T_C)^z]$, the fitting parameters were found to be A_0 = 0.054 meV · Å^2, c = 0.47 and z = 1.8.

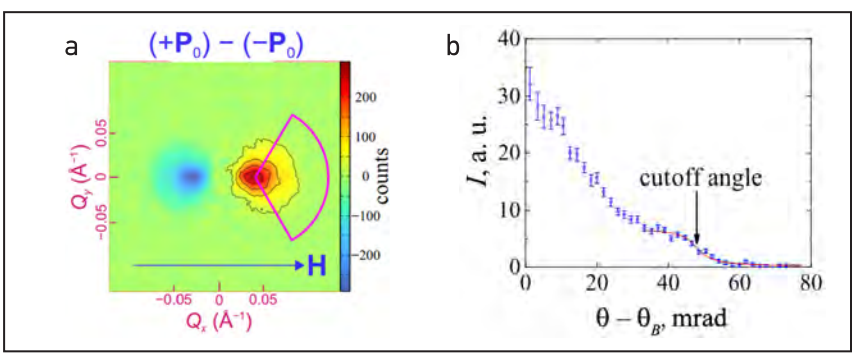

SANS map, MnSi at T = 15 K and H = 0.7 T (a) polarization-dependent scattering I_{SW} is shown. The profile of the averaged intensity, cut-off angle is observed (b)

Grigoriev S.V., Sukhanov A.S., Altynbaev E.V. ..., Maleyev S.V. // Phys. Rev. B. 2015. V. 92. P. 220415(R).

Spin structure of the quasi-two-dimensional honeycomb-lattice $Na_3Co_2SbO_6$ antimonate

M.D. Kuchugura, A.I. Kurbakov, S.Yu. Podchezertsev – Neutron Research Division, PNPI NRC "Kurchatov Institute"
J. Rodriguez-Carvajal – Institut Laue-Langevin
V.B. Nalbandyan – Southern Federal University

We present a comprehensive diffraction study (neutron and synchrotron powder diffraction) of the quasi-two-dimensional (2D) monoclinic $Na_3Co_2SbO_6$ compound with honeycomb superstructures of the cation layers. A new generation of layered complex compounds with honeycomb superstructures is currently one of the most intriguing materials from the point of view of their unique physical properties including low-dimension magnetism. Magnetic (and transport) properties of the studied oxides depend on the nature of all cations and their electronic, spin, and orbital states determined by the neighboring crystallographic environment.

The crystal structure of $Na_3Co_2SbO_6$ was described as a honeycomb-type structure with monoclinic space group *C*2/*m*. The compound is built upon the structural motives on the basis of edge-related oxygen octahedral layers with low-charged, relatively large cations of *d*-element in the centers of 2/3 octahedra. Ordered mixed layers consisting of magnetic cations Co^{2+} and nonmagnetic Sb^{5+} inside oxygen octahedra alternate with Na layers (see the *left* Figure). Magnetic cations in the oxygen-octahedral layers form honeycomb grids, which in condition of an antiferromagnetic type interaction between nearest neighbors, can lead to a frustration in the magnetic subsystem and the emergence of unusual types of magnetic moments ordering, which was actually observed in this study.

The appearance of additional reflections related to the antiferromagnetic ordering organization of the $Na_3Co_2SbO_6$-sample at T_N below 7 K is clearly visible on the low-temperature neutron powder diffraction patterns. The magnetic ordering is characterized by the presence of two propagation vectors; one of them is slightly incommensurate. The most intense peaks correspond to $\mathbf{k}_1$ = (1/2, 1/2, 0), and there is a prominent peak corresponding to $\mathbf{k}_2$ = (0, 1/2 + δ, 1/2) with δ ≈ 0.011 that is very close to the most intense peak of the $\mathbf{k}_1$-component. The presence of two independent propagation vectors leads to the fact that the diffraction pattern alone does not give the unequivocal description of the spin ordering; because the phase factor between the corresponding Fourier coefficients is not available in the experiment. Assuming a zero phase between them, we can suggest the simplest magnetic structure corresponding to the experimental data. This spin structure is formed by the superposition of a collinear AFM ($\mathbf{k}_1$) in a general direction with a long period transversal sinusoidal ($\mathbf{k}_2$) component along the *a*-axis (see the *right* Figure).

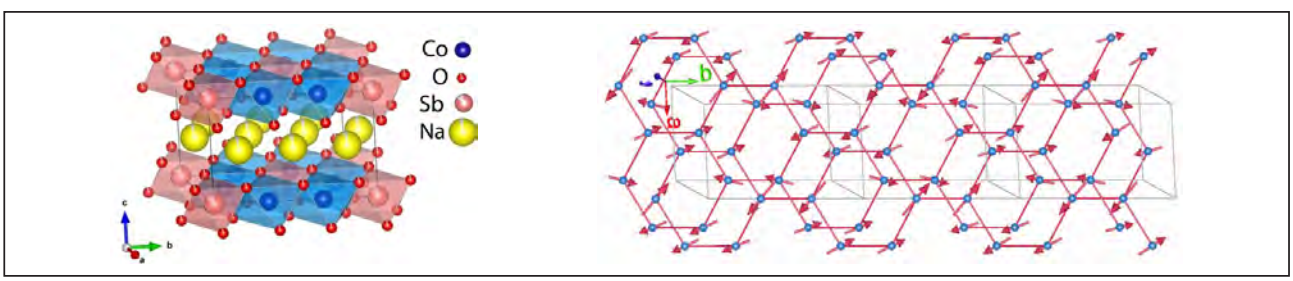

Polyhedral view of a layered crystal structure (*left*) and model of spin structure of $Na_3Co_2SbO_6$ (*right*)

Kurbakov A., Kuchugura M., Podchezertsev S. et al. // Proc. of the 1st IEEE Conf. Advances in Magnetics. Bormio, Italy, March 14–16, 2016. P. 70.

Neutron diffraction study of the $(BiFeO_3)_{1-x}(PbTiO_3)_x$ solid solution – nanostructured multiferroic system

I.V. Golosovsky – Neutron Research Division, PNPI NRC "Kurchatov Institute"
S.B. Vakhrushev – Ioffe Institute
J.L. García-Muñoz – Institut de Ciéncia de Materials de Barcelona
M. Brunelli – Institut Laue-Langevin
W.-M. Zhu, Z.-G. Ye – Simon Fraser University
V. Skumryev – Institució Catalana de Recerca i Estudis Avançats

Today, the search and studies of the materials with new properties for practical application is the most important task of the condensed matter physics. In this respect, the materials with improved ferroelectric properties, which also have a magnetic order, i. e., multiferroics, are in focus. Therefore, the new attempts of the solid solution synthesis with the purpose to organize the "instability" in the system due to the "connection" of the ferroelectrics with different crystal structure do not stop.

Our work is devoted to the systematic study of such a system – $(BiFeO_3)_{1-x}(PbTiO_3)_x$. The compound of $BiFeO_3$ is known as the only multiferroic, whose magnetic order and polarization coexist at room temperature. However, the polarization is small and much less than the theoretical prediction. It was found that in the solid solutions $(BiFeO_3)_{1-x}(PbTiO_3)_x$ the gained polarization can be several times greater than in the initial compounds. The samples were synthesized in Simon Fraser University, neutron diffraction studies were carried out on the diffractometer D20 and D2B of the Institut Laue-Langevin. The obtained results follow below.

1. The studied system is a mixture of two nanoscale phases: rhombohedral $(Bi_{0.8}Pb_{0.2})(Fe_{0.8}, Ti_{0.2})O_3$ and tetragonal $(Pb_{0.5}Bi_{0.5})(Fe_{0.5}, Ti_{0.5})O_3$. The average nanoparticle size is about 20–50 nm, and the ratio of Fe and Ti in the two phases was almost constant for all the samples, the relative phase content differs only.

2. The magnetic moments in $BiFeO_3$-phase, in contrast to the parent composition of the $BiFeO_3$, deviate from the basal plane. Temperature dependences of the spin component along the hexagonal axis and in perpendicular plane are different, resulting in the spin-orientation transition. The antiferromagnetic order in $PbTiO_3$-phase corresponds to a simple antiferromagnetic structure. At low temperatures, a weak ferromagnetic moment due to "canted" sublattices was found.

3. Analysis of the results shows a strong magnetic coupling between two systems. These effects were interpreted as the "exchange bias" between particles with different magnetic order: the phase with a larger Neel temperature is magnetizing the phase with a lower temperature. It is not surprising, taking into account the nanoscale nature of the constituent phases, which involves the well-developed interface between the nanoparticles with different magnetic structure.

Thus, the system $(BiFeO_3)_{1-x}(PbTiO_3)_x$ demonstrates a new scenario, where "proximity effects" in unstable nanostructured system play a crucial role in the emergence of unusual magnetic properties.

Golosovsky I.V. et al. // J. Phys.: Cond. Matt. 2015. V. 27. P. 046004.

Origin of the large dispersion of magnetic properties in nanostructured oxides: Fe_xO/Fe_3O_4 nanoparticles as a case study

I.V. Golosovsky – Neutron Research Division, PNPI NRC "Kurchatov Institute"
O.L. Makarova – NRC "Kurchatov Institute"
M. Estrader, S. Estradé, L. López-Conesa, F. Peiró – Universitat de Barcelona
L. Bergström, M. Estrader, G. Salazar-Alvarez – Stockholm University
A. López-Ortega – Università degli Studi di Firenze
J. Nogué – Institució Catalana de Recerca i Estudis Avançats
J. Nogué, A.G. Roca – Institut Catala de Nanociencia i Nanotecnologia
D. Tobia, E. Winkler, R.D. Zysler – Centro Atómico Bariloche
J.D. Ardisson, W.A.A. Macedo, M. Vasilakaki – Centro de Desenvolvimento da Tecnologia Nuclear
A. Morphis, K.N. Trohidou, M. Vasilakaki – Institute of Nanoscience and Nanotechnology, NCSR "Demokritos"
A. Gukasov, I. Mirebeau – Laboratoire Leon Brillouin
M.D. Baró – Universitat Autònoma de Barcelona

A systematic study of the core/shell nanosystem Fe_xO/Fe_3O_4 with characteristic sizes: large nanoparticles – 21(1)/8.8(3) nm and small nanoparticles: 10.1(5)/2.0(2) nm, for the core and shell, respectively, was performed. It is the largest and the smallest size, known in the literature for similar systems. It was shown that a combination of factors, namely, non-stoichiometry, the internal stress and size-effects govern a wide range of properties exhibited by the transition metal oxides at nanoscale. To identify these effects, various techniques primarily neutrons and *X*-ray diffraction (synchrotron) were employed. The magnetic measurements, magnetic circular dichroism (XMCD) and electron microscopy (HRTEM – High Resolution Transmission Electron Microscopy) in combination with EELS (Electron Energy Lost Spectroscopy) and GPA-HRTEM (Geometric Phase Analysis) were used as well.

The parameters of nanoparticles derived from the diffraction experiments proved to be very close to those obtained from electron microscopy. The diffraction revealed no significant internal stresses. However, the geometric phase analysis method, which allows defining a local deformation from TEM micrographs of a high-resolution showed their presence.

The neutron diffraction from small nanoparticles at low temperatures shows the magnetic contribution from the magnetite shell only. Contribution from the FeO core was not detected. The ordered magnetic moment in the core is very small, if it exists. At magnetic transition the cubic FeO undergoes the rhombic distortion due to magnetostriction. Therefore, *X*-ray measurements were carried out at low temperatures. Deviations from a cube within 0.1 degree at 10 K were not found, which is consistent with the absence of magnetic ordering in the core. Apparently, then large number of defects deploys the long-range order.

For a sample with a large core and shell a strong magnetic reflection ½ ½ ½ from the core FeO was observed, which in the bulk is strongly suppressed. This means that the magnetic moments deviate from the [111] direction, characteristic of the bulk FeO. The ratio of the intensities clearly indicates that in the core moment is aligned along the direction [110]. The temperature dependence of the magnetic reflection implies that the Neel temperature (T_N) in the core is significantly higher than in the bulk FeO, which can be interpreted as a "proximity effect", when the magnetite shell with greater T_N biases the core with smaller T_N.

Estrader M. ..., Golosovsky I.V. et al. // Nanoscale. 2015. V. 7. P. 3002.

Temperature evolution of superparamagnetic clusters in single-crystal $La_{0.85}Sr_{0.15}CoO_3$ from nonlinear magnetic *ac* response and neutron depolarization

A.V. Lazuta – *Theoretical Physics Division*
V.A. Ryzhov – Molecular and Radiation Biophysics Division
V.V. Deriglazov, V.P. Khavronin, V.V. Runov – Neutron Research Division,
PNPI NRC "Kurchatov Institute"

Doped cobaltites are characterized by a complicated character of the magnetoelectronic phase separation at low enough temperatures, resulting from strong electronic correlations. A particular feature of $La_{0.85}Sr_{0.15}CoO_3$ consists in the proximity of its Sr content to the boundary $x_c = 0.17$ separating the insulating and the metal states, below and above x_c, respectively. Below 250 K, spin polarons arise, while below 65 K, the spin-glass state occurs.

Measurements of the phase components Re(Im)$M_2(H, T)$ for the 2nd harmonic of the nonlinear magnetic response on the weak *ac*-field $h\cos 2\pi ft$ (f = 15.7 MHz) in the parallel *dc*-field H in the temperature range $96 < T < 213$ K showed ferromagnetic clusters to form upon cooling, generating the typical signals with extrema in the weak fields $H < 300$ Oe in both components (Fig. 1).

Below 140 K, the cluster system exhibits the superparamagnetic behavior. These signals were fitted with the Gilbert–Landau–Lifshitz formalism in the uniaxial approximation, which yields a solution of the Fokker–Planck kinetic equation describing such systems. As a result, the temperature dependences for a set of parameters characterizing magnetic and dynamical properties of the system were obtained, viz., the mean cluster magnetic moment, the total saturation magnetization, the width of the cluster-volume distribution and the characteristic dipolar energy of the cluster system, the concentration of clusters and the mean intercluster distance, the anisotropy field and energy, and also the damping factor of the cluster magnetic moment and the mean diffusion relaxation time. The measurement of the neutron depolarization in the same temperature interval additionally enabled the determination of the mean cluster size, the volume fraction of the cluster system, the mean magnetic moment of an incluster magnetic ion, and the anisotropy constant. The temperature dependences for some of the parameters are presented in Fig. 2.

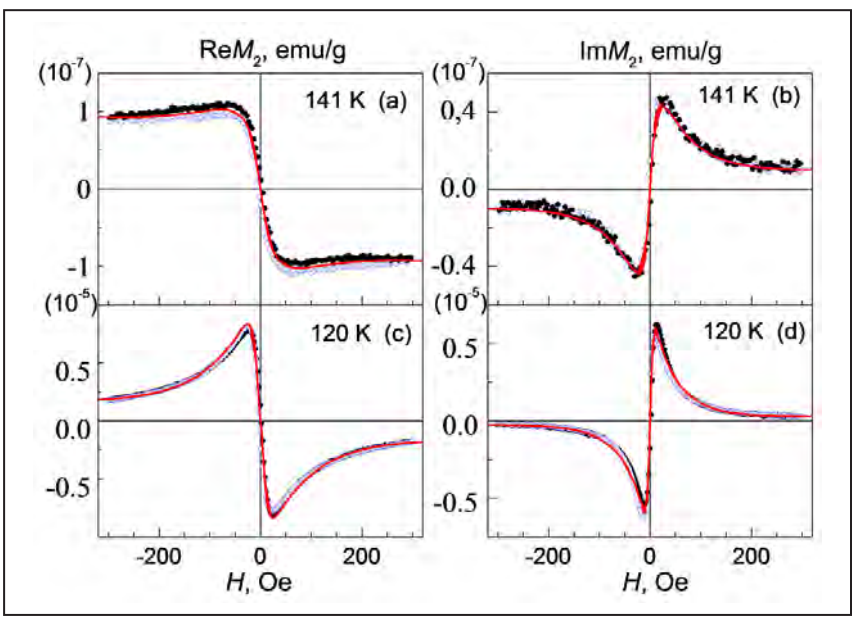

Fig. 1. The real and imaginary parts of the response on the 2nd harmonic as functions of the *dc* magnetic field for two typical temperatures 141 K (a, b) and 120 K (c, d). The solid curves are best fits

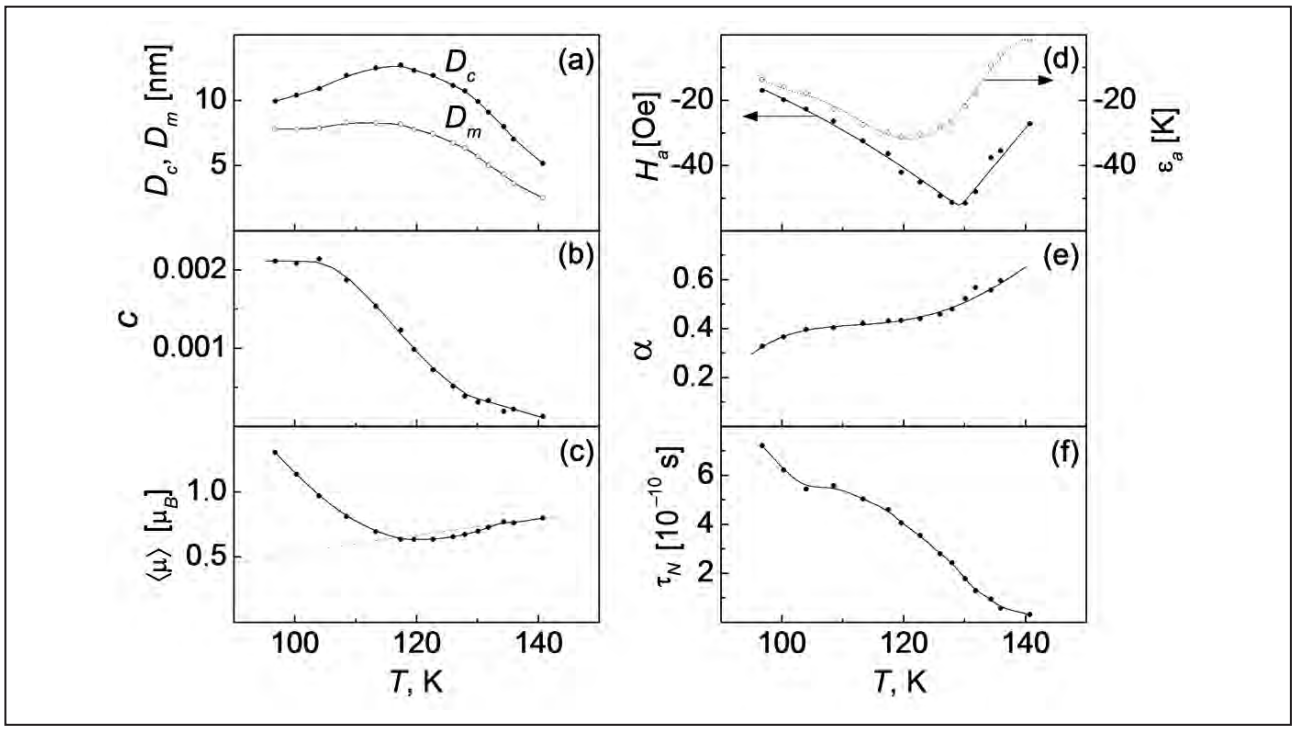

Fig. 2. The mean cluster size D_c and the size in the distribution maximum D_m (a); the cluster volume fraction (b); the mean magnetic moment of an intercluster magnetic ion, the dashed curve is $-\mu_0\exp(-\Delta/T)$, $\mu_0 = 2.15$, $\Delta = 140$ K (c); the anisotropy field H_a and energy ε_a (d); the damping factor (e); the diffusion relaxation time (f). The solid curves are guides for the eye

Upon cooling, the cluster system evolves via several stages.

In the region $140 < T < 213$ K, the clusters and their magnetic moments are pinned at magnetic inhomogeneities, their size slowly increasing upon cooling not exceeding a few nanometers.

At 140 K, the cluster size starts to considerably exceed the size of the inhomogeneities, the magnetic moment becomes of the order 10^2 μ_B, the pinning of the magnetic moment fails and the relaxation time starts to grow, acquiring the values typical for superparamagnetic particles. The incluster ion magnetic moment follows the activation law for Co^{3+}, so that the hole concentration in the clusters only a little exceeds that of the matrix.

Below 130 K, homogeneous nucleation occurs. Clusters arise in the whole volume, and their concentration and size strongly increase, enlarging the volume fraction and the saturation magnetization of the cluster system.

Below 115 K, the clusters cease to grow and their volume fraction stabilizes. On the contrary, the mean incluster ion magnetic moment starts to intensely rise due to commencing enrichment of the clusters with holes.

In the whole range below 140 K, the cluster-volume distribution width decreases with temperature, manifesting the tendency to stabilization of the cluster system. The damping factor monotonously reduces; its values of the order 0.1 imply an essential role of precession in the thermal relaxation of the cluster magnetic moment.

The obtained parameters of the cluster system made it possible to recover a contribution of the clusters to the linear low-frequency magnetic response. A comparison to the measured linear susceptibility evidenced the main contribution of the cluster system to the magnetism below 120 K, despite the little volume fraction of the latter < 0.002.

Lazuta A.V., Ryzhov V.A., Runov V.V., Khavronin V.P., Deriglazov V.V. // Phys. Rev. B. 2015. V. 92. P. 014404.

Structural studies of a new type of proton-conducting polymer membranes

S.S. Ivanchev, Yu.V. Kulvelis, V.T. Lebedev – Neutron Research Division, PNPI NRC "Kurchatov Institute"
S.S. Ivanchev, V.S. Likhomanov, O.N. Primachenko – Saint Petersburg Department of Boreskov Institute of Catalysis of the Siberian Branch of RAS
Gy. Török – Research Institute for Solid State Physics and Optics, Wigner Research Centre for Physics, Hungarian Academy of Sciences

Supramolecular structure of a new type of polymer membranes (Fig.) for hydrogen fuel cells has been studied by small angle neutron scattering. These membranes were designed at the Institute of Catalysis SB RAS using a new effective aqueous emulsion method for synthesis. The membranes are based on fluorine-containing macromolecules with sulfonic acid groups and grafted with short side chains. Such new prospective materials for hydrogen fuel cells have advantages over long side chain Nafion-type membranes (foreign analogs) due to optimal chemical structure and a type of macromolecules' packaging that creates stable conduction channels for protons. The results of neutron experiments allowed the discovery of the interrelation between the structural and functional properties of membranes by using physical modeling of membrane structure having a system of linear and branched diffusion channels with diameter of ~ 1 nm and the sides covered with SO_3H-groups that provide proton hopping conductivity. The results were published.

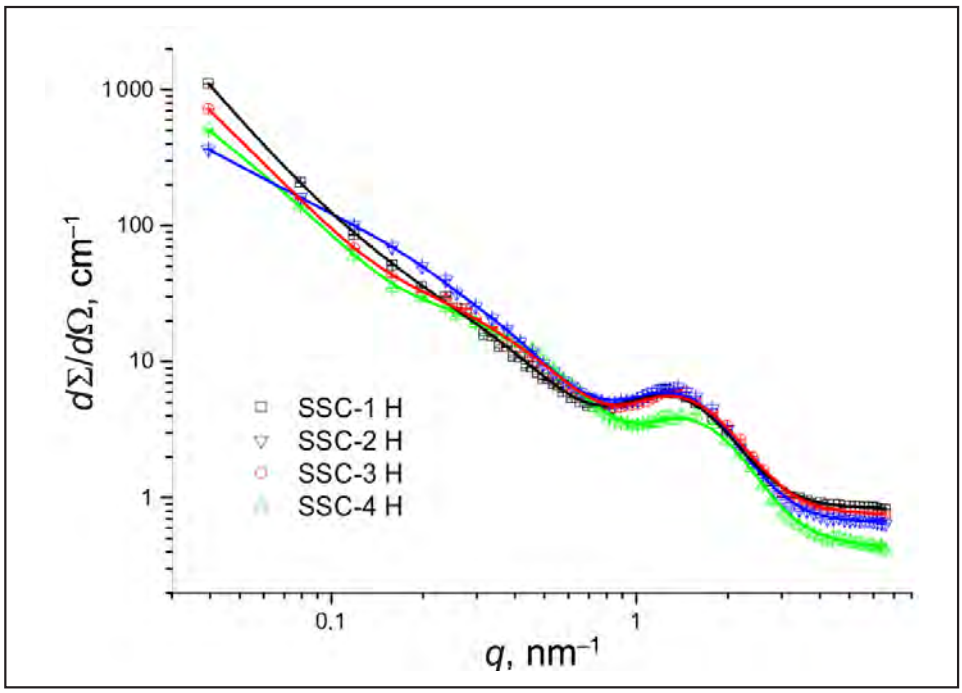

Scattering cross sections of membranes saturated with H_2O as dependent on momentum transfer. The samples SSC-1–4 H have different equivalent weight per a SO_3H-group in polymer chain (752; 804; 807; 1 021). Curves are the approximation functions used by modeling

Kulvelis Yu.V., Ivanchev S.S., Lebedev V.T. et al. // RSC Advances. 2015. V. 5. P. 73820–73826.

Neutron reflectometry: conditions of maximum filling of Δq with neutrons

N.K. Pleshanov
Neutron Research Division, PNPI NRC "Kurchatov Institute"

Luminosity of the reflectometer is defined in this work as the neutron flux incident onto the sample surface for measurements made with a given resolution Δq. Proceeding from this definition, new optimization criteria for a class of instruments – neutron reflectometers – are substantiated. The filling of Δq with neutrons near a certain momentum transfer q depends not only on the source luminance and the source-sample tract transmittance, but also on the beam tailoring. It is shown that the correct choice of the working wavelength and other beam parameters may increase the luminosity of the reflectometers in several times.

So far the luminosity of neutron reflectometers was implied to be maximum for the wavelength λ_{max} at the maximum of the spectral flux density $A(\lambda)$. The analysis showed that, when a conventional collimation system made with two diaphragms is used, the luminosity is maximum at the wavelength λ_{opt}, at which the product $A(\lambda)\lambda^3$ is maximum. In particular, for a beam of thermalized neutrons the transition from λ_{max} to $\lambda_{opt} = \sqrt{5/2}\,\lambda_{max}$ increases the luminosity of the reflectometer in $e^{3/2} \cdot 2/5 \cong 1.79$ times.

Furthermore, taking account of the correlation between the divergence and the beam width in measurements in the slit geometry with two diaphragms leads to new conditions for the beam parameters yielding maximum intensity with a given resolution Δq:

$$\Delta\theta/\theta = \sqrt{2}(\Delta\lambda/\lambda) = \sqrt{2/3}\,(\Delta q/q),$$

where θ and $\Delta\theta$ are the glancing angle and the beam divergence, λ and $\Delta\lambda$ are the mean wavelength and the wavelength spread (if the mentioned correlation is absent, the optimum measurement condition is known to be $\Delta\theta/\theta = \Delta\lambda/\lambda$). The decrease in the luminosity as compared to its possible maximum is given by the formula (see also Fig.)

$$\varepsilon = (3\sqrt{3}/2)\kappa(1 + \kappa^2)^{-3/2},$$

where $\kappa = (\Delta\lambda/\lambda)/(\Delta\theta/\theta)$.

The analysis of the existing schemes of realization of neutron reflectometry showed that the transition to the regime of optimum measurements may increase the luminosity in several times, e. g., when neutron velocity selectors on the basis of aperiodic multilayers are used. Such innovations as the time-of-flight technique with a fan beam formed by a chopper of special design (drum chopper) and small angle Soller collimators with absorbing traps for neutrons reflected from the channel walls are proposed to further increase the luminosity of the reflectometers.

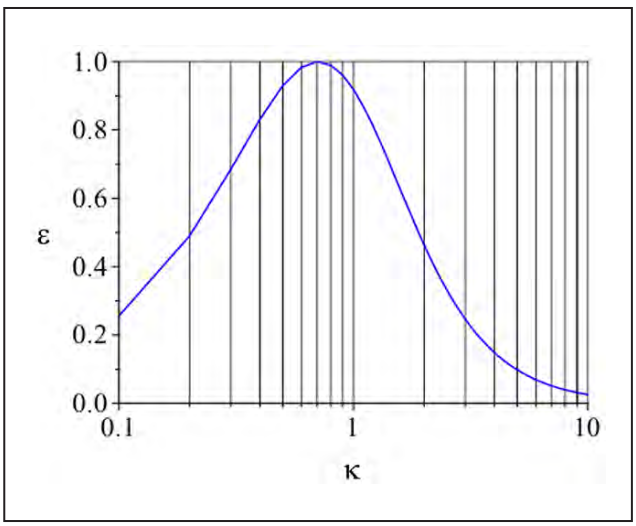

The optimality ε of measurements with a fixed resolution Δq as a function of κ for the slit geometry realized with two diaphragms. The κ-axis is in the logarithmic scale

Pleshanov N.K. // Nucl. Instr. Meth. A. 2016. V. 820. P. 146–155.

Investigation of magnetic properties of a ferrofluid with $CoFe_2O_4$ nanoparticles using the μSR-method

A.L. Getalov, E.N. Komarov, S.A. Kotov, V.G. Shcherbakov, S.I. Vorobyev
High Energy Physics Division, PNPI NRC "Kurchatov Institute"

Currently, the interest in development of technologies for production of materials possessing new properties increased significantly, as such properties are important for practical applications. Among such materials, a special place is occupied by systems in which magnetic nanoparticles are distributed in a nonmagnetic medium. Particularly, such materials include ferrofluids, ultrastabilized suspensions of single-domain magnetic nanoparticles (usually, Fe_3O_4, $CoFe_2O_4$, *etc.*) in a liquid medium. The cobalt ferrite is known to have the Curie temperature 793 K and the highest constant of anisotropy among the ferrite family. The magnetic properties of ferrofluids have been studied earlier by means of the different methods including the use of a quantum magnetometers (SQUID), a slow neutron scattering at the small angles and the Mössbauer spectroscopy.

The present work is devoted to the study of water based ferrofluid samples with different volumetric concentrations of $CoFe_2O_4$ nanoparticles (0.5% and 3.0%) with the mean size of 8.5 nm. The experiment was performed using the μSR-setup located at the exit of the polarized muon beam channel of the PNPI NRC KI synchrocyclotron with the momentum 90 MeV/*c* and polarization $P_\mu = 0.9$ (Fig. 1).

The investigation of samples was performed within the temperature range of 25–300 K. The experimental time spectra of the muon magnetic momentum precession in the external magnetic field have been described by the function

$$N(t) = N(0)\exp(-t/\tau_\mu)\cdot[1 + b\frac{P_0}{3}\exp(-\lambda t)\cos(\omega t + \varphi) + B],$$

where τ_μ = 2.197 μs is the life time of muon; P_0 is the primary polarization of the muon beam; λ is the relaxation rate of the muon polarization;

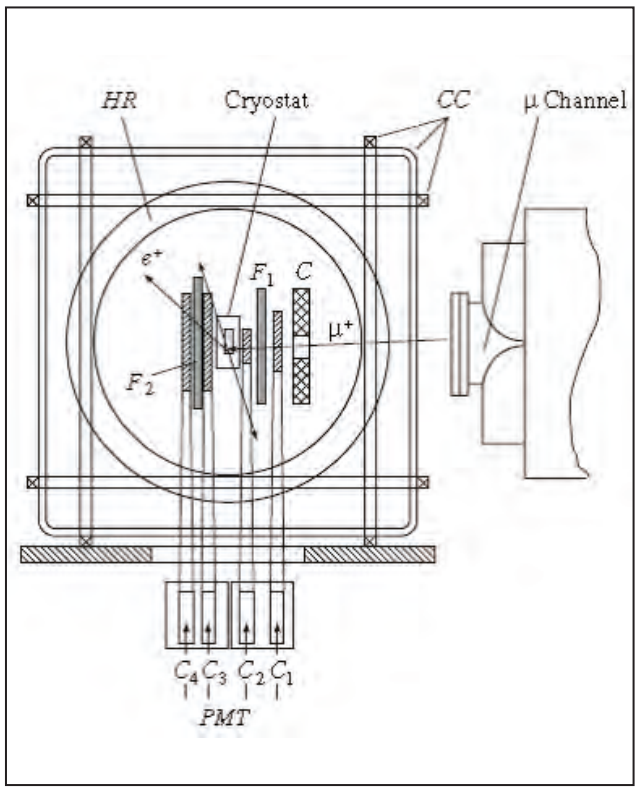

Fig. 1. Setup for the μSR experiments: HR – Helmholtz rings; CC – compensating coils; C – collimator; F_1, F_2 – filters; PMT – photomultiplier tube; C_1–C_4 – scintillation counters

ω is the precession frequency of the muon magnetic moment; φ is the initial phase; *B* is the background level; a value $b \simeq 1$ and it depends on the parameters of the setup. The characteristics of the relaxation function (*a*, ω, λ) were determined by means of the time spectra analysis. The temperature dependencies of nanoparticles in a sample with 3% concentration are presented in the Fig. 2 for two cooling conditions: in the presence of an external transverse magnetic field (FC) and in the absence of the field (ZFC).

As we can see, the amplitude a is smaller than the amplitude a(Cu) = 0.308 ± 0.003 determined by processing of the data received from a copper sample in an external transverse magnetic field B = 525 G. This fact is caused by a rapid polarization loss due to formation of muonium; it is not possible to detect the muonium spin precession effect at a given time resolution of 5 ns. In case of a asymmetry, the diamagnetic (muon) fraction in both samples is produced approximately in the same ratio as in pure H_2O, regardless of the cooling conditions. However, the relaxation rate λ and the precession frequency of the muon spin ω in aferrofluid with 3% concentration of nanoparticles depend on the cooling condition applied to the sample (see the Fig. 2), and differ significantly from similar data for H_2O.

In case of cooling, the ferrofluid in the absence of a magnetic field (ZFC), magnetic moments of nanoparticles are frozen in space in random directions. In case of FC measurements, the magnetic moments of nano-particles are ordered, and for this reason the magnetic field magnitude in the sample differs from that of the external field. As a result, the relaxation rate λ and the precession frequency of the muon spin ω in the medium are different depending on the cooling mode used. In case of FC cooling, nanoparticles induce an additional magnetic field in the medium. Using the average value of the muon spin precession frequency Δω within the temperature range of 26–175 K for FC and ZFC measurements, it was discovered that, in case of a ferrofluid with 3% concentration, nanoparticles cooled in the external magnetic field B = 525 G induce in the medium an additional magnetic field of about 4.7 ± 0.2 G.

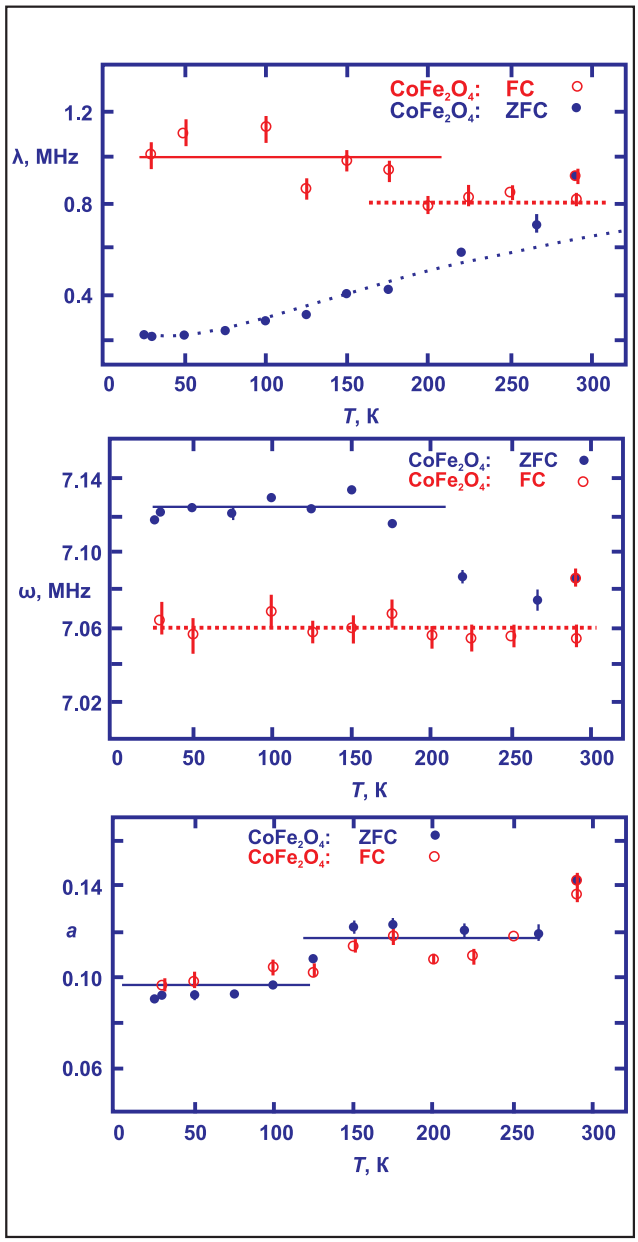

Fig. 2. Temperature dependence of asymmetry a, precession frequency ω, and relaxation rate λ in a sample with 3% concentration of nanoparticles (B = 525 G).

Mamedov T.N. ..., Getalov A.L., Komarov E.N., Kotov S.A. ..., Scherbakov V.G., Vorob'ev S.I. et al. // J. Optoelectr. Adv. Mater. 2015. V. 17. No. 7–8. P. 1086.

Critical state and low field electrodynamics in a new type of the granular superconductors

A.V. Aldushchenkov, O.V. Gerashchenko, I.S. Okunev – Neutron Research Division, PNPI NRC "Kurchatov Institute"
A.L. Kholmetskii, V.A. Lomonosov, L.V. Makhnach – Belarus State University
M. Mashlan – Palacky University
T. Yarman – Okan University

It is well known that superconducting oxypnictides of the 1111-type ($LaO_{1-x}F_xFeAs$) are characterized by a very high value of $H_{C2} \sim 1–10 \cdot 10^5$ Oe and, accordingly, by a small coherence length $\xi \sim 10$ Å. In this case, even a small defect in the material plays the role of a Josephson junction. Such a system known as a Josephson medium behaves analogously to a conventional type II superconductor. The role of the upper critical field is played by quantity $H_g \sim \Phi_0/a^2 \sim 10–100$ Oe, a is a grain size. The Ginzburg–Landau parameter is $\kappa >> 1$, and the vortex size is $\lambda_J \sim (\Phi_0/\mu_{eff}H_{C1})^{1/2} >> a$.

Such inhomogeneous systems obviously exhibit strong pinning of vortices, leading to nonlinear and irreversible effects that can be described using Bean's critical state concept. In this concept, the magnetic pressure force is balanced by pinning force $\alpha(h)$, and non uniform magnetic field $h(r)$ in the superconductor satisfies the critical state equation

$$\left|\frac{dh(r)}{dr}\right| = 4\pi j_C(H), \qquad j_C(h) = \frac{\alpha(h)}{h},$$

where $j_C(h)$ is the critical current density determined experimentally.

Another source of information on the magnetic flux dynamics is associated with the electric and transport properties of the superconductor. It is well known that in a type II superconductor in a magnetic field applied perpendicularly to the current, the passage of a current $j > j_C$ induces the electric field:

$$E(j) = \rho_{FF}(H, T)(j - j_C(H, T)).$$

Analysis of the current-voltage characteristics makes it possible to determine independently the temperature and field dependences of resistivity ρ_{FF} of the superconductor in the flux flow regime and critical current density $j_C(H, T)$ and to match the results of magnetic and electric measurements.

In this work, we have experimentally studied the penetration of a weak magnetic field into a $LaO_{0.85}F_{0.15}FeAs$ polycrystalline superconductor on the same samples using two mutually complementing methods: analysis of higher harmonics of the nonlinear magnetization and measurement of the I–V characteristics. We found that the given superconductor is a typical granular type II superconductor with nonlinear magnetic and electric properties that can be described by the low field electrodynamics of a Josephson medium; therefore, we have experimentally confirmed the universality of the concept of the low-field electrodynamics for a new class of polycrystalline superconductors.

Thus, the temperature and field dependences of the critical current can be written in the form:

$$j_C(H, T) = j_0 \frac{H_0}{|H| + H_0}\left(\frac{T_C - T}{T_C}\right)^2,$$

where $j_0 = 20$ A/cm^2, $H_0 = 90$ Oe, $T_C = 21.5$ K.

Gerashchenko O.V. ..., Alduschenkov A.V., Okunev I.S. et al. // JETP. 2015. V. 120. Iss. 6. P. 1034–1040.

Angular distribution and anisotropy of the fragments from neutron-induced fission of U and Th in 1–200 MeV energy range

A.M. Gagarski, O.A. Shcherbakov, A.S. Vorobyev – Neutron Research Division
L.A. Vaishnene – High Energy Physics Division,
PNPI NRC "Kurchatov Institute"
A.L. Barabanov – NRC "Kurchatov Institute"

Experimental data on angular distributions and anisotropy of the fragments from neutron-induced fission in the energy range 1–200 MeV, as well as the data on neutron fission cross sections, are necessary for the development of theoretical models of the fission reaction induced by intermediate and high energy neutrons, and also for the practical calculations, first of all – in nuclear power industry of new generation. In 2015, at the neutron time-of-flight spectrometer GNEIS, the measurements of angular distributions of fission fragments for ^{235}U, ^{238}U and ^{232}Th nuclei were performed in the incoming neutron energy range 1–200 MeV. A registration of the fission fragments was carried out with the use of position-sensitive detector enclosing two multiwire proportional counters located at the 36 m flight path. An event read-out from the electrodes of each counter (cathode and a pair of *X*, *Y*-anodes) and their subsequent digitization were carried out using the eight-channel registration system based on a FLASH-ADC, as shown in Fig. 1. The angular distributions of fission fragments measured in the angle range $0.3 < \cos\theta < 1$, were fitted by a function $W(\theta) \sim 1 + A_2 \cdot P_2(\cos\theta)$, where θ is an angle between neutron beam axis and a vector of fission fragment momentum, $P_2(\cos\theta)$ – is a Legendre polynomial of the 2nd order. An anisotropy $W(0^o) / W(90^o)$ was calculated using the fitting results. The data on anisotropy for ^{232}Th nucleus are shown in Fig. 2 together with the data by other authors. The ^{232}Th data set measured at the PNPI NRC KI is the most exhaustive and accurate one. An analogous data have been obtained for ^{235}U and ^{238}U. At present, the theoretical analysis of the experimental data obtained for ^{235}U, ^{238}U and ^{232}Th is underway, while the measurements for ^{233}U have been recently started.

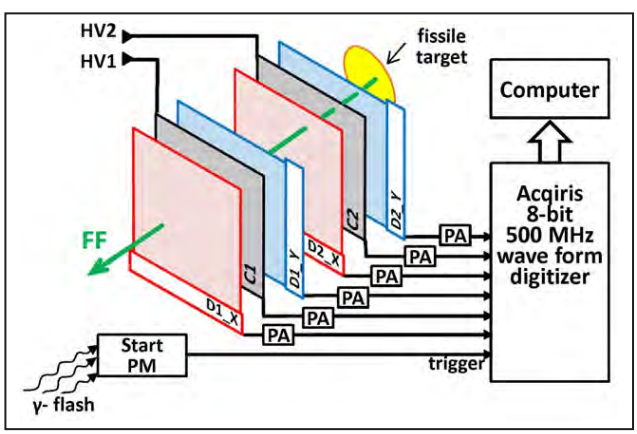

Fig. 1. Scheme of the experimental set-up

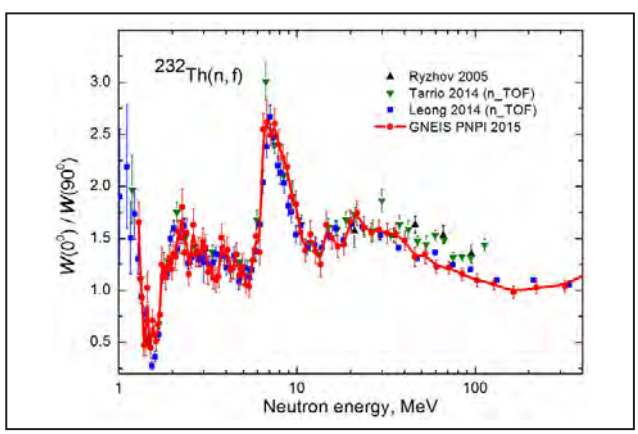

Fig. 2. Anisotropy of ^{232}Th fission fragments

1. *Vorobyev A.S., Gagarski A.M., Shcherbakov O.A., Vaishnene L.A., Barabanov A. L.* // Book of Abstracts of the XXIII Int. Seminar on Interaction of Neutrons with Nuclei. Dubna, Russia, May 25–29, 2015. JINR, E3-2015-29. P. 39.
2. *Vorobyev A.S., Gagarski A.M., Shcherbakov O.A., Vaishnene L.A., Barabanov A.L.* // JETP Lett. 2015. V. 102. No. 4. P. 203.

The development of techniques for instrumental and radiochemical neutron activation determination of Pt, Pd, Re, Ir, Au and other elements in samples of the tagamite and suevite selected in the Kara astrobleme

A.I. Egorov, Yu.E. Loginov, I.A. Mitropolsky, I.S. Okunev, S.L. Sakharov, G.I. Shulyak, P.A. Sushkov, T.M. Tyukavina, V.G. Zinovyev
Neutron Research Division, PNPI NRC "Kurchatov Institute"

The term astrobleme is closely related to the terms meteorite impact crater. Astrobleme is formed on the Earth's surface, generally in the form of a circular crater when a meteorite falls on the earth's surface. High temperature (15 000 °C) and high pressure ($5 \cdot 10^6$ atm) are the unique conditions created by the meteorite shock wave. The unique conditions form the vitreous impact melt rock (tagamite) in the crater. Sulfides, sulfoarsenides, oxides or alloy of heavy elements, Platinum Group Elements (PGE), Rare Earth Elements (REE) are separated and are accumulated with gravity as the microscopic impregnations in the lower layers of the melt at the temperature of 1 700–3 000 °C.

The Kara astrobleme is a meteor crater in the Yugorsky peninsula, Yamalo-Nenetsky region in Russia. It is 65 km in diameter and the age is estimated to be 70.3 ± 2.2 million years old. In recent years, the Geology Institute of Ural Branch of RAS started work on the study of mineral and element composition of tagamites from Kara impact structure for the purpose of substantiation of mineral formation and mineralization due to the Kara impact event. The company "Polargeo" started sampling the ore from the Kara astrobleme in order to estimate the gravity separation of the PGE, REE, Ag, Au, Ni, Co, Cr and other elements in the lower layers of the tagamite.

To study the composition and assessment of the degree of accumulation of Pt, Au, PGE and REE in the samples of tagamite and suevite we have proposed techniques of the instrumental (INAA) and radiochemical (RNAA) neutron activation analysis. An instrumental technique has allowed us to determine the weight content C of 28 elements with detection limits DL in the range from 10^{-4} to 10^{-8}% and a measuring error of 3–20%. The results of this analysis are shown in the Table 1.

For the determination of Pt and the improvement of the detection limits for Au, Re, Pd and Ir their radiochemical separation from the sample was carried out. The Figure shows the full absorption peaks for ^{199}Au, ^{186}Re, ^{188}Re and ^{99}Mo in the γ-ray spectrum of the sample analyzed in a solution of 0.2 M HCl missed through the ion exchange chromatographic column with the strongly acidic cation exchange resin Purolite C100 in the H^+-form.

Chemical yields of Au, Pt, Re, Pd and Ir in the chromatographic system, specified by the method "introduced-found", close to 100%. So, when eluent volume is 5 and 25 ml of eluate, for Au, Pt and Ir yields appeared to be equal to 88.6, 88.8 and 100%, respectively, while Re and Pd chemical yield was 95.9 and 96.7%, respectively. It was established that the volume of eluate 40–50 ml provides almost complete allocation of these elements from the sample. The Table 2 shows the results of determination of the Pt, Re, Ir and Au in rock samples from the Kara impact structure, obtained using RNAA.

In the work it is established that the cation exchange chromatographic system "Purolite C100 in H^+-form – 0.2 M HCl" can be used for separation of Pt, Re, Ir, Pd and Au from a large number of base metals. The detection limits of radiochemical techniques for the determination of Pt, Re, Ir, Au and Pd are in the range from $n \cdot 10^{-9}$ to $n \cdot 10^{-4}$% with an error of measurement 3–25%.

Table 1. The results of the INAA method for the elemental composition of rocks of the Kara impact structure

Element	Isotope	Suevite 1057 *C*, % wt	Suevite 1004 *C*, % wt	Tagamite 3000 *C*, % wt	DL, % mass
Na	^{24}Na	$1.24 \pm 5.47 \cdot 10^{-4}$	$2.51 \pm 1.53 \cdot 10^{-3}$	$1.87 \pm 7.85 \cdot 10^{-4}$	$6 \cdot 10^{-6}$
K	^{42}K	$1.9 \pm 9.61 \cdot 10^{-3}$	$1.5 \pm 2.58 \cdot 10^{-2}$	$1.71 \pm 1.27 \cdot 10^{-2}$	$1 \cdot 10^{-4}$
Rb	^{86}Rb	$6.01 \cdot 10^{-3} \pm 1.19 \cdot 10^{-3}$	$4.90 \cdot 10^{-3} \pm 7.96 \cdot 10^{-4}$	–	$5 \cdot 10^{-4}$
Cs	^{134}Cs	$1.22 \cdot 10^{-4} \pm 1.46 \cdot 10^{-5}$	$6.13 \cdot 10^{-4} \pm 1.58 \cdot 10^{-5}$	$4.03 \cdot 10^{-4} \pm 3.74 \cdot 10^{-5}$	$1 \cdot 10^{-5}$
Sr	^{85}Sr	$2.90 \cdot 10^{-2} \pm 1.16 \cdot 10^{-3}$	$2.02 \cdot 10^{-2} \pm 2.15 \cdot 10^{-3}$	$3.35 \cdot 10^{-2} \pm 2.33 \cdot 10^{-3}$	$3 \cdot 10^{-3}$
Ba	^{131}Ba	$7.24 \cdot 10^{-2} \pm 1.86 \cdot 10^{-3}$	$5.01 \cdot 10^{-2} \pm 2.94 \cdot 10^{-3}$	$6.00 \cdot 10^{-2} \pm 3.21 \cdot 10^{-3}$	$4 \cdot 10^{-4}$
Sc	^{46}Sc	$3.29 \cdot 10^{-4} \pm 1.40 \cdot 10^{-6}$	$1.71 \cdot 10^{-3} \pm 3.39 \cdot 10^{-6}$	$2.15 \cdot 10^{-3} \pm 3.65 \cdot 10^{-6}$	$3 \cdot 10^{-5}$
Cr	^{51}Cr	$2.19 \cdot 10^{-3} \pm 3.89 \cdot 10^{-5}$	$3.19 \cdot 10^{-2} \pm 1.36 \cdot 10^{-4}$	$2.23 \cdot 10^{-2} \pm 1.16 \cdot 10^{-4}$	$2 \cdot 10^{-5}$
Fe	^{59}Fe	$7.55 \cdot 10^{-1} \pm 1.78 \cdot 10^{-2}$	$5.51 \pm 5.04 \cdot 10^{-2}$	$5.4 \pm 4.20 \cdot 10^{-2}$	$5 \cdot 10^{-8}$
Co	^{60}Co	$6.02 \cdot 10^{-4} \pm 8.38 \cdot 10^{-6}$	$2.01 \cdot 10^{-3} \pm 1.63 \cdot 10^{-5}$	$2.74 \cdot 10^{-3} \pm 1.82 \cdot 10^{-5}$	$1 \cdot 10^{-8}$
Ni	^{58}Co	$2.00 \cdot 10^{-3} \pm 6.68 \cdot 10^{-4}$	$1.28 \cdot 10^{-2} \pm 1.62 \cdot 10^{-3}$	$1.36 \cdot 10^{-2} \pm 1.73 \cdot 10^{-3}$	$3 \cdot 10^{-5}$
Zn	^{65}Zn	$2.67 \cdot 10^{-2} \pm 2.83 \cdot 10^{-4}$	$1.28 \cdot 10^{-2} \pm 1.60 \cdot 10^{-3}$	–	$1 \cdot 10^{-4}$
Zr	^{97}Zr	$2.00 \cdot 10^{-2} \pm 7.96 \cdot 10^{-4}$	–	$1.16 \cdot 10^{-2} \pm 2.43 \cdot 10^{-4}$	$1 \cdot 10^{-4}$
Lu	^{177}Lu	$2.09 \cdot 10^{-5} \pm 1.19 \cdot 10^{-6}$	$3.72 \cdot 10^{-5} \pm 2.19 \cdot 10^{-6}$	$4.77 \cdot 10^{-5} \pm 2.29 \cdot 10^{-6}$	$2 \cdot 10^{-7}$
Hf	^{181}Hf	$9.15 \cdot 10^{-4} \pm 1.60 \cdot 10^{-5}$	$3.36 \cdot 10^{-4} \pm 2.29 \cdot 10^{-5}$	$5.11 \cdot 10^{-4} \pm 1.46 \cdot 10^{-5}$	$3 \cdot 10^{-6}$
Ta	^{182}Ta	$2.96 \cdot 10^{-5} \pm 3.13 \cdot 10^{-6}$	$6.92 \cdot 10^{-5} \pm 5.12 \cdot 10^{-6}$	$6.93 \cdot 10^{-5} \pm 6.16 \cdot 10^{-6}$	$1 \cdot 10^{-7}$
La	^{140}La	$1.37 \cdot 10^{-3} \pm 3.78 \cdot 10^{-5}$	$1.80 \cdot 10^{-3} \pm 4.85 \cdot 10^{-5}$	$2.33 \cdot 10^{-3} \pm 4.95 \cdot 10^{-5}$	$1 \cdot 10^{-7}$
Ce	^{141}Ce	$2.85 \cdot 10^{-3} \pm 2.35 \cdot 10^{-5}$	$4.75 \cdot 10^{-3} \pm 3.70 \cdot 10^{-5}$	$5.04 \cdot 10^{-3} \pm 3.52 \cdot 10^{-5}$	$4 \cdot 10^{-7}$
Nd	^{147}Nd	$1.30 \cdot 10^{-3} \pm 1.41 \cdot 10^{-4}$	$2.03 \cdot 10^{-3} \pm 2.31 \cdot 10^{-4}$	$2.50 \cdot 10^{-3} \pm 4.28 \cdot 10^{-4}$	$1 \cdot 10^{-5}$
Eu	^{154}Eu	$6.66 \cdot 10^{-5} \pm 3.95 \cdot 10^{-6}$	$1.38 \cdot 10^{-4} \pm 6.51 \cdot 10^{-6}$	$1.47 \cdot 10^{-4} \pm 1.05 \cdot 10^{-5}$	$7 \cdot 10^{-7}$
Gd	^{153}Gd	$1.89 \cdot 10^{-4} \pm 3.32 \cdot 10^{-5}$	–	$5.79 \cdot 10^{-4} \pm 5.55 \cdot 10^{-5}$	$2 \cdot 10^{-5}$
Tb	^{160}Tb	$8.62 \cdot 10^{-5} \pm 2.92 \cdot 10^{-6}$	$7.06 \cdot 10^{-5} \pm 4.33 \cdot 10^{-6}$	$9.73 \cdot 10^{-5} \pm 5.82 \cdot 10^{-6}$	$8 \cdot 10^{-7}$
Yb	^{177}Yb	$5.17 \cdot 10^{-4} \pm 2.03 \cdot 10^{-5}$	$2.12 \cdot 10^{-4} \pm 1.66 \cdot 10^{-5}$	$2.44 \cdot 10^{-4} \pm 1.41 \cdot 10^{-5}$	$5 \cdot 10^{-6}$
Th	^{233}Th	$3.23 \cdot 10^{-4} \pm 2.68 \cdot 10^{-5}$	$4.44 \cdot 10^{-4} \pm 6.17 \cdot 10^{-5}$	$7.81 \cdot 10^{-4} \pm 4.58 \cdot 10^{-5}$	$4 \cdot 10^{-6}$
U	^{239}U	$1.56 \cdot 10^{-4} \pm 1.36 \cdot 10^{-5}$	$2.11 \cdot 10^{-4} \pm 1.61 \cdot 10^{-5}$	$3.37 \cdot 10^{-4} \pm 1.76 \cdot 10^{-5}$	$1 \cdot 10^{-6}$
As	^{76}As	$6.12 \cdot 10^{-4} \pm 5.34 \cdot 10^{-6}$	$8.57 \cdot 10^{-4} \pm 9.17 \cdot 10^{-6}$	$1.12 \cdot 10^{-3} \pm 7.00 \cdot 10^{-6}$	$8 \cdot 10^{-6}$
Br	^{82}Br	–	$3.73 \cdot 10^{-4} \pm 3.24 \cdot 10^{-5}$	$1.55 \cdot 10^{-4} \pm 1.72 \cdot 10^{-5}$	$9 \cdot 10^{-7}$
Sb	^{124}Sb	$5.95 \cdot 10^{-5} \pm 2.47 \cdot 10^{-6}$	$4.84 \cdot 10^{-5} \pm 4.26 \cdot 10^{-6}$	$7.88 \cdot 10^{-5} \pm 4.80 \cdot 10^{-6}$	$5 \cdot 10^{-7}$

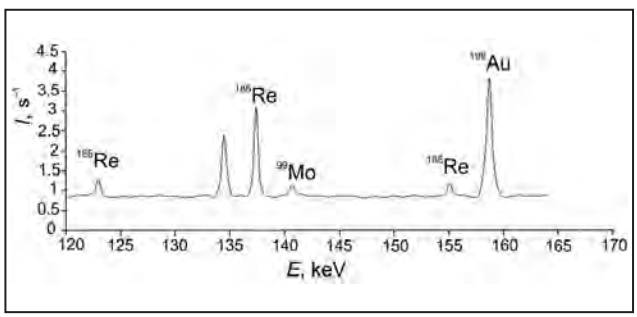

The full absorption peaks for ^{199}Au, ^{186}Re, ^{188}Re and ^{99}Mo in the γ-ray spectrum of the sample analyzed

Table 2. The contents of Pt, Re, Au (% wt) in samples of rocks of the Kara impact structure

Sample	Pt	Re	Ir	Au
Suevite 1057	$3.1 \cdot 10^{-6} \pm 1.2 \cdot 10^{-6}$	$3.1 \cdot 10^{-5} \pm 5.5 \cdot 10^{-6}$	$3.2 \cdot 10^{-7} \pm 8 \cdot 10^{-8}$	$7.5 \cdot 10^{-9} \pm 1.9 \cdot 10^{-9}$
Suevite 1004	$9.7 \cdot 10^{-6} \pm 2.1 \cdot 10^{-6}$	–	$7.8 \cdot 10^{-8} \pm 2 \cdot 10^{-8}$	$1.5 \cdot 10^{-6} \pm 1.4 \cdot 10^{-8}$
Tagamite 3000	–	$4.6 \cdot 10^{-5} \pm 3.8 \cdot 10^{-6}$	$2.9 \cdot 10^{-8} \pm 6.3 \cdot 10^{-9}$	$9.2 \cdot 10^{-6} \pm 1.6 \cdot 10^{-7}$

Zinovyev V.G., Egorov A.I., Shulyak G.I., Sushkov P.A., Tyukavina T.M., Mitropolsky I.A., Sakharov S.L., Okunev I.S., Loginov Yu.E. // J. Radioanal. Nucl. Chem. 2016. V. 307. P. 1315–1324.

Ultracold neutron source based on superfluid helium at the WWR-M reactor

A.V. Chechkin, A.K. Fomin, S.A. Ivanov, A.G. Kharitonov, V.A. Lyamkin, D.V. Prudnikov, A.P. Serebrov, M.E. Tchaikovsky
Neutron Research Division, PNPI NRC "Kurchatov Institute"

At present the project of Ultracold Neutron (UCN) source has been developed for the WWR-M reactor at PNPI NRC KI. The project is based on the use of superfluid helium for UCN production. The UCN source has to be placed in the thermal column near the reactor core. The task of helium maintaining in superfluid state at temperature of 1.0–1.5 K at conditions of reactor irradiation is extremely hard because the heat load is 15–20 W. It is a very high heat load for this level of temperatures. Due to the need to check the possible solutions of such an extreme task, a full-scale model of the source has been created, which includes all necessary cryogenic, vacuum equipment and a cryostat of the UCN source. Superfluid helium is received (Fig. 1) on a full-scale model.

After the practical experiments were performed on the technological complex of UCN source the following results were obtained: 1) trouble-free operation of

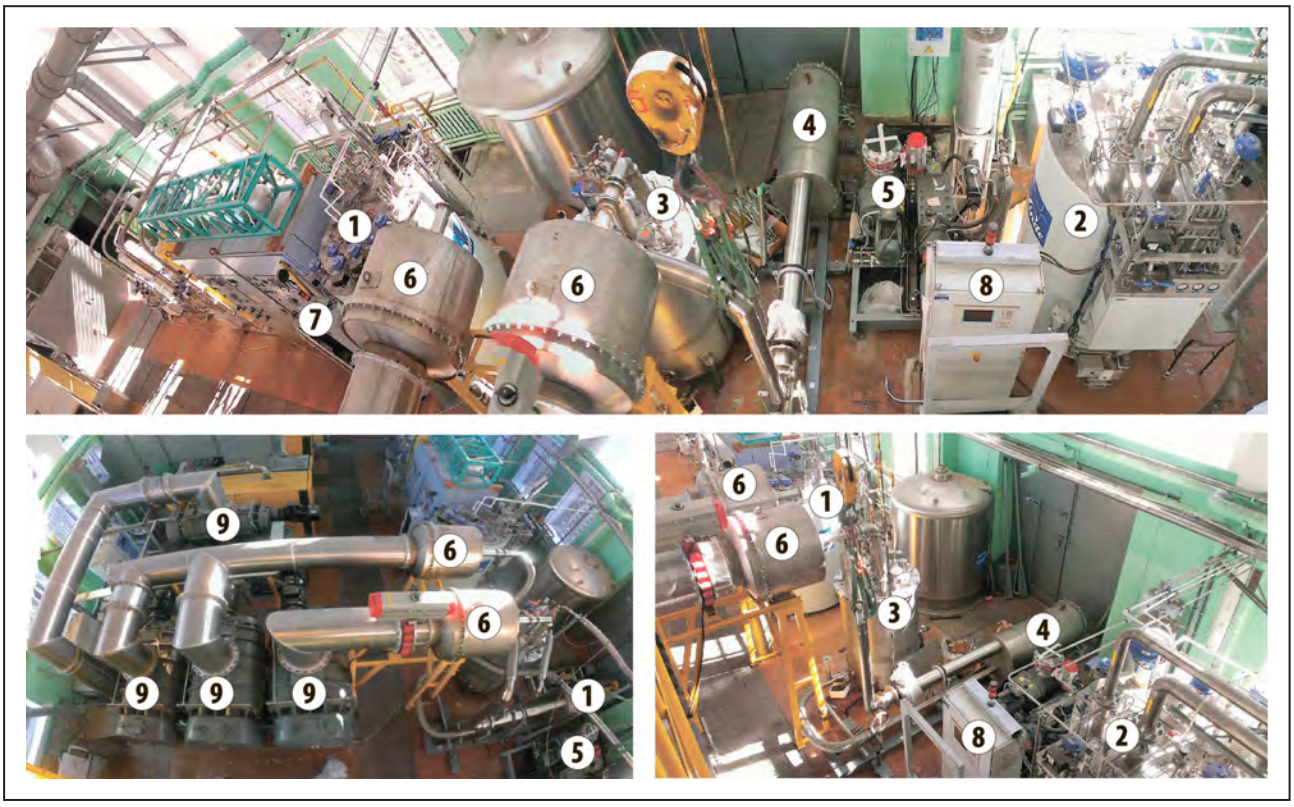

Fig. 1. Full-scale model of UCN-source at the WWR-M reactor: 1 – helium liquefier L-280 (98 l/h); 2 – helium refrigerator TCF-50 (3 000 W), 3 – helium cryostat (T = 1.08 K); 4 – model of UCN-source; 5 – vacuum pump of isotope pumping; 6 – heaters of helium vapors; 7 – box of liquefier management L-280; 8 – box of refrigerator management TCF-50; 9 – vacuum pumps EDWARDS HV30000

all technological complex of UCN source with maintenance of working temperature and level of helium in UCN source model bathtub is ensured; 2) temperature T = 1.08 K is obtained without heat load; 3) temperature T = 1.29 K is obtained with heat load P = 15 W. It is a very important result which shows possibility of realization of the project of UCN source at the WWR-M reactor and possibility of use of superfluid helium in nuclear technologies.

It would seem natural to assume it possible in the future to obtain an even higher UCN density at the high-flux reactor PIK. However, careful examination of the issue shows this is not so. PIK reactor is good for thermal and cold neutrons, but WWR-M reactor is better for UCN because it has the thermal column. In our work comparative calculations of two projects – for the WWR-M reactor and for the PIK reactor were carried out. Calculations show, that it is possible to obtain UCN density of $1.3 \cdot 10^4$ cm^{-3} in the trap of EDM-spectrometer with UCN source in the thermal column of the WWR-M reactor, and $1.3 \cdot 10^3$ cm^{-3} in the extracted beam of the PIK reactor. Therefore, the UCN source in the thermal column of the WWR-M reactor is ten times more effective (Fig. 2).

The difference lies in the fact that at the PIK reactor the UCN-source based on superfluid helium can only be situated in the extracted neutron beam. But transition to the scheme in the extracted beam of the PIK reactor leads immediately to a loss in the initial neutron flux density, which is proportional to the solid angle of the beam relative to 4π (about four orders of magnitude).

The implementation of the UCN source project with superfluid helium at the WWR-M reactor in Russia will allow the construction of the best UCN source in the world, whose intensity is about 100 higher than that achieved at the best UCN source in the international neutron center at the ILL reactor in Grenoble, France.

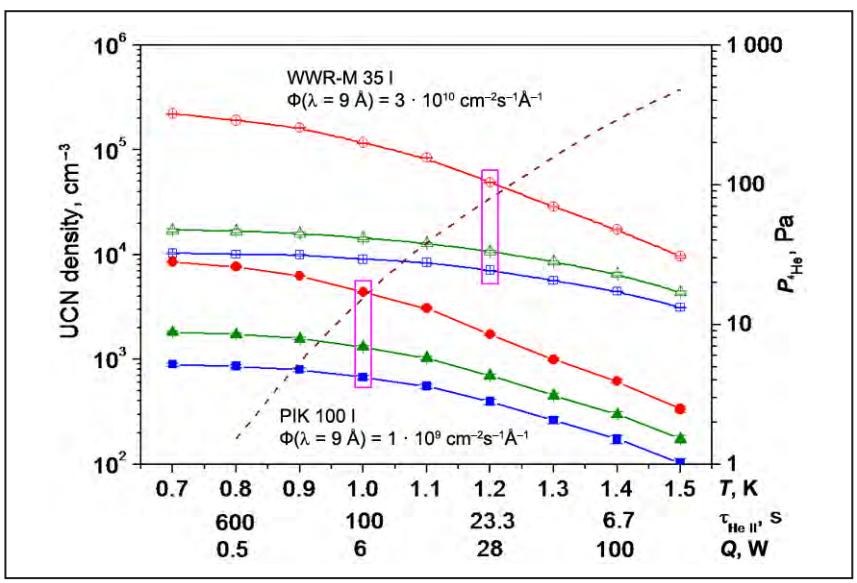

Fig. 2. Comparison of UCN densities in different traps for UCN-source projects at the WWR-M reactor and at the PIK reactor: ● – closed source chamber; ▲ – trap with a volume of 35 l; ■ – trap with a volume of 350 l. The dotted line is the temperature dependence of the saturated helium vapor pressure. On abscissa axis except temperature are shown: neutron lifetime in superfluid helium and the power which can be removed at this temperature for the fixed pumping speed

1. *Serebrov A.P.* // Physics-Uspekhi. 2015. V. 185. Iss. 11. P. 1179.
2. *Serebrov A.P., Fomin A.K., Kharitonov A.G. et al.* // Vestnik of Saint Petersburg University. Ser. 4. 2015. V. 2 (60). Iss. 1. P. 27–41.
3. *Serebrov A.P., Fomin A.K.* // Tech. Phys. 2015. V. 60. P. 1238.

Research Based on the Use of Protons and Ions. Neutrino Physics

Pentaquarks observation in the LHCb experiment

LHCb Collaboration
G.D. Alkhazov, N.F. Bondar, A.A. Dzyuba, O.E. Maev, N.R. Sagidova, Yu.A. Shcheglov, A.A. Vorobyev – High Energy Physics Division, PNPI NRC "Kurchatov Institute"

In the traditional quark model, the strongly interacting particles (hadrons) are formed either from quark-antiquark pairs (mesons) or three quarks (baryons). The existence of other (colourless) combinations, for example tetraquarks ($qq\bar{q}\bar{q}$) or pentaquarks ($qqqq\bar{q}$), are not forbidden by QCD first principles. On the other hand, up to now only one observed state $Z(4430)^+$ was reliably classified as an exotic (tetraquark) state.

A great achievement of the LHCb experiment in 2015 was the observation of the pentaquark – particle, which consists of four quarks and one antiquark. The decay of the Λ_b^0-baryon (particle with the *udb*-quark content) into a proton (*uud*) and K^- ($s\bar{u}$) and J/ψ ($c\bar{c}$) mesons was investigated. During the Large Hadron Collider Run 1, a high purity sample of approximately 26 000 events of this decay was collected. It was expected that the main contribution into $\Lambda_b^0 \to J/\psi p K^-$ decay is given by the processes with production of intermediate Λ^*-resonances, which later decay into pK^-. At the same time, the data demonstrate also another intermediate channel $\Lambda_b^0 \to K^- P_c^+(\to pJ/\psi)$, where a new heavy particle P_c^+ is produced together with the K^--meson (Fig. 1).

The data could not be satisfactorily described with conventional hadrons from the traditional quark model, including fourteen Λ^*-resonances. In order to get a satisfactory description of the data, two new pentaquark resonances were added in the multidimensional event-by-event amplitude analysis. The first one has a mass of 4 449.8 ± 1.7 ± 2.5 MeV and a width of 39 ± 5 ± 19 MeV, while the second one is wider, with a mass of 4 380 ± 8 ± 29 MeV and a width of 205 ± 18 ± 86 MeV (Fig. 2). The statistical significance of these resonances is 12 and 9 standard deviations, respectively. The amplitude analysis prefers the opposite parity for these states and gives restrictions on their spins.

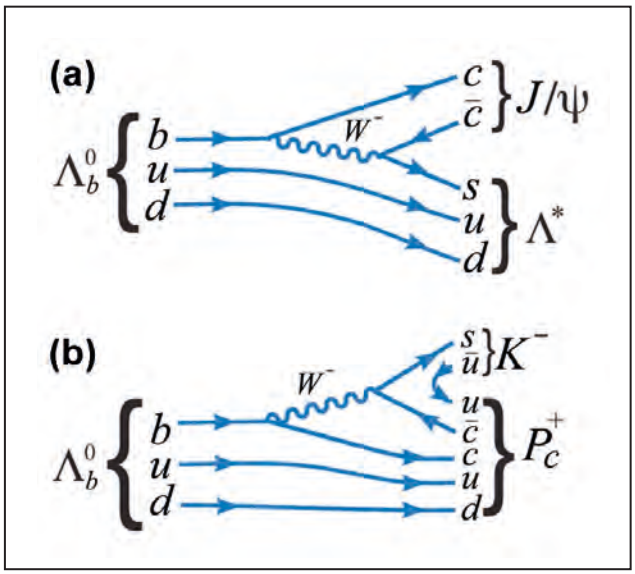

Fig. 1. Feynman diagrams corresponding to $\Lambda_b^0 \to J/\psi\Lambda^*(\to pK^-)$ (a) and $\Lambda_b^0 \to K^- P_c^+(\to pJ/\psi)$ (b) decays

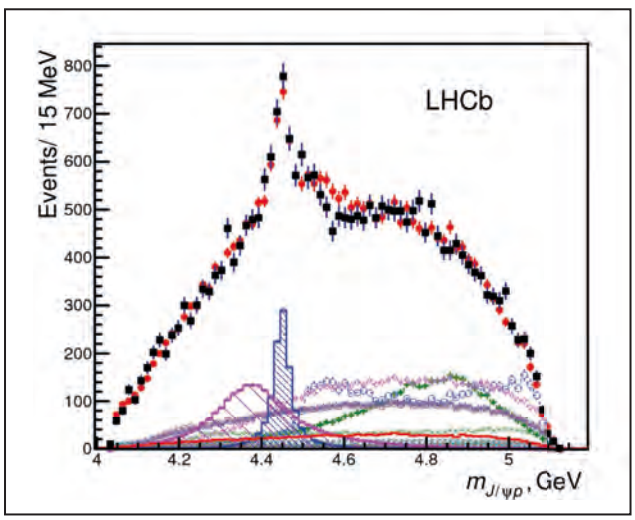

Fig. 2. Invariant mass distribution for the pJ/ψ-system. Experimental data are presented by the black points while the best result of the full amplitude analysis of the $\Lambda_b^0 \to J/\psi p K^-$ decay is shown by red. Hatched histograms indicate contributions from the pentaquark states

LHCb Collaboration // Phys. Rev. Lett. 2015. V. 115. P. 072001.

Combined measurement of the Higgs boson mass in the ATLAS and CMS experiments at the Large Hadron Collider

A.E. Ezhilov, O.L. Fedin, V.T. Grachev, M.P. Levchenko, V.P. Maleev, V.A. Schegelsky, V.M. Solovyev (ATLAS Collaborations); V.L. Golovtsov, Yu.M. Ivanov, V.T. Kim, E.V. Kuznetsova, P.M. Levchenko, V.A. Murzin, V.A. Oreshkin, I.B. Smirnov, V.V. Sulimov, L.N. Uvarov, S.A. Vavilov, A.A. Vorobyev (CMS Collaborations) – High Energy Physics Division, PNPI NRC "Kurchatov Institute"

The main result of the ATLAS and CMS experiments at the moment is the discovery in 2012 of the Higgs boson with a mass of about 125 GeV, a scalar quantum of the fundamental vacuum field which is responsible for spontaneous symmetry breaking of electroweak interactions and for the mass origin of elementary particles in the Standard Model (SM). The main parameter of the SM Higgs boson is the value of its mass. In 2015, the ATLAS and CMS experiments for the first time presented the results of the combined measurements of the mass of the Higgs boson based on 2010–2012 data. In ATLAS and CMS, the Higgs boson is now observed in all major SM modes of bosonic and fermionic decays. For the mass measurement of the Higgs boson, the most significant Higgs decay modes into bosons were used: decays into two photons $H \to \gamma\gamma$ and decays into two Z-bosons (into four charged leptons) $H \to ZZ \to 4l$, where $l = \mu, e$ (Fig. 1).

The measured mass of the Higgs boson in the combined analysis of the ATLAS and CMS experiments is 125.09 ± 0.21 (stat.) ± 0.11 (syst.) GeV. The consistency of the signal strength $\mu = \sigma\mathrm{Br}/(\sigma\mathrm{Br})_{\mathrm{SM}}$ (the ratio of the measured value of the product of the cross section and the branching ratio to the value expected in the SM) is shown in Fig. 2.

In summary, the new result, obtained in the combined analysis of the ATLAS and CMS experiments, is in even better agreement with the SM expectations than the results of the individual experiments.

An important role in the Higgs boson discovery and in its property measurements was played by the End-Cap Muon detector in the CMS (EMU system) and the Central Tracker of the ATLAS, the Transition Radiation detector (TRT system), where PNPI NRC KI has made a significant contribution to its designs, constructions and technical supports.

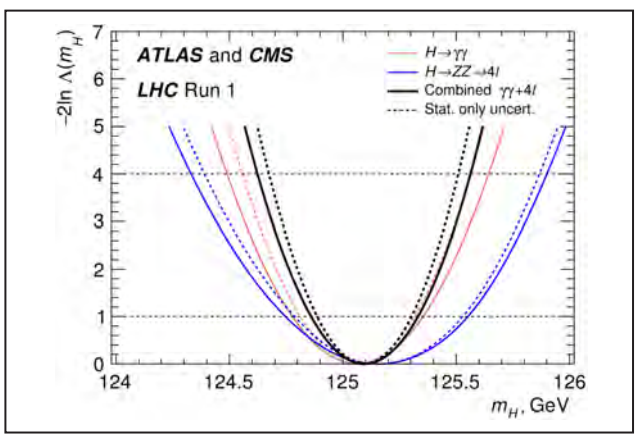

Fig. 1. Likelihood function $-2\log(\Delta m_H)$ is shown as a function of the SM Higgs boson mass in the combined analysis of ATLAS and CMS data for the major decay modes $H \to \gamma\gamma$ (blue curves) and $H \to ZZ \to 4l$ (red curves). Black curves show the results for both modes. The dashed curves show the results which take into account statistical uncertainties only, with the fixed best-fit values of the parameters responsible for systematic uncertainties

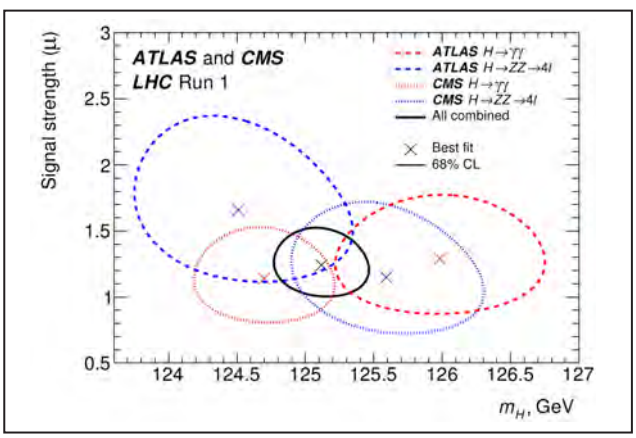

Fig. 2. Signal strength $\mu = \sigma\mathrm{Br}/(\sigma\mathrm{Br})_{\mathrm{SM}}$ (the ratio of the measured value of the product of the cross section and the branching ratio to the value expected in the SM) is shown as function of the Higgs boson mass. The dashed curves show the results of the ATLAS and CMS experiments in the corresponding decay modes with the 68% confidence level regions, and the solid curve shows the region of the combined analysis. The markers indicate the best-fit values

ATLAS and CMS Collaborations // Phys. Rev. Lett. 2015. V. 114. P. 191803.

A search for solar axions produced in M1-transition of ^{83}Kr nucleus

A.V. Derbin
Neutron Research Division, PNPI NRC "Kurchatov Institute"

An axion is a hypothetical particle that was introduced in theory as an attempt to solve the strong *CP*-problem, and which also is commonly considered as a viable dark matter candidate. If the axions do actually exist, then the Sun should be an intense source of these particles.

The research groups from the PNPI NRC KI low-background measurements laboratory and Institute for Nuclear Research (INR) of the Russian Academy of Sciences performed the search for the resonant absorption of 9.4 keV axions, produced by M1-transition of ^{83}Kr nuclei in the Sun: $A + {}^{83}Kr \rightarrow {}^{83}Kr^* \rightarrow {}^{83}Kr + \gamma$ (9.4 keV). In order to detect γ-quanta and electrons produced by the discharge of the nuclear level a proportional ionization chamber was used. The chamber was filled with gaseous Krypton and installed inside the low-background setup located at the underground laboratory at the Baksan Neutrino Observatory of INR RAS. As a result, the new limit on the isoscalar and isovector axion-nucleon coupling constants was obtained $|g_{AN}^{3} - g_{AN}^{0}| \leq 1.29 \cdot 10^{-6}$. The interpretation of this limit within the "hadronic" axion theoretical model yields the new limit on the axion mass: $m_A \leq 100$ eV (95% c. l.).

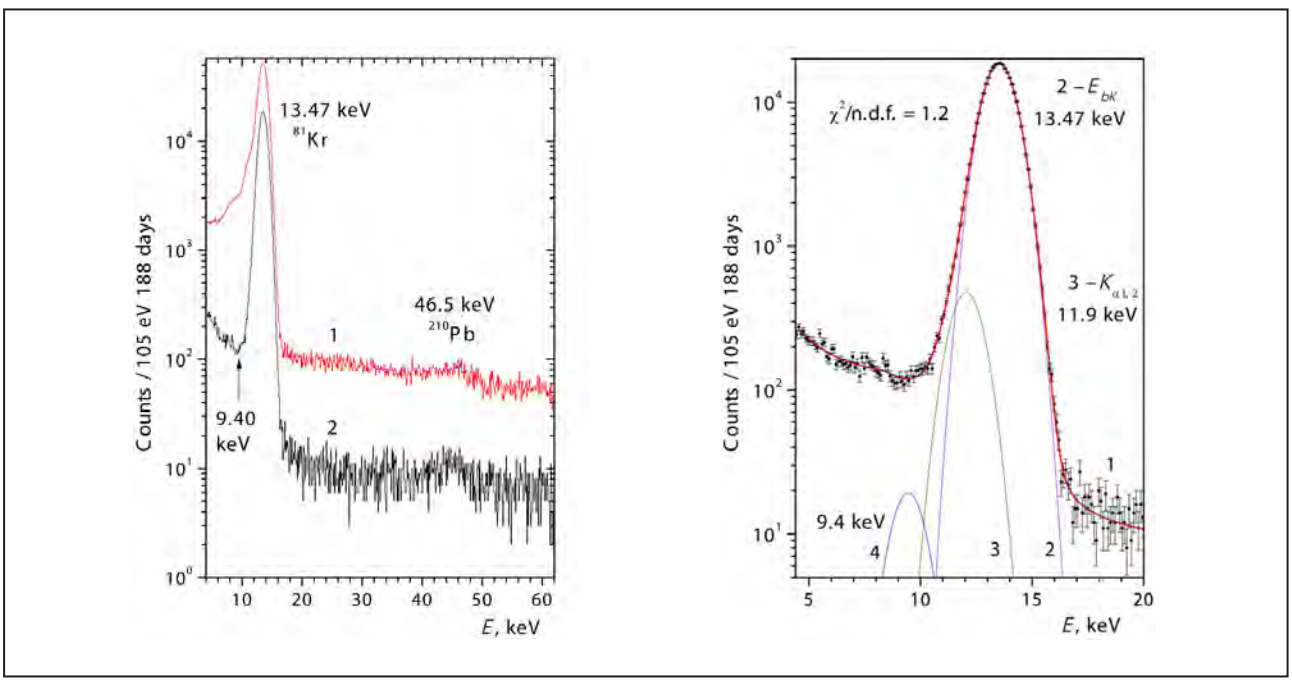

The energy spectra measured by Kr-chamber during 188.3 days of exposure (*left*): 1 – all registered events;
2 – signal rise time and primary/secondary pulse amplitude ratio cuts applied.
Fit results (*right*): 1 – events from the central part of the chamber; 2, 3 – Gaussians, describing the characteristic *X*-ray peaks of Br and Kr;
4 – the expected 9.4 keV axion peak (the intensity corresponds to the upper limit on the number of resonant absorption events)

1. *Gavrilyuk Yu.M. ..., Derbin A.V., Drachnev I.S., Muratova V.N. ..., Semenov D.A. ..., Unzhakov E.V. et al.* // JETP Lett. 2015. V. 101. No. 10. P. 664–669.
2. *Gavrilyuk Yu.M. ..., Derbin A.V. ..., Muratova V.N. ..., Semenov D.A. ..., Unzhakov E.V.* // Phys. Part. Nucl. 2015. V. 46. P. 152.

Measurement of quark coupling strength $|V_{ub}|$

LHCb Collaboration
G.D. Alkhazov, N.F. Bondar, A.A. Dzyuba, O.E. Maev, N.R. Sagidova, Yu.A. Shcheglov, A.A. Vorobyev – High Energy Physics Division, PNPI NRC "Kurchatov Institute"

In the Standard Model of particle physics, the transition of one quark to a quark with another flavor is mediated by the $W^{\pm}$-boson emission. This process is described by the 3 · 3 unitary Cabibbo–Kobayashi–Maskawa (CKM-matrix). The element $|V_{ub}|$, which describes the decay of a *b*-quark to a *u*-quark, is the smallest in the CKM-matrix with the highest uncertainty up to date. The most precise measurements of $|V_{ub}|$ have been performed by the Belle and BaBar experiments in two different ways – inclusive and exclusive. The difference between the two ways of $|V_{ub}|$ determination is approximately three standard deviations. This discrepancy is an intriguing puzzle in flavor physics.

In 2015, the LHCb experiment at the Large Hadron Collider presented a new method of the $|V_{ub}|$ determination based on the measurement of the branching fraction of the $\Lambda_b^0 \to p\mu\bar{\nu}_\mu$ decay (Fig. 1).

The baryonic decay was used for the measurement of $|V_{ub}|$ for the first time. The first observation of this decay was possible because of the high integrated luminosity collected by LHCb. Due to kinematical reasons, the events of the $\Lambda_b^0 \to p\mu\bar{\nu}_\mu$ decay have high invariant masses in the proton-muon system (Fig. 2).

This provides a way to discriminate the signal events from the background. Combined with theoretical calculations of the strong interaction and a previously measured value of $|V_{cb}|$ element, the determined $|V_{ub}|$ value is:

$$|V_{ub}| = (3.27 \pm 0.15_{exp} \pm 0.16_{\mathrm{LQCD}} \pm 0.06_{V_{cb}}) \cdot 10^{-3}.$$

The obtained result is in agreement with previous exclusive measurements. Due to the different spin of the Λ_b^0-baryon compared to the *B*-mesons used previously, the new measured value of $|V_{ub}|$ disfavors the explanation of the tension between exclusive and inclusive ways by introducing of a new particle, in addition to the *W*-boson, contributing to the quark transition. The new $|V_{ub}|$ measurement will have a significant impact on the global fits to the parameters of the CKM-matrix, whose values are connected by unitarity relations.

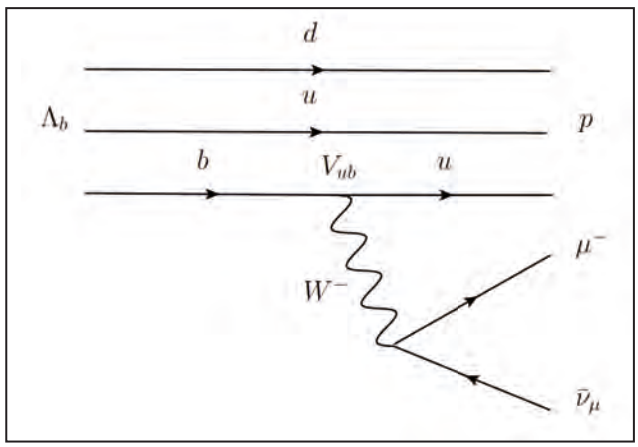

Fig. 1. Feynman diagram for the $\Lambda_b^0 \to p\mu^-\bar{\nu}_\mu$ decay

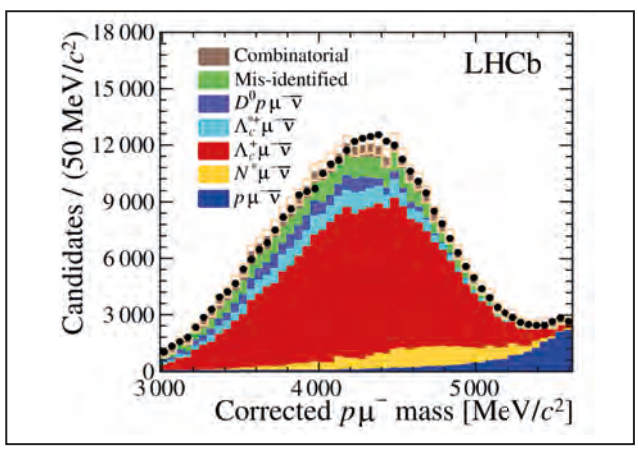

Fig. 2. Proton-muon invariant mass corrected on the flight direction of the Λ_b^0-baryon. Colored histograms demonstrate contributions of the process of interest and different sources of the background

LHCb Collaboration // Nature Phys. 2015. V. 11. P. 743.

HERMES experiment and baryon spin structure

HERMES Collaboration
S.L. Belostotski, G.E. Gavrilov, A.A. Izotov, A.Yu. Kisselev, P.V. Kravchenko, A.G. Krivschich, S.I. Manaenkov, O.V. Miklukho, Yu.G. Naryshkin, D.O. Veretennikov, V.V. Vikhrov – High Energy Physics Division, PNPI NRC "Kurchatov Institute"

Measurements of the European Muon Collaboration (EMC) showed that only a small fraction of proton (neutron) spin is carried by quarks. The total quark and antiquark spin in the nucleon (singlet axial charge $a_0 = \Delta\Sigma_q = 0.12 \pm 0.09_{exp} \pm 0.14_{theor}$) was found compatible with zero. This unexpected result, the so called "spin crisis", together with other poorly investigated aspects of spin physics, motivated the HERMES experiment, which was commissioned at DESY (Hamburg) in 1995. In the experiment, the quark and gluon polarizations and their orbital motions in the nucleon were investigated with the help of the 27.6 GeV longitudinally polarized positron (electron) beam of the HERA accelerator scattered off the polarized H, D or ^{3}He gas target. After integration of the measured spin-dependent structure functions, it has been obtained $\Delta\Sigma_q = 0.330 \pm 0.025_{exp} \pm 0.028_{theor}$. An important question about the strange quark polarization was also answered in this study: the "strange sea" was found to be weakly polarized opposite to the nucleon spin direction: $\Delta q_S = -0.085 \pm 0.008_{exp} \pm 0.009_{theor}$. Independently, in semi-inclusive reactions with pion and kaon production the value $\Delta\Sigma_q = 0.347 \pm 0.024_{exp} \pm 0.066_{theor}$ has been obtained by summing up the contributions from quarks of various flavours. Here the explored range of the Bjorken scaling variable was limited by its minimum value of 0.023. Polarization of gluons, an intriguing question of the nucleon spin structure, was measured using a possibility to enhance the sensitivity to gluons by selection of inclusively produced hadrons with high transverse momenta. It was obtained $\Delta g/g = 0.071 \pm 0.034$.

Using formulas of the SU(6)-symmetry rotation and proceeding from the value of $\Delta\Sigma_q$ and the flavour decomposition measured for the proton, one can determine the quark spin structure of any member of the spin-1/2 baryon octet. Thus, for the Λ-hyperon $\Delta u/u = \Delta d/d = -0.16$, $\Delta s/s = 0.64$, i. e., the light quarks are noticeably polarized opposite to the Λ-spin. On the other hand, it is commonly agreed that the light quark polarization in the Λ-hyperon is close to zero. The light quark contribution can be estimated by measuring the spin transfer to the Λ from the longitudinally polarized lepton beam. The integrated number of the spin transfer $D^{\Lambda}_{Lz} = 0.074 \pm 0.039$ obtained by HERMES is compatible with zero which confirms the second ("classical") variant of the Λ-spin structure.

Effects of "the transverse spin" like Collins fragmentation and Sivers distribution functions, as well as the generalized parton distributions, the spin-dependent vector meson production and some other interesting topics were also intensively studied by HERMES. Albeit the data taking period is over, the data analysis and paper publications are still going on. The PNPI NRC KI contribution to the experiment was essential at all its stages.

1. *HERMES Collaboration* // Eur. Phys. J. C. 2015. V. 75. Iss. 12. P. 600.
2. *HERMES Collaboration* // Eur. Phys. J. C. 2015. V. 75. Iss. 8. P. 361.
3. *HERMES Collaboration* // Phys. Rev. D. 2015. V. 91. No. 5. P. 057101.

Polarization structure in the reaction $p + {}^{40}Ca \rightarrow p' + X$ at the energy 1 GeV

G.M. Amalsky, V.A. Andreev, G.E. Gavrilov, A.A. Izotov, A.Yu. Kisselev, N.G. Kozlenko, P.V. Kravchenko, M.P. Levchenko, O.V. Miklukho, D.V. Novinsky, A.N. Prokofiev, A.V. Shvedchikov, S.I. Trush, A.A. Zhdanov
High Energy Physics Division, PNPI NRC "Kurchatov Institute"

The polarization (P) in the inclusive reaction $p + {}^{40}Ca \rightarrow p' + X$ at 1 GeV was studied at the PNPI NRC KI synchrocyclotron as a function of the scattered proton momentum (K). The measurements were performed using a precision magnetic spectrometer equipped with a multiwire-proportional chambers polarimeter.

The measured polarization demonstrates an appreciable growth at $K > 1\,590$ MeV/c (Fig.). The latter cannot be explained by scattering off uncorrelated nuclear nucleons. Note that in the considered momentum range a contribution from this scattering is strongly suppressed since an uncorrelated nucleon should have a momentum much higher than the Fermi momentum ($K_F \sim 250$ MeV/c). A structure observed in the polarization data more probably can be related to scattering off nucleon clusters (correlations) in the ${}^{40}Ca$ nucleus consisting of a few correlated nucleons.

The dotted line segments in the Figure cover the K intervals in which the polarization has different values. This difference is possibly due to quasielastic scattering off the different nucleon correlations. K_2, K_3 and K_4 correspond to the final proton momenta in the scattering off the ${}^2H$-, ${}^3He$-, and ${}^4He$-like immovable clusters. The width of the momentum intervals mentioned above is determinated by motion of the correlations. The polarization in the quasielastic scattering off the four-nucleon cluster is somewhat smaller than that in the free elastic scattering on the ${}^4He$ nucleus. This can apparently be related to modification of proton-nucleon interaction in the ${}^{40}Ca$ nucleus due to relativistic distortion of the nucleon spinor in the nuclear medium.

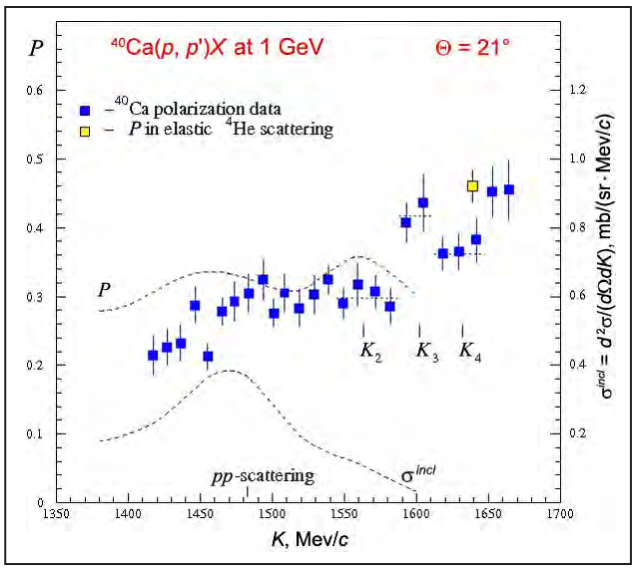

Dashed curves correspond to polarization P and differential cross section σ^{incl} calculated in the framework of the spin-dependent Distorted Wave Impulse Approximation taking into account modification of the nucleon spinor in the nuclear medium. Reaction kinematics: at $K > 1\,480$ MeV/c, the four-momentum Q transferred to the nucleus is practically constant and equal to 600 MeV/c ($Q > 2\,K_F$)

Miklukho O.V., Kisselev A.Yu., Amalsky G.M., Andreev V.A., Gavrilov G.E., Izotov A.A., Kozlenko N.G., Kravchenko P.V., Levchenko M.P., Novinskiy D.V., Prokofiev A.N., Shvedchikov A.V., Trush S.I., Zhdanov A.A. // JETP Lett. 2015. V. 102. No. 1. P. 11–13.

High-precision measurements of π–p elastic differential cross sections

EPECURE Collaboration
V.A. Andreev, E.A. Filimonov, V.V. Golubev, A.B. Gridnev, N.G. Kozlenko, V.S. Kozlov, A.G. Krivshich, D.V. Novinsky, V.V. Sumachev, V.I. Tarakanov, V.Yu. Trautman – High Energy Physics Division, PNPI NRC "Kurchatov Institute"

Differential cross sections for elastic scattering of positive and negative pions on protons were measured with high precision in the momentum interval 800–1 200 MeV/c with the set-up EPECURE at the ITEP accelerator pion beam. The total systematic errors were not larger than 2.6%. About 10 000 experimental points were obtained. The data demonstrate two narrow resonance structures at the energies $W \approx 1.686$ and $W \approx 1.720$ GeV. A tentative analysis indicates that these two structures can be described as two narrow (~ 25 MeV wide) resonances. The accuracy of the received data permits to define them accordingly as S_{11}- and P_{11}-resonances. The latter $P_{11}(1720)$ resonance is observed for the first time and can be considered as a good candidate to pentaquarks.

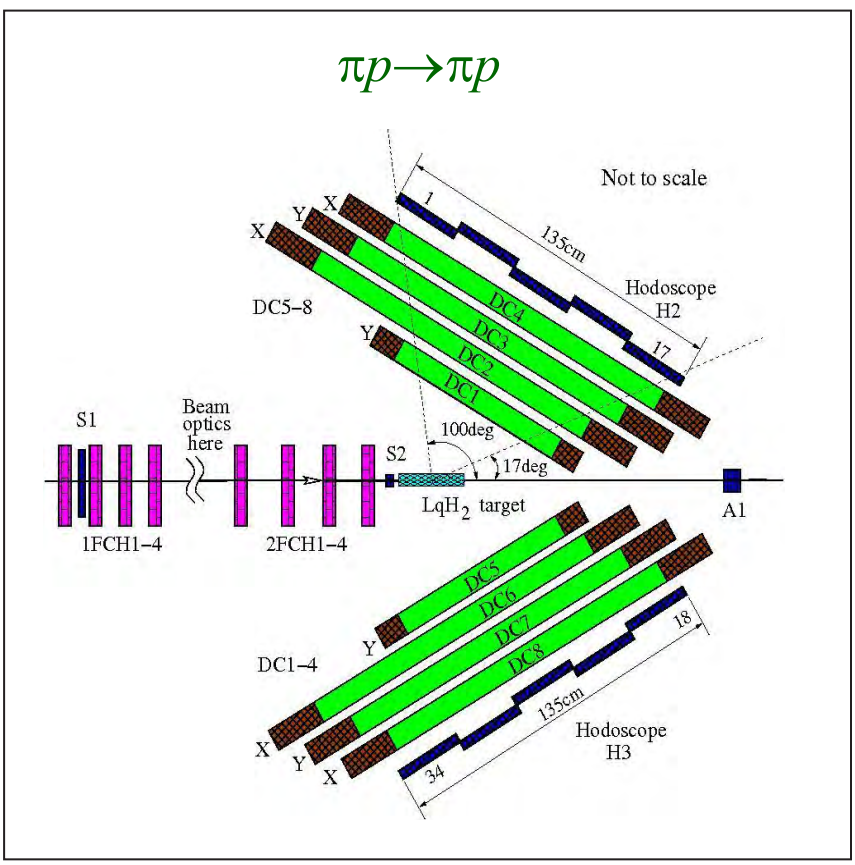

Set-up for measuring π-p elastic scattering:
1FCH1-4, 2FCH1-4 – proportional chambers with 1 mm pitch in the first focus and in front of the target;
LqH_2 – liquid hydrogen target;
DC1–DC8 – modules of drift chambers;
S1, S2, A1 – scintillation counter of a trigger;
H2, H3 – hodoscope counters

Andreev V.A. et al. // Phys. Rev. C. 2015. V. 91. P. 025205.

Long-range correlations in collisions of light and heavy nuclei at $\sqrt{s_{NN}}$ = 200 GeV

PHENIX Collaboration
V.V. Baublis, D.A. Ivanischev, L.M. Kochenda, A.V. Khanzadeev, B.G. Komkov, D.O. Kotov, V.G. Ryabov, Yu.G. Ryabov, V.M. Samsonov, A.E. Shevel –
High Energy Physics Division, PNPI NRC "Kurchatov Institute"

Recently, the PHENIX Collaboration, where NRC KI is represented by groups from PNPI NRC KI, NRC KI and Institute for High Energy Physics (IHEP), discovered a very intriguing phenomenon in collisions of ultrarelativistic light and heavy nuclei at $\sqrt{s_{NN}}$ = 200 GeV. A noticeable correlation was observed between two effects – significant collective flows of hadrons and the double-ridge structure observed in events with high multiplicity of the produced particles. Both these phenomena were observed earlier in ultrarelativistic heavy ion collisions at the Relativistic Heavy Ion Collider (RHIC) and at the Large Hadron Collider (LHC). The discovery of the elliptic flow of hadrons formed at the early stage of ultrarelativistic heavy ion collisions was considered as one of the key signatures of formation of the new state of matter – Quark-Gluon Plasma (QGP) with properties of nearly ideal strongly-interacting liquid characterized by a very low ratio of shear viscosity to entropy. The double-ridge structure, which reveals existence of significant azimuthal correlations between hadrons separated by some rapidity interval, was also successfully explained by collective hydrodynamic flows resulting from large pressure gradients in the hot and dense partonic medium formed in the overlap region of the colliding ultrarelativistic heavy ions. The study of interactions of ultrarelativistic light and heavy nuclei with selection of high multiplicity events was motivated by observation of double-ridge structures in proton-nucleus collisions at the LHC, as shown in Fig. 1.

One can expect that the similarity of the double-ridge phenomenon found in *p*A- and AA-collisions is due to their common nature. Hence, the collective flows of hadrons could also be revealed in ultrarelativistic collisions of light and heavy nuclei. In particular, one of the most interesting cases is ^{3}He + Au collisions where a different initial geometry of the interaction zone, realized due to symmetry properties of ^{3}He, can result in formation of the elliptic and triangular flows. Figure 2 shows an example of azimuthal correlations measured by PHENIX in 5% of the most central ^{3}He + Au collisions for charged particles separated in pseudorapidity by $\Delta\eta \approx 3$.

The correlation function $C(\Delta\phi, p_T)$ is fit to a four-term Fourier cosine expansion:

$$C(\Delta\phi, p_T) = 1 + \Sigma_{n=1}^{4}\, 2c_n(p_T)\cos(n\Delta\phi),$$

where $\Delta\phi$ is the difference of the azimuthal angles for two particles. Each of the components and their

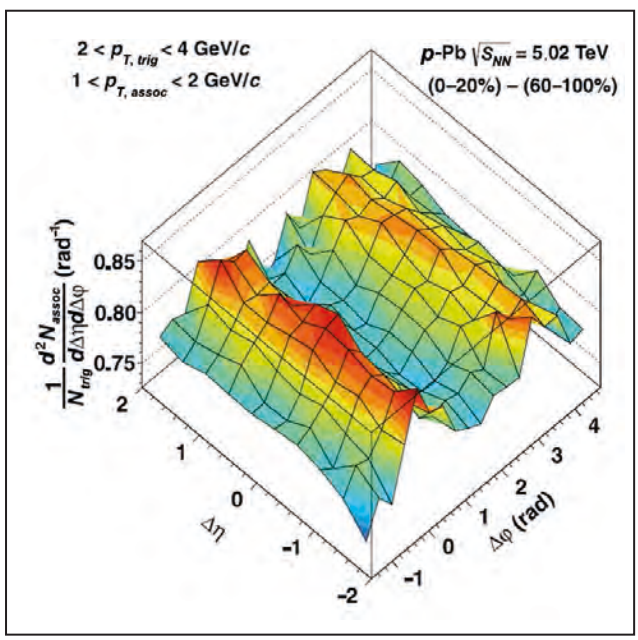

Fig. 1. Double ridge structure observed by ALICE at the LHC in high multiplicity *p*-Pb collisions at $\sqrt{s_{NN}}$ = 5.02 GeV

sum are shown in Fig. 2. In the most central ^{3}He + Au collisions, one can see a clearly visible enhancement of near-side pairs, producing a local maximum in the distribution at $\Delta\phi \approx 0$, described by the quadrupole component of the anisotropy shown with the red dotted curve.

The azimuthal anisotropy of the produced particles can be quantified by the Fourier coefficients v_n in the expansion of the particle distribution as

$$dN/d\phi = N_0 \{1 + \Sigma_{n=1} 2v_n \cos(n(\phi - \Psi_n))\},$$

where n is the harmonic order, ϕ is the azimuthal angle of the particle and Ψ_n is the azimuthal angle of the corresponding reaction plane. Figure 3 shows elliptic (v_2) and triangular (v_3) flows measured for inclusive charged hadrons at the midrapidity $|\eta| < 0.35$ in dependence on the transverse momentum.

The obtained results reveal presence of long-range correlations between the charged hadrons in the most central ^{3}He + Au collisions at $\sqrt{s_{NN}}$ = 200 GeV. A sizeable value of the v_3 flow is observed supporting an idea that the hot spots formed by the impact of the three ^{3}He nucleons on the Au nucleus expand hydrodynamically to generate the triangular flow. The measured values of v_2 and v_3 flows can be described only by the theoretical models that assume hydrodynamic expansion of the produced system, which can be considered as an indication of formation of spots of low-viscosity quark-gluon plasma with a typical size of the ^{3}He nucleus in the central ^{3}He + Au collisions.

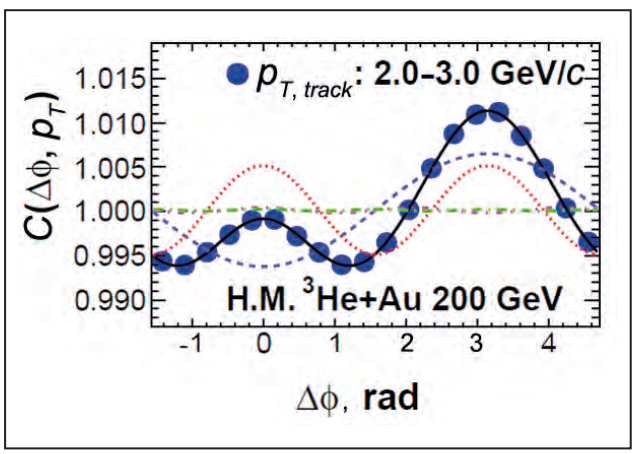

Fig. 2. Azimuthal correlation measured in 5% of the most central ^{3}He + Au collisions at $\sqrt{s_{NN}}$ = 200 GeV. Blue circles – experimental results; blue dashed and red dotted curves are dipole and quadrupole components of the Fourier expansion

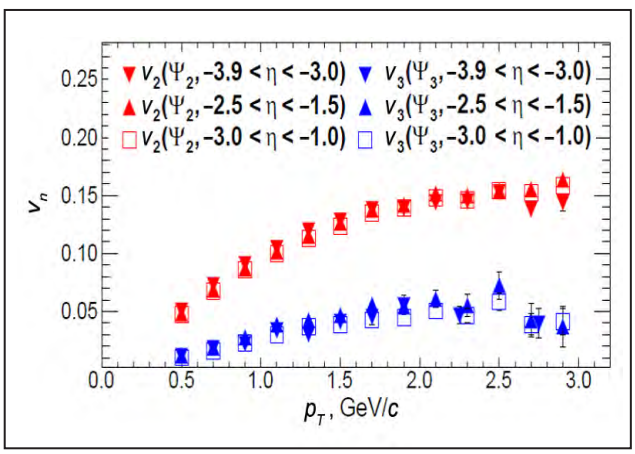

Fig. 3. Elliptic (v_2) and triangular (v_3) flows measured for charged hadrons in the most central ^{3}He + Au collisions at $\sqrt{s_{NN}}$ = 200 GeV

Direct high-precision mass-difference measurement of ^{163}Ho and ^{163}Dy with a Penning trap

Collaborations SHIPTRAP and TRIGATRAP
S.V. Chenmarev, S.A. Eliseev, P.E. Filianin, Yu.N. Novikov –
High Energy Physics Division, PNPI NRC "Kurchatov Institute"

The nuclide ^{163}Ho is characterized by the smallest decay energy in the capture process. Therefore, it is the best candidate for a neutrino mass determination. The neutrino mass limit determined so far is 225 eV, whereas for the antineutrino it is less than 2 eV. A considerable progress in the Penning Trap Mass Spectrometry, as well as in the Cryogenic Microcalorimetry, has allowed one to put forward an idea to combine both methods for the neutrino mass determination. The neutrino mass can be obtained from the bolometric de-excitation spectrum with a use of the exact value of the decay energy Q_{EC} measured with a Penning trap. This concept is being realized in the ECHo-1 project. Meanwhile, the first pilot bolometric measurements have shown that the derived Q_{EC}-value differs dramatically (by more than 7σ) from 2.56(2) keV – the value evaluated in literature (Fig.). To solve this puzzle, direct measurements of the mass difference ^{163}Ho–^{163}Dy were undertaken with the Penning trap mass spectrometer SHIPTRAP (GSI, Darmstadt). The collaboration had developed beforehand a technique for a production of ^{163}Ho at the ILL reactor in Grenoble, for its careful chemical and mass-spectrometric separation and for manufacturing of a holmium target with subsequent probing measurements at TRIGATRAP (Mainz). High-precision measurements of the cyclotron frequencies of singly charged ^{163}Ho and ^{163}Dy ions in SHIPTRAP have been performed with the novel phase-imaging method. The obtained result of 2 833(35) eV is in good agreement with 2 800(60) eV determined by microcalorimetry (see the filled box in the Fig.). This result confirms the validity of the concept for the neutrino mass determination proposed. It paves the way to the mass determination at a level of 1 eV, or even better. However, higher intensity sources of ^{163}Ho with advanced microcalorimetry and the new ultra-precise Penning trap mass spectrometer PENTATRAP should be used within the frame-work of the project ECHo-2.

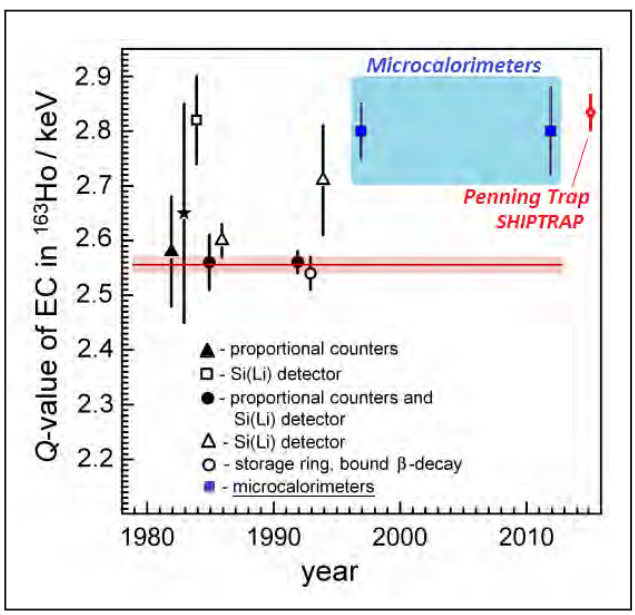

Comparison of the new SHIPTRAP measurement with other results

1. *Gastaldo L. et al.* // Low Temp. Phys. 2014. V. 176. P. 876.
2. *Schneider F. et al.* // Eur. Phys. J. A. 2015. V. 51. P. 89.
3. *Eliseev S. et al.* // Phys. Rev. Lett. 2015. V. 115. P. 062501.

Test of *CPT*-symmetry in light nuclear systems in the ALICE experiment

ALICE Collaboration
V.V. Ivanov, A.V. Khanzadeev, E.L. Kryshen, V.N. Nikulin, M.V. Malaev, V.G. Ryabov, Yu.G. Ryabov, V.M. Samsonov, M.B. Zhalov – High Energy Physics Division, PNPI NRC "Kurchatov Institute"

One of the most fundamental symmetries of quantum field theory is formulated in terms of the *CPT*-theorem, which states that all physical phenomena are invariant under the simultaneous time reversal (*T*), charge conjugation (*C*) and parity transformation (*P*). A direct consequence of the *CPT*-theorem is equality of the particle and its antiparticle masses. Presently, this equality has been tested in the weak interaction in the boson sector to the unprecedented precision of $\delta M(K^0\overline{K}^0) \leq 5 \cdot 10^{-19}$ GeV using the measurements of neutral kaon decays in the KLOE experiment. In the baryon sector, the most precise test of the *CPT*-symmetry comes from the measurement of the mass-to-charge ratios for protons and antiprotons: $R = m_{\bar{p}}Z_{\bar{p}}/m_pZ_p = -0.999999999839(90)$. Note that this value deviates by 1.8σ from the $R = -1.0$ followed from the *CPT* invariance; the ATRAP collaboration plans to measure this quantity with a higher precision.

In 2015, the ALICE collaboration, where NRC KI is represented by groups from PNPI NRC KI, NRC KI, Institute for High Energy Physics and Institute for Theoretical and Experimental Physics, published in the journal Nature Physics the results of the measurements of yields of D, ^{3}He, $\overline{\text{D}}$, $^3\overline{\text{He}}$ nuclei in Pb-Pb collisions at $\sqrt{s_{NN}}$ = 2.76 TeV. An important

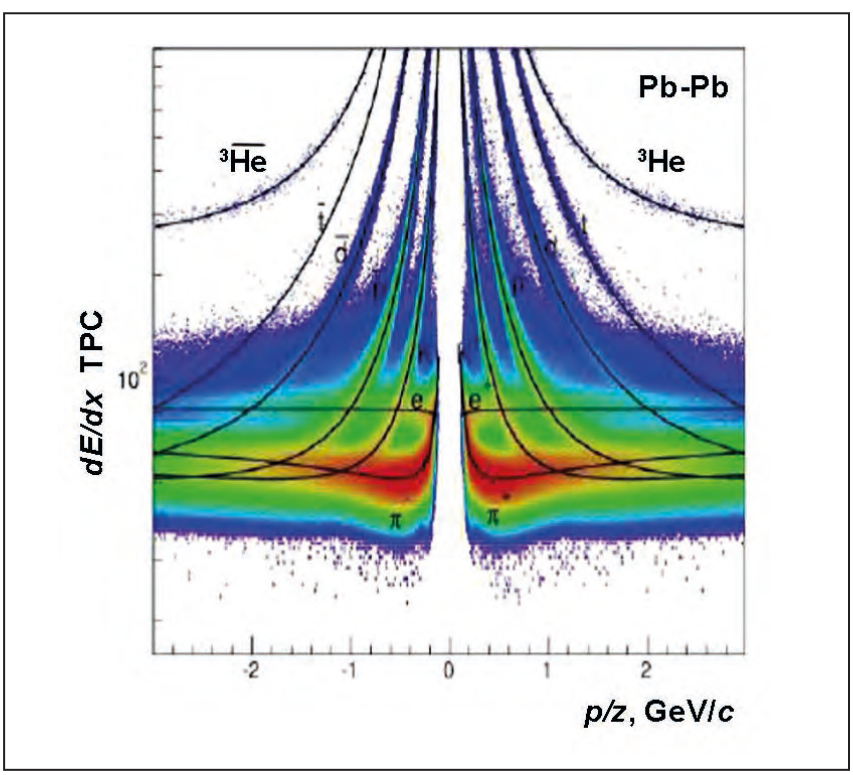

Fig. 1. Identification of nuclei and antinuclei using their energy losses in the ALICE detector

feature of the ALICE detector is that it allows one not only to reliably identify tracks of nuclei and antinuclei (Fig. 1), but also to measure the track length, the particle time-of-flight and the rigidity (the momentum-to-charge ratio) of its trajectory in the magnetic field. Hence, it enables one to determine the masses of light nuclei and antinuclei assuming that the magnitudes of their charges are equal.

As a result, it was obtained that the differences in the mass-to-charge ratios for nuclei and antinuclei are consistent with zero within the experimental uncertainties, which are at the level of $3 \cdot 10^{-4}$ for the D–$\overline{\text{D}}$ system and $3 \cdot 10^{-3}$ for the ^{3}He–$^3\overline{\text{He}}$ system (Fig. 2, *left*).

Along with the obtained masses of nuclei and antinuclei, the binding energies of these systems were also calculated using the CODATA recommended values for the nucleon and antinucleon masses. The difference of the binding energies of the nuclei and antinuclei is consistent with zero within the experimental uncertainties (Fig. 2, *right*). Note that for the ^{3}He–$^3\overline{\text{He}}$ system, this estimate has been obtained for the first time. These results demonstrate that within the experimental uncertaities, the effective nuclear forces responsible for formation of the ground-state of light nuclei do not violate the *CPT*-symmetry.

It is important to emphasize that a test of *CPT* invariance in light nuclear systems was not considered as one of the priority problems of the ALICE experiment aimed at studies of the mechanisms and the properties of the quark-gluon matter created in central collisions of ultrarelativistic nuclei at the LHC. The results presented above have been obtained due to the unique capabilities of the ALICE detector and the LHC. One can anticipate that the analysis of the data collected in 2015–2017 at the increased luminosity and the higher collision energy will enable one not only to significantly improve the existing estimates, but also to measure with high precision the difference between the masses of the nucleus and the antinucleus of ^{4}He and to estimate the limits for violation of *CPT* invariance in bound four-nucleon systems.

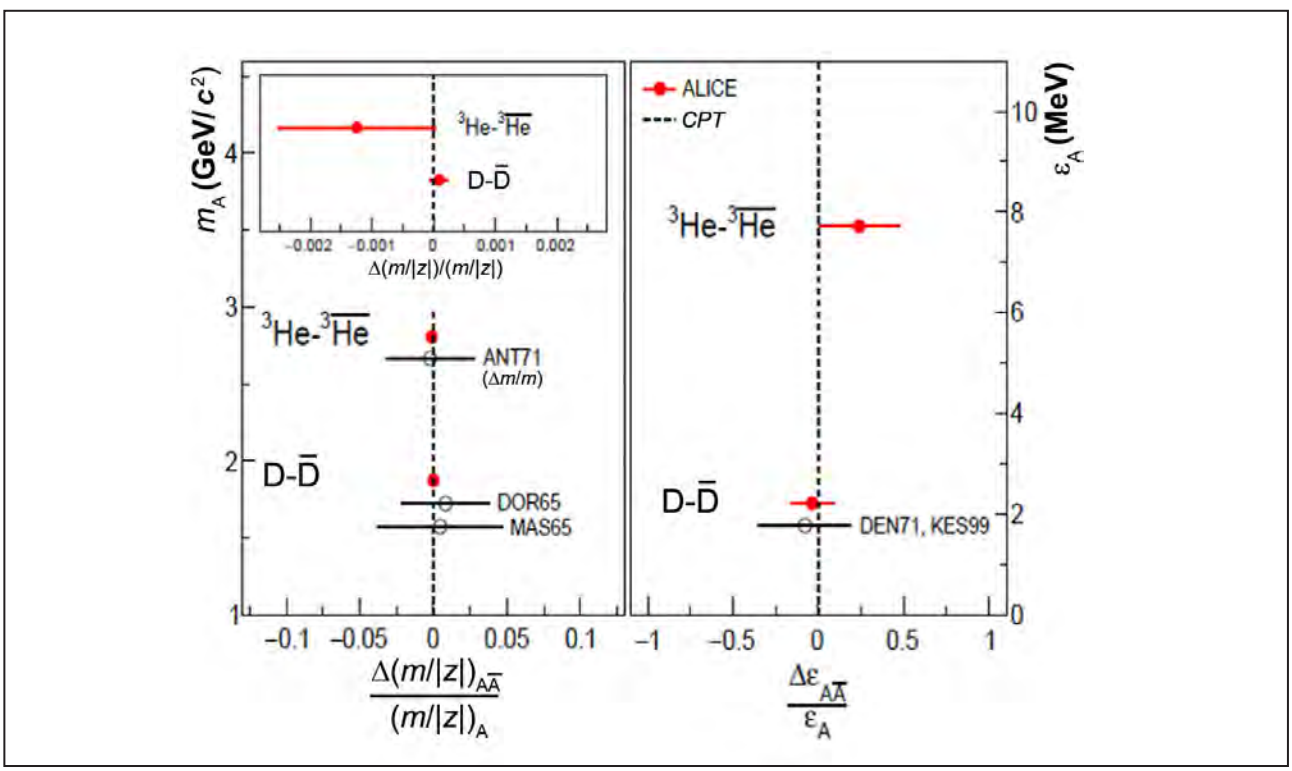

Fig. 2. The measured difference of the mass-to-charge ratios for nuclei and antinuclei (*left*). The measured difference of the binding energies of nuclei and antinuclei (*right*)

ALICE Collaboration // Nature Phys. 2015. V. 11. P. 811–814.

Changes in the mean square charge radii and electromagnetic moments of neutron-deficient Bi nuclei

Experiments ISOLDE (CERN) and IRIS (PNPI NRC KI)
A.E. Barzakh, L.Kh. Batist, D.V. Fedorov, V.S. Ivanov, P.L. Molkanov, F.V. Moroz, S.Yu. Orlov, V.N. Panteleev, M.D. Seliverstov, Yu.M. Volkov –
High Energy Physics Division, PNPI NRC "Kurchatov Institute"

Understanding the shape evolution and shape coexistence in atomic nuclei is one of the greatest challenges faced by theories of nuclear structure. The neutron-deficient isotopes near $Z = 82$ exhibit the richest manifestation of shape evolution shape coexistence phenomena. The behavior of the ground and isomeric states shape differs markedly for different Z nuclei in this region. While in the Hg isotopic chain ($Z = 80$) the jump-like odd-even shape staggering was observed at $N < 106$, for Po nuclei ($Z = 84$) an early onset and gradual increase of deformation was found at $N < 113$. At the same time, the neutron-deficient Pb and Tl nuclei ($Z = 82, 81$) remain essentially spherical, up to and beyond the neutron mid-shell at $N = 104$. The investigations of neutron-deficient Bi isotopes ($Z = 83$) plays an important role in understanding of the shape evolution and shape coexistence phenomena in this region of the nuclide chart. Nuclei of these isotopes reveal, along with the near spherical ground states, the presence of oblate and prolate structures resulting from the occupancy of $\pi i_{13/2}$ and $\pi s_{1/2}$ orbitals. Observables that give a model-independent information on the ground and isomeric states shape are charge radius changes determined by the atomic spectroscopy. So far, atomic spectroscopy measurements for a restricted set of bismuth isotopes $^{202-213}$Bi have been performed. The previous laser spectroscopic investigations ended at $N = 119$, well before $N = 112$ where the structural change in the adjacent Po isotopic chain occurs. It is of importance to extend these studies towards the mid-shell.

The available data for the magnetic moments of different Bi nuclear states are presented and compared with the magnetic moments of the adjacent Tl isotopes/isomers with the same spin (Fig. 1). The newly measured magnetic moments follow the isotopic trend for the heavier nuclei with the same spin fairly well. At the same time, within the error bars limits they do not differ from the magnetic moments of the corresponding Tl nuclei. It should be noted that nuclear states with the same spin in Tl and Bi are of different nature: $\pi h_{9/2}$ state is normal for Bi and an intruder ($1p–2h$) for Tl nuclei; $\pi s_{1/2}$ state is an intruder ($2p–1h$) for Bi and normal for Tl nuclei. Therefore, the newly measured magnetic moments of Bi nuclei support the observation that the sensitivity of μ to the normal or intruder character of the nuclear state is very low.

Relative radii changes $\delta\langle r^2\rangle$ (RDRs) for even-neutron Bi isotopes are compared with those for even-neutron Pb isotopes (Fig. 2a). Bismuth RDRs follow Pb-trend until $N = 110$ and markedly deviate from this trend at $N < 110$. It was shown previously that

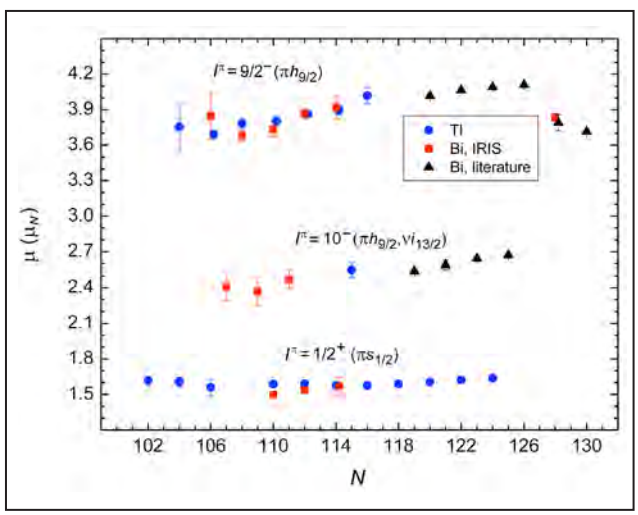

Fig. 1. Magnetic moments for Bi and Tl isotopes and isomers. Squares – Bi, present paper; triangles – Bi, literature data; circles – Tl

thallium RDRs perfectly follow Pb-trend even beyond the mid-shell (N = 104) whereas polonium RDRs display a substantial deviation which was interpreted as the onset of deformation at N < 113. One can conclude therefore that the deformation change for even-neutron Bi isotopes is "intermediate" between the ones for $_{82}$Pb and $_{84}$Po. At the same time, the RDR evolution (i. e. the shape evolution) in the Bi and Tl isotopic chains differs from each other, although these chains are "mirrors" in respect to the filled proton shell (Z = 82). One can also see that intruder Bi isomers (I = 1/2) have bigger radii (deformation) than the corresponding ground states. A similar behavior was observed previously for Tl intruder isomers (I = 9/2). At the same time, the radii trend of the odd-neutron Bi isotopes does not deviate noticeably from the radii trend for Pb (Fig. 2b). It is worth noting recent shell-model calculations indicate a spherical Bi ground state down to ^{193}Bi, while the deviation from the calculations observed in the lighter isotopes was attributed to the onset of deformation. Some structural change between ^{193}Bi and ^{191}Bi was also previously observed. These assumptions are supported by our results for $\delta\langle r^2\rangle$.

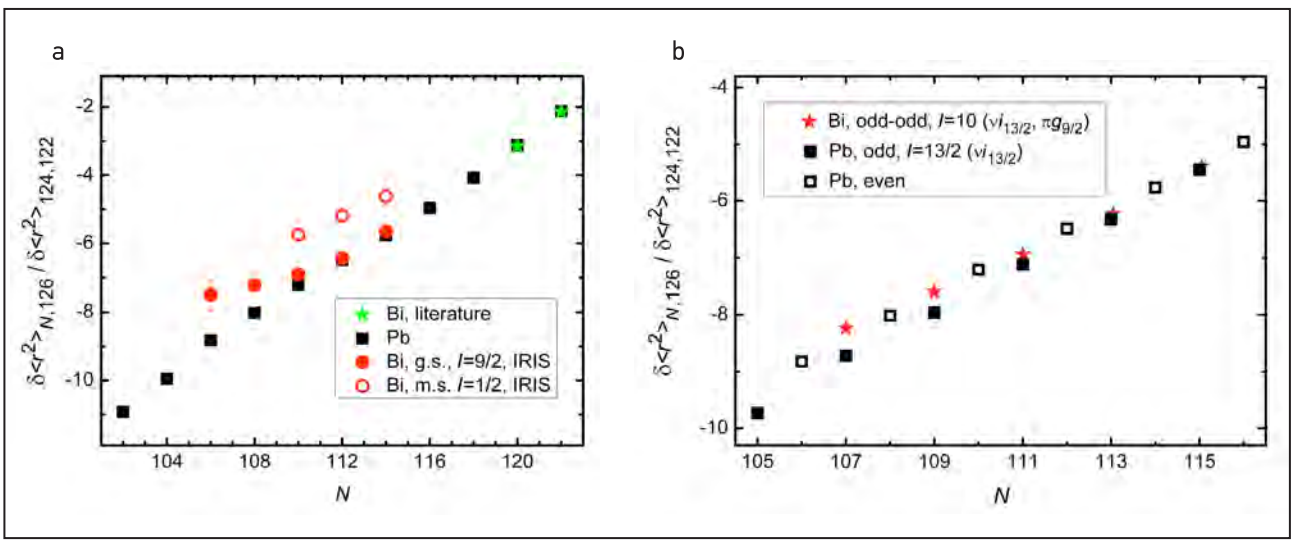

Fig. 2. Relative changes in $\delta\langle r^2\rangle$ for even-neutron lead and Bi isotopes (a): boxes – even Pb isotopes; full circles – odd Bi ground states with I = 9/2; open circles – odd Bi isomers with I = 1/2. Relative changes in $\delta\langle r^2\rangle$ for odd-neutron lead and Bi isomers (b): stars – Bi isomers with I = 10, configuration ($\nu i_{13/2}$, $\pi h_{9/2}$) (present paper); full boxes – odd-neutron Pb isomers with I = 13/2, configuration $\nu i_{13/2}$; open boxes – the values for even-neutron Pb isotopes are also presented

1. *Seliverstov M.D. et al.* // Phys. Rev. C. 2014. V. 89. P. 034323.
2. *Barzakh A.E., Batist L.Kh., Fedorov D.V., Ivanov V.S., Molkanov P.L., Moroz F.V., Orlov S.Yu., Panteleev V.N., Seliverstov M.D., Volkov Yu.M.* // AIP Conf. Proc. 2015. V. 1681. P. 030011.

New data from the geo-neutrino study at the Borexino experiment

A.V. Derbin
Neutron Research Division, PNPI NRC "Kurchatov Institute"

Geo-neutrinos are the electron anti-neutrinos, produced by the β-decays of uranium and thorium decay chains that take place inside the Earth. In order to detect such anti-neutrinos the reaction of inverse β-decay is used: $\nu + p \rightarrow e^{+} + n$. Two sequential events, occurring within the time window determined by the lifetime of neutrons in the scintillator (250 μs), allow one to effectively register this reaction. The main advantages of the Borexino experimental setup are the low levels of the background components connected with reactor anti-neutrinos, cosmic muons and natural radioactivity.

In 2015 the Borexino collaboration published the data of the measured geo-neutrino flux at the Gran Sasso National Laboratory accumulated during 2 056 days of exposure time. The total amount of 77 anti-neutrino events was registered, among which 24 events proved to be geo-neutrino events. By calculating the expected geo-neutrino flux from the Earth crust, it became possible for the first time to reliably establish the presence of the geo-neutrino flux from the mantle, which is important for studying the inner structure of the Earth. The number of reactor anti-neutrinos (53) registered at the record-breaking distance from the reactors (over 500 km) is in good agreement with the oscillation solution.

The results were obtained with active participation of Russian researchers from PNPI NRC KI, Joint Institute for Nuclear Research and Skobeltsyn Institute of Nuclear Physics of Lomonosov Moscow State University.

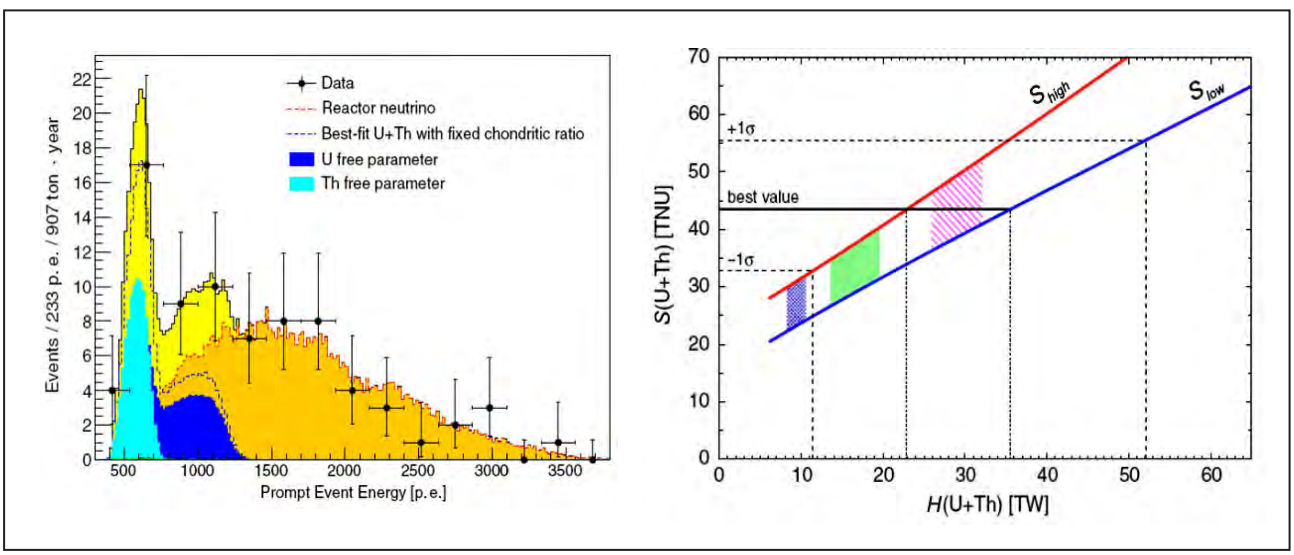

On the left – anti-neutrino spectrum containing 77 events. Light- and dark-blue regions denote neutrinos produced by Th and U decay chains correspondingly. Red line shows the contribution of reactor neutrinos.
On the right – the dependence of the geo-neutrino registration rate *S* (in TNU units – 1 event per 10^{32} protons per year) on the heat power *H*, produced inside the Earth, for different models (denoted by color). The most probable *S* value, obtained by the experiment, corresponds to the heat generation *H* of 23–36 TW, which should be compared to the overall heat power of Earth *H* = (47 ± 2) TW

Agostini M. et al. (Borexino Collaboration) // Phys. Rev. D. 2015. V. 92. P. 031101.

Creation of neutrino laboratory for carrying out experiment on search for a sterile neutrino at the SM-3 reactor

A.V. Chernyi, A.K. Fomin, V.G. Ivochkin, L.N. Matrosov, M.Yu. Matrosova, R.M. Samoilov, A.P. Serebrov, V.A. Solovei, M.E. Tchaikovsky, M.E. Zaytsev, O.M. Zherebtsov, V.G. Zinov'ev – Neutron Research Division
V.L. Golovtsov , N.V. Gruzinskii, P.V. Neustroev – High Energy Physics Division,
PNPI NRC "Kurchatov Institute"
V.P. Martem'yanov, V.G. Tsinoev, V.G. Tarasenkov, V.I. Aleshin – NRC "Kurchatov Institute"
V.V. Afanas'ev, M.O. Gromov, A.L. Izhutov, S.V. Pavlov, A.L. Petelin,
D.K. Ryazanov, S.A. Sazontov – JSC "SSC RIAR"

To check the existence of a sterile neutrino, a neutrino laboratory aimed at searching reactor antineutrino oscillations is created at the SM-3 reactor. A prototype of a neutrino detector with a scintillator volume of 400 l is moved at distances 6–11 m from the reactor core (Fig. 1).

The background of cosmic rays depends on the distance from the reactor core because of the distribution of concrete masses of the building. Furthermore, the background of cosmic rays varies over time owing to fluctuations of the atmospheric pressure and temperature in the lower layers of the atmosphere.

The use of the active shielding makes it possible to reduce the correlated background of cosmic rays only by 66%. This is apparently the muon component of the background of cosmic rays and can be controlled by the active shielding. The neutron component is hardly controlled by the active shielding; for this reason, it is necessary to separate signals from recoil protons and positrons according to the pulse shape.

Fig. 1. General view of the passive shielding from neutrino detector at the SM-3 reactor outside (*left*) and inside (*right*)

Background conditions are measured. It is shown that the cosmic rays background is the main problem in the experiment. Test measurements of dependence of reactor antineutrino flux on distance to the reactor core are carried out.

After cosmic rays background studies, measurements were made of antineutrino flux from SM-3 reactor and its distance dependence. Difference of correlated signals measurements depending on distance with the reactor on and off is presented in Fig. 2a. Treatment of the same data on deviation from the $1/R^2$ law is shown in Fig. 2b. So far statistical accuracy with model of the detector is not enough for any conclusions. Increase by order of magnitude in volume of the detector is required.

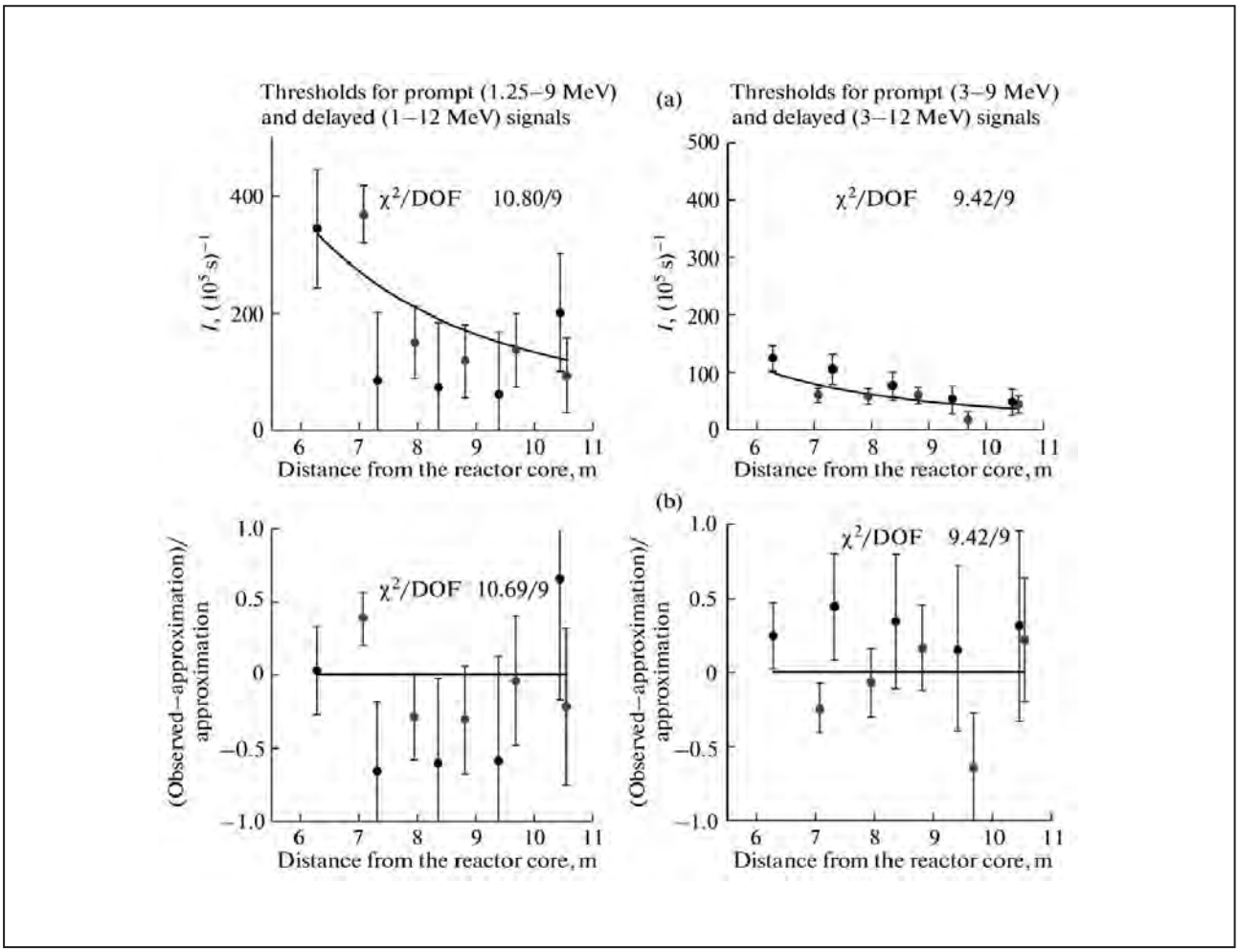

Fig. 2. a) Difference between the count rates of correlated events in the cases of the working and stopped reactor: for prompt signals in an energy range of 1.25–9 MeV (*left panel*) and 3–9 MeV (*right panel*) and for delayed signals in an energy range of 1–12 MeV (*left panel*) and 3–12 MeV (*right panel*).
b) Deviation of the data shown in panel from the $1/R^2$ law. The black and grey points were obtained with the first and last (current) versions of the active shielding

1. *Serebrov A.P.* // Physics-Uspekhi. 2015. V. 185. P. 1179.
2. *Serebrov A.P., Ivochkin V.G., Samoylov R.M. et al.* // JETP. 2015. V. 121. P. 578.
3. *Serebrov A.P., Ivochkin V.G., Samoylov R.M. et al.* // Technic. Phys. 2015. V. 60. P. 1863.

Observation of the Large Hadron Collider beam channeling in bent crystals

UA9 Collaboration
A.S. Denisov, Yu.A. Gavrikov, Yu.M. Ivanov, L.P. Lapina, L.G. Malyarenko, V.V. Skorobogatov – High Energy Physics Division, PNPI NRC "Kurchatov Institute"

The UA9 experiment is a part of the PNPI NRC KI-CERN Collaboration program. The main goal of the experiment is the design and study of crystal collimation of Large Hadron Collider (LHC) beams within the program of the LHC luminosity increase. Groups from PNPI NRC KI, Institute for High Energy Physics and Joint Institute for Nuclear Research are the Russian participants of the experiment. The recent 10 year studies carried out at the PNPI NRC KI synchrocyclotron and at the CERN SPS accelerator have created the base for application of crystal collimation in the high energy hadron colliders. It has been shown that bent silicon crystals in the channeling regime used as primary collimators may significantly reduce the beam halo, thus reducing irradiation of the critical zones in the accelerator ring. Also, the absorbing efficiency of the secondary collimators is significantly increased as the beam halo particles are more deviated from the collimator edge (Fig. 1). Based on the results of these studies, the LHC management took the decision for direct testing of crystal collimation in the LHC accelerator ring.

Two high precision goniometers equipped with the bent crystals produced in PNPI NRC KI and Instituto Nazionale di Fisica Nucleare (Italy) were installed in the LHC ring during 2013–2014 (Fig. 2). First tests were carried out in the LHC beams in 2015. The studies were carried out with 450 GeV and 6.5 TeV energy protons and with 450 GeV ion beams. For all these cases (at the maximum LHC energy as well) it was found that optimal crystal orientation relative to the beam direction leads to strong reduction of the number of inelastic nuclear interactions (Fig. 3), which witnesses obvious channeling effect. Thus, for the first time the channeling of particles of such high energies was demonstrated and the possibility of crystal beam collimation in LHC was proved. The measurements were carried at low beam intensity. Tests for higher intensities are under preparation.

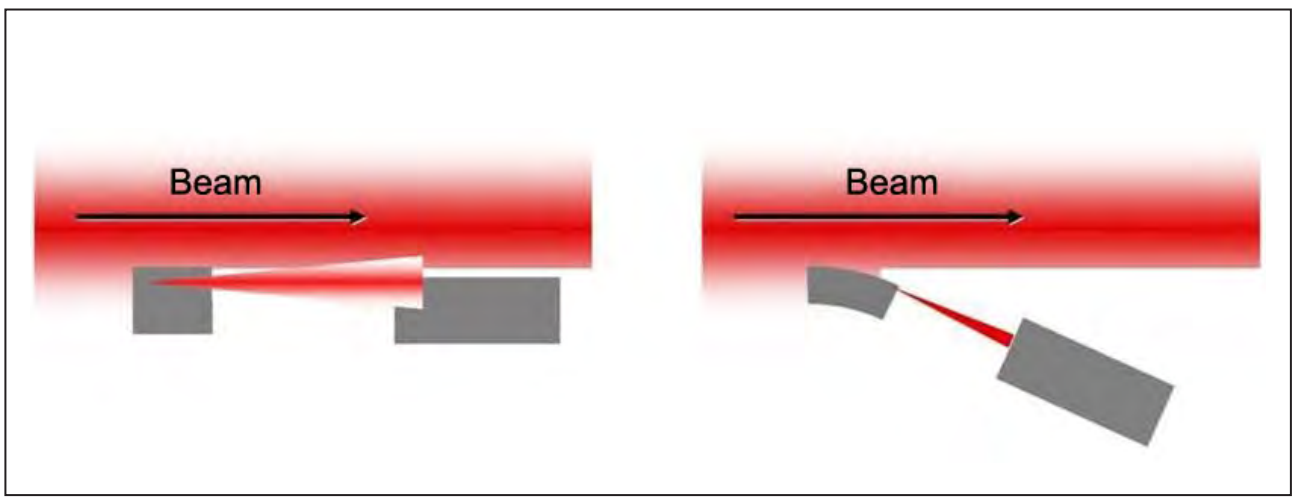

Fig. 1. Traditional (*left*) and crystal (*right*) collimation of charged particle beams

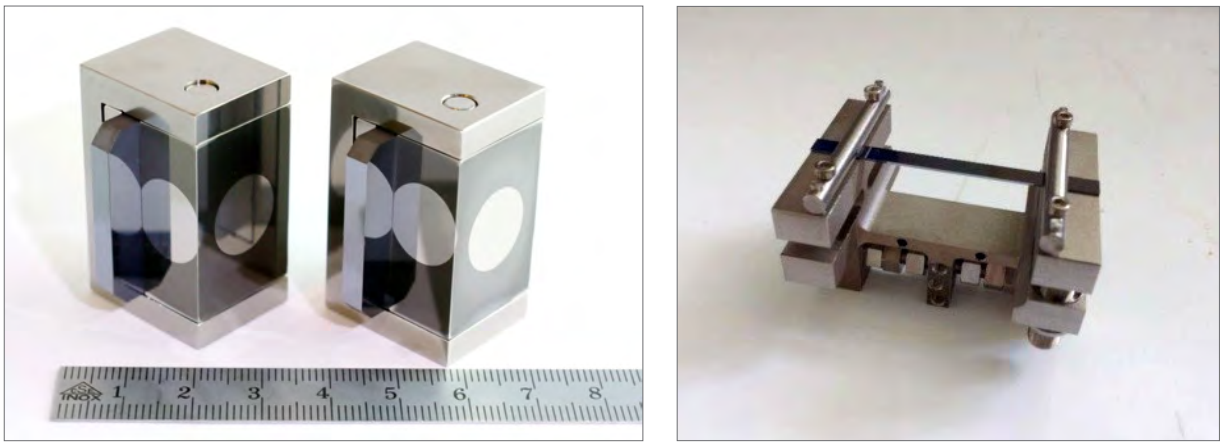

Fig. 2. Bent crystals for LHC prepared by PNPI NRC KI (*left*) and INFN (*right*)

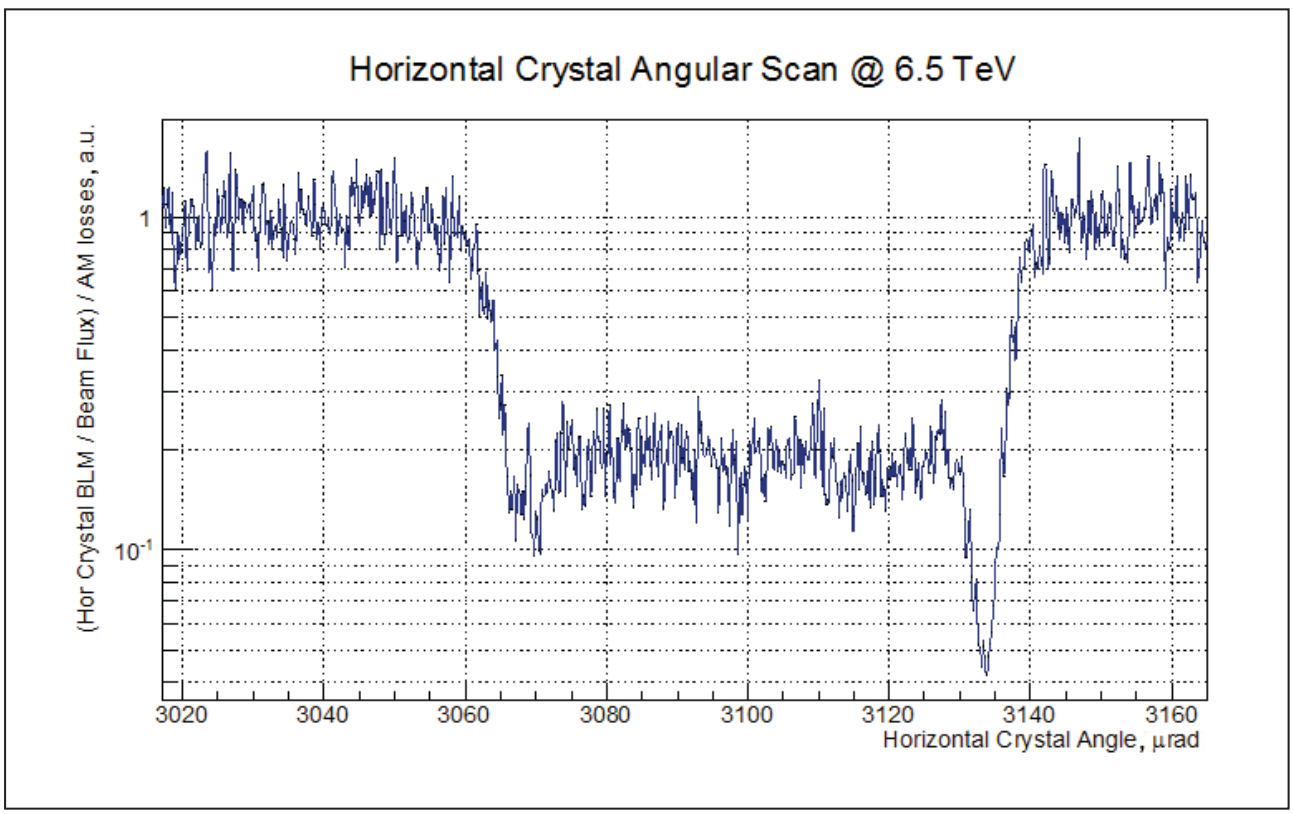

Fig. 3. Dependence of nuclear interaction rate in a crystal on its orientation for 6.5 TeV protons

1. *CERN Bulletin*. http://cds.cern.ch/journal/CERNBulletin/2015/49
2. *UA9 Collaboration*. Observation of Proton Channeling in the Crystal Assisted Collimation Set-Up for LHC. Submitted to Phys. Lett. B.

Generation of molecular hydrogen with high nuclear polarization

CELGAS Collaboration
K.Yu. Grigoryev, L.M. Kotchenda, P.A. Kravtsov, V.A. Trofimov, A.A. Vasilyev – High Energy Physics Division, PNPI NRC "Kurchatov Institute"
R. Engels – Forschungszentrum Jülich

Polarized charged particle beams and polarized targets are an important part of nuclear physics experiments. Internal hydrogen and deuterium gas targets with nuclear polarization are widely used in experiments at high-energy particle accelerators (HERMES at DESY, COSY FZ-Jülich). These experiments utilize a beam of polarized hydrogen or deuterium atoms with high degree of polarization. Further improvements in the accumulation of polarized atoms and in the polarization persistence are as yet lacking. The major problem is connected with recombination of atoms into molecules at the storage cell surface with a significant polarization loss.

Investigations of the polarization persistence in molecular hydrogen (deuterium), obtained by the recombination of atomic polarized hydrogen (deuterium), were started in 2001 at PNPI NRC KI. An experimental set-up built up at PNPI NRC KI enables us to study the recombination of polarized atoms on a variety of surfaces (Au, Cu, organic surfaces, etc.) at a wide temperature range (45–200 K) and magnetic field up to 1 T. To measure the polarization, hydrogen molecules are ionized by electron impact, and molecular ions are extracted to the polarimetry system. A uniform magnetic field is formed by superconducting magnets at liquid-helium temperatures. Further measurements were carried out at the Institut für Kernphysik, Forschungszentrum Jülich using a polarimeter and a polarized atomic beam source.

A unique technique of measurements of the nuclear polarization of molecular hydrogen has been developed using a Lamb shift polarimeter. Experimental investigations of the polarization of molecular hydrogen were carried out in the past, but it was impossible to get more than 50% polarization in strong magnetic fields, regardless of the type of the surface. In the PNPI NRC KI experimental set-up, the surfaces on which the recombination was performed were surrounded with cryogenic adsorption pumps at liquid helium temperature. This arrangement ensured the absence of water traces on the surface under investigation.

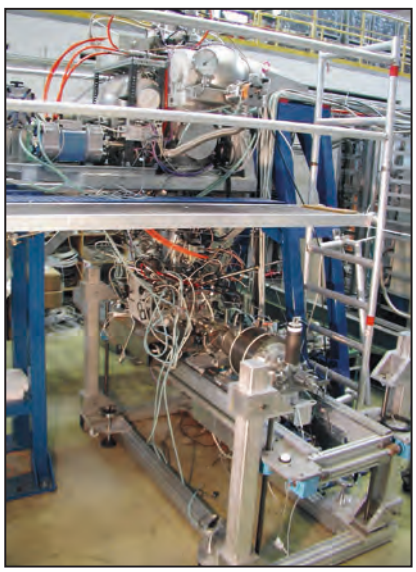

Experimental set-up for production and investigation of polarized molecules (COSY FZ-Jülich)

For the first time, the polarization of 97% was reached in molecular hydrogen formed by recombination of the polarized atoms in the storage cell covered with perfluoropolyether (Fomblin). Thus, a possibility of obtaining polarized molecular hydrogen with a high degree of polarization has been proven experimentally.

1. *Engels R. et al.* // Rev. Sci. Instrum. 2014. V. 85. P. 103505.
2. *Engels R. et al.* // Phys. Rev. Lett. 2015. V. 115. P. 113007.

Non-invasive method of recovery of gas discharge detectors working in high intensity irradiation fields

V.A. Andreev, A.A. Fetisov, G.E. Gavrilov, A.G. Krivshich, D.A. Maysuzenko, N.Yu. Shvetsova
High Energy Physics Division, PNPI NRC "Kurchatov Institute"

Studying the aging of gas discharge detectors in many modern physical experiments has shown that silicon (Si) compounds appearing in the gas mixture are a general reason of detectors degradation. Usually, sources of Si-compounds in the working space are the construction materials, elements of the gas supply system or fiberglass electrodes.

In the absence of Si-compounds in the gas volume, another aging mechanism appears at the accumulated charges of a few 1 $C \cdot cm^{-1}$ – anode wire swelling. It has been found that active oxygen radicals produced in the gas avalanche plasma penetrate through the pores in the wire gold-plating and oxidize tungsten – the material from which the anode wire is made. This causes a break of the gold plating, and then tungsten oxides (WO_x) appear on the wire surface through the cracks. Both types of aging lead to the anode diameter increase that results in the gas gain drop and diminishing of the signal amplitude. A universal solution of the aging problem is not found, therefore it would be useful to find a non-invasive method to recover the aged detector or, in other words, to perform the detector recovery without disassembling it.

At PNPI NRC KI, a new method has been developed to clean the anode wire surface off Si and WO_x compounds. It is based on plasma chemistry reactions widely used in microelectronic. Etching of the compounds takes place in the plasma formations of the 80% CF_4 + 20% CO_2 gas mixture discharge in vicinity of the wire surface to which a negative potential is applied. The bases of the process are the reactions between the active radicals of fluorine and compounds of silicon or tungsten in the gas discharge at the wire. The result of these reactions is the formation of volatile compounds which are removed from the bulk of detector by the gas flow. During the process of the detector restoration, the damaged area is irradiated with *X*-ray photons from ^{55}Fe. The photons with the energy of 6 keV provide maintaining of ionization in the gas discharge plasma and desorption of the etching products.

A study of plasma-chemical etching of silicon and tungsten formations was carried out at PNPI NRC KI using proportional straw-type counters. The straw cathode tube used in our tests was made of carbon coated polyamide film and was 4 mm in diameter, the anode consisted of 50 μm gold-plated tungsten wire. The aging study of the straw with a 60% Ar + 30% CO_2 + 10% CF_4 working gas mixture was carried out using a ^{90}Sr β-source with the intensity of 15 MHz. To test the applicability of the non-invasive method, two straws (Straw-1 and Straw-2) counters with the working gas mixture specially contaminated by silicon were aged three times (up to 35% of the amplitude drop), and then each time were successfully restored. Figure 1, *left*, shows the spectra – results of the wire surface fluorescence analysis (XEM) before and after recovery. The dependences of the gas gain upon the charge accumulated on the unit of the anode wire length are shown in Fig. 1, *right*.

To achieve the effect of anode wire swelling during counters irradiation we used a clean gas system eliminates any contaminants in the working volume of the detectors. Under these conditions, two straws were repeatedly aged and recovered by non-invasive method application. Four cycles of "aging-recovery" tests with Straw-1 held to 3% drop of the signal amplitude, Straw-2 aged three times to 6% drop of amplitude and each time successfully restored. The test results and XEM-analysis of the anode wires surfaces from multiple aged and recovered staws are shown in Fig. 2.

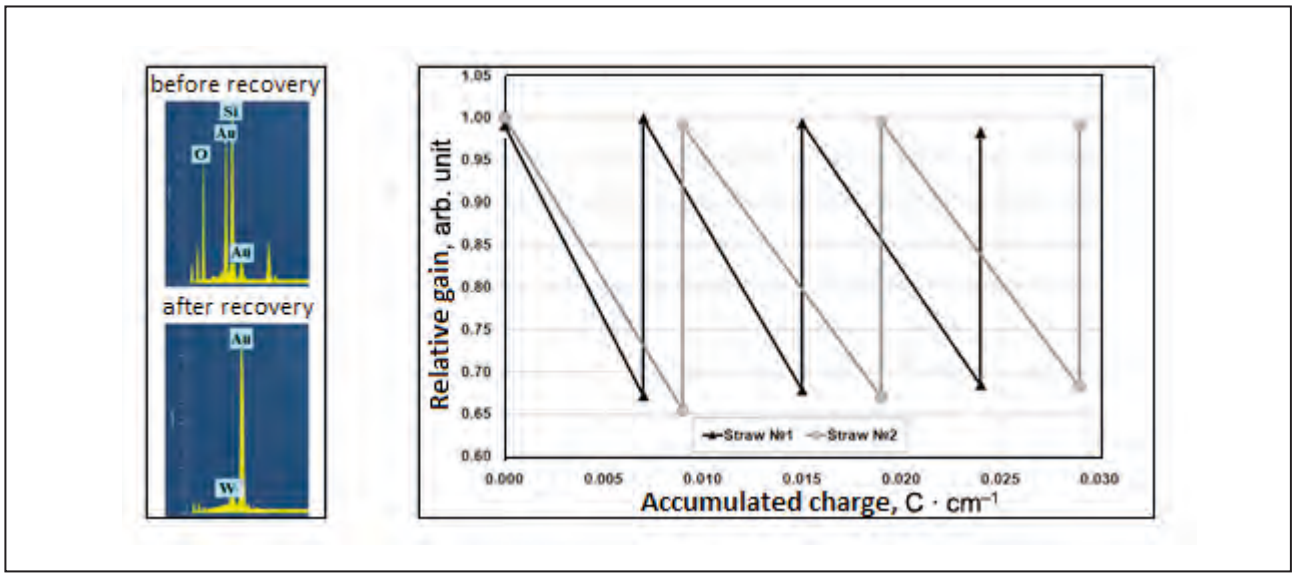

Fig. 1. *On the left* – the results of XEM-analysis of the anode wires surfaces: aged in 60% Ar + 30% CO_2 + 10% CF_4 (top); aged three and three free of silicon compounds by etching in a mixture of 80% CF_4 + 20% CO_2 (bottom). *On the right* – the gas gain dependence from the accumulated charge after repeated restoration of two straws. Diagonal lines – gas gain drop in the counters due aging process; vertical lines – gas gain recovery as a result of a non-invasive method application

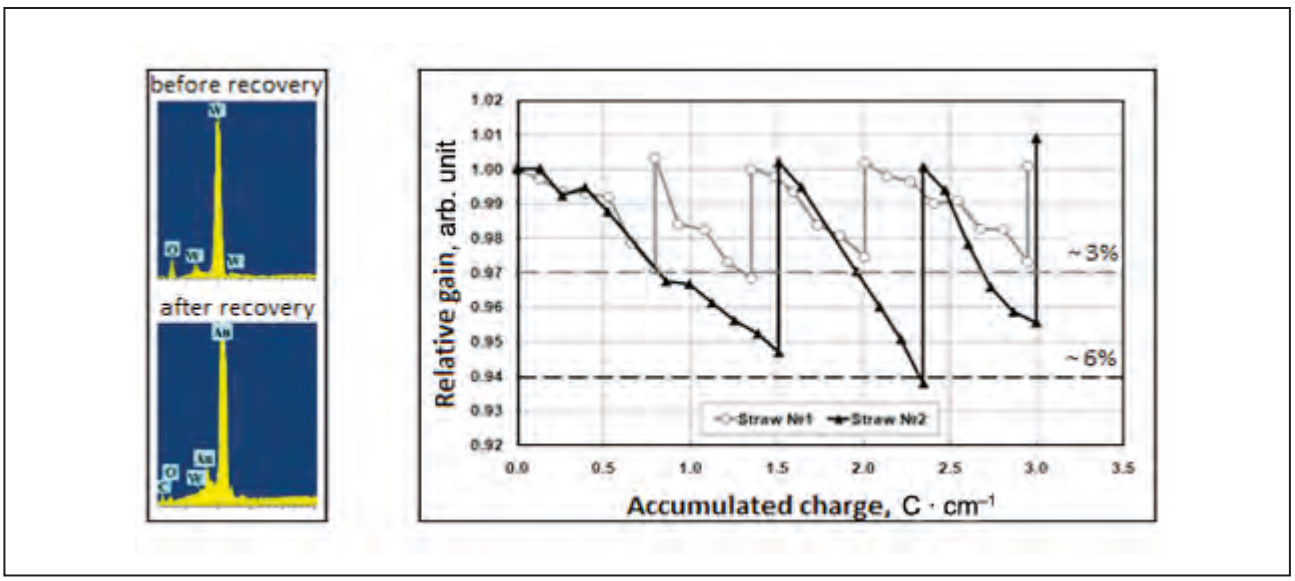

Fig. 2. *On the left* – the results of XEM-analysis of the anode wires surfaces: aged due to swelling in working mixture of 60% Ar + 30% CO_2 +10% CF_4 (top); three times aged and three times treated from tungsten compounds by etching in a mixture of 80% CF_4 + 20% CO_2 (bottom). *On the right* – gas gain dependence from the collected charge per unit of the wire length in multiple aging – restoring tests of two counters Straw-1 and Straw-2

Gavrilov G.E., Vakhtel V.M., Krivshich A.G. et al. // PNPI-Preprint 2983. Gatchina, 2015. 16 p.

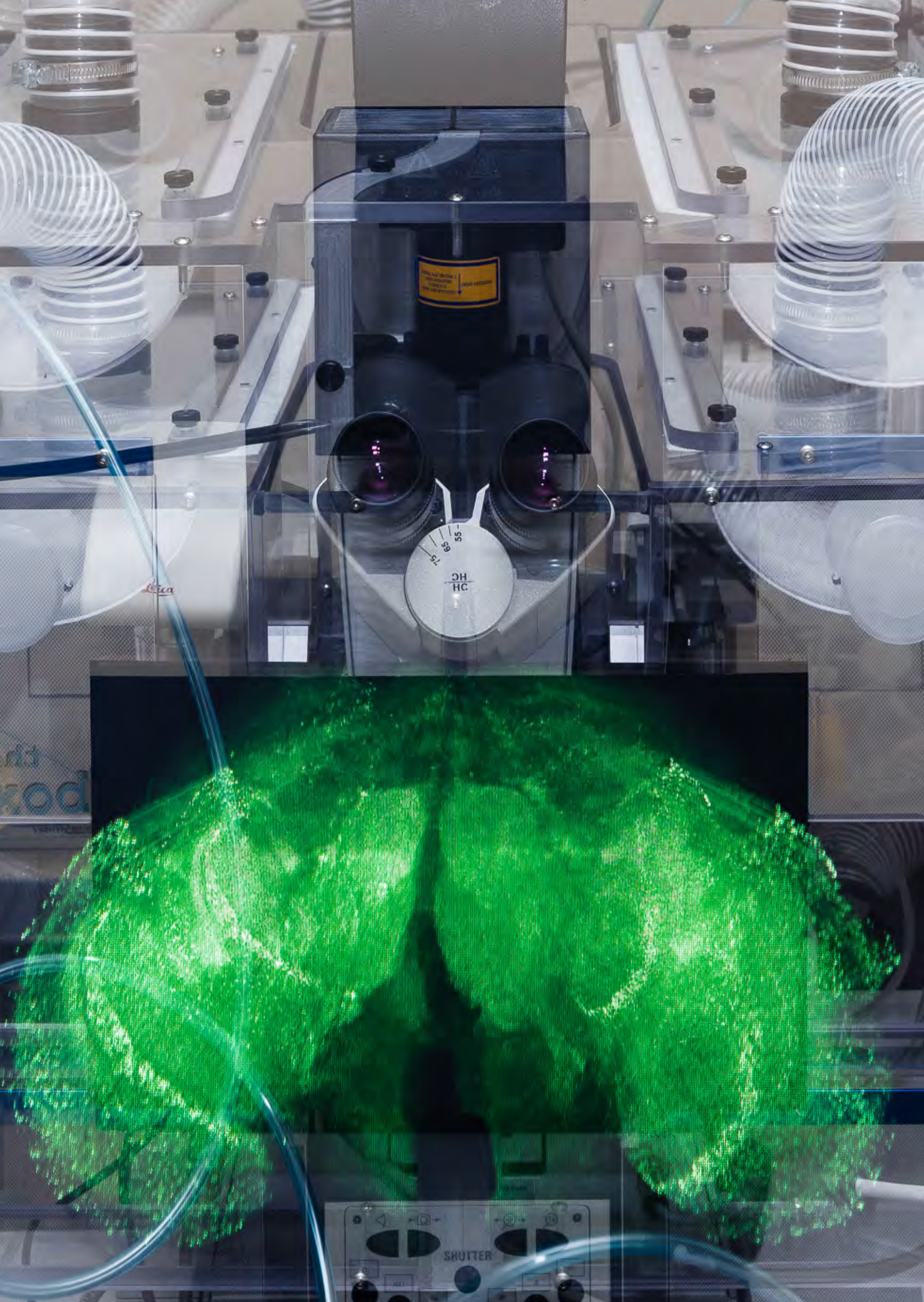
Leica
SHUTTER

Molecular and Radiation Biophysics

Structure of the *Escherichia coli* ribosome–EF-Tu complex at < 3 Å resolution by C_s-corrected cryo-EM

A.L. Konevega
Molecular and Radiation Biophysic Division, PNPI NRC "Kurchatov Institute"

Ribosome is a complicated macromolecular complex that consists of several dozens of proteins and ribonucleic acids. In the cells of all living organisms ribosomes perform an important function – synthesis of protein molecules using the genetic information stored in the messenger RNA (mRNA). Deciphering of the spatial structure of the ribosome has been recognized the most important result and awarded the Nobel Prize in Chemistry 2009.

Bacterial ribosomes are targets for the action of more than 50% of used in the therapy antibiotics – specific inhibitors of protein biosynthesis. Due to the emergence of bacterial strains resistant to existing antibiotics and posing a threat to the national (and international) security in the health of mankind, the study of the ribosome can be judged as one of the most important tasks of modern biomedicine.

For the first time in 2015 a group of researchers from Germany and Russia managed to surpass the results obtained by *X*-ray crystallography. Three-dimensional structures of ribosomal complexes were obtained with a resolution of less than 3 Å using the method of cryoelectron microscopy. New, optimized methods of the preparation of functional ribosomal complexes and methods of microimages' sorting allowed researchers to obtain the most accurate and complete model of the bacterial ribosome in complex with the elongation factor EF-Tu, stalled by antibiotic kirromysin during decoding (reading) of mRNA (Fig.). For the first time in the world the structure of the ribosome was obtained, which the structure of all 35 modified bases of the ribosomal RNA.

The results were produced with the active participation of Russian scientists from PNPI NRC KI.

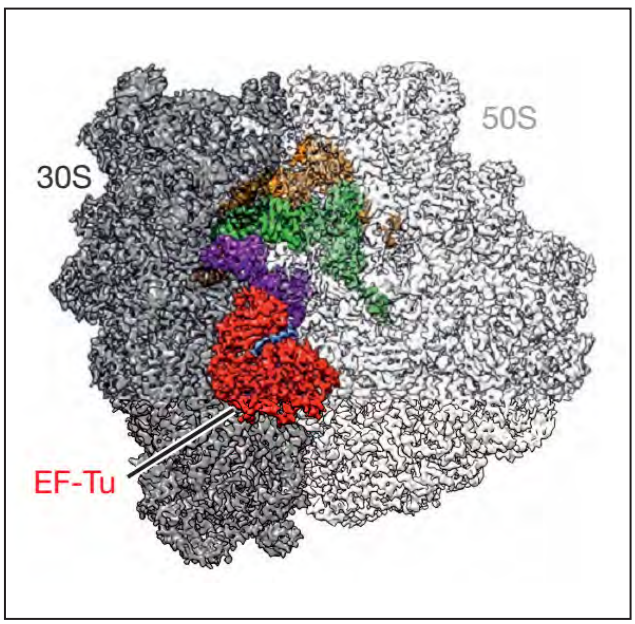

Structure of the ribosome (gray) with a protein factor EF-Tu (red), antibiotic kirromysin (cyan), Phe-tRNA^{Phe} in A/T-state (purple), fMet-tRNA^{fMet} in P-site (green) and tRNA^{fMet} in E-site (orange)

Fischer N., ..., Konevega A.L., ..., Rodnina M.V. et al. // Nature. 2015. V. 520. P. 567–70.

Sequencing, biochemical characterization, crystal structure and molecular dynamics of cellobiohydrolase Cel7A from *Geotrichum candidum 3C*

K.S. Bobrov, A.S. Borisova, E.V. Eneyskaya, F.M. Ibatullin, A.A. Kulminskaya – Molecular and Radiation Biophysic Division, PNPI NRC "Kurchatov Institute"
A.S. Borisova, U. Saleem, M. Sandgren, J. Stahlberg – Swedish University of Agricultural Sciences Uppsala
S. Jana, Ch.M. Payne – University of Kentucky
A.A. Kulminskaya – Peter the Great Saint Petersburg Polytechnic University
A.L. Lapidus – Saint Petersburg National Research Academic University of RAS
A.A. Logachev, D.E. Polev – Saint Petersburg University

The ascomycete *Geotrichum candidum* is a versatile and efficient decay fungus that is involved, for example, in biodeterioration of compact discs; notably, the *3C* strain was previously shown to degrade filter paper and cotton more efficiently than several industrial enzyme preparations. Glycoside hydrolase (GH) family 7 cellobiohydrolases (CBHs) are the primary constituents of industrial cellulase cocktails employed in biomass conversion, and feature tunnel-enclosed active sites that enable processive hydrolytic cleavage of cellulose chains. Understanding the structure–function relationships defining the activity and stability of GH7 CBHs is thus of keen interest. Accordingly, we report the comprehensive characterization of the GH7 CBH secreted by *G. candidum* (GcaCel7A). The bimodular cellulase consists of a family 1 cellulose-binding module (CBM) and linker connected to a GH7 catalytic domain that shares 64% sequence identity with the archetypal industrial GH7 CBH of *Hypocrea jecorina* (HjeCel7A). GcaCel7A shows activity on Avicel cellulose similar to HjeCel7A, with less product inhibition, but has a lower temperature optimum (50 °C versus 60–65 °C, respectively). Five crystal structures, with and without bound thio-oligosaccharides, show conformational diversity of tunnel-enclosing loops, including a form with partial tunnel collapse at subsite –4 not reported previously in GH7 (Figs. 1 and 2).

Also, the first O-glycosylation site in a GH7 crystal structure is reported – on a loop where the glycan probably influences loop contacts across the active site and interactions with the cellulose surface. The GcaCel7A structures indicate higher loop flexibility than HjeCel7A, in accordance with sequence modifications. However, GcaCel7A retains small fluctuations in molecular simulations, suggesting high processivity and low endo-initiation probability, similar to HjeCel7A.

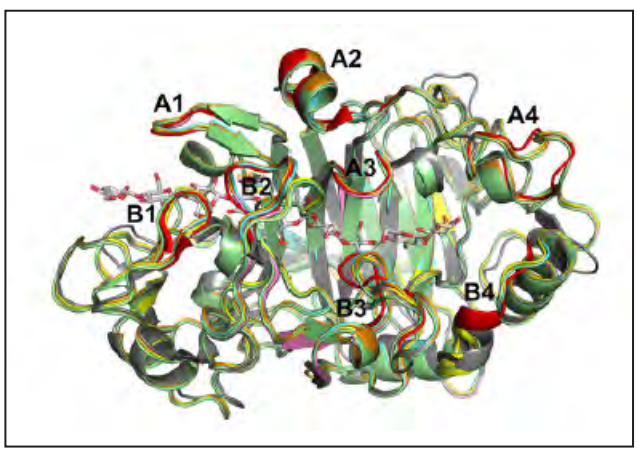

Fig. 1. Overall structural alignment of the five GcaCel7A structures with the HjeCel7A cellononaose complex (PDB code 4C4C)

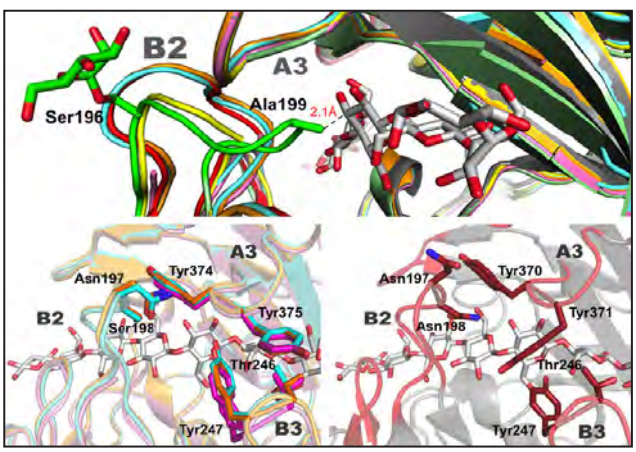

Fig. 2. Tunnel-enclosing loop contacts

Borisova A.S., Eneyskaya E.V., Bobrov K.S., ..., Ibatullin F.M., ..., Kulminskaya A.A. et al. // FEBS J. 2015. V. 282. No 23. P. 4515–4537.

BASP1 – an axon terminal protein forming amyloid-like oligomers

N.Ya. Gil'yano, O.S. Vityuk, V.V. Zakharov
Molecular and Radiation Biophysic Division, PNPI NRC "Kurchatov Institute"

A broad group of human conformational diseases called amyloidoses is accompanied by formation and accumulation of amyloid protein aggregates (fibrils and oligomers), which are inherently toxic. On the other hand, amyloid protein aggregates have a number of physiological functions. In addition, non-pathological amyloid-like aggregates are widely distributed in nature. The brain protein BASP1, which is critically important for the organism's vital functions, forms *in vitro* oligomers in the presence of anionic phospholipids or SDS and also forms fibril-like aggregates (Fig. a). In this study we have investigated the amyloid properties and toxicity of the BASP1 aggregates. We have also studied whether the BASP1 oligomers are present on the presynaptic membrane of rat brain neurons. The *N*-terminal myristoylated peptide myr-BASP1(1–13) containing the BASP1 aggregation domain forms fibrils (Fig. b). The birefringence of Congo red bound to myr-BASP1(1–13) fibrils (Fig. c) and the enhanced fluorescence of Thioflavin T in the presence of the peptide fibrils confirmed their amyloid-like structure. Using the conformation-specific antibodies to amyloid oligomers (A11) showed that BASP1 oligomers have a structure similar to that of amyloid protein oligomers (Fig. d). Native protein complexes were cross-linked by glutaraldehyde treatment of the presynaptic membrane fraction of rat brain neurons. BASP1 oligomers were revealed as a part of these complexes. BASP1 oligomers were shown to be non-toxic to PC12 cells. We conclude that BASP1 oligomers are a non-pathological functional form of this brain protein. Presumably, the oligomers sequester a membrane phosphatidylinositol-4,5-diphosphate.

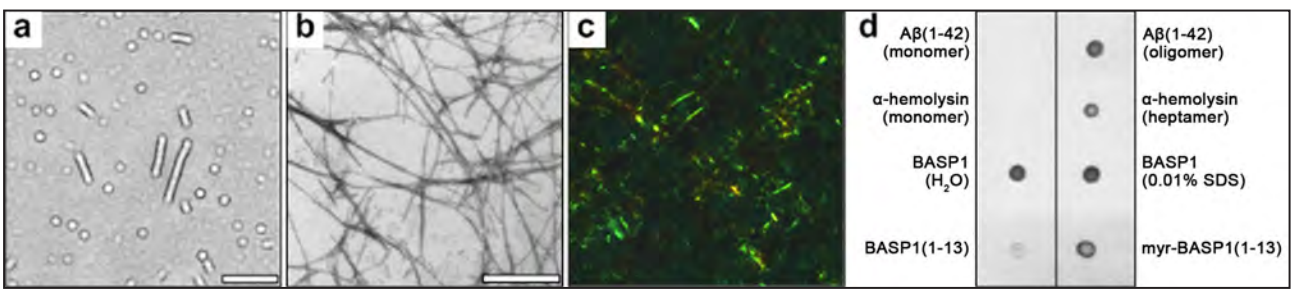

Electron micrograph of the oligomers and fibril-like aggregates of BASP1 protein, scale bar is 100 nm (a).
Electron micrograph of myr-BASP1(1–13) fibrils, scale bar is 500 nm (b).
Congo red birefringence in the presence of myr-BASP1(1–13) fibrils (c).
Interaction of conformation-specific antibodies A11 with protein monomers and oligomers on the dot-blot (d)

Vityuk O.S., Gil'yano N.Ya., Zakharov V.V. // Neurosci. Behav. Physiol. 2015. V. 45. No. 5. P. 523–527.

Deinococcus radiodurans RecA nucleoprotein filaments characterized at the single-molecule level with optical tweezers

D.M. Baitin – Molecular and Radiation Biophysic Division, PNPI NRC "Kurchatov Institute"
A.A. Alekseev, G.A. Cherevatenko, M.A. Khodorkovskii, O.D. Kovaleva, N.E. Morozova, G.E. Pobegalov, A.V. Sabantsev, A.D. Vedyaykin – Peter the Great Saint Petersburg Polytechnic University

Deinococcus radiodurans can survive extreme doses of ionizing radiation due to the very efficient DNA repair mechanisms that are able to cope even with hundreds of double-strand breaks. RecA, the critical protein of homologous recombination in bacteria, is one of the key components of the DNA-repair system. Repair of double-strand breaks requires RecA binding to DNA and assembly of the RecA nucleoprotein helical filaments. The *Escherichia coli* RecA protein (EcRecA) and its interactions with DNA have been extensively studied using various approaches including single-molecule techniques, while the *D. radiodurans* RecA (DrRecA) remains much less characterized. Here we combine microfluidics and single-molecule DNA manipulation with optical tweezers to follow the binding of DrRecA to long double-stranded DNA molecules and probe the mechanical properties of DrRecA nucleoprotein filaments at physiological pH. DrRecA forms complexes with dsDNA more rapidly, and DrRecA nucleoprotein filaments exhibit slightly shorter length and greater flexibility compared to EcRecA. Both binding profiles of DrRecA and EcRecA are highly nonlinear indicating that multiple nucleation events occurred during filaments assembly. In case of DrRecA nucleoprotein filaments assembly, end-to-end distance of the DNA-tether was extended by 25% about five times faster and reached the maximum value of extension about 1.5 times faster than in the case of EcRecA. Furthermore, the final end-to-end distance increase in the case of DrRecA was reproducibly smaller compared to that of EcRecA, 45.8 ± 0.5% and 48.3 ± 1.2% respectively. To probe the mechanical properties of DrRecA and EcRecA nucleoprotein filaments force-extension curves were obtained after RecA polymerisation on DNA was finished. In case of EcRecA nucleoprotein filaments determined values of P = 960 ± 120 nm. Analysis of force-extension data of DrRecA nucleoprotein filaments revealed notably lower values of the persistence length, P = 690 ± 90 nm, compared to that of EcRecA. These observations are more likely due to the presence of more discontinuities in the protein-DNA complexes as a result of the greater ratio between filament nucleation and growth. Overall, our results provide new insights into the assembly of the DrRecA-dsDNA nucleoprotein filaments and their mechanical properties and support the model that in contrast to EcRecA, DrRecA forms numerous short-length patches along the DNA, potentially leading to more effective recruitment of the protein for DNA repair.

Pobegalov G., ..., Baitin D. et al. // Biochem. Biophys. Res. Commun. 2015. V. 466. No. 3. P. 426–430.

Major reorientation of tRNA substrates defines specificity of dihydrouridine synthases

P.C. Kasatsky, A.L. Konevega
Molecular and Radiation Biophysic Division, PNPI NRC "Kurchatov Institute"

A characteristic feature of tRNA molecules is the presence of a large number of modified nucleotides. All modifications of tRNA nucleotides occur post-transcriptionally, arising in the process of maturation of the primary transcript of tRNA. One of the most common modified nucleosides – dihydrouridine – is formed by reduction of the double bond C5-C6 in the uridine molecule. Dihydrouridine is located in certain positions of D-loop and plays an essential role in regulation of the conformational rigidity of tRNA molecule. Formation of dihydrouridine in the tRNA molecule is catalyzed by an entire class of enzymes known as dihydrouridine synthases. Three enzymes of this class (DusA, DusB and DusC) are found in *Escherichia coli*.

Elevated levels of dihydrouridines in tRNA in eukaryotic cells are associated with the development of certain cancers, including non-small cell lung cancer. Thus, a detailed study of the molecular mechanisms of action of dihydrouridine synthases is required for the creation of anticancer drugs acting on modifying enzymes.

The study of the molecular mechanism of dihydrouridine synthases action was carried out using structural methods (*X*-ray crystallography) and functional studies, including biochemical and biophysical methods, performed by a group of researchers from the UK, Germany and Russia.

Because the catalytic center of all Dus enzymes is conserved, it is unclear how the same protein fold can be reprogrammed to ensure that nucleotides exposed at spatially distinct faces of tRNA can be accommodated in the same active site. Unexpectedly, crystal structures of DusC complexes with $tRNA^{Phe}$ and $tRNA^{Trp}$ show that Dus subfamilies that selectively modify U16 or U20 in tRNA adopt identical folds but bind their respective tRNA substrates in an almost reverse orientation that differs by a 160° rotation. The tRNA docking orientation appears to be guided by specific clusters of amino acids together with differences in the shape of the positively charged tRNA-binding surfaces. tRNA orientations are further constrained by positional differences between the C-terminal recognition domains. The exquisite substrate specificity of Dus enzymes is therefore controlled by a relatively simple mechanism involving major reorientation of the whole tRNA molecule. Such reprogramming of the enzymatic specificity appears to be a unique evolutionary solution for altering tRNA recognition by the same protein fold.

Byrne R.T. ..., Kasatsky P.S., Rodnina M.V. ..., Konevega A.L. et al. // PNAS. 2015. V. 112. No. 19. P. 6033–6037.

AquaBridge – a new method for the systematic search of structural water molecules in the active sites of proteins

A.S. Afanasyeva, M.G. Petukhov – Molecular and Radiation Biophysic Division, PNPI NRC "Kurchatov Institute"
S.A. Izmailov – Saint Petersburg University
M.Yu. Grigoriev – Paul Sabatier University

Globular proteins normally function in an aqueous environment, and therefore water plays a role not only in maintaining the stability of folded biologically active forms of these proteins, but often is directly involved in the chemical reactions catalyzed by these proteins such as the hydrolysis of ATP, the main energy source for a living cell. In particular, the water molecules are often observed in the active sites of proteins in their crystalline forms, both in the absence and in the presence of ligands. Taking this phenomenon into account in the design and docking of the ligands can be complicated. For this reason the standard practice is to remove water from the entire structural protein crystallographic data. It is quite possible that due to various technical reasons structural water is not fully represented even in high-resolution crystallographic data.

In order to clarify this issue, as well as to explore the possible impact of accounting for active site water on the effectiveness of advanced algorithms for docking and designing ligands in the active sites of proteins, we developed AquaBridge, a new method of searching all possible conformations of structural water in the active site of proteins. The method was implemented as the utility AquaBridge, intended for use in ICM-Pro, commercially available molecular modeling software package.

The effectiveness of the approach was studied by various methods, including using the molecular dynamics simulation of several protein systems from a representative set and docking of small ligands into active site of proteins. Analysis of the effectiveness of the docking of small organic molecules in the active site of proteins under study suggests a significant improvement in selectivity of the docking algorithms and in the prediction of the conformation of the ligands in the case when structural water is present in the active site of the proteins (Fig.).

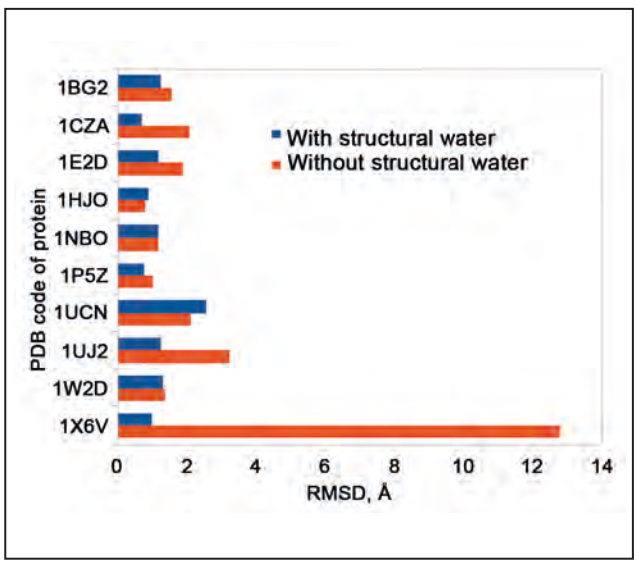

RMSD between theoretically predicted and experimental ATP conformations in ATP binding sites of several human ATPases

Afanasyeva A. ..., Petukhov M. // J. Comput. Chem. 2015. V. 36. P. 1973–1977.

Ionizing radiation improves glioma-specific targeting of superparamagnetic iron oxide nanoparticles conjugated with cmHsp70.1 monoclonal antibodies (SPION–cmHsp70.1)

V.A. Ryzhov – Molecular and Radiation Biophysic Division, PNPI NRC "Kurchatov Institute"
A.V. Dobrodumov – Institute of Macromolecular Compounds of RAS
M.A. Parr, V.I. Rolich – Saint Petersburg University
Y.Y. Marchenko, B.P. Nikolaev, L.Y. Yakovleva – Research Institute of Highly Pure Biopreparations
A.L. Mikhrina – Sechenov Institute of Evolutionary Physiology and Biochemistry of RAS
E. Pitkin – University of Pennsylvania
G. Multhoffb, M.A. Shevtsov – Technische Universität München

The stress-inducible 72 kDa heat shock protein Hsp70 is known to be expressed on the membrane of highly aggressive tumor cells including high-grade gliomas, but not on the corresponding normal cells. Membrane Hsp70 (mHsp70) is rapidly internalized into tumor cells and thus targeting of mHsp70 might provide a promising strategy for theranostics. Superparamagnetic iron oxide nanoparticles (SPIONs) are contrast negative agents that are used for the detection of tumors with MRI. Herein, we conjugated the Hsp70-specific antibody (cmHsp70.1) which is known to recognize mHsp70 to SPIONs to assess tumor-specific targeting before and after ionizing irradiation. *In vitro* experiments demonstrated the selectivity of SPION–cmHsp70.1 conjugates to free and mHsp70 in different tumor cell types (glioblastoma C6, leukemia K562, cervix carcinoma HeLa) in a dose-dependent manner. High resolution MRI (11T) on T_2-weighted images showed the retention of the conjugates in C6 glioma model (Fig. 1). Accumulation of the latter in the glioma resulted in a nearly two-fold drop of T_2^* values in comparison to nonconjugated SPIONs. Biodistribution analysis using measurements of second harmonic of nonlinear response to a weak *ac* magnetic field (NLR-M_2) in parallel to it *dc* field *H* showed a seven-fold increase in tumor-to-normal brain uptake ratio of SPION–cmHsp70.1 conjugates in

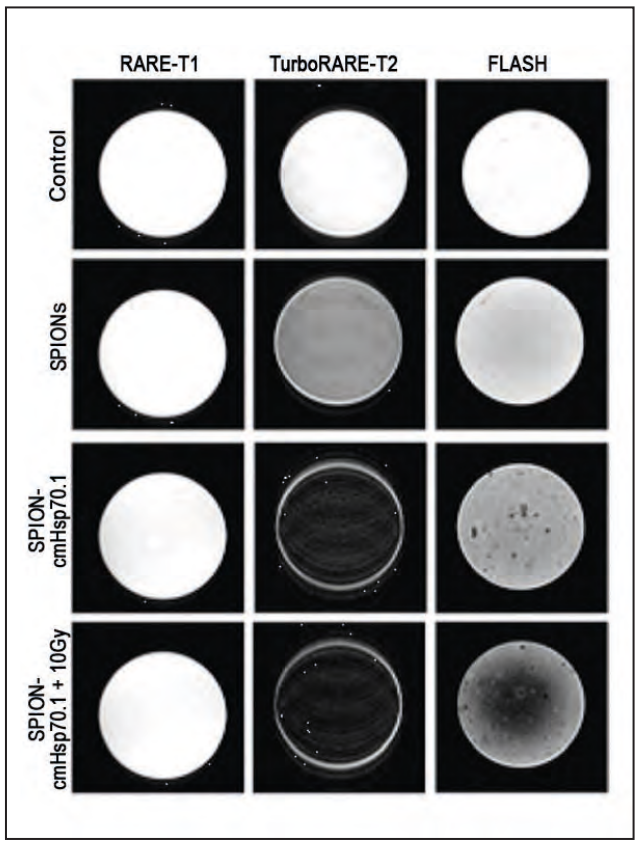

Fig. 1. T_1-, T_2-weighted and FLASH (gradient echo) MR scans of C6 glioblastoma cells in 0.1% agarose gel. The images were obtained for control, cells incubated with SPIONs, SPION–cmHsp70.1 conjugates. Additionally following irradiation (10 Gy) cells were incubated with SPION–cmHsp70.1

glioma-bearing rats relative to SPIONs (Fig. 2). This storing within Hsp70-positive glioma was further enhanced after a single dose (10 Gy) of ionizing radiation. Elevated uptake of the magnetic conjugates in the tumor (four-fold) due to radiosensitization proves the combination of radiotherapy and application of Hsp70-targeted agents in brain tumors. Our approach has the potential to be clinically applied for Hsp70-targeted anti-tumor diagnostic and/or therapeutic approaches. The important for the latter data on biodistribution of nanoparticles in other tissues and organs were also obtained.

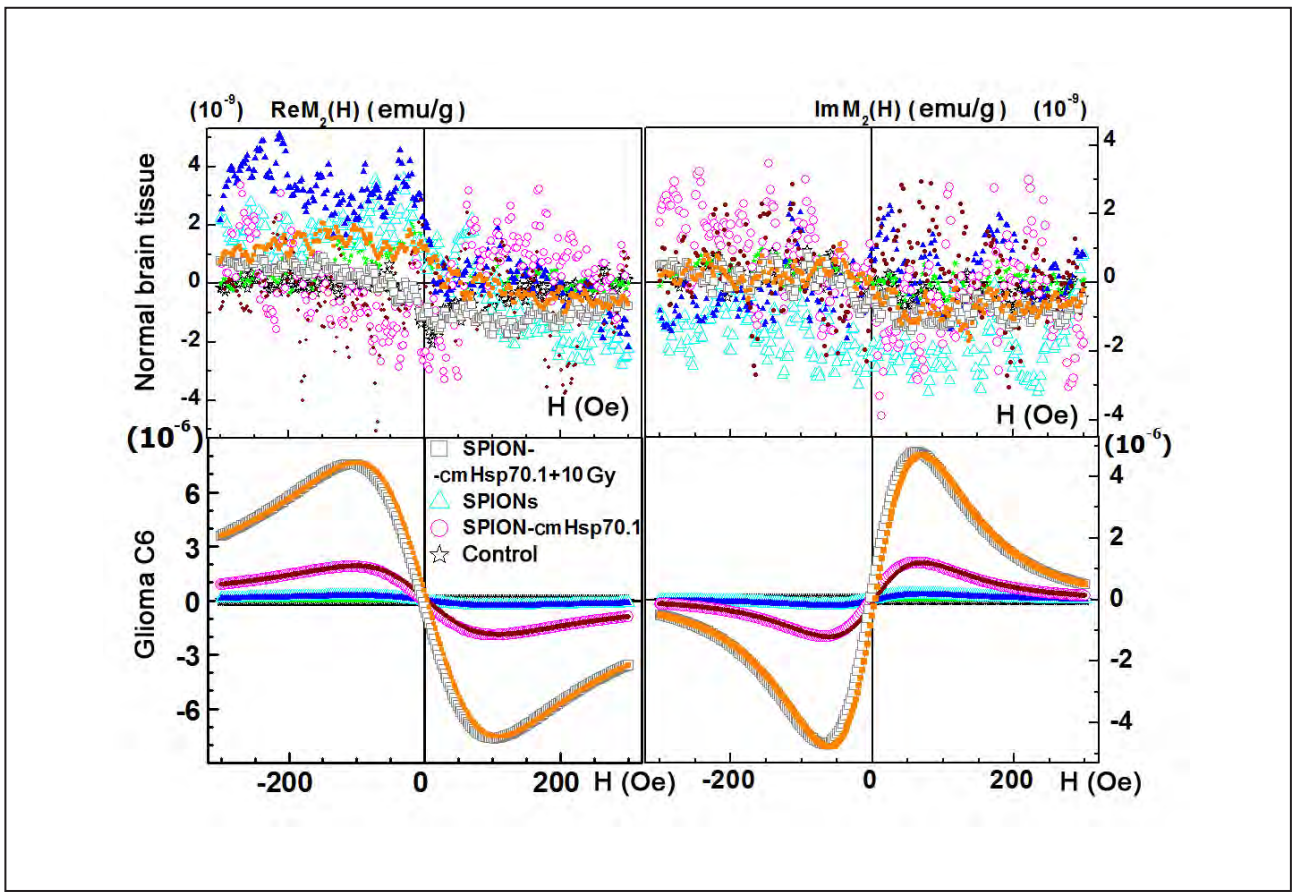

Fig. 2. Biodistribution of nanoparticles in normal brain and tumor of the non-irradiated rats treated by SPIONs, SPION–cmHsp70.1 and irradiated rodents (10 Gy) treated with SPION–cmHsp70.1 from NLR-M_2 data

Shevtsov M.A. ..., Ryzhov V.A. et al. // Nanoscale. 2015. V. 7. P. 20652–20664.

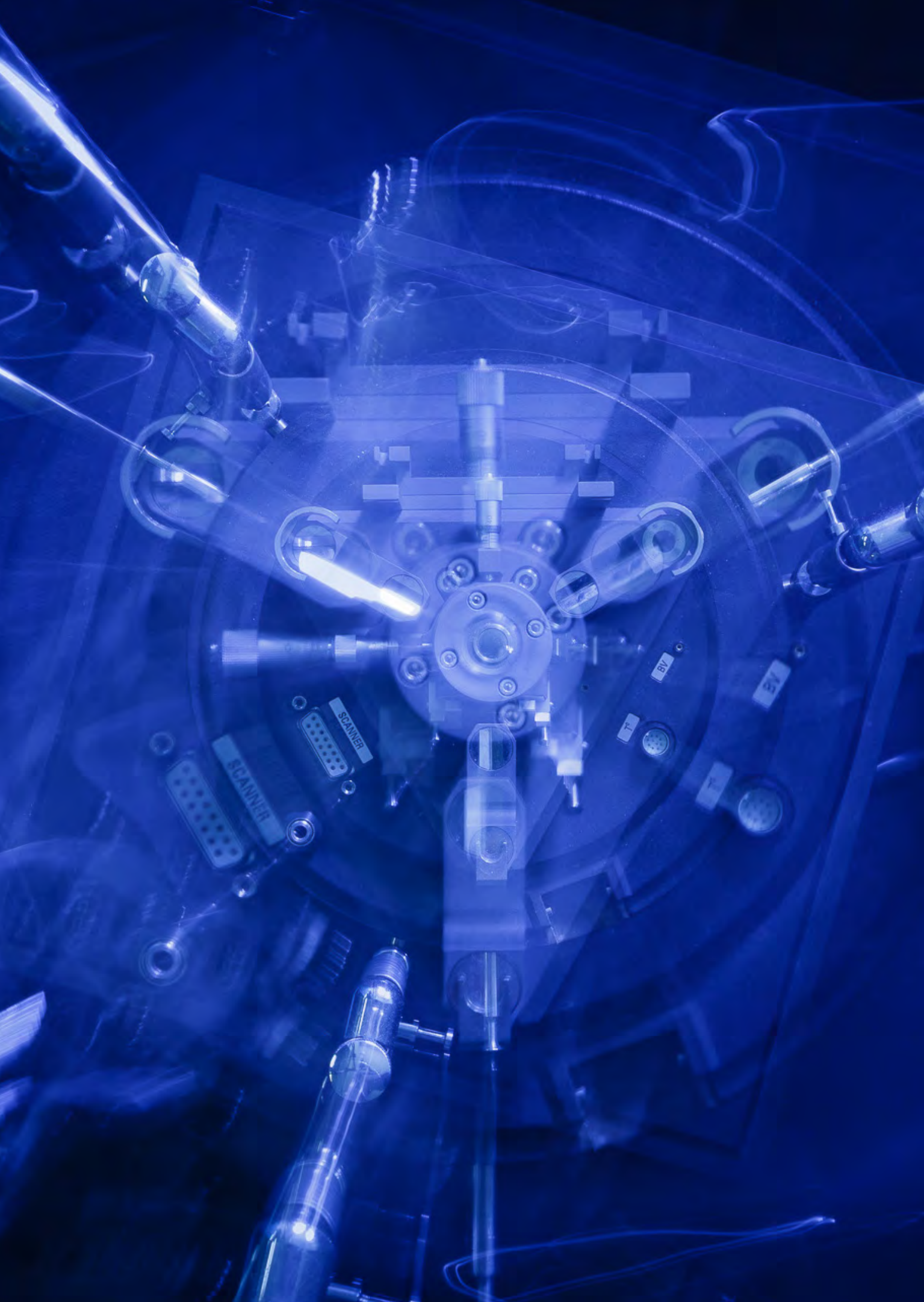
SCANNER
SCANNER
BV

Nuclear Medicine (Isotope Production, Beam Therapy, Nano- and Biotechnologies for Medical Purposes)

Generation, release and uptake of the NAD precursor nicotinic acid riboside by human cells

K.A. Shabalin, A.P. Yakimov – Molecular and Radiation Biophysics Division, PNPI NRC "Kurchatov Institute"
M.A. Khodorkovskiy, V.A. Kulikova, K.B. Nerinovski, A.A. Nikiforov, K.A. Shabalin, A.P. Yakimov – Peter the Great Saint Petersburg Polytechnic University
K.B. Nerinovski – Saint Petersburg University
A.A. Nikiforov – Institute of Cytology of RAS
C. Dölle, M. Niere, M. Ziegler – University of Bergen
M. Migaud, P. Redpath – Queen's University Belfast

Nicotinamide adenine dinucleotide (NAD) is an essential coenzyme of redox reactions in central metabolic pathways. Moreover, NAD is used as a substrate and is degraded by several families of regulatory proteins such as protein deacetylases (Sirtuins), ADP-ribosyltransferases, poly-ADP-ribose polymerases and ADP-ribosyl cyclases, which govern vital processes including gene expression, progression of the cell cycle, insulin secretion, DNA repair, apoptosis and aging. Proper control of these NAD-dependent metabolic and signaling processes depends on how efficiently cells can maintain their NAD contents. Dysregulation of NAD homeostasis can lead to a variety of pathologies such as neurodegenerative diseases, diabetes, metabolic syndrome and cancer.

Generally, human cells regulate their NAD supply through the biosynthesis using various precursors delivered with the diet. The major precursors in humans are nicotinamide (Nam) and nicotinic acid (NA). Both nicotinamide riboside (NR) and nicotinic acid riboside (NAR) also serve as NAD precursors. However, their role in physiological NAD generation is less clear.

In this study we explored whether the ribosides NR and NAR can be generated in human cells, not only delivered with the diet (Fig.). We demonstrate that purified, recombinant human cytosolic 5'-nucleotidases (5'-Nts) CN-II and CN-III, but not CN-IA, can dephosphorylate the mononucleotides NMN and NAMN and thus catalyze NR and NAR formation *in vitro*. In addition, they point to the possibility that different cell types might facilitate each other's NAD supply by providing alternative precursors.

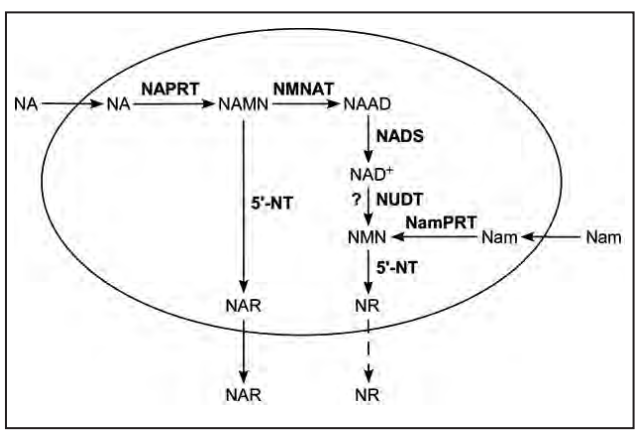

Biosyntesis of NAR and NR by human cells

Kulikova V., Shabalin K. ..., Yakimov A. et al. // J. Biol. Chem. 2015. V. 290. P. 27124–27137.

Plasma oligomeric alpha-synuclein is inversely associated with glucocerebrosidase activity in Gaucher disease type 1 patients

A.K. Emelyanov, S.N. Pchelina, T.S. Usenko – Molecular and Radiation Biophysics Division, PNPI NRC "Kurchatov Institute"
T.M. Boukina, E.P. Nuzhnyi, A.P. Yakimovskii, E.Y. Zakharova – Pavlov First Saint Petersburg State Medical University

In 2015 we studied correlation between plasma oligomeric alpha-synuclein levels and leukocytes glucocerebrosidase (GBA) activity in patients with Gaucher disease. The genetic link between Gaucher disease and Parkinson's disease (PD) is now widely accepted. Heterozygous GBA mutations are strong risk factor for PD, increasing the disease risk in 6–7 times. In homozygote state *GBA* mutations lead to rare inherited disorder, Gaucher disease. Alpha-synuclein oligomerization is believed to be the major neurotoxic event in neurodegenerative process in PD. We hypotezysed that mutation in the *GBA* gene, decreasing GBA activity could contribute to the accumulation and oligomerization of alpha-synuclein.

21 GD type 1 patients were involved in the study. The oligomeric alpha-synuclein levels were estimated by enzyme-linked immunosorbent assay (ELISA) with Human Synuclein OLIGO kit (ajRoboscreen, Germany). Leucocytes GBA activity was measured before treatment using fluorescent enzyme substrate (4-methylumbelliferyl-β-D-glucopyranoside (4MU-β-glc), Sigma-Aldrich). An exponential regression analysis revealed a statistically significant negative correlation of oligomeric alpha-synuclein level measured in plasma of 21 GD patients and leucocyte GBA activity determined before treatment (R^2 = 0.487, $p < 0.001$) (Fig.).

This is the first report assessing the correlation between plasma oligomeric alpha-synuclein levels in GD patients with leucocyte GBA activity. We showed a highly significant irreversible correlation between GBA activity and oligomeric alpha-synuclein levels in GD patients. Present study supports the notion that insufficiency in GBA activity may influence alpha-synuclein oligomerization and suggests that therapeutic strategies augumenting GBA activity might be potentially helpful for treatment of *GBA*-associated PD.

The work was supported by Russian Foundation for Basic Research (№ 13-04-01510, № 14-04-31665).

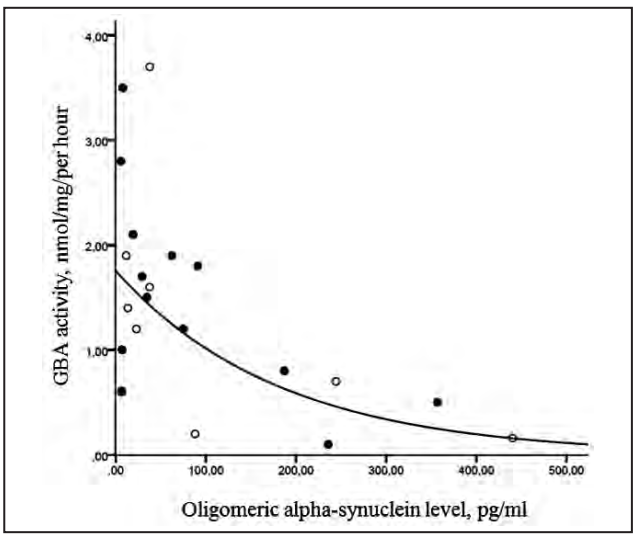

Negative correlation between levels of plasma oligomeric alpha-synuclein and GBA activity in GD patients (R^2 = 0.487, $p < 0.001$). Patients who have not received ERT are marked with whites dots, who received ERT less than five years – with black dots

Nuzhnyi E., Emelyanov A. ..., Usenko T. ..., Pchelina S. // Mov. Disord. 2015. V. 30. Iss. 7. P. 989–991.

A study of the unilamellar vesicles in aqueous solutions of sucrose

V.L. Aksenov – PNPI NRC "Kurchatov Institute"
M.A. Kiselev – Joint Institute of Nuclear Research

A development of the market of nanodrugs and their carriers requires a development of adequate methods for their diagnosis, including research methods of the vesicular systems of phospholipids used as delivery medicine systems. Methods of neutron small-angle scattering (SANS method) and of *X*-ray synchrotron radiation are the main methods of studying the structure of the vesicular systems. The use of small-angle *X*-ray scattering (SAXS method) requires an increase in the contrast between the lipid biolayer and aqueous medium. Disaccharides stabilize the lipid biolayer. The vesicles prepared in aqueous solutions of disaccharides fully retain their properties after lyophilization and subsequent hydration. This property of disaccharides (maltose) is applied in the manufacture of the phospholipid delivery nanosystem used as a container for drugs (Institute of Biomedical Chemistry – IBMC). The disaccharides (sucrose and maltose) substantially (many factors of ten) increase a contrast on the monolayer vesicles of the phospholipids in the experiments by the SAXS methods. In this case, the question of the disaccharide influence on the structure of the lipid bilayer remained open. A study of the influence of sucrose on the structure of single-layer vesicles of dimyristoyl phosphatidylcholine (DMPC) by the methods of SANS and SAXS has been made.

The method of separated form factors has been used for the analysis of SANS data. It has been shown that an increase in the concentration of sucrose results in a significant decrease in the average radius of vesicles and the thickness of the biolayer as well as in a slight decrease in the population polydispersity.

The results are shown in the Table, where $\langle R \rangle$ – the average radius of a vesicle; m – the polydispersity coefficient (fit option); the membrane thickness d and the thickness of the hydrophilic region D – free parameters; ρ_0 – the density of the scattering length.

The methods employed open up the possibility of the characterization of nanosystems for the drug delivery.

Table. The parameters of 1% (*w*/*w*) population of DMPC vesicles in aqueous (D_2O) sucrose solutions*

Sucrose concentration, %	$\langle R \rangle$, Å	m	σ, %	d, Å	D, Å	χ^2	ρ_0, cm^{-2}
0	307.5 ± 4.9	9.8 ± 0.8	30.4	49.8 ± 0.8	16.5 ± 1.7	1.1	$6.37 \cdot 10^{10}$
5	270.6 ± 4.8	9.7 ± 0.9	30.7	48.1 ± 2.1	19.9 ± 2.9	6.9	$6.11 \cdot 10^{10}$
10	243.5 ± 3.2	12.8 ± 0.8	26.9	47.6 ± 1.9	23.0 ± 3.1	6.6	$5.85 \cdot 10^{10}$
20	213.4 ± 2.2	13.7 ± 0.5	26.1	44.5 ± 2.1	25.1 ± 2.8	9.5	$5.33 \cdot 10^{10}$
40	190.6 ± 1.6	13.2 ± 0.7	26.5	34.8 ± 0.6	27.2 ± 1.3	0.7	$10.94 \cdot 10^{12}$

* Sucrose concentration 0–20% (SANS experiment).The results of the SAXS spectrum fitting for the case of 40% sucrose concentration are given in the last line H_2O.

Kiselev M.A. ..., Aksenov V.L. // Crystallography. 2015. V. 60. No. 1. P. 140–150.

Characterization of nanosystems for the drug delivery

V.L. Aksenov – PNPI NRC "Kurchatov Institute"
M.A. Kiselev – Joint Institute of Nuclear Research

A morphology of the phospholipid transportation nanosystem (PTNS) (Fig. 1) developed by Institute of Biomedical Chemistry has been studied for the first time on the synchrotron of NRC "Kurchatov Institute" by the small-angle *X*-ray scattering method. PTNS is proved to be a vesicular system (Fig. 2) rather than a micellar one. For the concentration of PTNS in water 25% (5% – phospholipids, 20% – maltose, 75% – water), the phospholipid transport mean radius is shown to be R_{PTNS} = 160 ± 2 Å and the thickness of the lipid biolayer – d = 43.5 ± 0.5 Å.

Soy phospholipids present a complex multicomponent system (five different saturated and unsaturated phospholipids with a different length of the hydrocarbon tail (Fig. 3)). A possibility to determine the structural parameters of the vesicles formed from the soy phospholipids has been experimentally proved. These results open up a new direction of the nanodrug research by neutron and synchrotron sources. In this case, synchrotron experiments allow one to study the nanodrugs at the pharmaceutical concentrations.

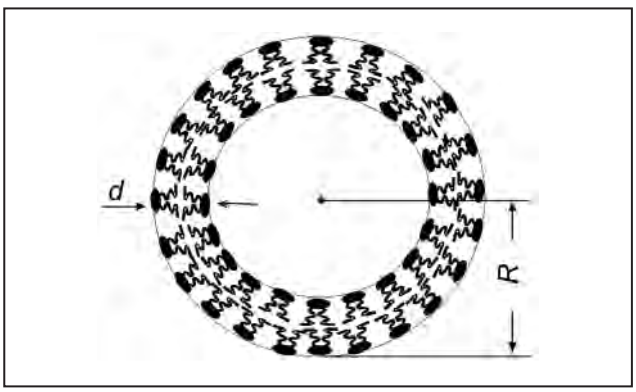

Fig. 2. The structure of the PTNS vesicle

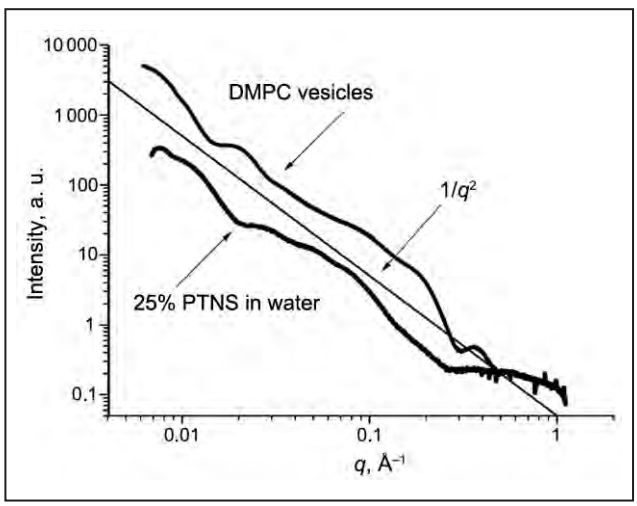

Fig. 1. Synchrotron small-angle scattering spectra of *X*-ray beams from the extruded vesicles of dimyristoyl phosphatidylcholine (DMPC) and PTNS

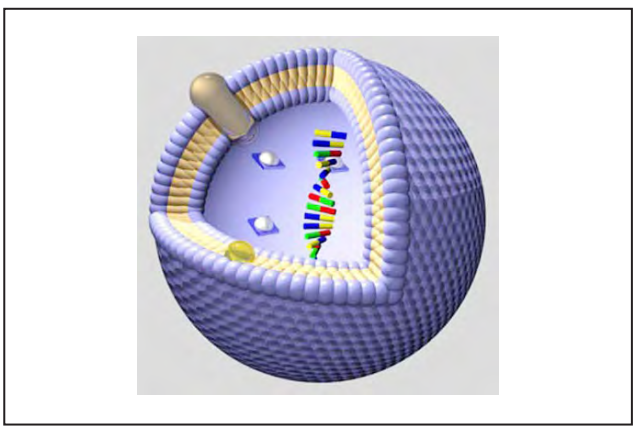

Fig. 3. The structure of the nanodrug based on the PTNS that incorporates water-soluble molecules (water volume within the vesicle) and insoluble (lipid biolayer) drugs

Aksenov V.L. et al. // J. Pharm. Biomed. Anal. 2015. V. 114. P. 288–291.

Radiobiological effectiveness of protons: the current state

N.A. Ivanov, Zh.S. Lebedeva
Knowledge Transfer Division, PNPI NRC "Kurchatov Institute"

Previously created calculation program for the formation of the proton beam line of the cyclotron C-80 can be applied to create a modified Bragg peak for the biological dose. The aim of the study is to convert an absorbed dose to the biological. The constant value relative biological effectiveness (RBE) of protons with energies 0–200 MeV equal to 1.1, is used in clinical practice. However, many radiobiological experiments show an increase in the RBE with decreasing proton energy. The Figure compares the biological dose based on clinically used RBE = 1.1, and on a phenomenological model using the relation between RBE and linear energy transfer (LET).

The Figure shows a significant increase in the biological effect in the distal part of the SOBP, which can lead to the overdosage of critical structures located beyond the target in most clinical situations.

These results indicate that the data available for the absorbed to biological dose convertion is not sufficiently accurate for use in clinical practice, and the gap in the understanding of the biological effects produced by protons does not allow to realize the potential of the method for proton therapy fully. In this connection it is necessary to initiate further experimental and theoretical research in this field.

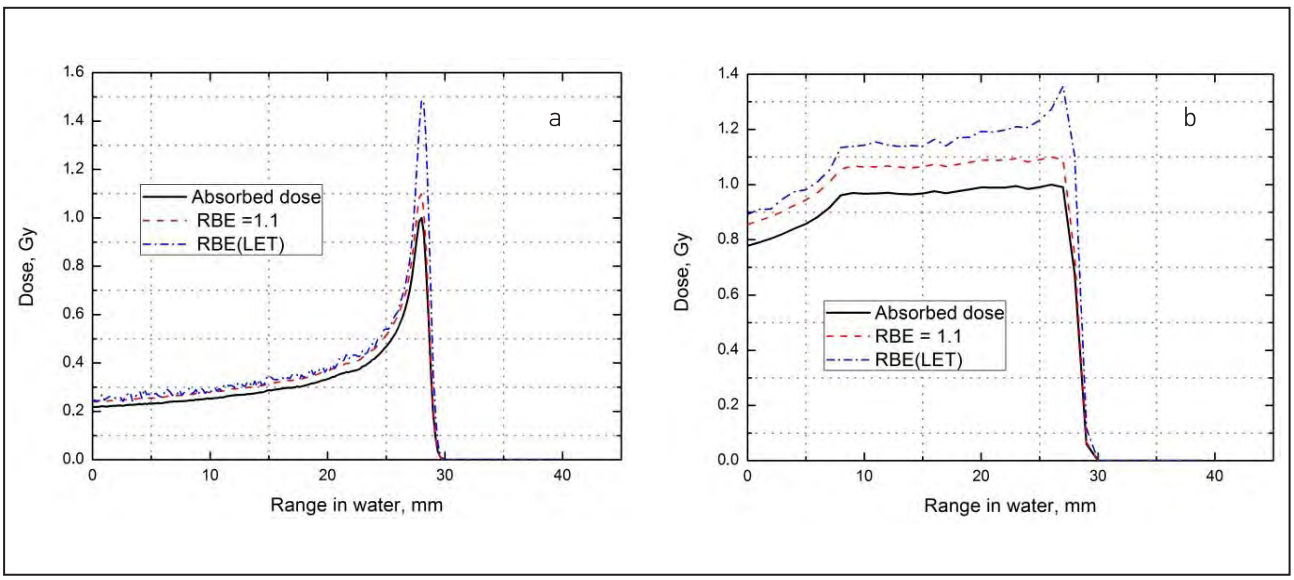

The 60 MeV protons Bragg peak: individual (a); spread out Bragg peak (SOBP) (b)

Ivanov N.A., Lebedeva Zh.S. Report PNPI NRC KI 2981. Gatchina, 2015. 24 p.

Target development for ^{82}Sr and $^{223, 224}$Ra production at the RIC-80 facility

A.E. Barzakh, L.Kh. Batist, D.V. Fedorov, V.S. Ivanov, P.L. Molkanov, F.V. Moroz, S.Yu. Orlov, V.N. Panteleev, Yu.M. Volkov
High Energy Physics Division, PNPI NRC "Kurchatov Institute"

The cyclotron C-80 (beam energy 40–80 MeV, intensity up to 200 μA) will be soon put into operation at PNPI NRC KI. This cyclotron is aimed at production of a wide spectrum of medical radionuclides for diagnosis and therapy. The radioisotope complex RIC-80 facility will be installed at C-80. The parameters of the C-80 cyclotron allow the production of a broad nomenclature of radioisotopes promising for diagnosis and therapy. One of the target stations will be equipped with a mass-separator. It will allow one to get some radionuclides of ultra-high purity. The unique parameters of the RIC-80 will allow the production of a broad range of radioisotopes. Among these are ^{68}Ge, ^{82}Sr, ^{111}In, $^{123, 124}$I, $^{223, 224}$Ra, ^{64}Cu, ^{67}Cu, ^{67}Ga, ^{77}Br and ^{81}Rb.

The essential components of the accelerator facilities for medical isotope production are the target materials and the target devices – a determinant of the production spectrum of medical radionuclides, the production efficiency and purity. This is a reason why the new target device development is the key factor for successful isotope production at RIC-80. In the first experimental tests for production of ^{82}Sr (the radionuclide widely applied in PET diagnostics) we used pills of yttrium carbide as the target material irradiated in the proton beam of the PNPI NRC KI synchrocyclotron. The irradiated target was then heated at 2 000 °C under vacuum, and the evaporated strontium was collected at a cooled collector. Figure 1 presents a gamma spectrum of the collected radioactivity at the collector. The final efficiency of strontium extraction was about 90%.

The radio nuclides decaying by alpha particle emission can be an effective tool for the therapy of different malignant tumors at an early stage of their formation. Among such nuclides are ^{223}Ra and ^{224}Ra, which can be produced by proton irradiation of uranium or thorium targets. Figure 2 demonstrates an alpha spectrum of species evaporated at 2 400 °C from a UC target and collected on a cooled tantalum collector. There is a possibility to increase the yields of Ra isotopes using the ThC target instead of the UC one. This material possesses good characteristics to be used as a target under high temperature coupled with the mass-separator ion source of surface ionization.

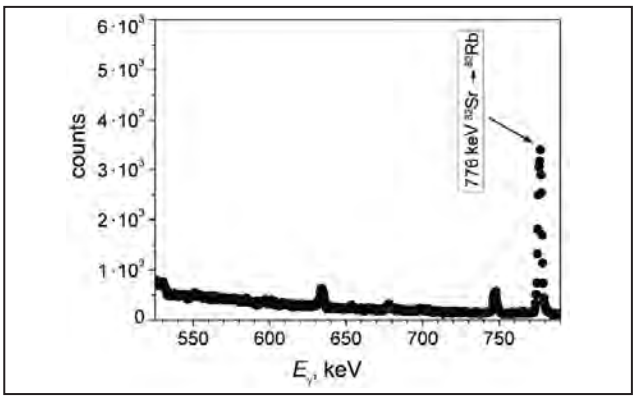

Fig. 1. Gamma spectrum of the collected radioactivity at a cooled collector during heating of the irradiated yttrium carbide samples at a temperature range 1 950–2 000 °C

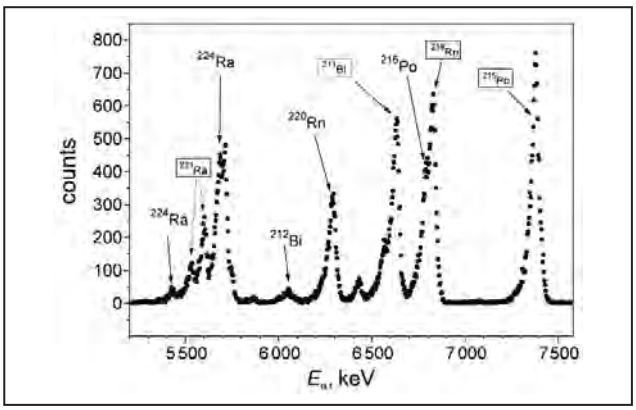

Fig. 2. Alpha spectrum of species evaporated at 2 400 °C from a UC target to a cooled tantalum collector. Isotopes from ^{223}Ra decay chain are placed in boxes

Panteleev V. N., Barzakh A. E., Fedorov D. V. et al. // Rev. Sci. Instrum. 2015. V. 86. P. 123510.

Nuclear Reactor and Accelerator Physics

Complex of calculations for safety ensuring of the PIK reactor

A.V. Korotynsky, A.S. Poltavsky, V.N. Tishchenko – Department of Nuclear and Radiation Safety
A.S. Zakharov – Department of Reactor Physics and Technology,
PNPI NRC "Kurchatov Institute"
E.V. Burlakov, A.A. Ivanov, A.V. Krayushkin et al. –
Kurchatov Nuclear Technology Complex, NRC "Kurchatov Institute"

The complex of calculations for safety ensuring of the PIK reactor was performed in the framework of paragraph 7 of "Safety ensuring of the PIK reactor operation (Stage 2)" under the Statement of R&D Works on "Research in the field of scientific, engineering and methodical foundation of development of nuclear power technologies, fuel supply and safety of use of nuclear energy for 2015 and planning period of 2016–2017". The Statement of R&D Works was approved by the Order of NRC "Kurchatov Institute" № 1965 dated 12/31/2014.

The following four joint scientific and technical reports were completed and approved:

– "The corrected calculations of the blackout accident of the reactor facility and accident caused by the break of outlet pipeline with diameter of 450 mm", where new conditions of the appearance of negative consequences of considered emergencies were identified, thus, it allows the provision of technical and organizational measures, which reduce or eliminate dangerous consequences of these emergencies;

– "Transient and accident computational analysis for the central experimental channel", that was performed with the use of three-dimensional model of coolant loop based on Relap5-mod3 computer code for the calculation of dynamic regimes of the PIK reactor. The accidents with the loss of coolant in this channel simultaneously can be a possible reason of a reactivity accident. Therefore, analysis considers additional failures and selection of different accident scenarios;

– "Carrying out of calculation for the purpose of verification of Relap5-mod3 code", during which model calculations of stationary, transient and emergency modes of the PIK reactor were performed for comparison with the results obtained with use of the SOCRAT/B1 code;

– "The corrected calculation of the radiation effects of beyond design basis events with fuel melting", which used a refined scenario of possible destructions of fuel in a beyond design basis accident with full blackout of a reactor complex. Modelling of radionuclide transport inside of the reactor complex and estimation of radioactive release into the environment with the dose assessment had been carried out in cases of ventilation system operation or its failure.

The results of obtained calculations will be used in the preparation of appendixes for the Safety Analyses Report of the PIK reactor.

1. The Corrected Calculations of the Blackout Accident of the Reactor Facility and Accident Caused by Break of Outlet Pipeline with Diameter of 450 mm. Report on R&D, Inv. No. 110.11-14/15-97. Moscow–Gatchina, 2015. 130 p.
2. Transient and Accident Computational Analysis for the Central Experimental Channel. Report on R&D, Inv. No. 110.11-14/15-98. Moscow–Gatchina, 2015. 127 p.
3. Carrying out Calculation Verification with the Use of Relap5-mod3 Code. Report on R&D, Inv. No. 110.11-14/15-99. Moscow–Gatchina, 2015. 106 p.
4. The Corrected Calculation of the Radiation Effects of Beyond Design Basis Events with Fuel Melting. Report on R&D, Inv. No. 110.11-14/15-100. Moscow–Gatchina, 2015. 66 p.

The neutron flux perturbations in the PIK reactor reflector

A.N. Erykalov – Theoretical Physics Division
K.A. Konoplev, I.M. Kosolapov, A.S. Zakharov – Department of Reactor Physics and Technology
A.S. Poltavsky – Department of Nuclear and Radiation Safety
S.L. Smolsky – Department of Exploitation of Nuclear Installations,
PNPI NRC "Kurchatov Institute"

One of the advantages of a heavy water reflector is that it is able to provide change of the form and sizes of experimental channels or new devices installation. Unperturbed thermal neutron flux at the PIK reactor in the reflection reaches $1.3 \cdot 10^{15}$ cm$^{-2} \cdot$ s^{-1} and $5 \cdot 10^{15}$ cm$^{-2} \cdot$ s^{-1} in a neutron trap that is located in the center of the core. The installation of any experimental devices in a reflector should take into account their influence on neutron fluxes.

The influence of neutron beam channel design on the density of thermal neutron flux in this channel and ambient space has been investigated previously in experiments at full-scale critical facility.

Using MCNP code the major factors of neutron flux perturbations in heavy water reflector were investigated for the first channels configuration (Fig. 1). The calculations were conducted for reflector states before and after the installation of channels. The increase in the sizes of channels is a main factor of neutron flux depression in a reflector. The reduction of density of thermal neutron flux at the channel bottoms or inside of the large – dimension channels reaches 50% and on the average ~ 35%. The appreciable factor is the insertion of a hydrogen-containing moderator in the channel volume. The channels also cause thermal neutron flux reduction in heavy water space between channels (Fig. 2). Due to the change of position of absorbing shutters – central control rods in a core or due to burnable poison depletion, the neutron flux deviates within 10% interval.

Possible approaches and criteria are considered for the estimation of each channel contribution to a share of useful consumed neutrons from a total number of generated ones. These estimations consider the neutron flux density, the geometrical size of a channel and its destination.

For the scientific program at the PIK reactor the most informative parameter is the spectral brightness of the channel – the differential characteristic that allow estimating intensity of extracted neutrons with needed energy in the unit of space angle from a horizontal neutron beam channel.

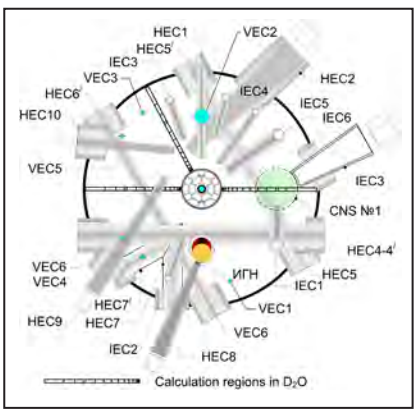

Fig. 1. Regions for neutron flux calculation

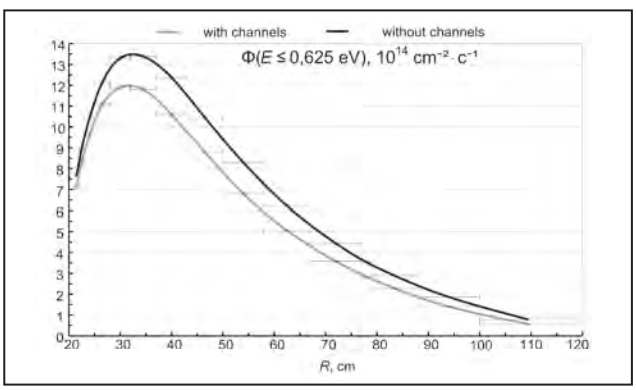

Fig. 2. Distribution of neutron flux in heavy water reflector

Erykalov A.N., Zakharov A.S., Konoplev K.A., Kosolapov I.M., Poltavsky A.S., Smolsky S.L. PNPI Preprint 2976. Gatchina, 2015. 21 p.

Measurement of tritium concentration in water coolant of the PIK reactor by the liquid-scintillation radiometry method

D.E. Romanova, D.Yu. Tugusheva, T.V. Voronina
Department of Nuclear and Radiation Safety, PNPI NRC "Kurchatov Institute"

Tritium concentration of heavy water can reach a few tens of Ci/l on heavy-water reactors. As a result tritium makes up a considerable part (up to 40%) of the personnel radiation dose. Two heavy-water systems are included on the project of the PIK reactor: a heavy-water reflector circuit and a liquid regulation cooling circuit. Its tritium concentration must not exceed 2 Ci/l. The organization of reliable tritium control of heavy-water coolant and technological water drain of the PIK reactor is required.

The most sensitive and exact method for the analysis of tritium water is a liquid-scintillation method. The calibration dependence of tritium concentration of water on radiometer account was determined by the modern spectrometry radiometer Thriathler LSC. The received calibration dependences (Fig.) are linear and stable. Their stability will allow one, not to carry out the regular adjustment of measurements. It is recommended to measure a single control solution of tritium water (with the known concentration) for every series of analysis (to control the state of the device and calibration).

The developed method can measure tritium concentration in the range ($3.7 \cdot 10^{-7}$–6) Ci/l. It will allow its application for both the control of the heavy water of reflector (up to 2 Ci/l) and for the control of light water of the primary coolant circuit (10^{-5}–10^{-3} Ci/l).

The preparation of one sample will take 15 min; the analysis on a radiometer – from 10 min (at measuring time = 60 s) to 2 h (at measuring time = 600 s). It is recommended to use the followings ratio of volumes sample/scintillation liquid for preparation of samples:

– 1 ml/10 ml – for the samples with middle tritium concentration (10^{-6}–$8.5 \cdot 10^{-3}$ Ci/l);

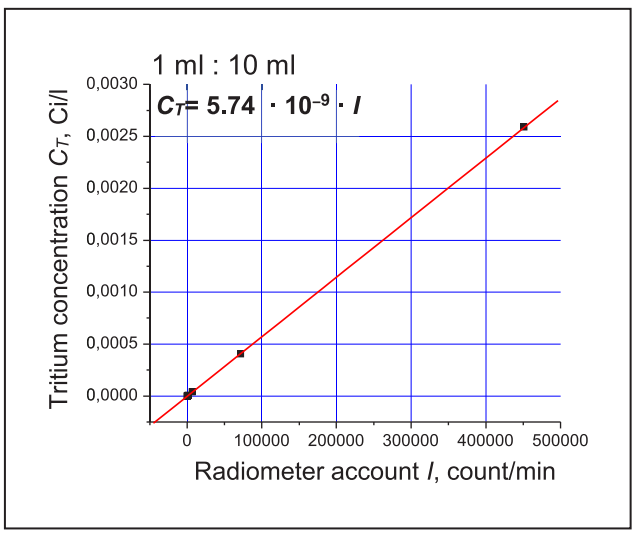

Calibration dependence of tritium concentration of water from radiometer account

– 8 ml/10 ml – for low-concentrated samples (< 10^{-6} Ci/l);

– 0.1 ml/10 ml – for high-concentrated samples (> $8.5 \cdot 10^{-3}$ Ci/l).

The relative error of determination of tritium concentration in the samples of water (intermediate- and high-concentrated) does not exceed 4%, while measuring the samples with low tritium concentration the error can amount to 10%.

Thriathler LSC allows measuring the spectra of water samples. It will allow reducing errors of analysis caused by the presence of the disturbing impurities. It is intended in the future to carry out the work on the determination of disturbing impurities (testing the influence of presumable corrosion products in heavy-water systems of the PIK reactor on the sampling data of a water coolant for the tritium content).

Measurement of Tritium Concentration in Light and Heavy Water by the Liquid-Scintillation Radiometry Method. Report of DNRS, Inv. No.15-02. Gatchina, 2015. 31 p.

Prototype of on-line safety system of the PIK reactor based on an industrial FT-NIR spectrometer

D.E. Romanova, T.V. Voronina
Department of Nuclear and Radiation Safety, PNPI NRC "Kurchatov Institute"

Detection of the reactor vessel disruption at its early stage is a relevant task to be solved at any operating reactor. Today, the Leak-Before-Break Concept is a modern approach to assure the safe operation of the reactor equipment. Such an approach demands a sure fixation of a leak for registration of through defects. It is impossible to organize an operating inspection of reactor vessel defects on the base of standard pressure and level detectors for the research heavy-water reactor PIK since the detection time for it is no less than one hour. However, it is possible to offer a more sensitive additional inspection method for the PIK reactor vessel integrity – on the decrease of deuterium content in heavy water of the Liquid Regulation Cooling Circuit (LRCC) that occurs at appearance of light water leakage in the primary cooling circuit. For this purpose, it is necessary to create a system of precise remote monitoring of the protium content in heavy water of the LRCC based on an on-line analyzer.

Previously it was shown that it is possible to solve this problem using the infrared (IR) spectrometry method (based on the FT-NIR spectrometer and the on-line cell with length of optical way 1–5 mm). At present, the system of permanent monitoring of heavy water concentration in the LRCC is included in the PIK reactor project. It is necessary to calibrate the on-line analyzer in laboratory, before setting it in the LRCC. It is not a simple task. The NIR range (12 500 to 4 000 cm^{-1}) consists of overtones and compound molecular vibrations of water (not main molecular vibrations of water), so the calibration dependence will be complex. The equipment for creation of an additional on-line safety system of the PIK reactor (industrial FT-NIR spectrometer MATRIX-F, industrial on-line steel cell in 2 mm thick and optical fiber) was given to in test exploitation in our laboratory in 2015. The prototype of the system was created under laboratory conditions, and the method of calibrating of the on-line heavy water analyzer was developed at this prototype. The optimum algorithm of calibration of analyzer was defined the organization of continuous circulation of heavy water through a cell on the closed design; stabilization of heavy water discharge through a cell by means (of) a pump; temperature control of the on-line cell.

The minimum of heavy water samples for calibrating of the analyzer is more than 20 in every range of concentrations. Calibration models were designed from received experimental data (the spectra of calibration solutions of heavy water, Fig.). The calibration error is 0.002 at.% for concentrated heavy water. The calibration error is 0.02 at.% for the wide range of heavy water concentration. Quality of calibration models was tested on independent heavy water samples.

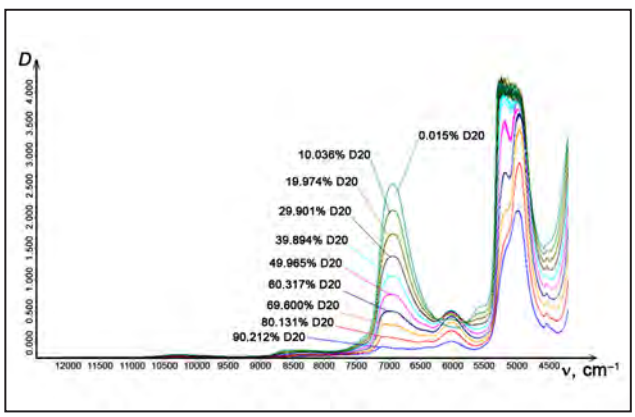

Spectra of calibration solutions of heavy water in the wide range of concentration

Voronina T.V., Zapitetskaya I.V. // Mat. of VI Scientific and Technical Conf. "Creation of an Additional Security System for the PIK Reactor Based on an Industrial FT-NIR Spectrometer". (Atomenergoanalitika-2014). Russia, 2014. P. 67–79.

Recent progress in the experimental study of LPCE process on EVIO pilot plant

I.A. Alekseev, S.D. Bondarenko, O.A. Fedorchenko, T.V. Vasyanina
Department of Reactor Physics and Technology, PNPI NRC "Kurchatov Institute"

A new LPCE column (LPCE-3) of 2 m packing height and 50 mm inner diameter expands the experimental possibilities of EVIO pilot plant (Table).

Experimental results are presented in comparison with those received on LPCE-1 and LPCE-2 earlier.

Fresh RCTU-3SM catalyst with a somewhat greater than average percentage of Platinum (1.33% versus 1.17%) and a little bit larger dimensions of SDBC carrier (spherical granules of 0.8–1.2 mm versus 0.5–1.0 mm) has been tested in LPCE-3. Both hydraulic and isotope separation characteristics of LPCE-3 filled with alternating layers of the catalyst and stainless steel spiral-prismatic packing in the volume ratio of 1 : 4 (the same packing and the same ratio as it used in LPCE-1 and LPCE-2 columns) have been studied.

LPCE-3 demonstrates very good capabilities. The throughput (Fig. 1) and performance (Fig. 2) of the column increased to a considerable extent compared to the characteristics of elder columns.

Dependence of separation performance on specific hydrogen load has been discovered.

Table. EVIO pilot plant columns

Column name	LPCE-1	LPCE-2	LPCE-3
Setting to work	2003	1995	2014
Packing height	5.4 m	5.9 m	2 m
Inner diameter	0.1 m	0.1 m	0.05 m
The number of sections	5	3	1
Packing / catalyst	4 : 1 (volume)		
Packing	Spiral-prismatic from stainless steel wire 2.2 × 2.2 × 0.2 mm		
Catalyst	RCTU-3		RCTU-3SM
Pt Content, mass % (NAA)	0.8–1 (1.17 ± 0.02)		0.8–1 (1.33 ± 0.02)
Carrier	SDBC		
Diameter of granules, mm	0.5–1.0		0.8–1.2

Separation performance expressed by a three-fluid model attribute K_c – mass-transfer coefficient for catalytic exchange (at fixed mass-transfer coefficient for phase exchange) is the same for different isotopes (H, D and T) in contrast to separation performance expressed by the overall mass-transfer coefficient, $K_y a$. Dependence of separation performance on column inner diameter (as on specific hydrogen load) can be explained by effect of channeling of fluids in counter-current flow because of poor liquid distribution.

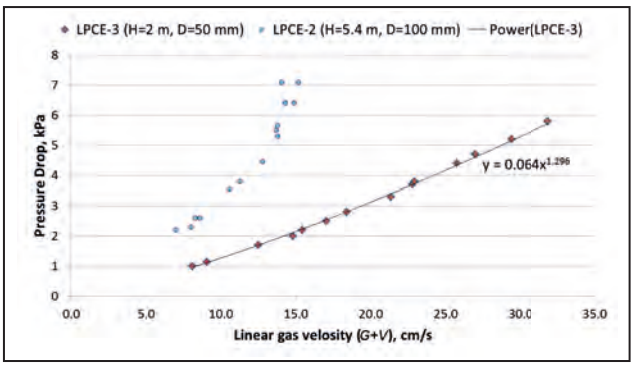

Fig. 1. Pressure drop versus linear gas velocity (hydrogen plus water vapour) for two columns

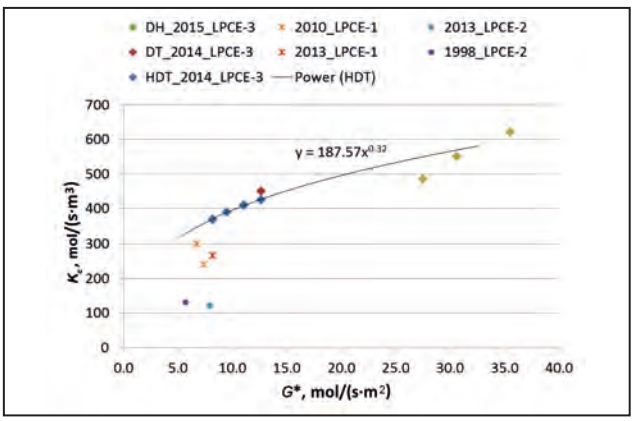

Fig. 2. K_c – mass-transfer coefficient for catalytic exchange versus specific hydrogen load (at fixed mass-transfer coefficient for phase exchange B_x = 500 mol/(m^3 · s))

To be presented at Tritium-2016 11th Int. Conf. on Tritium Science & Technology, April 17–22, 2016, Charleston, SC, USA.

Irradiation of structural materials in WWR-M reactor

S.R. Friedmann – Reactors Physics and Technology Department
S.P. Orlov – Department of Nuclear and Radiation Safety
V.L. Solovey – Neutron Research Division
O.P. Yakorev – Department of Exploitation of Nuclear Installations,
PNPI NRC "Kurchatov Institute"

Reactor WWR-M tests of structural materials have been carried out as part of background for physical and mechanical properties examination and radiation stability substantiation from 1985 to 2015. In 2015 analysis and examination of sample ampoules and witness samples have been performed.

The work content included determination of the following characteristics of ampoules and samples:

– irradiation conditions and duration for sample ampoules;
– neutron fluence for ampoules;
– loading pattern for samples and monitors in ampoules;
– samples material;
– type and characteristics of samples.

On the base of the work results, the list of basic irradiated materials and its characteristics has been made. This list can be used for investigations of physical and mechanical properties of materials aimed to service life substantiation of the PIK reactor vessel, in-vessel components and experimental channels.

The material list includes a wide range of materials science samples irradiated at WWR-M reactor:

– steel samples:
  • 08Cr18Ni10Ti; Cr18Ni10Ti-VAR, Cr18Ni10Ti;
  • ChS-42VI; ChS-42 TMP; ChS-42 (austenization); ChS-42 with Ti (austenization, aging);
  • Cr16Ni11Mo3BZr-VAR; Cr16Ni11Mo3; Cr16Ni11Mo3Ti-VAR;
  • 04Cr16Ni11Mo3Ti;
  • Cr15Ni35Mo3ChS56 (1 100 °C – 1 h);
– aluminum samples:
  • SAV-1, AT11, AD1, AMg3, AD33 (6061), SAV-6, AD31
– and also some pure Ge, Si and Al(999) samples.

The samples are suitable for investigations of physical and mechanical properties of materials after irradiation in the WWR-M reactor under temperature of ~ 70 °C up to various damaging doses. The maximum neutron fluence for steel samples was above $1 \cdot 10^{22}$ cm$^{-2} \cdot$ s^{-1} ($E > 1$ MeV); for aluminum samples the thermal neutron fluence was above $1 \cdot 10^{23}$ cm$^{-2} \cdot$ s^{-1} ($E < 0.2$ MeV). It is possible to examine mechanical properties both the base metal and joint weld.

On the base of the test results and investigation of the properties of the samples, the degradation of presented materials with neutron fluence typical for atomic reactor equipment at the coolant temperature to 100 °C can be determined.

Irradiation damage evolution of materials under temperatures 50–150 °C is underinvestigated. There are investigations analyzing current results for physical and mechanical properties of steel 08Cr18Ni10Ti irradiated up to fluence $5.6 \cdot 10^{22}$ cm$^{-2} \cdot$ s^{-1} ($E > 0.8$ MeV) under the temperature of 300–350 °C. It is of immediate interest for power reactors. Investigations of samples presented in the research report and available samples allow us to receive data on the properties of steels and aluminum alloys irradiated under the temperature to 100 °C. It is important both for the equipment substantiation and for the life extension of the reactors of PNPI NRC KI as well as many Russian research reactors.

Friedmann S.R., Orlov S.P., Solovey V.L. et al. Reactor Examination of Samples Tested within Material Science Ampoules in the Reactor WWR-M. Report, reg. No. 15ЯУ–03. Gatchina, 2015. 46 p.

20
30

Applied Research and Developments

Investigations of radiation hardness of the electronic components intended for aviation and space at the Roscosmos testing facility IS NP/GNEIS

L.A. Vaishnene – High Energy Physics Division
A.M. Gagarski, O.A. Shcherbakov, A.S. Vorobyev – Neutron Research Division
E.M. Ivanov – Knowledge Transfer Division,
PNPI NRC "Kurchatov Institute"
L.R. Bakirov – The Branch of JSC "United Rocket Space Corporation" – "Institute of Space Device Engineering"

Two shifts of the electronic components tests were done in 2015 by the Branch of JSC "United Rocket and Space Corporation" – "Institute of Space Device Engineering" at the neutron testing facility IS NP/GNEIS (Fig.) with a neutron spectrum resembling that of atmospheric neutrons in a wide energy range 1–1 000 MeV. For six samples of SRAM (Static Random Access Memory) of national (two technological norms) and foreign (four technological norms) production, used in aviation and space equipment, the single event upset (SEU) and latch-up (SEL) cross sections have been obtained. Simultaneously with the testing, methodological works were carried out with the aim of improving parameters of the neutron beam profile meter.

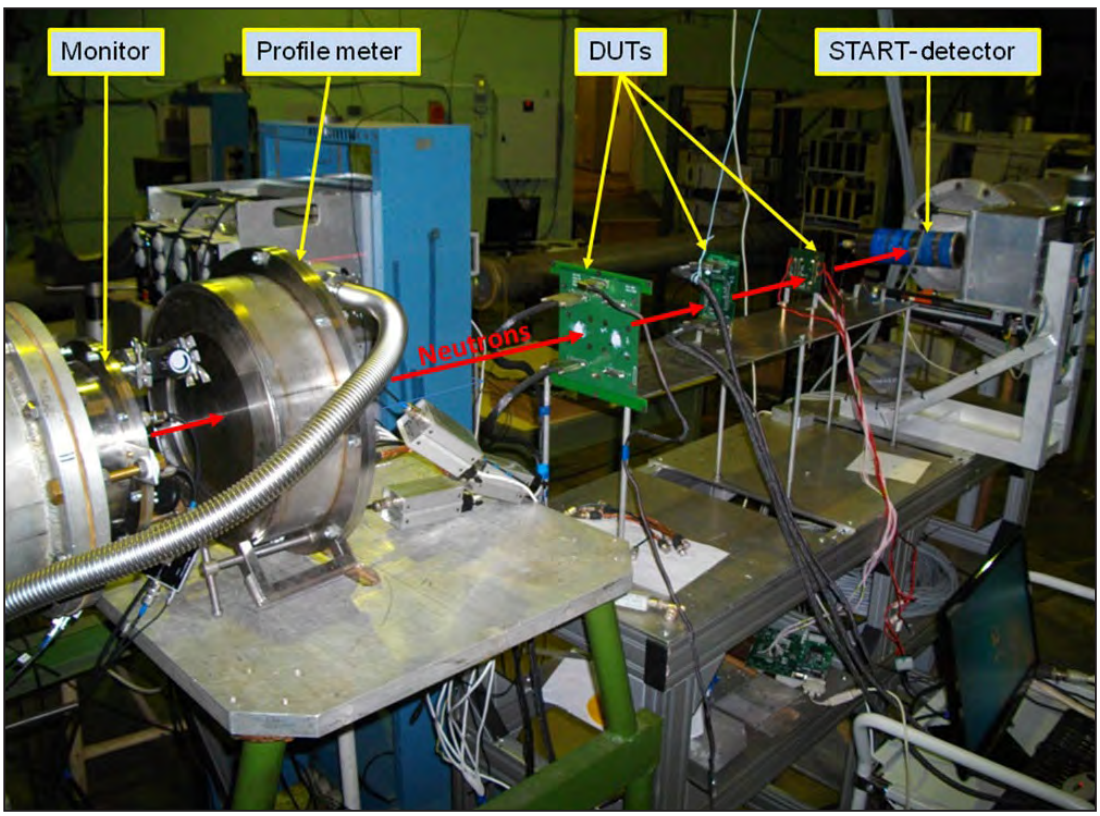

Neutron testing facility IS NP/GNEIS

1. *Shcherbakov O.A., Vorobyev A.S., Gagarski A.M., Vaishnene L.A., Ivanov E.M. et. al.* // Book of Abstracts of the XXIII Int. Seminar on Interaction of Neutrons with Nuclei. JINR, 2015. P. 76.
2. *Shcherbakov O.A., Vorobyev A.S., Gagarski A.M., Vaishnene L.A., Ivanov E.M. et. al.* // Proc. of 15th Eur. Conf. on Radiation and Its Effects on Components and Systems (RADECS-2015). 2015. P. 288.

Clusters of spikes in CCD-matrices, irradiated by nucleons

K.N. Ermakov, N.A. Ivanov, O.V. Lobanov, V.V. Pashuk –
Knowledge Transfer Division, PNPI NRC "Kurchatov Institute"
M.O. Prygunov – LLC "NPC "Granat"

Under the action of protons and neutrons in the CCD-matrices as a result of nuclear reactions the spikes are formed which are the long-term damages to the pixels, in which the dark currents I_{dc} significantly exceed the average value of the dark currents in the pixels of the original matrix. In the publication it was established that in CCD-matrices, irradiated by nucleons, clusters are formed from multiple adjacent spikes. In this paper we consider the kinetics of the behavior of such clusters, both in the process and after irradiation. We investigated the influence of protons with energy of 1 000 MeV and neutrons of the atmospheric spectrum with a maximum energy of 1 000 MeV on the CCD-sensor Sony ICX259AL that contain ~ $4 \cdot 10^5$ pixels with the size of 6.50×6.25 μm^2.

As an example, Fig. 1 shows the relief of one of the clusters in the process and after irradiation by neutrons. This cluster was formed when neutron fluence is $5.3 \cdot 10^8$ cm^{-2} (Fig. 1a). Immediately after this exposure, the cluster had dimensions of ~ 13×12.5 μm^2 and included four spike.

As a result of subsequent irradiation to a fluence of $3.2 \cdot 10^9$ cm^{-2} the brightness of the spikes in this cluster increased, their number increased to eight, and the transverse size of the cluster has increased to ~ 13×25 μm^2 (Fig. 1b). The growth mechanism of the cluster and the spikes brightness is perhaps due to the fact that the disturbed crystal structure of the semiconductor material in the cluster is the attractor for radiation defects formed near the cluster during subsequent irradiation.

Figure 1c shows the topography of the same cluster 214 h after irradiation. It is seen that there is a reduction in the number of spikes and the transverse cluster size, and also the reduction of the brightness of spikes in the cluster. There was also the disappearance with time of some clusters, in which the brightness of the spikes was reduced to I_{dc} values in non-irradiated CCD-matrix.

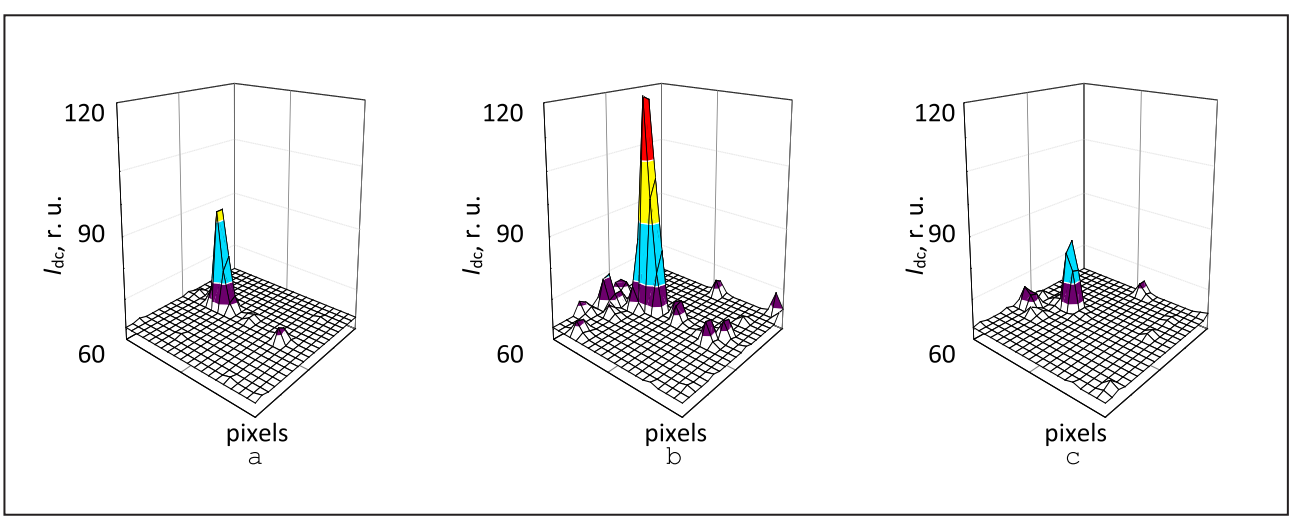

Fig. 1. Relief of spike cluster in the CCD irradiated by neutrons: fluence is $5.3 \cdot 10^8$ cm^{-2} (a); fluence is $3.2 \cdot 10^9$ cm^{-2} (b); after 214 h after exposure (c)

Figure 2 shows the time dependence of the distribution of pixels according to the magnitude of the dark current in the CCD after the exposure. The analysis of the speed of reduction of number of spikes in the CCD-matrix irradiated by nucleons showed that the time dependence of the number of spikes N can be approximated by an exponential function: $N \sim \exp(-t/\tau)$ when the value of $\tau \sim 3.5 \cdot 10^4$ s.

It should be noted that the emergence of clusters of spikes under the influence of nucleons indicates the possibility of multiple failures and failures in integrated circuits with the size of sensitive areas near and smaller pixel size in the studied CCD. The observed properties of the spike cluster growth during the irradiation and annealing of radiation defects in the damaged pixels provide grounds for continuing the research with the aim of increasing the reliability of the microelectronic devices in the radiation fields.

The research was supported by Russian Foundation for Basic Research, grant No. 14-29-09240.

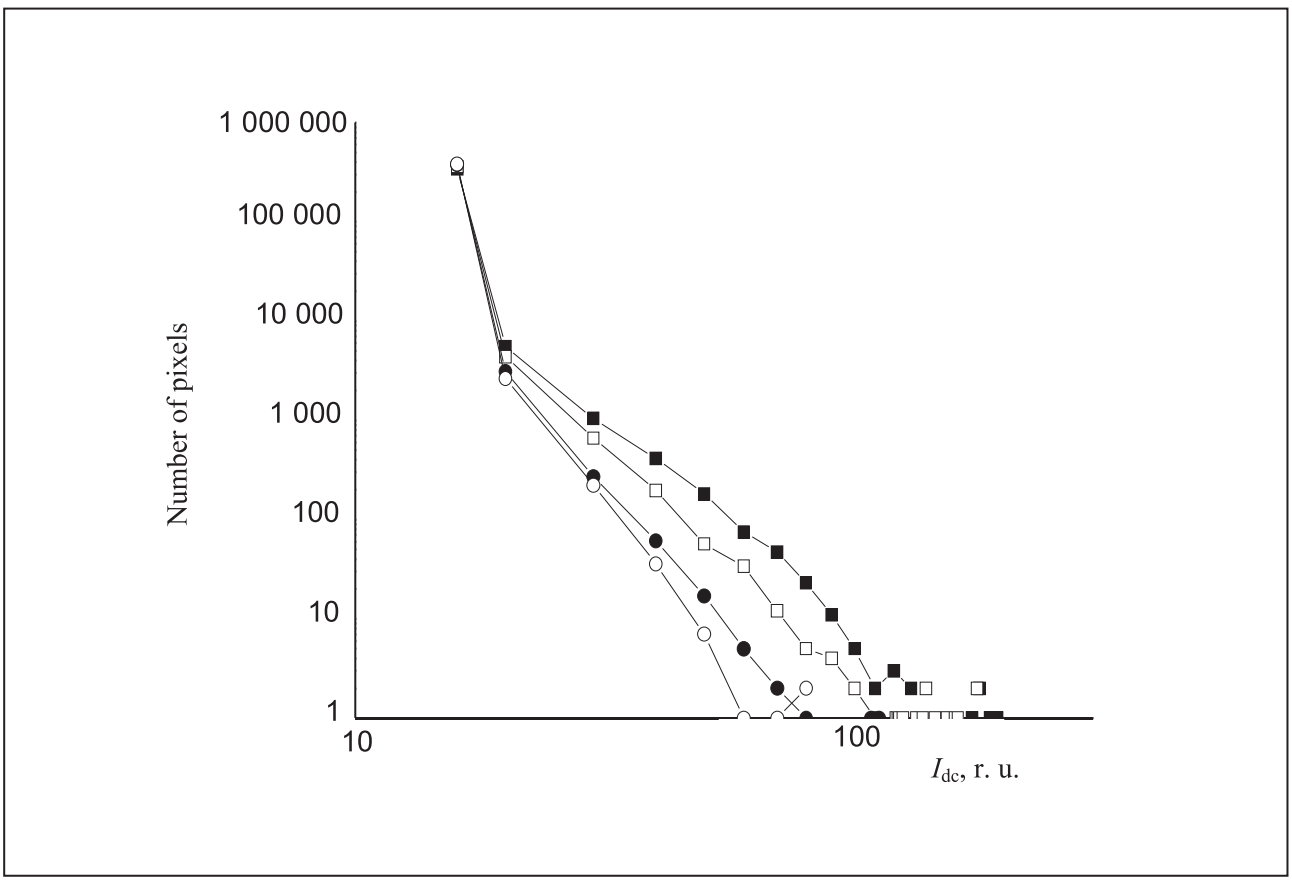

Fig. 2. Dependence of the distribution of pixels in the current value of the CCD irradiated by neutrons with a fluence of $3.2 \cdot 10^9$ cm^{-2}, on the time after the end of irradiation: ■ – 2.4 h, □ – 40 h, ● – 182 h, ○ – 428 h

Ivanov N. A., Lobanov O. V. ..., Pashuk V.V. et al. // Book of Abstracts of the 18th All-Russian Scientific-Technical Conf. on the Radiation Resistance of Electronic Systems "Resistance-2015". 2015. P. 134–135.

Final calculations and experimental adjustment of proton beams with energies in the range of 64–1 000 MeV for radiation resistance testing of electronic components

D.A. Amerkanov, S.A. Artamonov, G.I. Gorkin, V.P. Gres, E.M. Ivanov, G.S. Lebedeva, G.F. Mikheev, V.V. Pashuk, G.A. Riabov, V.A. Tonkikh, D.S. Udoldin – Knowledge Transfer Division
S.V. Kosianenko, V.G. Muratov, V.A. Solovei – Neutron Research Division,
PNPI NRC "Kurchatov Institute"

In order to ensure the successful operation of aviation and space techniques in radiation environment there is a need for radiation resistant electronic equipment. A universal center for testing of Electronic Components Base (ECB) for the needs of aviation and space research was created at PNPI NRC KI synchrocyclotron SC-1000 jointly with the Branch of the "United Rocket and Space Corporation" – "Institute of Space Design Engineering".

One of the main instruments of these tests is a variable energy proton beam. At the SC-1000, it was decided to create the quick-adjustable proton beams with energies of 64, 100, 200, 300, 400, 500, 600, 700, 800, 900, and 1 000 MeV with a set of predetermined properties for ECB radiation tests. For this purpose, the process of ECB irradiation had to be automated to the maximum. In particular, a copper degrader with remote variation of its length was designed and developed, which enabled the setting of the required value of the beam energy for each experiment in a fast and safe mode. The degrader was successfully positioned as close to the channel of the focusing lens as possible, which resulted in an increased capture of the beam and, consequently, in an increase in its intensity in the irradiation area. It provided a full computer control of the beam line magnetic elements.

A realization of such an extensive program required the intensive lenient calculations for each desired value of the beam energy. With the use of Geant4 Monte Carlo program complex, the trajectories of millions of protons with an energy of 1 000 MeV have been simulated tracking their propagation in the copper degrader. The parameters of the beam passing through the degrader, as well as the length of the degrader, which sets the desired beam energy, were also determined. These data were used as input for the MEZON and OPTIMUM programs, which allowed us to trace the trajectory of each proton in the channel, to optimize the beam parameters in it and to obtain the optimal modes of the beam line magnetic elements.

Being based on the calculations performed, the subsequent experimental adjustment of the proton beams of variable energy has allowed achieving of all necessary parameters for the ECB test. The required beams in the energy range 1 000–64 MeV with a density intensity of $1 \cdot 10^9$–$6 \cdot 10^5$ $cm^{-2} \cdot s^{-1}$ in the irradiation area, and 10% homogeneity within diameter of at least 25 mm were obtained.

Equipment for the radiation ECB tests

Artamonov S.A., Ivanov E.M., Lebedeva G.S., Riabov G.A. Numerical Simulation and Optimization of the Variable Energy 60–1 000 MeV Proton Beams at PNPI Synchrocyclotron for Testing of Radiation Resistance of Electronics // PEPAN Lett. 2015. In Press.

Neutron beam profile meter for energies up to 200 MeV

O.A. Shcherbakov, L.A. Vaishnene – High Energy Physics Division
A.M. Gagarski, A.S. Vorobyev – Neutron Research Division,
PNPI NRC "Kurchatov Institute"

In the course of the electronic components testing at the neutron test facility IS NP/GNEIS, a profile meter is used for the neutron beam profile measurements in the energy range 1–200 MeV. This device developed at the PNPI NRC KI is based on the two-coordinate Multiwire Proportional Counter (MWPC) 140 × 140 mm^2 in size (Fig. 1). The principle of operation of the profile meter is based on registration by means of MWPC of the fission fragments from ^{238}U(*n*, *f*)-reaction induced by beam neutrons in the converter material (Uranium), deposited on the MWPC cathode manufactured from the thin Mylar film. An information from the (*X*, *Y*)-anodes consisting of 140 gilded tungsten wires aligned parallel with the 1 mm gap is read out throughout the delay lines into the registration system. The fast FLAS-ADC (250 MSample/s, 12-bit) of this system is used for digitizing of the MWPC signals. The spatial resolution of the profile meter was found to be in the range of 2–4 mm. Its high processing speed in conjunction with the time-of-flight method enable one to measure the neutron beam profile as a function of neutron energy. A 3D-image of the beam profile shown in the Fig. 2 below corresponds to the neutron collimator 75 mm in diameter. By virtue of using ^{238}U with a negligibly small fission cross section below the threshold (~ 1 MeV), the developed profile meter has a very low sensitivity to the room background neutrons inside the IS NP/GNEIS facility room.

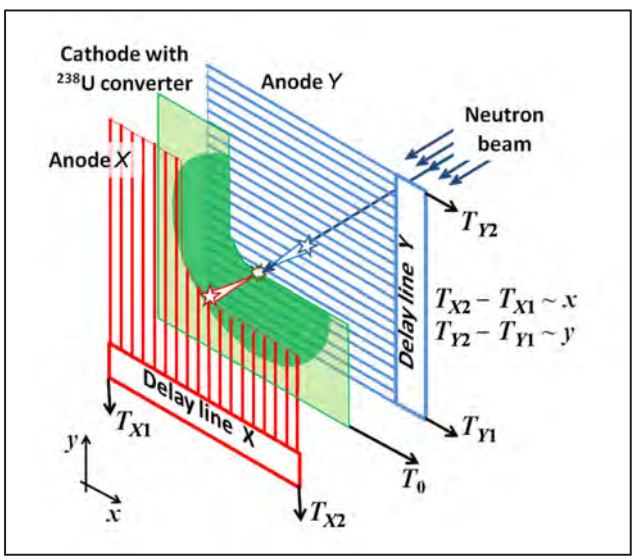

Fig. 1. Scheme of the profile meter

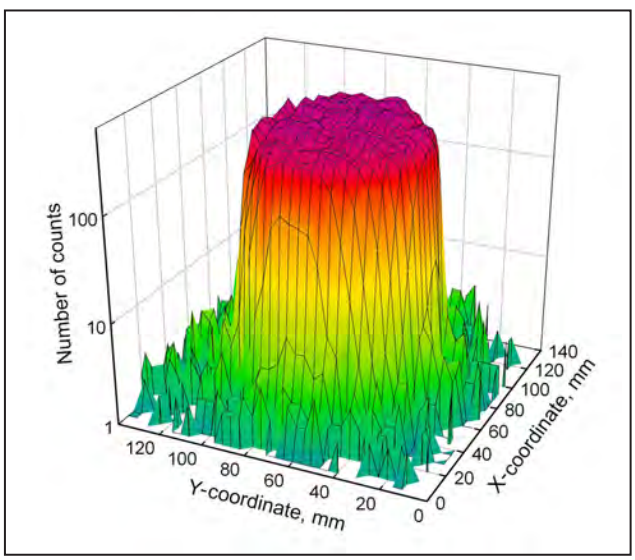

Fig. 2. 3D-image of the neutron beam profile

1. *Shcherbakov O.A., Vorobyev A.S., Gagarski A.M., Vaishnene L.A., Ivanov E.M. et al.* // Book of Abstracts of the XXIII Int. Seminar on Interaction of Neutrons with Nuclei. JINR, 2015. P. 76.
2. *Shcherbakov O.A., Vorobyev A.S., Gagarski A.M., Vaishnene L.A., Ivanov E.M. et al.* // Proc. of 15th Eur. Conf. on Radiation and Its Effects on Components and Systems (RADECS-2015). 2015. P. 288.

Results of PNPI NRC KI participation in collaboration on control of ATLAS experiment on Large Hadron Collider

V.M. Filimonov, V.P. Khomutnikov, Yu.F. Ryabov
Knowledge Transfer Division, PNPI NRC "Kurchatov Institute"

The discovery of the Higgs' boson in the ATLAS and CMS experiments on Large Hadron Collider (LHC) at CERN is a brilliant achievement of the world nuclear physics. The Detector Control System (DCS) has played a substantial role in providing the consistently reliable functioning of the ATLAS experiment The PNPI NRC KI team has been participating in the development and further support of that DCS from the very beginning.

The LHC upgrade consisting in the doubling of the beam power and the DCS system improvements were performed in 2013–2015. The main goals of the ATLAS detector control team during the year 2015 were completing of the reintegration of the system including 16 systems of experiment subdetectors and running it in the new Run 2 stage of the experiment. Activities on improvement of a CANOpen OPC server widely used at CERN and the top-level systems immediately supported by the PNPI NRC KI team (rack control, tools of configuring and monitoring of the subsystem, information exchange between DCS and LHC, ATLAS condition database tools, access control) have been combined with the support of subdetector teams in upgrade and including new hardware and software tools, reintegration and restart of their local systems. The main results of the PNPI NRC KI activities on these directions reported, in particular, at international conferences, can be listed as follows:

– Issuing of a production release of the CANOpen OPC server in accordance with the advanced standard OPC UA, running and support that server in both central systems and a series of subdetector control systems;

– Upgrade of the rack control system and the system of subdetector control system observation;

– Improvement of DCS–LHC data exchange interface;

– Developing of tools and coordination of moving to new implementation of the Condition database for the event reconstruction (in the DCS-related part) for all of ATLAS subdetectors.

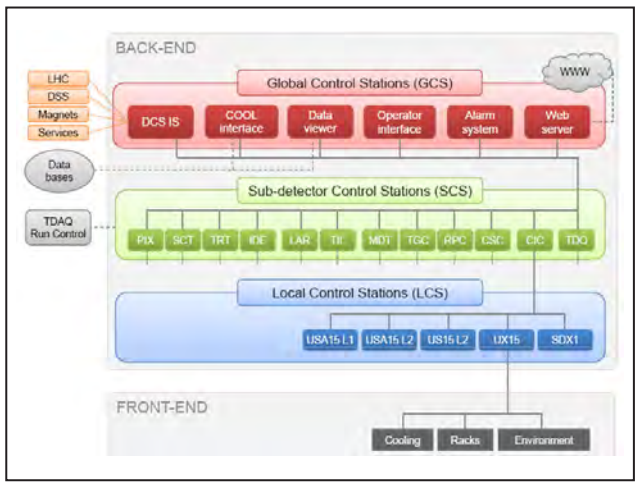

The architecture of ATLAS–DCS

1. *Nikiel P. ..., Filimonov V. et al.* // Proc. of 21th Int. Conf. Computing in High Energy Physics (CHEP2015). 2015. http://chep2015.kek.jp/
2. *Maciejewski J., Khomutnikov V. et al.* // Int. Workshop "Database & Metadata TIM in Genoa". 2015. https://indico.cern.ch/event/390140/session/2/contribution/21/attachments/1150664/1651791/DB_Future_08_09_2015_ATLAS_DCS.pdf

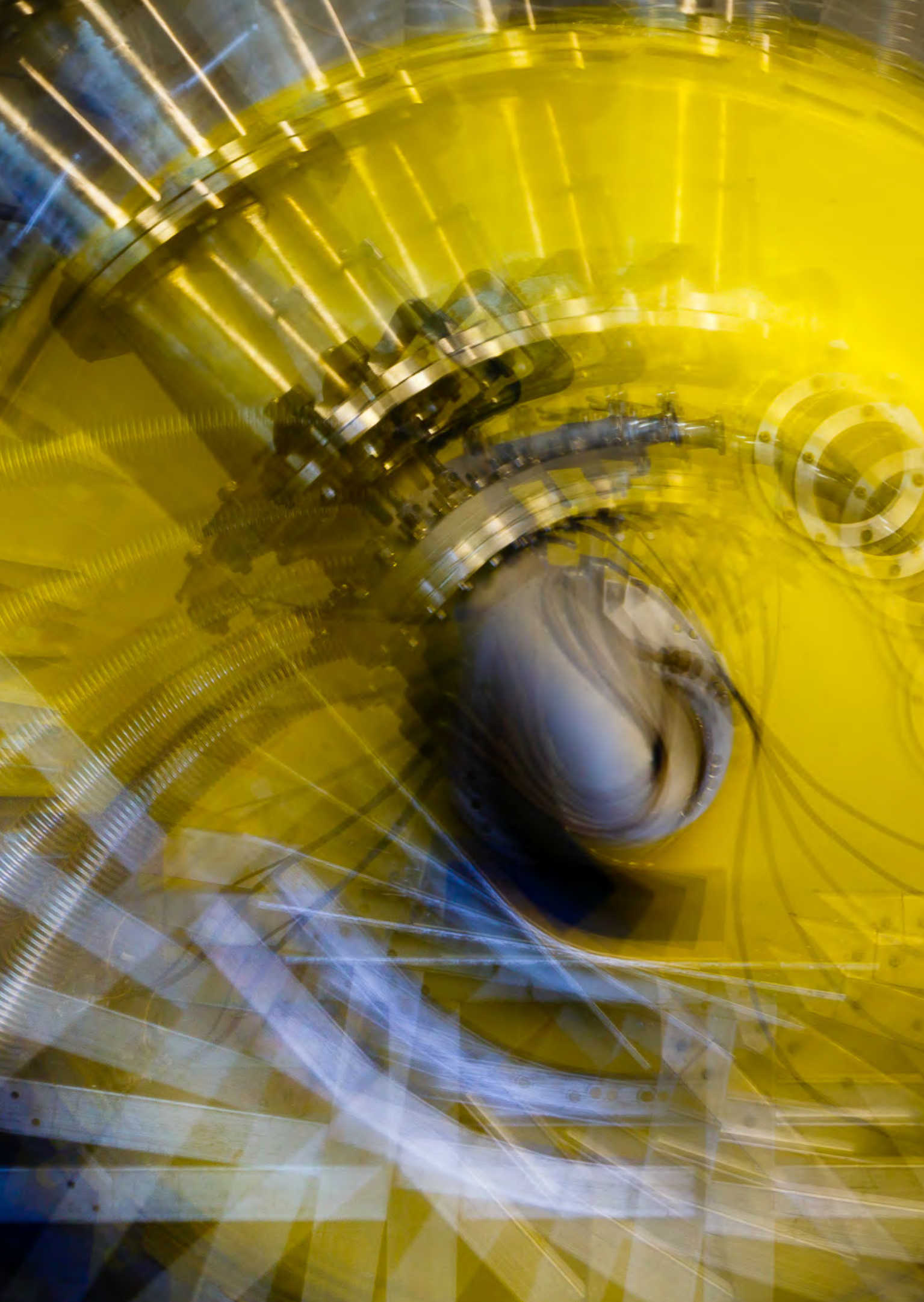

Basic Installations

The status of the 1 000 MeV synchrocyclotron PNPI NRC KI in 2015

S.A. Artamonov, E.M. Ivanov, G.F. Mikheev
Knowledge Transfer Division, PNPI NRC "Kurchatov Institute"

Synchrocyclotron SC-1000 at protons energy 1 000 MeV with the extracted beam intensity 1 mkA is one of the basic facility of PNPI NRC KI and it is widely used for fundamental research in particle physics, nuclear structure and nuclear reaction mechanisms, solid state physics, as well as in applied works on radiation testing and nuclear medical research.

In 2015 the accelerator has been in operation for 1 874 h. The chart shows the distribution of SC-1000 working time in certain areas of research carried out on its beam.

The most significant work in 2015 is the completion of development SC-1000-based testing center for aerospace electronics radiation resistance. This testing center includes two test stands of the proton beams, as well as the test stand of the neutron beam similar to the atmosphere spectrum.

Development of proton stands included the following main stages:

– Execution of calculations by SRIM code and manufacturing of copper degrader; calculation of additional option of tungsten degrader;

– Numerous calculations execution by Geant3 and Geant4 codes of protons passing through the degrader material that defines the initial conditions for the optimization of the parameters of the tract magnetic elements;

– Optimization of magnetic elements proton tract parameters;

– NMR magnetometer sensors in E-9 and a magnet of SP-40 installation for fixing energy of the transported proton beam;

– Development and manufacturing of an automated system of the proton beam energy absorption;

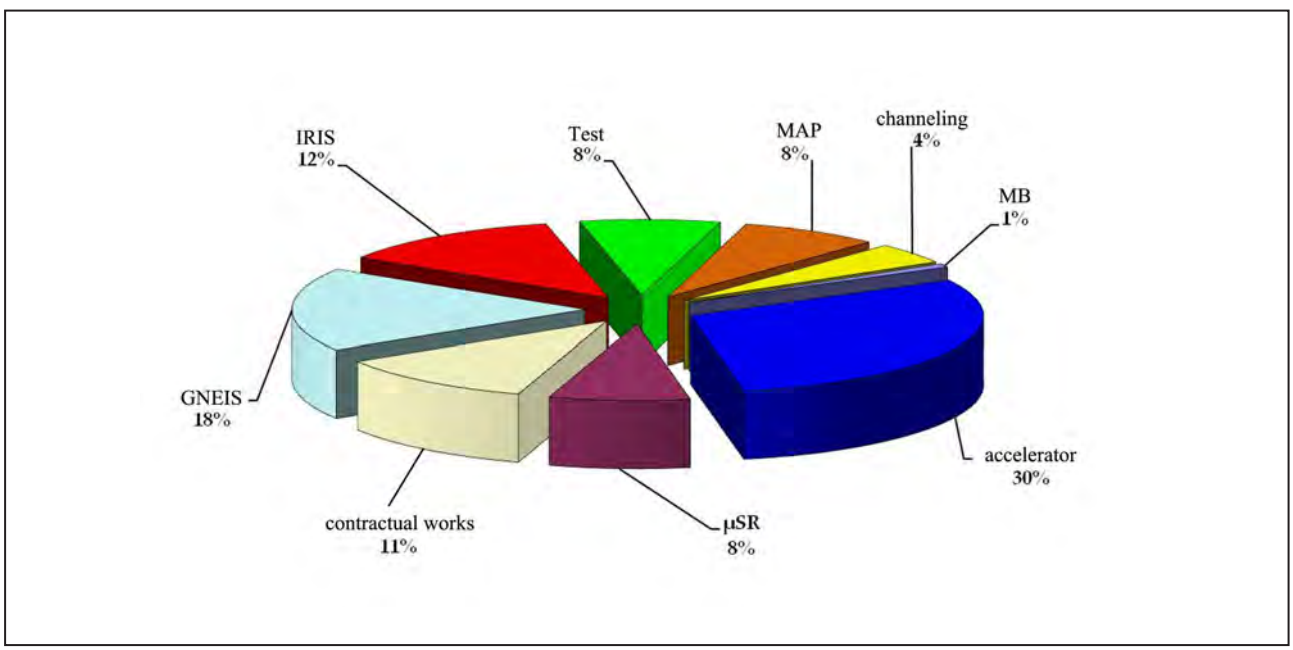

The directions of works carried out on the beams of synchrocyclotron SC-1000

– Development and manufacturing of Printed Circuit Board (PCB) for an automatic control system of currents in transport beam magnetic elements;

– The automated system of linear movement of PSB manufacturing;

– Producing of heating system for PCB placement box;

– Development and manufacturing of the profilometer with a possibility to measure protons distribution in a beam;

– On-line system of monitoring of a proton beam development.

The first test stand – at a constant proton beam energy E = 1 000 MeV has flux density at the site 10^8 cm$^{-2} \cdot$ c^{-1}, intensity heterogeneity of ≤ 5% in the irradiation diameter of 26 mm; on-line control of proton fluency is conducted. The Certificate No. 178/15 on its use is received.

There is the second test stand – in beams of variable energy 900–64 MeV. There are achieved: the intensity of the density at the target of irradiation from 10^9 to $8 \cdot 10^5$ cm$^{-2} \cdot$ c^{-1} in the energy range 900, 800, 700, 600, 500, 400, 300, 200, 100, 64 MeV and 10% in the beam intensity non-uniformity at the size of the area of at least 25 mm in diameter. The temperature of the test object may vary in the range +250 ÷ +125 °C. On-line controls of proton fluencies are conducted. The Certificate No. 177/15-1 on its use is received.

The description of the test stand based on a neutron beam of an atmospheric range is provided in other article of this collection.

All three stands are included in the Interagency Testing Center of the State Corporation Russian Space Agency “Roscosmos”, and stand in the neutron beam is included also in the international standard IEC-62396-2.

It is necessary to emphasize that the SC-1000 synchrocyclotron PNPI RNC KI is the exclusive accelerator in Russia, where in one place it is possible to conduct electronic components radiation testing in proton beams of variable energy, as well as in the neutron beam spectrum similar to atmospheric one.

Закрытое Акционерное Общество
«Инновационные технологии «Тест-Прибор»
ЗАО «ИТ «Тест-Прибор»

АТТЕСТАТ

№ 178/15

Дата выдачи 21 сентября 2015 года

Удостоверяется, что Испытательный стенд ИС ОП, ЦЛКТ.412110.013
наименование и обозначение испытательного оборудования
зав. № 75252253,
заводской или инвентарный номер
принадлежащий Филиалу ОАО «ОРКК» – «НИИ КП»,
наименование предприятия (организации), подразделения, центра
по результатам первичной аттестации признан пригодным для использования при испытаниях продукции, в соответствии с характеристиками, указанными в протоколе № НПК-1/4916 от 21 сентября 2015 года

Периодичность аттестации 24 месяца
(месяцев, лет)

Аттестат выдан ЗАО «ИТ «Тест-Прибор»

ГЕНЕРАЛЬНЫЙ ДИРЕКТОР
ЗАО «ИТ «Тест-Прибор» В. А. Подосинников

Экспертное заключение ФГУП «ВНИИФТРИ»,
подтверждающее возможность ЗАО «ИТ «Тест-Прибор» проводить аттестацию испытательного оборудования, применяемого при оценке соответствия оборонной продукции №10.003-2014

АТ N004518

Закрытое Акционерное Общество
«Инновационные технологии «Тест-Прибор»
ЗАО «ИТ «Тест-Прибор»

АТТЕСТАТ

№ 177/15-1

Дата выдачи 21 сентября 2015 года

Удостоверяется, что Испытательный стенд ИС НП, ЦЛКТ.412110.010,
наименование и обозначение испытательного оборудования
зав. № 75252247,
заводской или инвентарный номер
принадлежащий Филиалу ОАО «ОРКК» – «НИИ КП»,
наименование предприятия (организации), подразделения, центра
по результатам первичной аттестации признан пригодным для использования при испытаниях продукции, в соответствии с характеристиками, указанными в протоколе № НПК-1/4917 от 21 сентября 2015 года.

Периодичность аттестации 24 месяца
(месяцев, лет)

Аттестат выдан ЗАО «ИТ «Тест-Прибор»

ГЕНЕРАЛЬНЫЙ ДИРЕКТОР
ЗАО «ИТ «Тест-Прибор» В. А. Подосинников

Экспертное заключение ФГУП «ВНИИФТРИ»,
подтверждающее возможность ЗАО «ИТ «Тест-Прибор» проводить аттестацию испытательного оборудования, применяемого при оценке соответствия оборонной продукции №10.003-2014

АТ N004515

The Device for Measuring the Profile of the Beam of High-Energy Accelerators: a Utility Model Patent No. 152734 / E.M. Ivanov, S.V. Kosianenko, G.F. Mikheev, A.N. Suvorov, V.M. Suvorov; Priority of 21.01.2015.


ЯДЕРНОЙ
ПИК

Management and Research

PIK-based International Center for Neutron Research

International Center for Neutron Research (ICNR) is being created on the base of the PIK neutron facility. In 2010, PNPI NRC KI signed an agreement on cooperation with the Helmholtz-Zentrum Geesthacht (HZG) about the transfer of part of HZG neutron stations to the PIK reactor. In 2014, the National Research Center "Kurchatov Institute" signed an agreement with the Forschungszentrum Jülich (FZJ), the coordinator of the participation of German Research Centers in ICNR establishment in Gatchina. The cooperation with German Neutron Research Centers was discussed in detail at the workshop in October 2013 in Gatchina. The workshop participants stated the fact that the PIK reactor, along with the reactor of the European Center for Neutron Research, Institute Laue-Langevin (ILL) (Grenoble, France), and the spallation source being built in Sweden (Lund) based on the ESS proton accelerator, is included as a research base in a strategy of neutron science development in Europe.

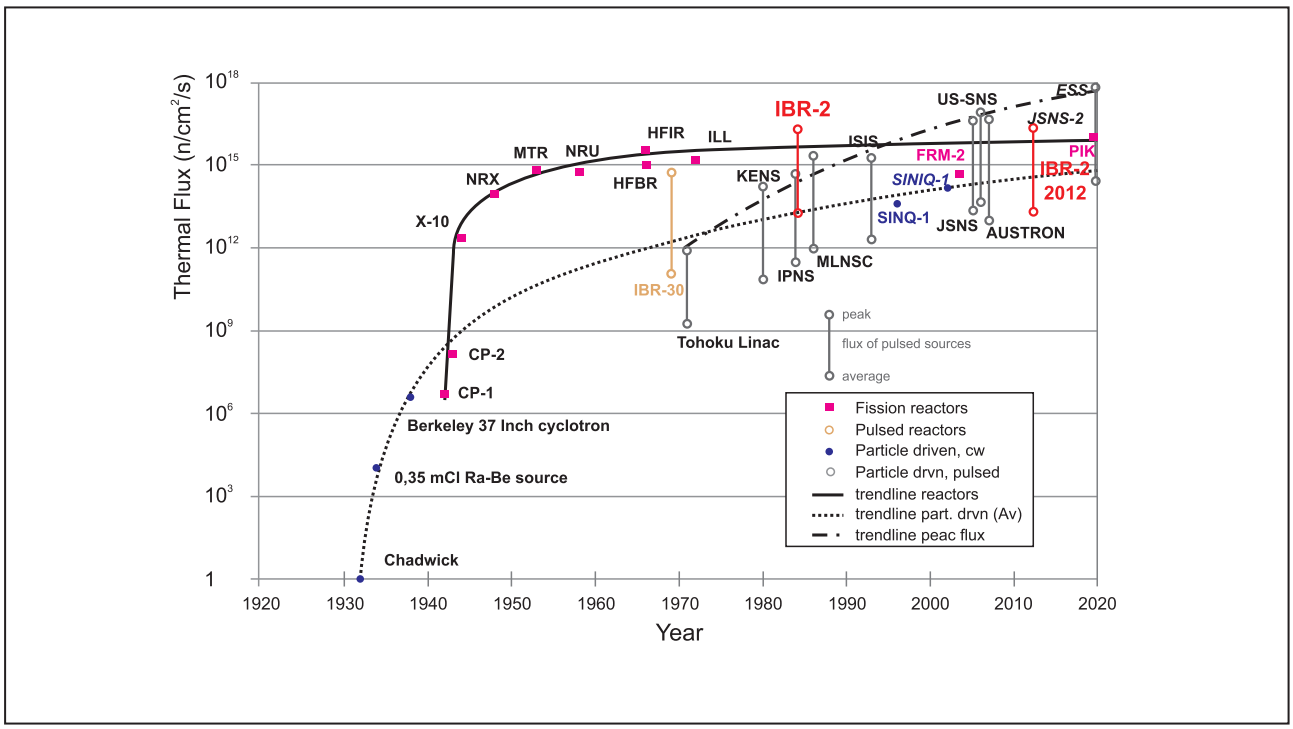

Evolution of a thermal flux at different European neutron sources over the past century

Formation of a scientific program and a program for design and construction of the PIK instrumentation base is performed in coordination with other neutron centers, such as Joint Institute for Nuclear Research (JINR) (Russia), FZJ on basis of Technische Universität München (TUM) (Germany), ILL (France) and ESS (Sweden). Physicists from all over the Europe are participating in development of the concept and further design and construction of experimental setups. ICNR starting point is the creation of experimental stations at the PIK reactor.

In June 2013, a workshop of NRC KI–ILL was held in Gatchina. As a result, an agreement on cooperation in research, creation of the instrumentation base of the PIK reactor and scientific examination of projects of experimental stations for the PIK reactor was signed between PNPI NRC KI and ILL. ILL agreed to take on the role of the international expert organization.

FRAMEWORK COOPERATION AGREEMENT

between

Forschungszentrum Jülich GmbH
52425 Jülich
Federal Republic of Germany
- hereinafter referred to as „*Forschungszentrum Jülich*" -

and

National Research Centre "Kurchatov Institute"
Moscow
Russia
- hereinafter referred to as "NRC Kurchatov Institute" -

A framework cooperation agreement was signed between NRC KI and FZJ on 16 June 2014. Prof. M.V. Kovalchuk and Prof. S. Schmidt at the signing ceremony

Within the framework cooperation agreement between NRC KI and FZJ of June 2014, the parties agreed to create an advisory committee and scientific subcommittees in order to discuss in detail the scientific program to be developed for the PIK reactor to establish a world-class suite.

In 2014, NRC KI established the International Advisory Committee on Photon and Neutron Sciences (Chairs Prof. H. Dosch and Prof. M.V. Kovalchuk) with two subcommittees: on photon sciences (chaired by Prof. F. Sette) and neutrons. The Neutron Scientific Advisory Committee (NSAC) of NRC KI acts as an international expert council for neutron sciences, chaired by Prof. S. Schmidt (FZJ). The current stage of NSAC activity is focused on the discussion of the proposed experimental stations and their placement on the neutron channels at the PIK reactor. The 1st meeting of NSAC was held on March 10–11, 2015.

The 1st meeting of NSAC on 10–11 March 2015 (Gatchina)

In the course of the 1st meeting, the committee (NSAC) has recommended the establishment of six subcommittees for further exploration of the fields of neutron diffraction, neutron spectroscopy, large-scale structures, fundamental physics with neutrons, neutron optics and moderators, detectors and monitors. In accordance to the NSAC recommendations, the established subcommittees have held their kick-off meetings in period from June to September 2015.

NSAC neutron spectroscopy subcommittee visits the PIK reactor

NSAC Members

Sebastian M. Schmidt	**Forschungszentrum Jülich (Germany) – chairman**
Sergey Grigoriev	**PNPI NRC "Kurchatov Institute" (Russia) – secretary**
Anatoly Balagurov	**Joint Institute for Nuclear Research (Russia)**
Olwyn Byron	**University of Glasgow (UK)**
Vyacheslav Em	**NRC "Kurchatov Institute" (Russia)**
Andrew Harrison	**Diamond Light Source (UK)**
Valery Nesvizhevsky	**Institute Laue-Langevin (France)**
Winfried Petry	**Technische Universität München (Germany)**
Dieter Richter	**Forschungszentrum Jülich (Germany)**
Mikhail Rychev	**European *X*-Ray Free Electron Laser (Russia)**
Helmut Schober	**Institute Laue-Langevin (France)**
Andreas Schreyer	**Helmholtz-Zentrum Geesthacht (Germany)**
Yaroslav Shtrombakh	**NRC "Kurchatov Institute" (Russia)**
James Yeck	**European Spallation Source (Sweden)**
Hartmut Zabel	**Ruhr-Universität Bochum (Germany)**

Subcommittee Members

Diffraction Subcommittee

A. Kurbakov (PNPI NRC KI, Gatchina) **– SC leader**
A. Balagurov (JINR, Dubna)
V. Em (NRC "Kurchatov Institute", Moscow)
A. Goukassov (CBA–LLB, Saclay)
M. Meven (RWTH, Aachen)
W. Schweika (FZJ, Jülich)
P. Staron (HZG, Geesthacht)

Fundamental Physics Subcommittee

V. Nesviszhevsky (ILL, Grenoble) **– SC leader**
H. Abele (TU Wien)
S. Baessler (UVA University of Virginia, Oak Ridge)
W. Furman (JINR, Dubna)
E. Lychagin (JINR, Dubna)
V. Voronin (PNPI NRC KI, Gatchina)
O. Zimmer (ILL, Grenoble)
M. Jentschel (ILL, Grenoble)

Spectroscopy Subcommittee

K. Schmalzl (JCNS–ILL, Grenoble) **– SC leader**
P. Alekseev (NRC "Kurchatov Institute", Moscow)
E. Klementjev (I. Kant Baltic Federal University, Kaliningrad)
J. Kulda (ILL, Grenoble)
M. Monkenbusch (FZJ, Jülich)
M. Russina (HZB, Berlin)
V.G. Sakai (ISIS, Didcot)
J. Voigt (FZJ, Jülich)

Neutron Optics and Moderators Subcommittee

F. Mezei (ESS, Lund) **– SC leader**
K. Batkov (ESS, Lund)
A. Bulkin (PNPI NRC KI, Gatchina)
T. Grosz (Budapest Neutron Centre, Budapest)
S. Kulikov (JINR, Dubna)
K. Lefmann (ESS, Lund)
P. Link (TUM, München)
V. Mitukhlayev (PNPI NRC KI, Gatchina)
A. Muzychka (JINR, Dubna)
U. Rücker (FZJ, Jülich)

Large Scale Structures Subcommittee

A. Ioffe (FZJ, Jülich) **– SC leader**
M. Avdeev (JINR, Dubna)
D. Lott (HZG, Geesthaht)
S. Mattauch (FZJ, Jülich)
A. Metwalli (TUM, München)
E. Moskvin (PNPI NRC KI, Gatchina)
B. Toperverg (PNPI NRC KI, Gatchina)

Detectors and Monitors Subcommittee

S. Kulikov (JINR, Dubna) **– SC leader**
B. Guerard (ILL, Grenoble)
R. Hall-Wilton (ESS, Lund)
D. Iljin (PNPI NRC KI, Gatchina)
G. Kemmerling (FZJ, Jülich)
S. Kosjanenko (PNPI NRC KI, Gatchina)
G. Novak (HZG, Geesthacht)
I. Stefanescu (ESS, Lund)

Main activities of the NSAC at PNPI of the National Research Center "Kurchatov Institute" from March to September 2015

Date	Activity	Milestones
10–11 March 2015	1st NSAC Meeting at PNPI NRC KI, Gatchina	Minutes of the Meeting. The person in charge – Sebastian Schmidt
	Kick-off Meeting of Neutron Optics and Moderators Subcommittee at PNPI NRC KI, Gatchina	Minutes of the Meeting. The person in charge – Victor Mitukhlayev
17 June 2015	Kick-off Meeting of Spectroscopy Subcommittee at PNPI NRC KI, Gatchina	Minutes of the Meeting. The person in charge – Karin Schmalzl
24 June 2015	Kick-off Meeting of Diffraction Subcommittee at PNPI NRC KI, Gatchina	Minutes of the Meeting The person in charge – Alexander Kurbakov
29–30 June 2015	Kick-off Meeting of Large Scale Structures Subcommittee at PNPI NRC KI, Gatchina	Minutes of the Meeting The person in charge – Alexander Ioffe
6–7 July 2015	1st Meeting of Neutron Optics and Moderators Subcommittee at ESS, Lund	Minutes of the Meeting. The person in charge – Ferenc Mezei
14–16 September 2015	Kick-off Meeting of Detectors and Monitors Subcommittee at PNPI NRC KI, Gatchina	Minutes of the Meeting. The person in charge – Sergey Kulikov
23–24 September 2015	Kick-off Meeting of Fundamental Physics Subcommittee at PNPI NRC KI, Gatchina	Minutes of the Meeting. The person in charge – Valery Nesvizhevsky

In framework of the meetings, the participants of the subcommittee meetings visited the PIK neutron facility and are now acquainted with its current state and the instrumentation concept designed previously by the Russian scientific community and the PIK representatives. The leaders of the Subcommittees have prepared the proceedings of the meeting and have worked out the first guidelines for the concept of the PIK instrumentation suite.

The current model of the ICNR can be clearly split in three parts (see the scheme below). The basis is founded on the neutron instrumentation starting with the PNPI–HZG neutron platform. The advisory committee NSAC represents the international community, their needs and requirements. The user center creates the infrastructure for those scientists who can derive maximum scientific benefit from the use of neutron scattering in biology, chemistry, material science and, of course, physics.

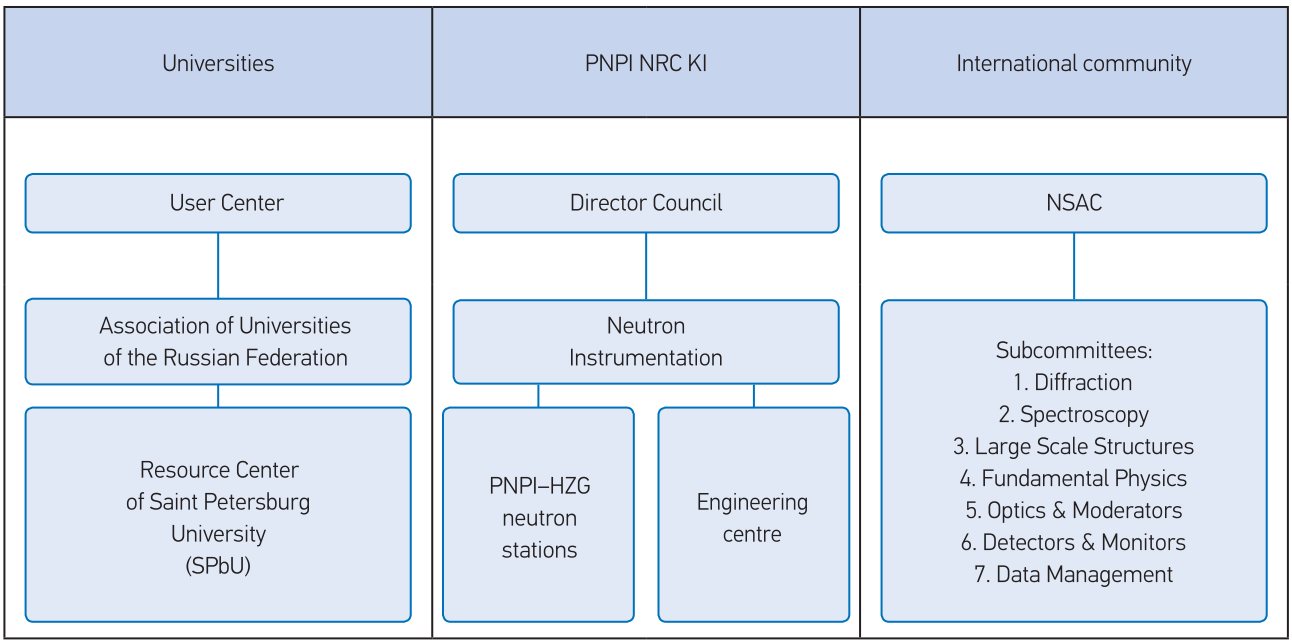

To support the infrastructure of the mega-science projects, the European Commission has implemented a new project "CREMLIN" with the aim to connect Russian and European measures in this rapidly developing branch of modern science. The PNPI NRC KI is responsible for the important task of coordinating measures in field of neutron science and particularly the activity of the international community around the PIK reactor.

Annual Winter School "Neutrons and Synchrotron Radiation for Condensed Matter Physics" of PNPI NRC KI

Research results in figures

PNPI NRC KI conducts more than 60 works supported by grants of the Russian Science Foundation (RSF), the Russian Foundation for Basic Research (PFBR), grants of the government of the Russian Federation, etc.

Number of grants

Grants	2015
RFBR	54
RSF	4
President of the RF	2
Education and Science Ministry Russia	1

Number of publications

Publications	2015
In Russian editions	170
In foreign editions	395

Six doctoral theses were defended in 2015.

Patents

In 2015, 15 patents were received including five invention patents, four useful model patents, and six certificates of the state registration of the computer program.

Awards. Prizes

PNPI NRC KI is an actively functioning institute keeping up with the current scientific trends, which is evidenced by scientific prizes and grants of its employees. The head of the Theoretical Physics Department academician L.N. Lipatov and doctor Yu.L. Dokshitzer were awarded by the Europe physical society “For the outstanding contribution to the high energy physics”.

L.N. Lipatov

Yu.L. Dokshitzer

On 28 September the Chairman of the State Duma of the Russian Federation S.E. Naryshkin paid a visit to PNPI NRC KI. The visit coincided with a professional holiday and the 70th anniversary of the atomic industry in Russia. Sergey Naryshkin conducted an awards ceremony, at which the employees of the Institute were given the certificates of gratitude on behalf of the Chairman of the State Duma. The Science Director, Corresponding Member of RAS V.L. Aksenov, the head of the High Energy Physics Division, the corresponding member of RAS A.A. Vorobyov, the head of the Knowledge Transfer Division V.F. Ezhov, the head of the reactor group K.A. Konoplev, the head of the Theoretical Physics Department academician L.N. Lipatov, the head of the Neutron Physics Department doctor A.P. Serebrov, and the Deputy Director S.L. Smolsky were awarded the memory gifts and gratitude for achievements and personal contribution to the development of the atomic industry.

Awarding of V.F. Ezhov

Awarding of K.A. Konoplev

Awarding of L.N. Lipatov

Awarding of A.P. Serebrov

Awarding of S.L. Smolsky

The rewards of the State Corporation on the Atomic Energy "Rosatom"

The merit badge "For a contribution to the atomic branch" second degree:

– V.F. Ezhov;
– D.L. Karlin;
– V.V. Pashuk;
– A.P. Serebrov;
– V.V. Fedorov.

The anniversary medal "70 years of the atomic branch of Russia":

– A.V. Korotynsky.

The winners of a competition for the prize named after I.V. Kurchatov

An active participation in a competition for a I.V. Kurchatov prize has become a good tradition among the employees of PNPI NRC KI. It is particularly pleasant that the organizers involve not only the leading and young researchers and engineers but also students. For this purpose, the Regulations of a competition contain special terms and conditions for their application. This year eight scientific works of PNPI NRC KI employees were recognized as the best ones.

In the area of the scientific investigation:

"Research of the structure and molecular mechanisms of the protein family TIP49" – A.S. Afanasyeva, A.P. Yakimov, A.V. Shvetsov, M.G. Petukhov.

In the area of the engineering and technological developments:

A series of works "A development of the technology of a productive synthesis and a functionalization of carbon structures for biomedicine, technical applications and standardization" – V.T. Lebedev, V.A. Shilin, V.S. Kozlov, V.P. Sedov, A.A. Szhogina, M.V. Suysova, Yu.V. Kulvelis, V.V. Runov, D.N. Orlova, S.P. Orlov.

Among the works of the young scientific and R&D-employees:

– "An interaction of the super-heavy elements with a surface of an amorphous selenium" – Yu.A. Demidov;
– "A search for a resonance absorption and axioelectric effect for the solar axions" – A.S. Kaynnov, D.A. Semenov, E.V. Unzhakov.

Among the works of students:

– "A sensivity of the tunnel-rotation transitions in ethylene glycol to a variation of a relation of an electron and proton masses" – A.V. Vyatkina;
– "A study of the chiral domains $TbMn_2O_5$ by the methods of the polarized neutron scattering." – M.D. Kuchugura;
– "A role of a cubic anisotropy in a transition from a helicoid to a ferromagnetic structure in the compounds of a B20-type" – A.S. Sukhanov;
– "A description of the experimental data of the spin-echo small angle neutron scattering on a base of the analysis of cross sections of the neutron scattering" – E.G. Yashina.

In 2015 the government of the Leningrad district prolonged the support of 22 works, which were previously awarded the prizes and scientific scholarships of the governor of the Leningrad district, besides, the government rewarded the following new research works:

1. A prize of the governor of the Leningrad district of the first degree for the best scientific work among the young researchers – for the research work "The molecular-genetic link of the Parkinson and Goshe diseases" (a MRBD employee A.K. Emelyanov);
2. A prize of the governor of the Leningrad district of the third degree for the best scientific work among the young researchers – for the research work "A calculation of the low-lying states of ions with a few valent elections" (a NRD employee E.A. Konovalova).

At the end of 2015 the results of the competition for scientific scholarships of the governor of the Leningrad district for the period 2016–2017 were announced. Nine employees of PNPI NRC KI were chosen at the scholarship-holders by the members of the competition committee. K.S. Bobrov (MRBD), O.I. Bolshakova (MRBD), P.A. Kravtsov (HEPD), O.V. Lobanov (KTD), V.N. Panteleev (HEPD), A.A. Szhogina (NRD), A.E. Sovestnov (NRD) became the winners in the "Leading Scientists" category. M.V. Suyasova (NRD) and A.E. Shmidt (MRBD) became the winners in the "Young Scientists" category.

Seminars

Schedule of seminars

The Institute seminars:
- The general seminar – once a month (Thursday);
- A seminar on the condensed state – every Thursday (except the day of the general seminar);
- A seminar on biology – once or twice a month (Wednesday);
- A combined seminar of the High Energy Physics Division and the Theoretical Physics Division – once a month (Thursday).

Seminars in Division:
- High Energy Physics Division – Thursday;
- Neutron Research Division – once a month (Wednesday);
  - The Section of Investigation of the Condensed States (Tuesday);
  - Laboratory of the *X*-ray and Gamma Spectroscopy – once a quarter (Wednesday);
  - The Section of the Neutron Investigation on the Atomic and Molecular Physics – once a quarter (Thursday);
- Theoretical Physics Division – once a week (Monday); in the Euler International Mathematical Institute (Saint Petersburg); in PNPI NRC KI (Gatchina) every Thursday;
- Molecular and Radiation Biophysics Division (seminars on articles sent to journals) – once or twice a month (Wednesday).

The schedule of seminars of laboratories within the Division:
  - Genetics of Eukaryotes – once a week (Friday);
  - Biophysics Macromolecules – twice a month (Wednesday);
  - Cell Biology – once a week (Tuesday);
  - Protein Biosynthesis – twice a month (Friday);
  - Proteomics – twice a month (Monday);
  - Experimental and Applied Genetics – once a week (Wednesday);
  - Enzymology – twice a month (Thursday);
  - Molecular Genetics – once a month (Wednesday);
  - Human Molecular Genetics – once a week (Wednesday);
- Knowledge Transfer Division – one a month (every third Thursday);
  - Accelerator Department – once a month (every second Thursday).

The Institute seminars

January 27. S.P. Gambaryan (I.M. Sechenov Institute of Evolution Physiobiology and Biochemistry RAS) – "Intracell signaling by the cyclical nucleotides".
January 29. P.N. Bibikov (Saint Petersburg University) – "Low temperature thermodynamics of *XXZ*-chain".
February 12. V.V. Fedorov (Neutron Research Division, PNPI NRC KI) – "Crystal-diffraction methods in physics. In honor of 85th anniversary of the first director of PNPI, the corresponding member of the USSR Academy of Sciences O.I. Sumbaev".
February 26. A.V. Rozhkov (Institute of Theoretical and Applied Electrodynamics RAS) – "Low-dimentional and anysotropical many body systems".
March 26. A.S. Sukhanov, S.V. Grigoriev (Neutron Research Division, PNPI NRC KI) – "Cubic anisotropy in the B20-compounds (of MnSi-type)".
April 2. V.N. Robuck (Laboratory of the Information Technologies of Joint Institute of Nuclear Research) – "Symmetry analysis of the linear uniform differential equations in particular derivations with the constant coefficients".
April 9. I.T. Dyatlov (Theoretical Physics Division, PNPI NRC KI) – "Quark and lepton mixing matricies: manifestation of the broken mirror symmetry".
April 16. N.E. Savitskaya (Theoretical Physics Division, PNPI NRC KI) – "Modeling of financial markets with the help of time-depending nets".
May 14. L.N. Lipatov (Theoretical Physics Division, PNPI NRC KI) – "Evolution equation of the parton distributions".
May 21. S.V. Maleev (Theoretical Physics Division, PNPI NRC KI) – "Dzyaloshinskii–Moriya interaction in spiral magnetics".
May 28. V.A. Schegelsky (High Energy Physics Division, PNPI NRC KI) – "AMS-experiment. Recent results in cosmic ray physics".
June 4. L.A. Batalov, A.V. Syromyatnikov (Theoretical Physics Division, PNPI NRC KI) – "Anomalous great relaxation of the longwave magnons in cubic antiferromagnetics with the dipole forces".
June 17. M.V. Filatov (Molecular and Radiation Biophysics Division, PNPI NRC KI) – "System manyfactor approach to study of processes of cancer transformation and oncogenesis".
June 18. O.I. Utesov, A.V. Syromyatnikov (Theoretical Physics Division, PNPI NRC KI) – "Defects in spiral magnetics with the Dzyaloshinskii–Moriya interaction".
June 25. S.V. Konyakhin (Saint Petersburg National Research Academic University, RAS and Ioffe Institute) – "Investigation of the optical and oscillation properties of carbon nanostructures".
August 26. T.V. Didenko (Research Scripps Institute. Kurt Wiitrich Laboratory") – "NMR-spectroscopy of receptors connected with G-proteins (GPCRs)".
September 24. Michael Jentschel (Institute Laue-Langevin) – "Nuclear Physics Instrumentation at a Neutron High Flux Reactor".
October 21. M.I. Mosevitskii (Molecular and Radiation Biophysics Division, PNPI NRC KI) – "New group of the outcall low specific peptidases, connected wih neurons".
October 22. O.V. Akilin (Department of the Resource Centers of Kurchatov complex NBICS-technologies of NRC KI) – "Resource centers of NRC "Kurchatov Institute".
November 5. V.V. Tarnavich (Neutron Research Division, PNPI NRC KI) – "Magnetic properties of Ho-Y and DY-Y-super lattices".
December 10. V.W. Robuk (Laboratory of Information Technologies of Joint Institute of Nuclear Research) – "Many parametric solution of the sehrodinger egnation in 1 + 3-dimension".
December 16. R.A. Shalek (Russian scientific center of Radiology and surgical technologies) – "40 years experience of clinical application of the proton beam on the base of the synchrocyclotron with the energy 1 000 MeV".

Conferences

In a framework of a wide range of scientific research subjects realized at PNPI NRC KI, the Institute convenes and hosts conferences, lectures and workshops, which are attended by the representatives from the leading scientific centers of Russia and abroad.

In 2015, our Institute organized 15 scientific events (workshops, conferences and schools) with more than 1 500 participants, including more than 500 foreign representatives of the world scientific community from such countries as Germany, Sweden, the USA, Switzerland, Japan, China, the Netherlands, Italy, Belgium, Ireland, *etc*.

The list of scientific events organized in 2015

1. "Neutron Diffraction – 2015" Discussion. **February 18–20.**
2. 49th PNPI Winter School on Nuclear and Particle Physics, Theoretical Physics, Nuclear Reaction Physics. **February 28 – March 6.**
3. Winter School for Young Scientists on Biophysics and Molecular Biology. **March 10–15.**
4. Winter School on Condensed State Physics. **March 16–12.**
5. Seminar devoted to the 85 anniversary of the corresponding member AS USSR V.N. Gribov. **March 26.**
6. Workshop "Small Angle Scattering in Biopolimers". **April 23–24.**
7. Workshop on the Inelastic Neutron Scattering "Spectrina-2015". **June 18–19.**
8. International Conference "Dzyloshinskii–Moriya Interaction and Exotic Spin Structures (DMI-2015)". **June 26–30.**
9. First Summer School on Personnel Training "Narova-2015". **June 28 – July 3.**
10. The 3rd Annual Conference on Large Hadron Collider Physics (LHCP2015). **August 31 – September 5.**
11. Conference on the Small Angle Neutron Scattering "Muromets-2015". **September 24–25.**
12. International Conference "Biogeochemical, Biophysical and Astrobiological Investigations at the Russian Station "Vostok" in Antarctica: Beginning and Prospects". **September 25–27.**
13. International Scientific and Practical Conference "Hadron Therapy and Nuclear Medicine". **October 5–7.**
14. Conference of Young Scientists "KMUS-2015". **November 11–13.**
15. Conference "School on Polarized Neutrons in Gatchina" (School PN – 2014). **December 17–18.**

Besides during 2015 the employees of the PNPI NRC KI took part in 139 Russian and international conferences as speakers.